

# University of **Strathclyde** **Glasgow**

*Strathclyde Institute of Pharmacy and Biomedical Sciences*

## Identification and Quantification of Antibiofilm Metabolite Extracts using Electrochemical Techniques

*Lily Riordan*

*Thesis presented in fulfilment of the requirement for the degree of  
Doctor of Philosophy*

*September 2023*

## Declaration

This thesis is the result of the author's original research. It has been composed by the author and has not been previously submitted for examination which has led to the award of a degree. The copyright of this thesis belongs to the author under the terms of the United Kingdom Copyright Acts as qualified by University of Strathclyde Regulation 3.50. Due acknowledgement must always be made of the use of any material contained in, or derived from, this thesis. The figures used in this thesis are a result of work carried out by the author.

Signed:

A handwritten signature in black ink, consisting of a large, stylized initial 'A' followed by a series of connected loops and a horizontal tail.

Date: 30<sup>th</sup> September 2023

## Acknowledgements

Firstly, I'd like to start off by thanking my family, and firstly to firstly is my huzzzzband, John. Sometimes I forget how lucky I am to be married to someone who just gets me; "Lily's the funniest person I know. And the funniest person she knows for that matter". Seriously though, thank you for being my forever squishy, and looking after me through my darkest thoughts. I'm so proud of both of us. You're sometimes more honest than I'd like, but I need it to pull myself together and battle through that imposter syndrome; I'm getting there. I can't wait to live together again and start planning those red cabbage practicals. There's truly no one I'd rather push a car to the garage with than you.

To Sal, Diego and Blue. Thanks for all the hugs, licks and 30 kg lap warmings. Sal, adopting you was the best thing I've ever done; I'll never forget our therapeutic toddles round the park (and the less therapeutic chasing of cats through the hedge).

My parents, Karen and Alan, taught me the value of education, the love of discovering and learning which took me to the point of studying for my PhD – "Lily's got sections on her CV which I haven't". Thank you for being so endlessly supportive and attempting to understand exactly what I do; "well, you poddle around with petri dishes and dangerous things". Hannah, who taught me to love reading and (according to mom) is why I'm so competitive. Nom, thank you for being my constant cheerleader "I don't understand what you said but you sounded like you knew what you were on about". I love you so deeply. Thank you for always being available for a rant. And of course Polly, for being the first Riordan to ever arrive early. You've made writing up infinitely harder as all I wanted to do was sit and tickle those toes all day. You are so very loved by all of us.

I have some of the best in-laws going, so to Dave, Glen, Dewi, Ieuan, Adam, and Matt; I never knew how infuriating having brothers was. I love all the board games, the random meet ups and meals, and the family chats and pet photos. You've all helped me survive the last several years, even if you've just been an island of normalcy in the ocean of insufferable long days and experiments crapping out. To my amazing grandparents, I apologise for making you travel so far for yet another graduation (last one, I promise!) – thank you for all the zoom calls, excitement for my life up here in Scotland and overall joy that being around you, even virtually, brings. Also to my grandparents who are no longer with us, not a day goes by that I wouldn't like to call you, with Nana answering "2 1 3 2". I know you'd be so proud of me,

and you wouldn't understand why I've moved so far away. To the remaining Riordans, Sindens, Rounds, Hadleys, Deeleys, Parsons, Francescuttis – thank you for being my eclectic family that I'm so proud to list. Thank you Sue for taking care of me on my North Carolina adventure, for being so amazed and overwhelmed by my science that I started to believe in myself again. I really needed that. Thank you for introducing me to your wacky, wonderful life on the other side of the pond, I'll be bringing John across soon.

To the random-af Glasgow-residing folk (in no particular order – don't read into the order, Darren): Darren, the most intimidating colleague I've ever met. We've gone through this journey together, and I couldn't have asked for a better friend to have by my side. We've made each other calmer, happier, or angrier, whatever the situation required. HVD, my personal shopper. I cannot begin to put into words how much our friendship has carried me through, I regret not sequestering you into my life sooner. Ally, my aggressive Irish cheerleader. Thank you for all the ~personalised~ advice ie. cups of tea, eg. dinner etc.. Jack (& Larry the Loop), I'm so forever grateful that you followed me to Glasgow (conscious or subconscious, we'll never know). Logan, from helping me move an incubator to pretending to father a koala with me. It's been real. Hannah, for the vegan tips and being fed eggs by 2 (!! ) people. Dave, I hope you know I laugh on the inside at (some of) your jokes. Thank you for switching between ridiculous and ridiculously caring at the droop of an eyelid. To all of you, I love you so, so much. Between you all, you've been through challenges I hope to never face (sorry not sorry), and you've never stopped being there for me or each other. Thanks for being my go-to dog-sitters, meme sendees, and people that make me smile every day.

To my non-Glasgow pals; Kizzy, I've known you for 23 years now which can't really be possible as I'm 22 in my head, but here we are. You are the most genuine, kind, and wonderful human I know, and it's been a blessing to have you in my life this whole time. Never stop smiling, and never let Noah win at games. Ali – oh deaaaaaar. I love our random 6-monthly meet ups with cups of tea and way too much talking, and of course Blake in his dressing gown. Rose, Rose knows. I'll make it out to Switzerland, I promise. I love our WhatsApp calls whilst you cook dinner, it feels like a low-budget Saturday Morning Kitchen. Peter, it feels like 23 years but it really isn't. Here's to our long-distance book club and tootling round Belfast greeting dogs. Andy, having lost contact, let's not do that again, that was silly. You always know what to say, whether it's genuine advice or cheer-me-up nonsense, it's always perfect. Brendan, Sophie, Bonnie & Lyra, your family is so beautiful.

This acknowledgments section marks the fact that I am on my way back down South soon. I can't wait to get back to our routine of meeting up and putting the world to rights over wine or Earl Grey. It's been way too long.

To MicroSoc, FEMS and ASM, thank you for funding some amazing conferences and experiences for me. It's a shame that I missed some experiences due to the pandemic, but I've made the most of the time I've had, facilitated by you, and for that I am grateful.

To the Strathclyde Microgroup members past and present; Gordon, Adriana, Tom Ha., Laia, Parra, Perrine, Marla, Diana, Connie, Kate M., Ainsley, Charlie, Eilidh, Tom He., Khadeejah, Lis, Elmira, Emily, Becca, Liam, Anna, Molly, Robyn, James, John B., John M., Dan L., Katherine, Kaisha, Stuart, Johnny, Derya, Anil, Jordan, Bea, and Angelika, thanks for putting up with my nonsense and breakdowns. I can only hope someone fills the procrastinating, tea-drinking void I'll leave behind. Keep complaining, keep elevating those mammals. Also a huge, huge thank you to Christine, Allison, Richie, Craig, and Susie, the building would fall apart without all of you. And of course, to all the PIs on Level 6; Arnaud, Paul He., Paul Ho., Nick, Dan W., Craig, Chris, Martin, Morgan, and Helina.

To the de Cogan group, Maddie, Stefana, and Alex, thank you for embracing my sarcasm and tea-drinking procrastination with open arms. I look forward to distracting all of you.

Lastly, I'd like to thank Dr. Kate Duncan for the opportunity to pursue my PhD, for taking a chance on a student she didn't know, and who was on holiday the day of the interviews. As well as Prof. Damion Corrigan, who says "no no that's not a stupid question" but chuckles anyway – thanks for all the support, advice and answering of said stupid questions. It would be remiss of me not to mention my other supervisors and mentors who have been cheering me on from the sidelines, and pushed me to apply for PhD positions (and then finish my PhD), so of course, my deepest thanks to Prof. Jon Aylott, Dr. Felicity de Cogan, Dr. Naa Dei Nikoi, Prof. Jess Blair, Prof. Sharon Huws, Dr. Linda Oyama, Dr. Luke Alderwick and Dr. Paco Fernandez-Trillo.

To those I've lost throughout the course of my PhD, I'll raise a glass of stolen pinot noir from floor 2, to absent family, friends, and hounds.

---

*“pushed from the precipice, climbed right back up the cliff, long story short I survived” – Taylor Swift, 2020*

---

## Contents

Declaration .....	2
Acknowledgements .....	3
List of figures .....	10
List of tables .....	12
Abstract .....	13
1.0 Introduction.....	14
1.1 Antimicrobial resistance – a global problem.....	14
1.2 Antimicrobial resistance: persistence and prevalence .....	19
1.3 Priority pathogens .....	23
1.4 <i>Pseudomonas aeruginosa</i> .....	23
1.5 Biofilms.....	27
1.6 Biofilms & their medical impact .....	30
1.7 Biofilm detection .....	33
1.8 Electrochemical techniques .....	36
1.9 Natural products .....	38
1.10 Microbial specialised metabolites.....	39
1.10.1 Actinobacteria .....	39
1.10.2 <i>Streptomyces</i> secondary metabolism .....	39
1.10.3 Antibiotic Discovery.....	40
1.11 Metabolomics.....	41
1.11.1 Mass spectrometry.....	41
1.11.2 Comparative metabolomics and dereplication .....	42
1.12 Aims and objectives.....	43
2.0 Materials and methodology .....	46
2.1 Bacterial growth and maintenance .....	46
2.2 Sediment collection and bacterial isolation .....	47
2.3 DNA extraction, polymerase chain reaction and phylogeny of environmental isolates .....	51
2.4 Metabolite extraction and fractionation.....	52
2.5 Antibacterial bioactivity assays (plug and disk).....	52
2.6 Mass spectrometry of bacterial metabolite extracts .....	53

2.7 Processing of mass spectrometry data .....	54
2.8 Molecular networking of mass spectrometry data .....	55
2.9 Initial biofilm formation and quantification (cuvettes).....	55
2.10 Biofilm formation and quantification (96-well plates).....	56
2.11 Electrochemical biofilm quantification methods .....	56
2.12 Pyocyanin concentration curve .....	60
2.13 Screening antibiofilm agents.....	60
2.14 Biofilm formation on Dacron graft material.....	61
2.15 Statistical analysis.....	62
2.16 Data storage and availability .....	62
3.0 The optimisation and use of both crystal violet and electrochemical measurements to quantify <i>Pseudomonas aeruginosa</i> biofilms .....	63
3.1 Introduction.....	63
3.2 Aims and objectives: .....	67
3.3 Results .....	69
3.4 Discussion .....	84
3.5 Conclusions and future work.....	87
4.0 The antibiotic and antibiofilm potential of Actinomycetota isolated from marine sediment .....	88
4.1 Introduction.....	88
4.2 Aims and Objectives .....	92
4.3 Results .....	92
4.4 Discussion .....	116
4.5 Conclusions and future work.....	119
5.0 Real world applications of electrochemical sensing .....	120
5.1 Introduction.....	120
5.2 Aims and objectives: .....	126
5.3 Results .....	127
5.4 Discussion .....	150
5.5 Conclusions and future work.....	152
6.0 General discussion, future work, and conclusions.....	154
6.1 Discussion.....	154
6.2 Future work .....	156

6.3 Conclusions.....	158
7.0 References.....	159
8.0 Supplementary information.....	181
8.1 Supplemental tables.....	181
8.2 Supplemental figures .....	192

## List of figures

Figure 1.1: Comparison of global deaths attributed to AMR, cancer, cholera, diabetes, diarrhoeal disease, measles, road traffic accidents, and tetanus.	16
Figure 1.2: UK Government efforts to combat AMR schematic.	18
Figure 1.3: Evolution of an antimicrobial-resistant bacterial population compared to persister cell survival after an antimicrobial challenge.	22
Figure 1.4: <i>P. aeruginosa</i> virulence factors and their associated mechanisms.	26
Figure 1.5: Lifecycle of a biofilm.	28
Figure 1.6: The development of subpopulations within a biofilm.	29
Figure 1.7: Properties of Dacron graft material.	32
Figure 1.8: Example of an <i>E. coli</i> biofilm forming on a biliary stent.	34
Figure 2.1: Front and back of a PalmSens 96-well plate with sensors in the bottom.	58
Figure 2.2: Photograph of equipment set up for electrochemical measurements.	58
Figure 3.1 DropSens <sup>TM</sup> plate layout and biofilm formation.	68
Figure 3.2: Crystal violet quantification of <i>P. aeruginosa</i> (PA14) biofilms with increasing seeding densities ( $OD_{600}$ 0.05 – 1).	72
Figure 3.3: Crystal violet quantification <i>P. aeruginosa</i> (LESB58) with increasing seeding densities ( $OD_{600}$ 0.05 – 1).	73
Figure 3.4: SWV Pyocyanin concentration curve.	75
Figure 3.5: SWV quantification of <i>P. aeruginosa</i> (PA14) with increasing seeding densities ( $OD_{600}$ 0.05 – 1).	77
Figure 3.6: SWV quantification of <i>P. aeruginosa</i> (LESB58) with increasing seeding densities ( $OD_{600}$ 0.05 – 1).	78
Figure 3.7: EIS quantification of <i>P. aeruginosa</i> biofilms over four hours.	80
Figure 3.8: Heatmap showing the efficacy of six antibiofilm agents recommended in the literature.	82
Figure 4.1: Bacterial isolate LR16 on ISP7 agar.	91
Figure 4.2: Antibacterial activity of isolated strains.	94
Figure 4.3: Antibacterial activity of environmental isolates.	96
Figure 4.4: Phylogenetic relationships of environmental isolates and closely related sequences.	99
Figure 4.5: Biofilm inhibition of <i>P. aeruginosa</i> by environmental bacterial metabolite crude extracts (in DMSO).	102
Figure 4.6: <i>P. aeruginosa</i> biofilm inhibition of fractions of crude extracts from three strains (four fractions per extract) which showed most antibiofilm activity previously.	104
Figure 4.7: Classical molecular network of KRD153 crude extract and its four fractions.	107
Figure 4.8: Classical molecular network of LR15 crude extract and its four fractions.	109
Figure 4.9: Classical molecular network of LR16 crude extract and its four fractions.	111
Figure 4.10: EIS quantification of <i>P. aeruginosa</i> (PA14) biofilm inhibition by LR16 (1 mg/mL).	113
Figure 4.11: EIS quantification of <i>P. aeruginosa</i> (PA14) biofilm inhibition by extract LR16 at decreasing concentrations.	115
Figure 5.1: Genome map of PA14.	124
Figure 5.2: Pyocyanin biosynthesis pathway.	125
Figure 5.3: Planktonic and biofilm growth of five PA14 insertion mutants.	128
Figure 5.4: Biofilm growth of three PA14 insertion mutants measured with EIS.	131
Figure 5.5: Planktonic growth of three PA14 insertion mutants measured with SWV.	132
Figure 5.6: Planktonic growth of PA14 grown alongside of four extract fractions measured with SWV.	135

<i>Figure 5.7: Planktonic growth LESB58 grown alongside of four extract fractions measured with SWV.</i>	136
<i>Figure 5.8: Biofilm growth of PA14 and LESB58 grown alongside MeOHdH<sub>2</sub>O extract fraction.</i>	138
<i>Figure 5.9: Biofilm growth of PA14 and LESB58 grown alongside MeOH extract fraction.</i>	140
<i>Figure 5.10: Biofilm growth of PA14 and LESB58 grown alongside ACN extract fraction.</i>	143
<i>Figure 5.11: Biofilm growth of PA14 and LESB58 grown alongside EtOAc extract fraction.</i>	144
<i>Supplementary Figure 3.1: CV-stained P. aeruginosa (PA14) biofilms at decreasing seeding densities (OD<sub>600</sub> 0.05 – 0.6).</i>	192
<i>Supplementary Figure 3.2: SWV quantification of P. aeruginosa (PA14 and LESB58) with increasing seeding densities (OD<sub>600</sub> 0.05 – 1).</i>	193
<i>Supplementary Figure 4.1: Biofilm formation of LESB58 in the presence of increasing concentrations gentamicin (µg/mL).</i>	194
<i>Supplementary Figure 4.2: OD and CV measurements of controls against both PA14 and LESB58.</i>	195
<i>Supplementary Figure 4.3: OD measurements of media solvent fractions against P. aeruginosa (PA14 and LESB58).</i>	196
<i>Supplementary Figure 4.4: CV measurements of media solvent extractions against P. aeruginosa (PA14 and LESB58).</i>	197
<i>Supplementary Figure 4.5: EIS measurements of decreasing concentrations of extract LR16 (1 – 0.25 mg/mL) over four hours.</i>	198
<i>Supplementary Figure 5.1: Photograph of Dacron graft post-CV staining.</i>	199

## List of tables

<i>Table 2.1: List of pathogens and insertion mutants (Is) used.</i>	46
<i>Table 2.2: List of culture media recipes used.</i>	48
<i>Table 2.3: List of bacterial isolation locations and corresponding co-ordinates.</i>	49
<i>Table 2.4: Full list of environmental isolated strains used.</i>	49
<i>Table 3.1 Biofilm formation of P. aeruginosa quantified spectroscopically.</i>	70
<i>Table 5.1: PA14 biofilm inhibition in the presence and absence of Dacron graft.</i>	147
<i>Table 5.2: LESB58 biofilm inhibition growth in the presence and absence of Dacron graft</i>	149
<i>Supplementary table 2.1: FASTA sequences of 16s rRNA genes of isolated environmental strains</i>	181
<i>Supplementary table 2.2: Closest related strains, and percentage similarity, to LR2 according to NCBI BLAST search</i>	187
<i>Supplementary table 2.3: Closest related strains, and percentage similarity, to LR3 according to NCBI BLAST search</i>	187
<i>Supplementary table 2.4: Closest related strains, and percentage similarity, to LR4 according to NCBI BLAST search</i>	188
<i>Supplementary table 2.5: Closest related strains, and percentage similarity, to LR6 according to NCBI BLAST search</i>	188
<i>Supplementary table 2.6: Closest related strains, and percentage similarity, to LR9 according to NCBI BLAST search</i>	189
<i>Supplementary table 2.7: Closest related strains, and percentage similarity, to LR10 according to NCBI BLAST search</i>	189
<i>Supplementary table 2.8: Closest related strains, and percentage similarity, to LR14 according to NCBI BLAST search</i>	190
<i>Supplementary table 2.9: Closest related strains, and percentage similarity, to LR15 according to NCBI BLAST search</i>	190
<i>Supplementary table 2.10: Closest related strains, and percentage similarity, to LR16 according to NCBI BLAST search</i>	191
<i>Supplementary table 2.11: Closest related strains, and percentage similarity, to KRD153 according to NCBI BLAST search</i>	191

## Abstract

Currently 2.29% of deaths worldwide are caused by antimicrobial resistance (AMR), this is compared to 1.16% caused by malaria, and 1.55% caused by human immunodeficiency virus and acquired immunodeficiency syndrome (HIV/AIDs). Furthermore, deaths from AMR are projected to increase to more than 10 million *per annum* by 2050. Bacteria within biofilms have shown resistance to 1000-fold higher concentrations of antibiotics than planktonic cells. This is due to the bacteria entering a dormant-like state, reducing their growth rate. As many antibiotics target mechanisms of active metabolism, these are less effective. New antibiofilm-metabolites are needed to inhibit biofilm formation and target established biofilms. Bacteria from the marine environment are a rich, untapped source of novel bioactive metabolites, many of which have not been tested for antibiofilm properties. However, the current methods of screening for antibiofilm activity and quantification of biofilms are slow, and do not provide crucial information, such as time to eradication.

This thesis aims to tap into this rich marine biodiversity. To fulfil this, strains were isolated from Scottish marine sediments, and screened these for their antibiotic and antibiofilm potential. Their metabolites were subsequently extracted and analysed using tandem mass spectrometry to identify the bioactive compound. Alongside this, we aimed to develop a method for biofilm quantification which could be translated into the clinical setting, as well as used in the screening of antibiofilm agents. This was carried out alongside crystal violet staining, as a published point of reference.

The developed electrochemical techniques, electrochemical impedance spectroscopy and square wave voltammetry, were able to detect *P. aeruginosa* biofilm formation within an hour after seeding *P. aeruginosa* on the sensor. This showed that there was a 40% decrease in impedance modulus when *P. aeruginosa* biofilm had formed, compared to the media only control. This was also compared to a non-biofilm forming mutant, which showed only a 9% decrease in impedance modulus also compared to the media only control. As such, this thesis offers a starting point for the development of real-time biofilm sensing technologies, which can be translated into implantable materials.

## 1.0 Introduction

### 1.1 Antimicrobial resistance – a global problem

Antimicrobial resistance (AMR) is currently the largest threat to humankind and human health. In fact, AMR infections are associated with nearly 5 million (4.95 million) deaths a year, with 1.27 million deaths directly attributed to these infections (1). To summarise the impact, in a commissioned report on global AMR in 2016, the O’Neill report shared a harrowing projection that ‘over one million people have died from AMR since [they] started this review in 2014’, with AMR responsible for 700,000 deaths annually (2). Deaths caused by AMR are predicted to increase to more than 10 million by 2050, more than cancer (8.2 million), cholera (120,000), diabetes (1.5 million), and measles (130,000) combined (**Figure 1.1**). In fact, patient deaths attributed to AMR have shown an 81% increase based on a 2022 Antimicrobial Resistance Collaborators report, climbing from 0.7 million in 2014 to 1.27 million in 2019. Of these deaths attributed to antibacterial resistance, nearly one million (929,000) deaths were caused by just six pathogens (1), known collectively as the ESKAPE pathogens; *Enterococcus faecium*, *S. aureus*, *Klebsiella pneumoniae*, *Acinetobacter baumannii*, *P. aeruginosa*, *Enterobacter* spp. (3), with these six pathogens associated with a further 3.57 million infections (1). Despite these alarming figures, the incidence of deaths caused by AMR infections in England decreased by 8.5% from 2018 to 2021. However, this figure was estimated from blood stream infections only, and the severe acute respiratory syndrome coronavirus 2 (SARS-CoV-2) pandemic led to an overall decrease in reported blood stream infections (4). In the United States of America (USA), a total of 2.8 million AMR infections are recorded annually, resulting in 35,000 deaths (5), although this is also likely to be underreported. China also has a particularly high AMR prevalence; the highest number of hospital-acquired resistant infections globally (38% of all infections) (6). One example of a prolific antibiotic-resistant infection is tuberculosis (TB), a chronic lung infection caused by *Mycobacterium tuberculosis*. Currently, 25% of the global population are infected with latent TB, with up to 15% active infectious TB (7). There are only a handful of antibiotics available to treat TB, categorized as either a first-line, or second-line treatment (8), such as the narrow spectrum antibiotic, isoniazid, used to target Gram-indeterminate pathogen, *M. tuberculosis* (9). A testament to the prevalence of this infection; it is interesting to note that studies on drug-resistant TB commonly refer to multi-drug resistant (MDR) TB and not single-drug

resistant TB. This is most likely a result of the high prevalence of MDR strains, as nearly 80% of cases with resistance to one of the first-line drugs was also resistant to another (7). MDR-TB is defined as being resistant to two of the first-line treatment drugs. There has also been reports of extensively drug resistant (XDR) TB, first seen in 2006, which is MDR-TB with additional resistance to a fluoroquinolone and one second line drug (8). One year later, totally drug-resistant (TDR) TB was discovered in two patients in Italy, where the strain was resistant to all currently available treatments and therefore the infection was untreatable (8). TDR-TB has now been seen in three countries; Italy in 2007 (8), Iran in 2009 (9), and India in 2012 (10). *M. tuberculosis* and Enterobacteriaceae both have a resistance enzyme called New Delhi metallo- $\beta$ -lactamase, which affords the bacteria resistance to nearly all  $\beta$ -lactams, including last-line antibiotics; carbapenems (11,12). Furthermore, some strains have shown antimicrobial resistance less than a year after an antibiotic was brought to market, such as methicillin-resistant *Staphylococcus aureus* (MRSA) (5). The resistant *Staphylococci* were first isolated in 1961 in South-East England, less than a year after the introduction of the  $\beta$ -lactam antibiotic, methicillin (13). Lastly, there have been no new classes of antibiotics approved for use since the introduction of Diarylquinolones in 2012 (14), and no new classes of antibiotics which target Gram-negative bacteria in 20 years (15). Despite this, the global incidence of deaths attributed to TB is declining by 2% annually (1.5 million deaths worldwide), due to an increase in accurate testing, as well as testing for drug resistance (7), meaning interventions are more successful. However, as shown previously, cases of AMR infections as a whole are still increasing, and have been previously estimated to rise to 10 million annual deaths globally by 2050 (2) if no further action is taken, and it is estimated that this will cost \$100 trillion globally per year (16).

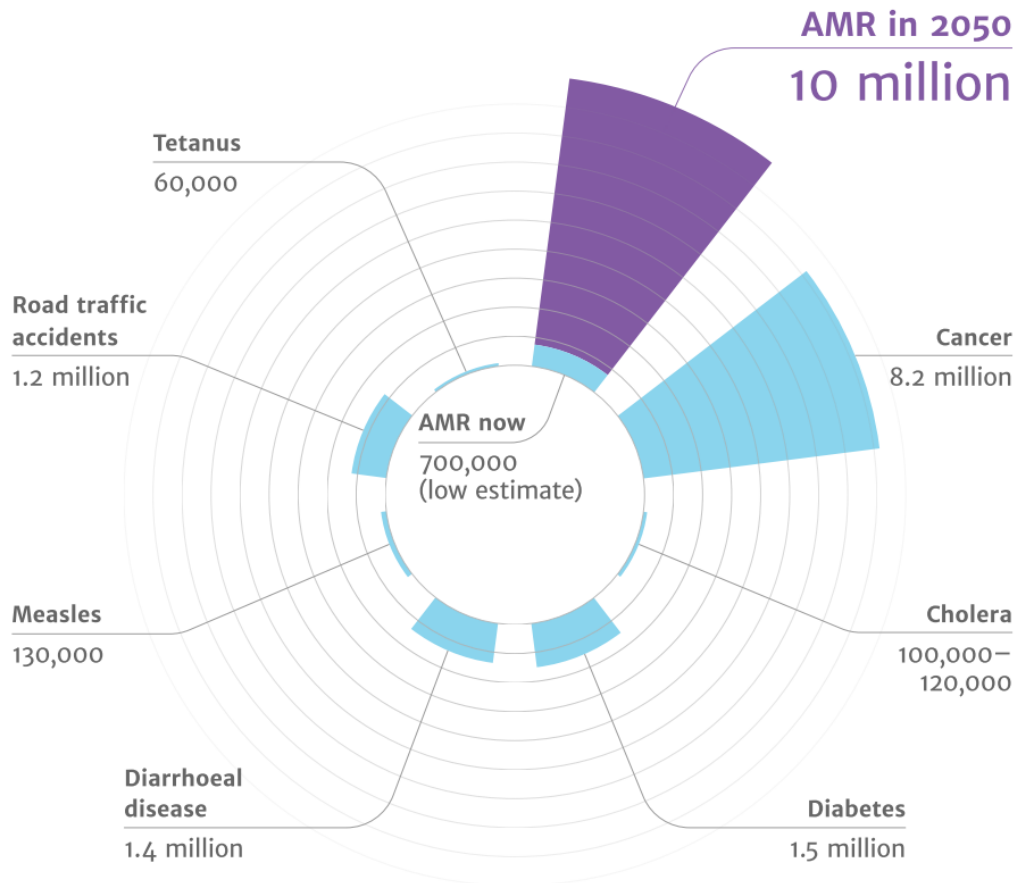


**Figure 1.1: Comparison of global deaths attributed to AMR, cancer, cholera, diabetes, diarrhoeal disease, measles, road traffic accidents, and tetanus.** Current values are shown in blue, and the estimated number of deaths caused by AMR in 2050 is shown in purple. Taken from a 2016 review by O’Neill (2).

The current global action plan for AMR, as outlined by the World Health Organisation (WHO) in 2017, involves increasing awareness of AMR by increasing communication and education, research, and surveillance of AMR infections, as well as reducing their incidence, optimising the use of current antimicrobials, and increasing investment in new medicines (17). The United Kingdom (UK) was one of the first countries to outline an AMR action plan, which was implemented in 2000, with less focus on novel antimicrobial discovery, and more on maintaining efficacy of current treatments and reducing infection rates (18). The current UK action plan now includes investing in the discovery, supply, and access to antimicrobials, alongside the reduction of unnecessary antimicrobial use (**Figure 1.2**) (16). The USA have a more comprehensive action plan, with a focus on research. For example, investing in new technologies to understand antimicrobial resistance, development of drugs and diagnostic tools, research into novel healthcare interventions, and data-driven solutions to guide public health interventions (19). Both the UK and the USA plan to optimise the use of antimicrobials, with reduced use in agriculture (16,19). Interestingly, the UK aims to utilise a point of care diagnostic test or 'decision support tool' by 2024 for microbial diagnostics and subsequent prescriptions (16).

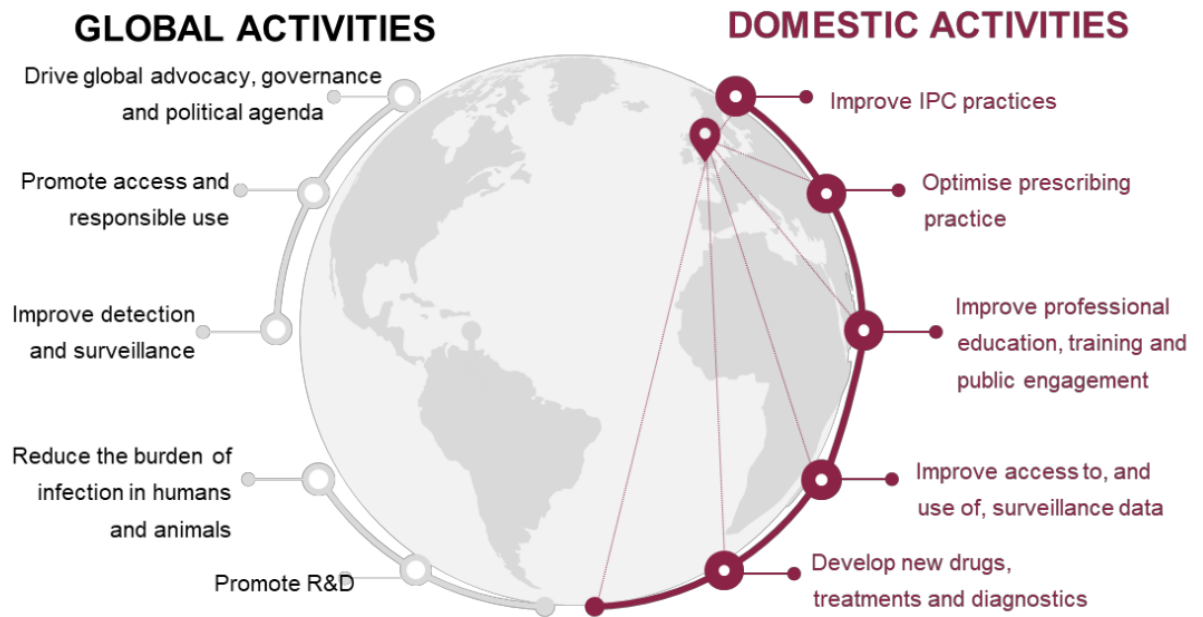


**Figure 1.2: UK Government efforts to combat AMR schematic.** Areas of focus for the UK Government to tackle AMR, separated into global objectives (grey) and UK-wide objectives (burgundy). Taken from the UK Government’s five-year national action plan, from 2019 to 2024 (16). Infection prevention and control abbreviated to IPC.

## 1.2 Antimicrobial resistance: persistence and prevalence

The prevalence of AMR strains is on the rise due to several factors which can be summarised as the overuse and misuse of antibacterial, antifungal, and antiviral drugs (20,21). A major factor in this is the increased global migration of people which allows antibiotic-resistant bacteria to travel between different countries easily (22), this was demonstrated previously in a study monitoring MDR *M. tuberculosis*, 46.6% of TB cases came from non-nationals (9). Another large contributor to AMR, is the use of antimicrobials in the farming industry. In fact more antimicrobials are added to animal feeds than are consumed by humans (21), globally 63,151 tons of antimicrobials consumed by farming animals, twice the amount consumed by humans (23). The antimicrobials are added to the feed to keep the farmed animals healthy in unsanitary and unsafe conditions to increase yield; this decreasing housing size has seen an increased need for antimicrobials in feed (21,23,24). Moser, *et al.*, demonstrated that the use of antimicrobials in farming drives AMR, which led to an increased number of AMR microorganisms present in the animals themselves; they found 69.3% of *Escherichia coli* isolates from a poultry farm had MDR, compared with 15.3% from domestic birds, and crucially, this was mirrored in the associated humans (24). Another major contributor to AMR, and perhaps one of the most well-known, is the over-prescription of antibiotics for human consumption in clinics (4). This is demonstrated in China, whereby 50% of all prescriptions contained at least one antibiotic (20). As well as this, during the outbreak of SARS-CoV-2, at the end of 2019, 95% of patients in China were given antibiotics prior to diagnosis (25). This reliance on antimicrobials, both by the patient and doctors, is also exacerbated in some countries, such as Saudi Arabia and Ethiopia (12), with the availability of antibiotics as over-the-counter medication (22) accounting for over 80% of their antibiotic usage (26). Lastly, perhaps less of a global contributing factor, but is nevertheless important, is the lack of education around prescriptions. For example, patients not finishing their course of antibiotics, as this permits the survival of bacteria which have been exposed to the antibiotic, allowing them to develop resistance (27). This has been demonstrated in the literature, looking at *P. aeruginosa*, repeated exposure to ciprofloxacin, starting at 50% of the MIC (0.1 mg/L), led to an MIC of 2 mg/L after just seven passages (28). One of the methods to improve antimicrobial stewardship and extend the lifespan of currently available antimicrobials is the AWaRe classification by the World Health Organization. This has categorised 258 commercially available antibiotics into four categories based on the

prevalence and impact of antimicrobial resistance associated with both the antibiotic and antibiotic class; access, watch, reserve, and not recommended. The WHO aims that at least 60% of all administered antibiotics would belong to the lowest risk group; 'access' (29).

As well as mismanagement and overuse of antimicrobials by humans contributing to AMR, microorganisms themselves have evolved some remarkable mechanisms to become resistant to these treatments. It is worth noting that AMR is an ecological function in nature to adapt to threats such as antibiotic-producing strains (30), however AMR has been exacerbated by our overuse. In fact, bacteria have a range of antibiotic resistance mechanisms. These changes in bacteria include the first-line defence mechanism against antibiotics; persister cells (31). These cells exist as a slow-growing, subpopulation within an otherwise antibiotic-susceptible population, without any specificity against particular antibiotics, but an overall decreased susceptibility to antibiotics (31,32). This has been shown to be due to their decreased growth rate and uptake of antibiotics (31). Their phenotypic change is not hereditary, and the persister cells change back to an antibiotic-sensitive state and reinitiate growth once the environmental stress has passed (**Figure 1.3**) (32,33). This ability of persister cells to survive has been demonstrated by the monitoring of single nucleotide polymorphisms (SNPs) from bacteria associated with recurring infections, using SNP typing and whole genome phylogenetics. For example, in HIV-infected adults with recurring bloodstream infections caused by invasive nontyphoidal Salmonella, Okoro, *et al.*, found that 78% of recurrences were from identical or highly related bacterial isolates (34). This was also demonstrated in an older study which used chromosomal restriction fragment length polymorphisms (RFLP) analysis with pulsed-field gel electrophoresis to identify the percentage of recurrent urinary tract infections caused by *E. coli*. Their analysis revealed that 68% of patients had a recurrent *E. coli* infection with the same RFLP profile as a strain previously isolated from that patient (35). Both studies therefore indicate that the majority of these infections were not cleared, and that the recurrence was not reinfection. Another line of defence against antibiotics used by bacteria, is the overexpression of efflux pumps (36). This is also accompanied by a change to the cells metabolism to compensate for the increased demand, as efflux pump formation is metabolically expensive (37). Efflux pumps transport a wide range of substrates, including antibiotics, out of the bacterial cell. These pumps are embedded in the membrane can decrease the concentration of antibiotic inside the bacterial cell to a sublethal concentration, leading to resistance. The most clinically

significant efflux pump system is the RND efflux family (36). For example, AdeABC, *Acinetobacter* drug efflux, is an RND efflux pump in *Acinetobacter*, and its over-expression positively correlates with the pathogen gaining multidrug resistance (38). Furthermore, some pathogens use efflux pumps to transport substrates for biofilm formation, such as *Pseudomonas aeruginosa* which uses MexAB-OprM and MexCD-OprJ efflux pumps to form biofilm in the presence of the antibiotic azithromycin (39). An increase in biofilm formation in the presence of antibiotics is not uncommon; this increase in resistance mechanisms in the biofilm phenotype is also seen in *E. coli* (40). However, the inactivation of efflux pumps is not straightforward, as the targeting and inactivation of particular efflux pumps has been shown to lead to increased gene expression of alternative efflux pumps (41). This is possibly to enable the pathogen to maintain the level of resistance, as well this demonstrates the need for efflux-inhibiting drugs to target more than one pump, or for the mechanism of action to be well-understood. Lastly, bacteria can develop resistance to specific antimicrobials, such as tetracycline (24). AMR can spread throughout a bacterial population using horizontal gene transfer (HGT) via mobile genetic elements (MGEs), such as plasmids and integrons (24,42). As such, these MGEs are capable of transferring genes which confer resistance between different bacterial genera (24). This was demonstrated by a study looking at antimicrobial use in animal feed. The authors found that this selected for *E. coli* containing specific MGEs, and *E. coli* sampled from humans working on the farms were subsequently found to also be carrying the same MGEs (24).

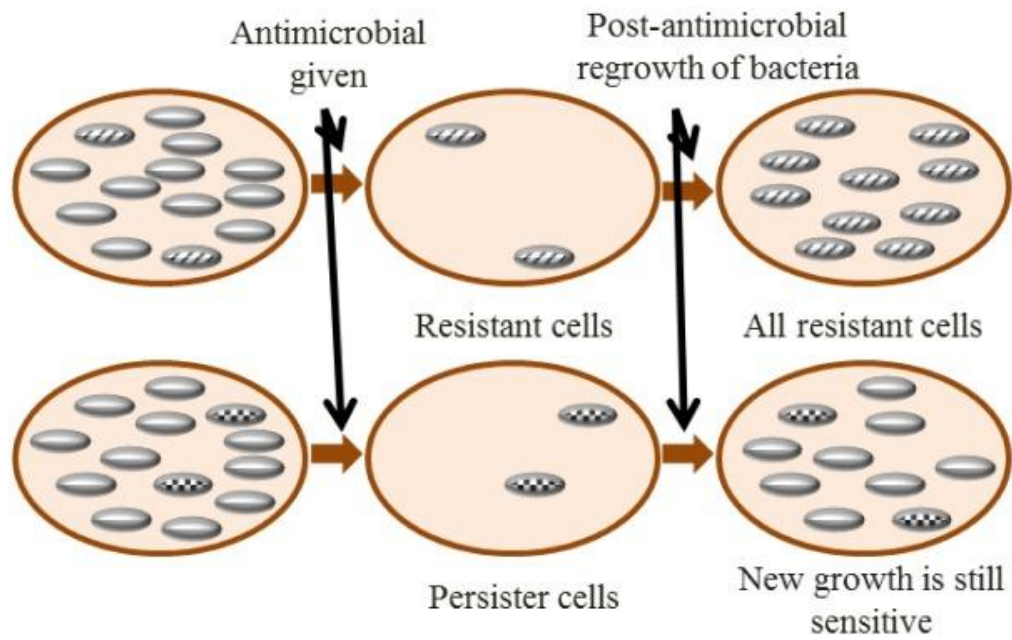


**Figure 1.3: Evolution of an antimicrobial-resistant bacterial population compared to persister cell survival after an antimicrobial challenge.** The survival and subsequent proliferation of antimicrobial-resistant bacteria shown in the top line, compared to the survival of persister cells underneath, which shows proliferation of antimicrobial-sensitive bacteria. Taken from a 2018 review by Reygaert (33).

### 1.3 Priority pathogens

Alongside *E. coli*, the majority of AMR infections are caused by only a few species of bacteria, known as the ESKAPE pathogens; *Enterococcus faecium*, *S. aureus*, *Klebsiella pneumoniae*, *Acinetobacter baumannii*, *P. aeruginosa*, *Enterobacter* spp. (3). *E. coli* is sometimes exchanged for *Enterobacter* spp., as they are from the same Family; *Enterobacteriaceae* (43). All of the ESKAPE pathogens belong to two phyla; Firmicutes and Pseudomonadota (formerly Proteobacteria). In 2017, the WHO released a list of global priority pathogens (GPP), which included the ESKAPE pathogens, and highlighted the need for new antimicrobials against these pathogens (44). However, despite the increased focus on developing novel treatments, the number of effective treatments against these ESKAPE pathogens is still declining (45). For example, a study looking at hospital-acquired infections (HAIs) found that the most commonly prescribed antibiotic for *S. aureus* infections was amikacin, however 60% of *S. aureus* isolates from patients had resistance to this antibiotic, with 100% of *S. aureus* isolates resistant to penicillin and 80% resistant to erythromycin and cotrimoxazole (46). These authors also found that HAIs led to an increase in the length of hospital stay required (36% of patients stayed longer than 15 days, compared to 15% of patients without a HAI) (46). As well as an increased length of hospitalisation, infection with an ESKAPE pathogen has also been shown to lead to an increased risk of mortality (2.1%) (47). These authors showed that approximately 400,000 patients with bloodstream infections, 42.2% of patients were infected with an ESKAPE pathogen. From these, more than one in five patients were infected with *S. aureus* (21.9%) and *E. coli* (22.6%), and despite not being listed as an ESKAPE pathogen, more people were infected with *E. coli* than *S. aureus*. Lastly, the study found that 14.7% of patients were infected with either *K. pneumoniae* or *P. aeruginosa* (47). These *P. aeruginosa* infections are of particular concern, as more than 55% of *P. aeruginosa* clinical isolates showed resistance to all assayed antibiotics (48), including last-line antibiotic, meropenem (49).

### 1.4 *Pseudomonas aeruginosa*

*P. aeruginosa* belongs to the phylum Pseudomonadota, a major phylum of Gram-negative bacteria; renamed from Proteobacteria in 2021 (50). Within this phylum, *P. aeruginosa* belongs to the genus *Pseudomonas*, which consists of species which are ubiquitous and

prosper in an array of environments (51,52), including water (53), soil (54), plants (53), and the human lung (55). Part of this environmental adaptation can be attributed to the bacterium's swimming, swarming and twitching motilities (52). These traits enable *P. aeruginosa* to colonise a range of ecological niches (52), including clinical environments (51,56,57), with multiple studies showing the prevalence of *P. aeruginosa* in hospital wards (55,58,59) and on medical devices (56,57). In particular, *P. aeruginosa* is infamous for its prolific ability to form biofilms in inhospitable environments (60), and its ability to develop antibiotic resistance, as mentioned previously. For example, a review looking at Nepalese clinical isolates found that 42% of *P. aeruginosa* isolates were resistant to two or more antibiotics (61), whilst another study showed more than 55% of *P. aeruginosa* clinical isolates were resistant to 12 antibiotics (48). This resistance to antibiotics might be explained in part as the *P. aeruginosa* genome hosts a disproportionately large number of regulatory genes associated with virulence and encoded virulence factors (62,63). For example, the *P. aeruginosa* gene, *lasR*, encodes a global regulator which regulates pyocyanin production and the synthesis of rhamnolipid (64), a biosurfactant required for biofilm maturation (65). As well, another *P. aeruginosa* virulence factor which causes extensive tissue damage upon infection upon a human host (66), the enzyme elastase, also requires *lasR*, and the subsequent transcription of *LasR*, in order to be activated (67). Unsurprisingly, it has been observed that the densely packed nature of the biofilm increases genomic mutations (68) and HGT (63), a key method *P. aeruginosa* uses to develop AMR. All these adaptations have contributed to *P. aeruginosa* being the etiological agent of 10% of all recorded nosocomial infections in the European Union (69), as well as being the leading cause of endoscope infections (56), and death amongst cystic fibrosis (CF) patients (51). Lastly, it should be noted that as *P. aeruginosa* is able to colonise an array of environments, it is usually assumed that *P. aeruginosa* infections in CF patients are environmentally-derived, and not a result of human transmission (51). Overall, CF-patient life expectancy sits at a median age of 46 years for males, and 41 for females (70); with *P. aeruginosa* infection increasing risk of mortality to 53.7% within 8 years (71).

There are two commonly used laboratory strains of *P. aeruginosa*; PAO1 and PA14 (72). PA14, originally isolated from a burn wound patient (54), has two additional pathogenicity islands to PAO1, and increased virulence (52,73). The work in this thesis focusses on PA14, as PA14 shows more consistent biofilm formation compared to PAO1 (74). The other *P.*

*aeruginosa* strain used in this thesis work is LESB58, which belongs to the LES group of *P. aeruginosa* isolates, which are the most common strains in CF patients (75). LESB58 was also the first identified *P. aeruginosa* clinical isolate (55), isolated from a CF patient in Liverpool in 1988 (51). LESB58 is a highly virulent strain of *P. aeruginosa*, encoding 99.2% of all known *P. aeruginosa* virulence factors (**Figure 1.4**) (76). Unusually for *P. aeruginosa*, LESB58 exhibits human transmission readily (55). Studies have shown that LESB58 has undergone loss-of-function mutations, increasing transmissibility (51), and therefore has been seen to cause infections in patients with other lung conditions (55), such as primary ciliary dyskinesia (51), as well as relatives of CF patients without lung conditions (59). One of these mutations includes the loss of the type VI secretion system (T6SS), a biological weapon used to kill surrounding pathogens (51). Other mutations in similar isolates include increased alginate production (57), making the biofilm more mucoid (57,77), impairment of efflux pumps (51), and loss of quorum sensing (51). The advantages of these mutations is not clear, however they may have an alternative role that is more important in adaptation to the CF lung (51). Crucially for this study, one of the virulence factors which LESB58 has not lost is the production of electrochemically active metabolites. Of specific interest to this work, is pyocyanin; a blue pigmented metabolite (78), produced by 95% of *P. aeruginosa* strains (79). Further to this, metabolite concentration typically increases as the optical density (OD) of the pathogen culture increases. This is particularly true in a closed system, where there is no movement of anything other than energy in or out of the system, therefore metabolite concentration can be used as a measure of growth if all other factors remain constant (80). Interestingly, many of the genes associated with pyocyanin production are also involved in biofilm formation; a key component of AMR (56). These genes include *lasR*, mentioned previously, as well as *pmtA* which encodes for pyocyanin, and the deletion of *pmtA* disrupts biofilm formation (81).

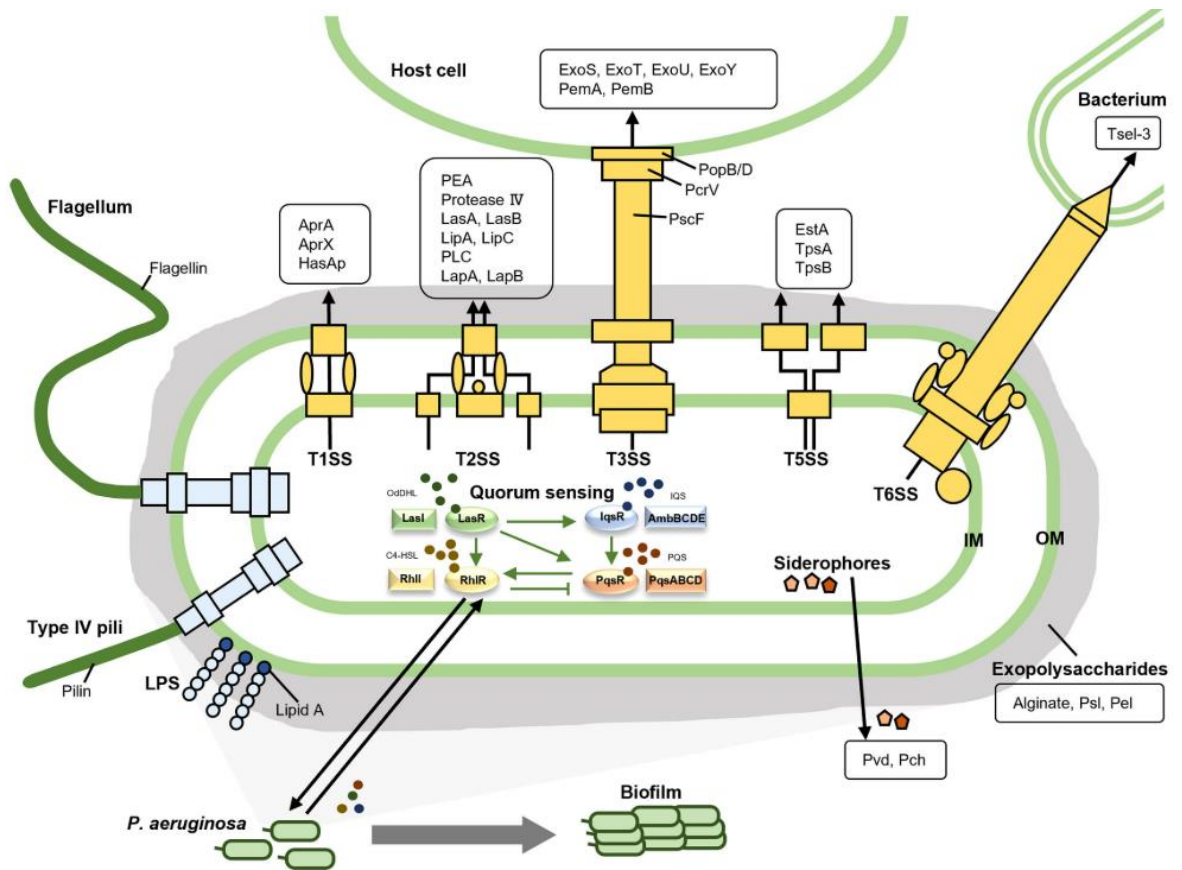


**Figure 1.4: *P. aeruginosa* virulence factors and their associated mechanisms.** The virulence factors of *P. aeruginosa* can be separated into three main categories (surface structures, secreted factors, and cell-to-cell interaction). Surface structures include the type secretion systems (abbreviated to TxSS), type IV pili, and flagellum. The secreted factors are outlined in dark grey, and biofilm and quorum sensing are cell-to-cell interactions. Taken from an 2022 review by Liao (82).

## 1.5 Biofilms

As mentioned previously, a major factor which makes certain bacteria harder to treat is their ability to form and maintain biofilms (**Figure 1.5**). Biofilms are a community of bacteria, usually mixed species (74), with increased resistance to antibiotics, antimicrobials, and other biocides, often with minimum biocidal concentrations of 1000-fold higher than planktonic cells (56,77,83,84). Biofilms have been shown to afford the bacteria environmental protection (74), such as against shear stress and decreased nutrient availability (60). Mechanisms also include the creation of a physical barrier of extracellular polymeric substances (60,85,86) through sequestration of environmental and own molecules. This includes molecules and material from the environment in which the biofilm has formed, for examples within an animal host, materials such as red blood cells, platelets, and fibrin (86,87), as well as the cell's own "junk" DNA (74) and polysaccharides (31). Furthermore, bacteria with increased antibiotic resistance have been shown to have an increased production of various polysaccharides, such as alginate in *P. aeruginosa* (88). Being in a biofilm allows bacteria to maintain a larger population number, as not all the bacteria are "exposed" to the outside of the biofilm, and therefore an antibiotic, at once, meaning that bacteria within a biofilm can withstand up to 1000 times higher antibiotic concentration than those not in biofilm (89,90), and additionally tolerate higher concentrations of organic compounds and salts (90). This is further demonstrated by the heterogeneous nature of a biofilm, as shown in **Figure 1.6** (40). For example, Høiby, *et al*, demonstrated that in a PAO1 biofilm, the cells in the core of the biofilm have reduced metabolism (57), and as some antibiotics, such as  $\beta$ -lactams target active metabolism (57), these cells have an increased tolerance to such antibiotics (31,32,91,92). Using GFP-expressing *P. aeruginosa* and then staining for dead cells, these non-dividing, dormant cells have been shown to be present in the centre of the biofilm, and actively growing cells on the outside. This study used ciprofloxacin, which targets active metabolism, killing all cells outside of the biofilm but leaving the inside cells alive. This was then confirmed using colistin, which is active against non-dividing cells (57).

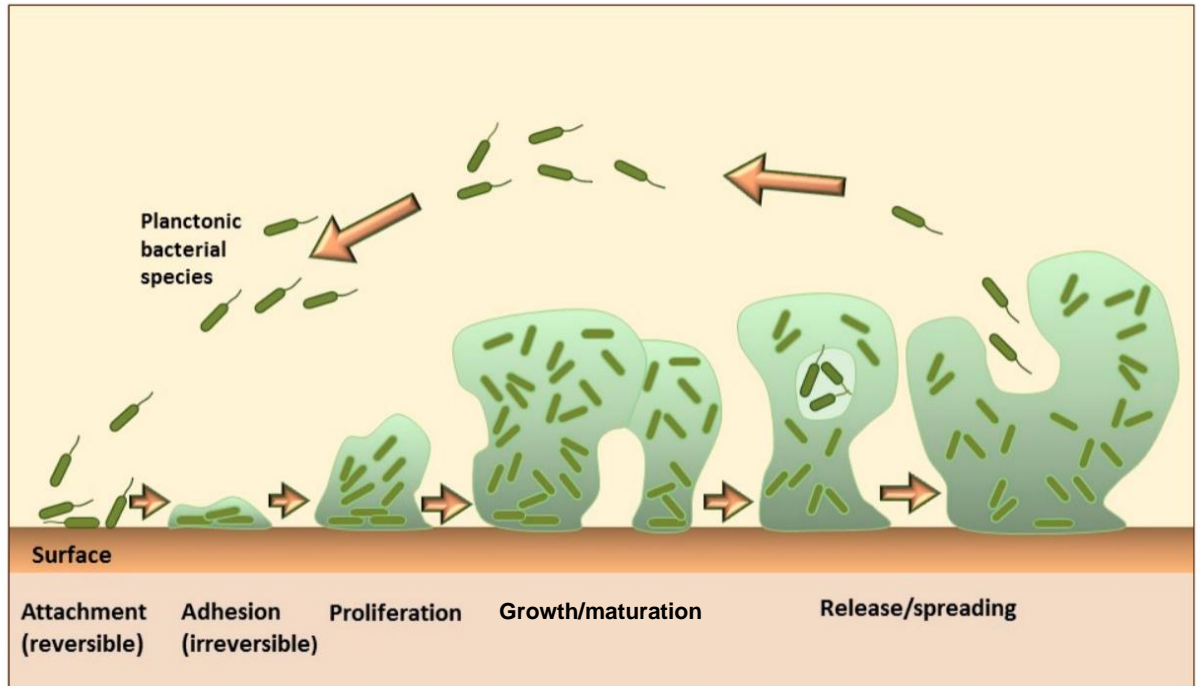


**Figure 1.5: Lifecycle of a biofilm.** The size stages in the lifecycle of a biofilm, from initial attachment of planktonic cells to the maturation and subsequent dispersion of further planktonic cells. Taken from an 2016 review by Rukavina (93).

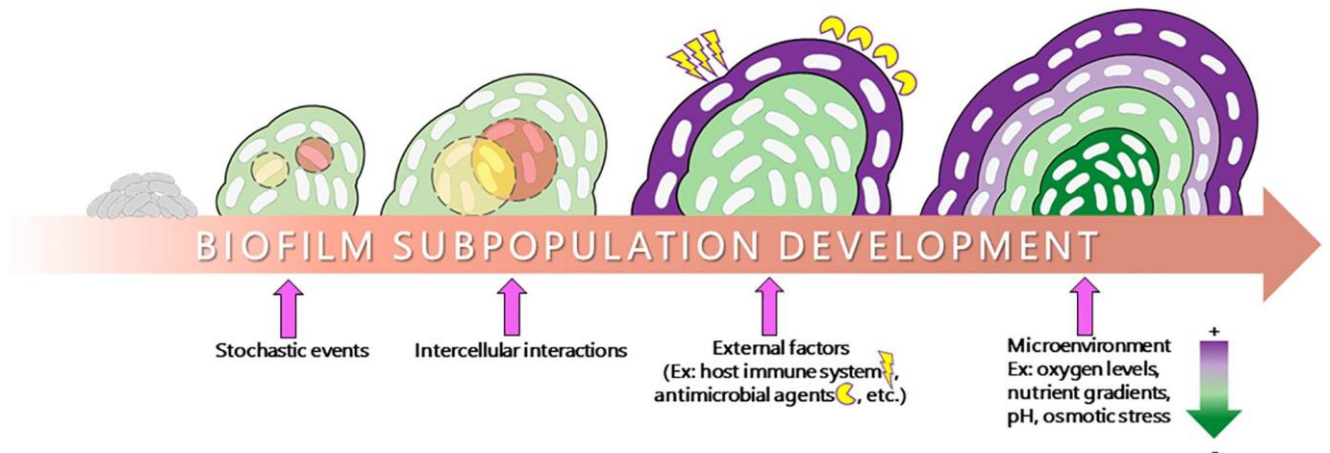


**Figure 1.6: The development of subpopulations within a biofilm.** The events both within a biofilm (stochastic events and intercellular interactions), and outwith a biofilm (external factors and microenvironment) lead to the development of a heterogenous biofilm as shown in the four different colours on the far-right image. Taken from an 2019 review by Bisht (94).

## 1.6 Biofilms & their medical impact

In a biofilm context, medical devices and implants, such as catheters (57,95,96), grafts (57,97,98), and endoscopes (56,99), are a particular issue, as they provide a surface on which the biofilm can form (56,57). In fact, it has been shown that 2% of knee and hip replacements become infected, with 57.1% of cases developing a second infection, leading to further surgeries and debridement (100,101). Furthermore, the incidence of bacterial implant infections ranges considerably, for example intraocular lenses have an infection rate of 0.1%, urinary tract catheter up to 33% (102), and open fractures have incidences reported to be 31% (102). One of the key factors influencing infection is the material used. The most commonly implanted orthopaedic material is stainless steel, specifically 316L (103), along with the most common materials for coronary surgeries is polytetrafluoroethylene or Dacron fabric (104).

Dacron fabric, **Figure 1.7**, was first invented in the 1950s with the intention of creating a synthetic material for repairing blood vessels (105). Since then, Dacron grafts have been routinely used for coronary surgeries (97,106,107), despite their prevalence, Dacron grafts induce a stronger inflammatory response than other implantable materials reported (106). This means that the implanted graft is more likely to be rejected compared to materials with a weaker inflammatory response (37). It is therefore unexpected that Dacron grafts have the same infection incidence of *S. aureus* biofilm formation as other implantable materials which induce a weaker immune response, such as fusion graft and polytetrafluoroethylene (PTFE) (108). However, this is potentially because implantable materials, along with Dacron grafts, are typically coated in host matrix proteins for improved host integration (109). Unfortunately, these proteins also create an ideal surface for bacteria to form biofilms (109). Unsurprisingly, the published estimates for biofilm-related infections vary; from up to 65% of all bacterial infections (74), to 70% of all implant infections (72). However, with this in mind, there are currently no antibiofilm agents on the US market (74,110,111). Taurolithocholic acid (TLCA) induces biofilm dispersal, however is not used clinically as it increases the virulence of *P. aeruginosa*, and the production of biosurfactants for greater cell adhesion (110). As such, biofilm prevention *in vivo* is limited to physically isolating infected patients to prevent cross-contamination (57), or aggressive oral antibiotic therapy (112). Ideally, an anti-quorum sensing (involved in biofilm formation) drug or natural product could be administered, limiting pathogenicity and biofilm formation (113–115).

Furthermore, the creation of antibacterial implant surfaces could remove the risk of biofilm formation on the implantable materials. With this in mind, impregnating antimicrobial peptides onto medical-grade stainless steel has shown great promise, with a study showing that inoculated *P. aeruginosa* was eradicated within 45 minutes upon such material (58). Furthermore, the sterile surfaces could also be employed for non-single use medical equipment, such as endoscopes, which are of particular concern due to their repeated use. One study showed that biofilms can survive typical cleaning regimens as the biocidal concentration of the cleaning solution is calculated for planktonic cells. Further, the authors found that the minimum biofilm eradication concentration of the same species is 100-fold higher, and increases with the biofilm age and biomass (56). Another study found that increasing the concentration of the antibiotic, isothiazoloquinolone, to a concentration 16-fold higher than the bacterial planktonic minimum inhibitory concentration (MIC) only reduced biofilm biomass by 33% (84).

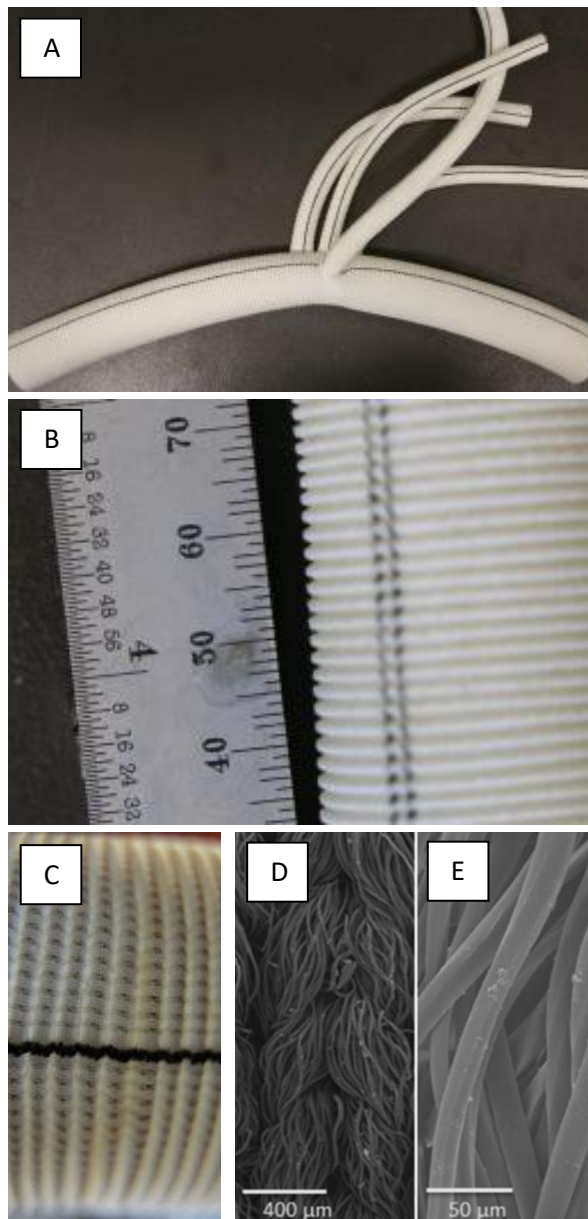


**Figure 1.7: Properties of Dacron graft material.** Dacron graft material pre-implantation into a patient (A), with a close-up demonstrating the ridges are  $\sim 1$  mm each (B), and showing the woven structure (C). Scanning electron micrographs of Dacron graft showing both the weaving (D) and individual fibers (E). A, B and C taken from an 2020 research article by Amabili (116), D and E taken from an 2017 research article by Herten (117).

## 1.7 Biofilm detection

As mentioned, biofilms can lead to complications when they form on medical implants and other surgery sites, these complications include bacteraemia and subclinical infections (89,118), which in turn lead to further surgeries or poor clinical outcomes (86). Currently the main method of identifying a medical implant biofilm is after the device has been explanted (86,89), or when bacteria break away from the biofilm and cause bacteraemia (89,118) (**Figure 1.8**). Prior to this, subclinical infections often go unnoticed due to very mild symptoms (89). Therefore, the available methods to identify a biofilm on an implant would involve surgery and a swab of the implant and site of infection, followed by bacterial culture. Aside from the invasive procedure, the main problem of this method is often the bacteria are in a dormant or slower growth state. If this is the case, the results would likely give a false negative or not include all bacteria present due to the growth conditions needed for different species (89). Alongside these methods, swabbing and then staining with crystal violet (CV) has been proposed. However, CV can create a large quantity of background stain, meaning it needs to be combined with measuring the optical density of the stained bacteria to produce a more accurate value (119). Further to this, polymerase chain reaction (PCR) can be used to identify the bacteria present via 16S rRNA sequencing (89), as well as AMR genes or virulence factors present in the bacterial genome (120). PCR can also be performed on blood, urine or sputum samples, and has been shown to successfully detect pathogenic bacteria in a patient's body fluids (120). Although, as highlighted by Xu, *et al.*, these sequence-based methods are not able to differentiate between planktonic and biofilm-forming bacteria (89).

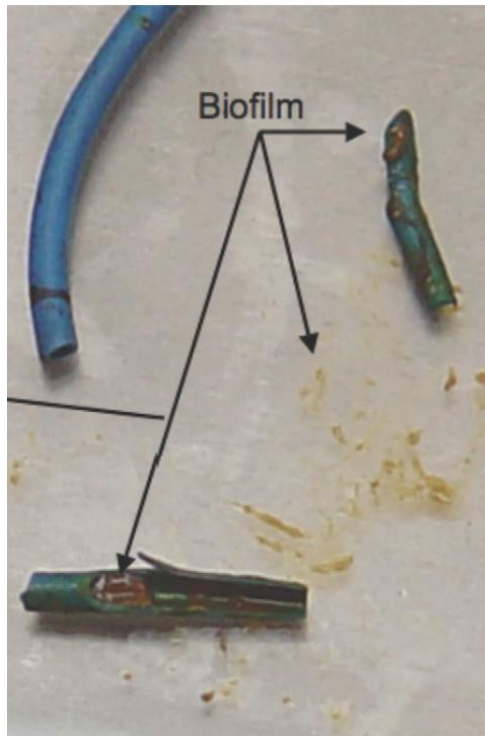


**Figure 1.8: Example of an *E. coli* biofilm forming on a biliary stent.** Biofilm led to bacteraemia and sepsis, and was ultimately fatal, however, the biofilm is only visible when the stent has been explanted. Figure from Høiby, *et al*, 2010 (57).

When considering biofilm-formation, as mentioned previously, within a biofilm, many bacterial species often regulate density via a chemical messaging system called quorum sensing, (89,90). As such, quorum signal profiling has been assessed as a method for biofilm detection. For example, during the development of the *P. aeruginosa* biofilm, the differentiation stage is initiated by two homoserine lactone molecules. Measuring the quantity of these molecules in sputum samples from patients with CF has enabled the identification of *P. aeruginosa* biofilm, as well as determining the biofilm growth stage (121). However, the use of acyl homoserine lactones for quorum sensing is also seen in the family Vibrionaceae, including human and fish pathogens *Vibrio cholerae* and *Vibrio fischeri* (122), and therefore these markers could not be used as *P. aeruginosa*-indicators. Another similar method includes measuring biofilm associated markers (BAMs), as during biofilm growth, metabolites specific to particular strains can be produced (89). For example, *S. aureus* and other *Staphylococcus* spp. produce a surface protein called Bap; the presence of this protein strongly correlates with the ability of the strain to form a biofilm, as gene knockout strains of these species have a reduced ability to form biofilms (123). Bap homologs have also been found in several other bacteria species including *A. baumannii* and *Staphylococcus epidermidis* (89,123), however, the protein has not been found in human *Staphylococcal* isolates (123), and therefore Bap and the homologs may not be a viable biofilm marker. BAMs can also be molecules which bacteria add to their biofilms, for example, uropathogenic *E. coli* (UPEC) biofilms contain cellulose, however planktonic UPEC cells do not. Therefore, Antypas, *et al.*, developed an assay to identify cellulose in urine as an indicator of UPEC biofilm infection (124). Further to this, Xu, *et al.*, suggested that this UPEC detection method could be combined with cell-free DNA testing. As mentioned above, some pathogens incorporate their own DNA into their biofilm, and therefore combining BAM detection with cell-free DNA testing could be used to detect and identify the bacterial species present in a biofilm (89).

Furthermore, a recent technology for monitoring biofilm formation in real-time, instead of after biofilm formation, uses surface acoustic waves (SAWs). SAWs are a type of vibrational wave which passes through a solid material and are affected by the elasticity of the material (89). This new technology can be attached to the inside of a liquid-filled tube and the deposition of materials onto the side of the tube is monitored. This is a promising technology for the real-time monitoring of biofilm formation on medical devices, such as catheters, as

the technology is also capable of differentiating between a soft or hard deposition, such as a biofilm or limescale layer, respectively (125). Another non-destructive method is Surface Enhanced Raman Spectroscopy (SERS). This is capable of detecting molecules with high sensitivity by detecting the scattering of photons from a material and their relative change in energy (89). This method has previously been used to detect the *P. aeruginosa* metabolite, pyocyanin (115). SERS is capable of detecting low abundance molecules (89), however due to the equipment cost and technical expertise required, it is unlikely to be used in a clinical setting. Another imaging technique which only visualises live bacteria is positron emission tomography (PET), which has been used to image biofilms *in vivo*. Sellmyer, *et al.*, developed a probe based on trimethoprim which is taken up by live bacteria only. In a mouse model, this probe allowed for the identification of live bacterial infections, without increased signalling in cancers and inflammation (oncogenic and proinflammatory markers) (126). These imaging techniques provide ways to detect biofilms *in situ* without the requirement to remove an infected implant from a patient. However, unless a patient was regularly going for PET scans, there is no way to monitor the formation of biofilms in real-time.

## 1.8 Electrochemical techniques

Electrochemical methods to detect bacteria in real-time have been gaining momentum in the last few years (127–130). One method which has been previously employed to monitor *P. aeruginosa* growth in real-time is square wave voltammetry (SWV) (128). SWV is an electrochemical quantification method which can be carried out using small sensors (0.5 cm), with the measurements solely based on medium dispersion (128). SWV applies a range of potential differences to the system, typically liquid such as growth media, and measures the current output. In this way, physiochemical properties of the system in the media can be determined from the analysis of the current output at a potential difference of interest (131,132). For example, the redox active metabolite, pyocyanin, has oxidation peaks at -0.560, -0.311, and 0.699 V (133), also reported at -0.25 V (128), and -0.37 (134). The intensity of the peak positively correlates to the quantity of pyocyanin present in the system (128). Other compounds are also able to be detected by SWV, for example LB growth media has an oxidation peak at 0.85 V. Hence, this study was carried out with measurements between -0.5 and 0.5 V. Previous studies identifying pyocyanin in LB media have similarly used

potential differences less than 0.6 V (128). As the potential difference applied is very small, it therefore does not affect the conditions of the system but outputs robust measurements (132). This has allowed SWV to be employed for the detection, identification, and quantification of microorganisms growing in culture. For this purpose, SWV can be measured either directly or indirectly (132). The direct measurement detects the metabolites the bacteria produce, for example pyocyanin, and these metabolites change the ionic composition of the medium, thereby changing the conductivity of the media, which is measured at the working electrode at a specific potential difference (128,132). Furthermore, SWV measurements can also be carried out indirectly, with the electrodes instead placed into an alkaline solution, and the gases released from bacterial metabolism are pumped through the solution. These gases decrease the conductance in the solution, which is then measured by the electrodes (132). However, as the measurements are based on the dispersion of metabolites within the media, SWV is only able to quantify planktonic growth in real-time, and not biofilm formation.

However, another electrochemical method which has been previously employed to monitor biofilms in real-time is electrochemical impedance spectroscopy (EIS) (89,127–130). Like SWV, EIS is also non-destructive (89), however instead measures the biofilm build up directly on the surface of the sensor (129). For EIS, measurements are based on the electrical impedance on the surface of an electrode. Electrical impedance is a form of resistance to a circuit which depends on the operating frequency of that circuit, and EIS can be used to measure this impedance. EIS measures across a wide range of frequencies, typically around 0.1 Hz – 100 kHz (130). This can be used to define the optimum frequency parameters, which has profound applications for point of care devices (129,130). EIS, along with other voltametric measurements, uses a sensor made up of three different electrodes: working, reference and counter. As in SWV, the working electrode is where the reaction happens in the system, and it measures the current output. The counter electrode sources the current required to enable the required potential at the working electrode to be maintained, and the reference electrode controls this potential at the working electrode. EIS has been used previously to detect *P. aeruginosa* and *S. aureus* biofilms, both separately and in polymicrobial biofilms (129,130,135). One study grew both strains separately over 69 hours, with peaks at 100 Hz after 24 hours observed for *P. aeruginosa* but not for *S. aureus* (135), however the authors only took a single scan every 11-24 hours, which means that any biofilm

formation earlier than 11 hours would not have been detected. Contrary to that study, *S. aureus* biofilms were detected at a higher frequency (100 kHz) in less than two hours in other work (129). For the most part, EIS data is often fit to a model circuit to extract further analytical parameters (128,129), however the raw impedance values have been demonstrated to be indicative of the biofilm on the sensor (130), providing easier access for point of care, real-time diagnostics. Lastly, there have been a couple of studies which have combined SWV and EIS to monitor bacterial growth. In one, for example, the real-time monitoring of the metabolite, pyocyanin, was correlated to the biofilm formation (128). However, the authors removed the biofilm from the wells prior to EIS measurements, and this may reduce the accuracy of the quantification.

## 1.9 Natural products

Natural products, also known as secondary metabolites or specialised metabolites, are produced by organisms (136–138). Typically, these are not required for the growth or immediate survival of the organism (139). Natural products have been found to have many properties, including anticancer (140–142), antibacterial (143,144), antifungal (145), antiparasitic (146), antiviral (142,147,148), and immunomodulatory effects (140,141). However, the medical properties of natural products are not a modern-day phenomenon; natural products have been used for thousands of years, although not in the same ways seen today. The earliest record of natural product usage is 2900 BC, the Ebers Papyrus, an Ancient Egyptian pharmaceutical record documenting more than 700 natural products and their producing organisms (149). Although historically plants were used directly for medicinal purposes, many have since been shown to produce natural products of medical interest, such as *Cannabis sativa* (cannabinoids) (106), *Cinnamomum camphora* (cinnamon oil) (150), and *Cuminum cyminum* (cumin) (151). As well, another natural product which has been used for the treatment of inflammation for more than 400 years, is the plant genus *Arnica* (152). However, despite its long usage, one of the natural products from *Arnica montana* was only identified in 1992 (153). As seen here, natural products have been extracted from a variety of plants, fungi, algae, and bacteria. For example, the antimicrobial properties of herb extracts have shown antibacterial efficacy against *S. aureus* and *P. aeruginosa* (154), as well as brown algal extract showed antibacterial efficacy against these two pathogens, as well as

activity against lung carcinomas (155). Although many of these early discoveries involved plants, most of the successful clinical drugs still in use today are of microbial origin (137,138,156,157).

## 1.10 Microbial specialised metabolites

### 1.10.1 Actinobacteria

One of the most important sources of natural products is the bacterial phylum, Actinomycetota, which is one of the largest and most diverse phyla within the Bacteria domain, comprising of over 150 genera (158) including *Streptomyces* (159), *Mycobacterium* (159), *Corynebacterium* (159), and *Rhodococcus* (158). Actinomycetota are distributed across many ecosystems, and are particularly abundant in soil and marine sediments (136,142,158,160,161). Due to the size of the phylum, Actinomycetota exhibit a diverse range of morphologies, such as bacillary or coccoid forms (158), with some genera, such as *Mycobacterium* falling into the category of Gram-indeterminate (162), where they are categorised as neither Gram-positive or Gram-negative. Furthermore, many Actinomycetota are able to form mycelium and spores in a range of colours (158). For example, *Streptomyces coelicolor* produces both aerial hyphae and spores, alongside actinorhodin, a blue-pigmented polyketide (141). Regarding their clinical interest, members of the Actinomycetota phylum produce up to 90% of all antibiotics, including synthetic derivatives (163–165), and of particular interest is the genus *Streptomyces*.

### 1.10.2 *Streptomyces* secondary metabolism

The genus *Streptomyces* is an important source of metabolites; between 1945 and 1978, during the 'Golden Age' of antibiotic discovery (138), 55% of all antibiotics isolated were from this genus (159). In fact, the first three antibiotics were all isolated from strains of *Streptomyces*; actinomycin, streptothricin, streptomycin, from *Streptomyces antibioticus* (166), *Streptomyces lavendulae* (167), and *Streptomyces griseus* (168), respectively. These metabolites isolated from *Streptomyces* can be divided into those from primary metabolism and those from specialised metabolism. Primary metabolites are essential for the survival of the bacteria, such as those involved in nutrient acquisition (169). Specialised metabolites,

also known as secondary metabolites, are non-essential molecules. Specialised metabolites confer an adaptational advantage (170), for example *Pseudonocardia* spp. exist in symbiosis with leaf-cutter ants, and produce an antifungal to protect their host (171), allowing them a fitness advantage (142,170). As well as this, a specialised metabolite isolated from *Streptomyces peucetius* showed activity against *E. coli* bacteriophages nearly 60 years ago (148). These metabolites can be extracted and then isolated, with the resulting compounds active against bacteria (172), fungi (172), cancers (142,172), viruses (142,148,172), and more (172). Despite this success, there has been a decline of research into these bacteria and their secondary metabolites, due to the issues of rediscovery, slow isolation methods, and low commercial profitability (157). It is these specialised metabolites which are of key clinical interest in the search for novel antibiotic and antibiofilm agents.

### 1.10.3 Antibiotic Discovery

The systematic screening of compounds against a particular pathogen was highly successful in the isolation of specialised metabolites from *Streptomyces* spp. during the “Golden Age” of antibiotic discovery, as highlighted previously. However, this method was also used prior to the isolation of the first *Streptomyces*-derived antibiotic, actinomycin (166). Instead, the methodology dates all the way back to the discovery of the very first antimicrobial therapeutic agent, Salvarsan, in 1910 (173). Salvarsan was used to treat syphilis, caused by *Treponema pallidum*. However, the screening process used *T. pallidum*-infected rabbits which were then injected with the agent (174) as a method to find novel antimicrobial compounds. Observing pathogen inhibition by a potential antimicrobial compound using zones of inhibition on pathogen-inoculated agar was not popularised until Fleming’s work on penicillin nearly 20 years later (27). Current methods for isolation of antibiotics still include the isolation of potentially novel strains from sediments (146,175–178), alongside the one strain many compounds (OSMAC) approach, in which one strain is grown on a range of media due to Actinomycetota altering their metabolism based on the nutrients available (179). This was shown previously by Soldatou, *et al.*, in which they cultured 25 strains on four different media each. They found that the specialised metabolites from one strain grown on tryptic soy agar was active against all six pathogens tested, however when the

strain was grown on the other three agar types, there was no inhibition against any of the pathogens (180).

## 1.11 Metabolomics

### 1.11.1 Mass spectrometry

Mass spectrometry was first used more than 120 years ago to search for the existence of electrons, then was slowly developed throughout the early 1900s to be able to measure the mass-to-charge ratio of ionized atoms, and later, of isotopes. This finding devastatingly allowed mass spectrometry to be used in the separation of uranium isotopes for use in the first atomic bombs (181).

In 1956, gas chromatography was coupled to mass spectrometry (GC-MS), which revolutionised mass spectrometry by allowing the separation of ions prior to analysis (182). GC-MS can be used to separate biological compounds, however, only those which are thermally stable (183). Following the coupling of GC-MS, liquid chromatography mass spectrometry (LC-MS) was introduced. LC-MS is also used for separating biological molecules, however this method can also separate non-thermally stable molecules (184). LC-MS has since become somewhat of a gold-standard for high-throughput mass spectral analyses (143,185). Alongside nuclear magnetic resonance (NMR), a technique which provides structural information (183), these three technologies present themselves as the best options for performing microbial mass spectrometry analyses. LC-MS collects signals from the microbially-sourced metabolites, their fragments and isotopes, as well a degree of instrument noise (186). Typically, MS techniques use electrospray ionisation (ESI) as the ionization method of choice (143,187,188), as it is a soft ionisation method, which causes little fragmentation (183). In positive ionisation mode, this results in the peaks of a certain  $m/z$  in a spectrum representing the protonated form of the metabolite ( $[M+H]^+$ ), allowing simpler downstream spectrum interpretation and metabolite identification (189). The combination of LC-MS and ESI has proved fruitful (143), however, this single quadrupole detection method is often overlooked in favour of other soft ionization methods, such as matrix-assisted laser desorption ionization (MALDI). This is currently the most commonly used ionisation source for proteomics research, despite only giving qualitative data (183).

In the last 15 years, triple quadrupole, referred to as ‘tandem’ MS has gained popularity over LC-MS, as LC-MS/MS has increased specificity and sensitivity (184). Furthermore, LC-MS/MS has been used to characterise specialized metabolites from Actinomycetota. For example, the presence of known antibiotic, chloramphenicol, was anticipated from sequence data of a *Rhodococcus* sp. and was confirmed using LC-MS/MS (180). Further, three metabolites extracted from Actinomycetota isolated from the rhizosphere of olive and rosemary plants were identified by LC-MS/MS, and shown to have anti-fungal activity against plant pathogen, *Penicillium expansum*, as well as growth-promoting activity towards *Ocimum basilicum* (basil) (190).

As well as LC-MS/MS use in identifying microbial produced metabolites, MS technologies have also been developed to be able directly identify microbial organisms. For example, MALDI time of flight mass spectrometry (MALDI-ToF) has been employed in the dereplication process of specialised metabolite discovery, providing spectra used to identify identical strains within the screen, as well as previously discovered strains (191). Finally, imaging mass spectrometry has also been employed for strains growing in co-culture, such as *Pseudomonas* sp. and *Bacillus* sp.. This method allows detection, identification, and localisation of the bioactive metabolites (192).

### 1.11.2 Comparative metabolomics and dereplication

One of the main bottlenecks in the discovery of novel microbial specialised metabolites is the rediscovery of known metabolites, which fed into the relative collapse of the Waksman discovery pipeline by the 1960s (2). As alluded to previously, it is therefore important to develop reliable methods for distinguishing between known and unknown metabolites, in a process is known as dereplication (193). Dereplication seeks to identify and subsequently remove previously discovered natural products from datasets, and is highly necessary to combat rediscovery of known specialised metabolites (165). The creation of the Global natural products social molecular networking (GNPS) brought all natural product databases together (193). GNPS is the largest public natural product database of MS/MS spectra and exists as an open-access knowledge database of raw or processed LC-MS/MS data (193). However, it cannot be used to analyse valuable single quadrupole MS data, and there is currently no platform which integrates single and tandem mass spectral data libraries.

Ultimately, the success of databases, such as GNPS, relies on the community sharing of data as publicly available natural product databases. As of 2020, it is estimated that the GNPS libraries contain only 2.5% of known natural products (194).

One of the methods used for the visualization of the chemical space present in MS is molecular networking, which facilitates the detection of groups of spectra from related metabolites. Networks of related metabolites appear as clusters which represent molecular families of metabolites; this is based on their structural similarity. This information is provided by the molecules' MS/MS fragmentation pattern and retention time (193,195). Molecules which cannot be identified by a mass spectral library, such as GNPS, can then be prioritized for further chemical analysis (193). The use of molecular networking MS/MS data has been utilized previously in the search for novel chemistry. For example, two potentially novel antimicrobial agents were identified as the already known prodigiosin and cycloprodigiosin, following GNPS analysis and molecular networking (196). Counter to this however, is the screening of polar Actinomycetota extracts, which found 1652 parent ions with no matches to the GNPS database, indicating novel chemistry within their extract collection (197).

### 1.12 Aims and objectives

Biofilm research and quantification has been focussed around the use of crystal violet staining as a method to quantify biofilms. This chapter has evidenced that CV and the other commercially available quantification techniques have not developed in the last 40 years since their conception. Furthermore, the characterisation of biofilms comes decades after the identification of antimicrobial resistance, despite biofilm formation being a key antimicrobial resistance strategy used by pathogens. Therefore, identification of biofilms, and isolation of novel antibiofilm agents are of utmost importance in the fight against antimicrobial resistance. This thesis aims to bring together these point of care technologies and antibiofilm drug discovery to combat biofilm formation on implantable materials. This was achieved through the following objectives and aims:

### **Objective 1: Electrochemical quantification of biofilms**

A model system for monitoring the growth and inhibition of biofilm formation, using clinically relevant pathogen, *P. aeruginosa*, was developed for electrochemical impedance spectroscopy (EIS), and validated using crystal violet (CV)

Aim 1: To optimise *P. aeruginosa* biofilm growth in 96-well plates (required for downstream EIS measurements)

Aim 2: To quantify PA14 and LESB58 biofilms using CV

Aim 3: To quantify PA14 and LESB58 biofilms using EIS

Aim 4: To compare CV and electrochemical data for biofilm quantification

### **Objective 2: Isolation of antibacterial and antibiofilm Actinomycetota**

Actinomycetota strains were isolated from four locations, and their crude metabolite extracts were assayed for their antibiotic and antibiofilm activity, using both traditional methods and developed EIS quantification

Aim 1: To isolate marine actinomycetes, test their antibacterial activity, and taxonomically and phylogenetically identify them using 16S rRNA gene sequencing

Aim 2: To culture these strains and extract their bacterial metabolites, and assess the antibiofilm activity using CV and EIS methodologies

Aim 3: To fractionate these bacterial crude extracts and assess their antibiofilm activity using CV and EIS methodologies

### **Objective 3: Biofilm formation and reduction on clinically-relevant material**

*P. aeruginosa* biofilms (PA14 and LESB58) were formed on Dacron graft material and quantified in real-time using EIS, both in the presence and absence of the crude metabolite extract and fractions

Aim 1: To establish a method for biofilm formation on medically relevant materials

Aim 2: To quantify biofilms in real-time on medically relevant materials using both CV and EIS

Aim 3: To assay with EIS the fractionated metabolite extracts against these clinically relevant biofilms, formed using the established method for biofilm formation

## 2.0 Materials and methodology

### 2.1 Bacterial growth and maintenance

*Escherichia coli*, *Pseudomonas aeruginosa* (PA14 & LESB58) and *Staphylococcus aureus* were cultured from glycerol stocks and streaked onto LB agar and incubated (37 °C, 18 hours, static) (Tables 2.1 and 2.2). Following growth, LB broth (5 mL) was inoculated with a single colony and incubated (37 °C, 18 hours, 250 rpm). For bioactivity and biofilm assays, pathogens were diluted to an OD<sub>600</sub> of 1, unless stated otherwise.

**Table 2.1: List of pathogens and insertion mutants (Is) used.**

Strain	Genotype	Reference
<i>Escherichia coli</i> ATCC 25922	WT	American Type Culture Collection (ATCC)
<i>Staphylococcus aureus</i> ATCC 43300	WT	ATCC
<i>Pseudomonas aeruginosa</i> (PA14)	WT	PA14 (198)
<i>P. aeruginosa</i> (LESB58)	WT	LESB58 (76)
<i>P. aeruginosa</i> (PA14)	<i>IsrhII</i>	Liberati, <i>et al.</i> , 2006 (199)
<i>P. aeruginosa</i> (PA14)	<i>IsrhIR</i>	Liberati, <i>et al.</i> , 2006 (199)
<i>P. aeruginosa</i> (PA14)	<i>IspqsA</i>	Liberati, <i>et al.</i> , 2006 (199)
<i>P. aeruginosa</i> (PA14)	<i>IsphzM</i>	Liberati, <i>et al.</i> , 2006 (199)
<i>P. aeruginosa</i> (PA14)	<i>Islasl</i>	Liberati, <i>et al.</i> , 2006 (199)

## 2.2 Sediment collection and bacterial isolation

Sediment samples were collected from four locations; Apple Cross Beach, Cape Wrath, Duck Bay and Loch Lomond shores (**Table 2.3**) and incubated (50 °C, 1 hour) to kill non-spore forming bacteria and fungi. To selectively target the isolation of spore forming Actinomycetales, a dry stamping pre-treatment was carried out (200). Briefly, the sediment was stamped clockwise over six sections of both international *Streptomyces* project medium 2 and 7 (ISP2 and ISP7) (**Table 2.2**) with the following antibiotics added: 10 µg/mL nalidixic acid, 25 µg/mL cycloheximide, 25 µg/mL nystatin. The stamping was carried out using a sterile foam bung (30 mm) to create a serial dilution effect, with three Petri dishes for each sediment sample. Following incubation (7 days, 30 °C), colonies with actinomycete-like growth, characterised as matte or powdery colonies and hyphae growth, were morphologically identified and sub-cultured until pure. For dereplication and simplification of the screening assays, if two or more strains isolated from the same location had similar morphologies on the same agar, only one was taken. Once pure cultures were obtained, glycerol stocks (20% glycerol) of the bacterial isolates were made from single colonies and stored at -80 °C (**Table 2.4**). This methodology was also followed in the isolation of the Arctic and Antarctic strains (**Table 2.4**) (180).

**Table 2.2: List of culture media recipes used.**

Media	Components (per 1 litre)	pH	Reference
<b>Lysogeny broth (LB)</b>	10 g tryptone, 5 g NaCl, 5 g yeast extract	7.4	Bertani, 1951 (201)
<b>LB agar</b>	10 g tryptone, 5 g NaCl, 5 g yeast extract, 15 g agar	7.4	Bertani, 1951 (201)
<b>International <i>Streptomyces</i> Project (ISP) 2 medium</b>	10 g malt extract, 4 g yeast extract, 4 g dextrose	7.2	Shirling & Gottlieb, 1966 (202)
<b>ISP2 agar</b>	10 g malt extract, 4 g yeast extract, 4 g dextrose, 15 g agar	7.2	Shirling & Gottlieb, 1966 (202)
<b>ISP7 medium</b>	15 g glycerol, 0.5 g L-tyrosine, 1 g L-asparagine, 0.5 g K <sub>2</sub> HPO <sub>4</sub> , 0.5 g MgSO <sub>4</sub> ·7H <sub>2</sub> O, 0.5 g NaCl, 0.01 g FeSO <sub>4</sub> ·7H <sub>2</sub> O	7.2	Shirling & Gottlieb, 1966 (202)
<b>ISP7 agar</b>	15 g glycerol, 0.5 g L-tyrosine, 1 g L-asparagine, 0.5 g K <sub>2</sub> HPO <sub>4</sub> , 0.5 g MgSO <sub>4</sub> ·7H <sub>2</sub> O, 0.5 g NaCl, 0.01 g FeSO <sub>4</sub> ·7H <sub>2</sub> O, 15 g Agar	7.2	Shirling & Gottlieb, 1966 (202)
<b>Difco nutrient agar (NA)</b>	4 g Difco nutrient broth powder, 15 g agar	7.4	Difco
<b>Soft nutrient agar (SNA)</b>	4 g Difco nutrient broth powder, 7.5 g agar	7.4	Difco

**Table 2.3: List of bacterial isolation locations and corresponding co-ordinates.**

<b>Location ID</b>	<b>Geographic co-ordinate</b>
<b>Apple Cross Beach</b>	57.434167, -5.814167
<b>Cape Wrath</b>	58.553056, -4.789444
<b>Duck Bay</b>	56.016800, -4.611399
<b>Loch Lomond</b>	56.006056, -4.589719

**Table 2.4: Full list of environmental isolated strains used.**

<b>Strain</b>	<b>Growth medium</b>	<b>Isolation ID</b>
<b>LR1</b>	ISP2	Loch Lomond
<b>LR2</b>	ISP2	Apple Cross Beach
<b>LR3</b>	ISP2	Apple Cross Beach
<b>LR4</b>	ISP2	Apple Cross Beach
<b>LR5</b>	ISP2	Duck Bay
<b>LR6</b>	ISP2	Apple Cross Beach
<b>LR7</b>	ISP2	Apple Cross Beach
<b>LR8</b>	ISP2	Apple Cross Beach
<b>LR9</b>	ISP2	Apple Cross Beach
<b>LR10</b>	ISP2	Apple Cross Beach
<b>LR11</b>	ISP2	Loch Lomond
<b>LR12</b>	ISP2	Loch Lomond
<b>LR13</b>	ISP2	Duck Bay

<b>LR14</b>	ISP2	Apple Cross Beach
<b>LR15</b>	ISP2	Cape Wrath
<b>LR16</b>	ISP7	Cape Wrath
<b>KRD026</b>	ISP2	Antarctic (180)
<b>KRD070</b>	ISP2	Arctic (180)
<b>KRD077</b>	ISP2	Arctic (180)
<b>KRD096</b>	ISP2	Arctic (180)
<b>KRD168</b>	ISP2	Antarctic (180)
<b>KRD175</b>	ISP2	Arctic (180)
<b>KRD185</b>	ISP2	Antarctic (180)
<b>KRD188</b>	ISP2	Antarctic (180)
<b>KRD140</b>	ISP2	Antarctic (180)
<b>KRD153</b>	ISP2	Arctic (180)
<b>KRD182</b>	ISP2	Antarctic (180)

### 2.3 DNA extraction, polymerase chain reaction and phylogeny of environmental isolates

DNA was extracted from a single colony of each environmental bacterial strain using a method previously reported (203). Briefly, a single colony was added to 25  $\mu\text{L}$  nuclease-free  $\text{H}_2\text{O}$ , vortexed and incubated at  $-80\text{ }^\circ\text{C}$  (10 minutes), and then immediately incubated at  $95\text{ }^\circ\text{C}$  (10 minutes). These were then vortexed again and kept on ice until needed.

Polymerase chain reaction (PCR) of the 16S rRNA gene was carried out in 25  $\mu\text{L}$  reactions using the following: 5  $\mu\text{L}$  5x OneTaq<sup>TM</sup>, 0.5  $\mu\text{L}$  10 mM dNTPs, 0.125  $\mu\text{L}$  OneTaq<sup>TM</sup> polymerase, 2.5  $\mu\text{L}$  each of the following primers; forward (5'- AGA GTT TGG ATC MTG GCT CAG -3') and reverse (5'- CGG TTA CCT TGT TAC GAC TT -3') 16S primers (27F and 1492R, respectively), 1  $\mu\text{L}$  extracted DNA, and 17.375  $\mu\text{L}$  nuclease free water. The PCR was performed in the Applied Biosystems Veriti 96-well thermal cycler, to the following protocol:

Stage	Temperature ( $^\circ\text{C}$ )	Time (seconds)
<b>Initial denaturation</b>	95	2 minutes
<b>Denaturation</b>	95	45 seconds
<b>Extension</b>	55	30 seconds
<b>Annealing</b>	72	90 seconds
<b>Final extension</b>	72	5 minutes
<b>Hold</b>	4	$\infty$

} 35 cycles

Gel electrophoresis of the PCR amplicons (5  $\mu\text{L}$ ) were carried out using 1% agarose and ethidium bromide gel, and run for 60 minutes at 90 V with a Promega 1kb DNA ladder (4  $\mu\text{L}$ ) and Promega Blue/Orange 6X loading dye (1  $\mu\text{L}$ ). The gel was visualised under UV and the presence of bands at 1500 bp on the ladder was confirmed. The PCR products were then cleaned up as per the BiLine PCR clean-up kit protocol and sent for sequencing (Eurofins)

at a concentration of 20 ng/ $\mu$ L. FASTA sequences of 16S rRNA genes in **Supplementary table 2.1**. A nearest-neighbour maximum likelihood phylogenetic tree was constructed using the Tamura-Nei method (204) and bootstrap resampling (bootstrap value of 1000) using MEGA-X (version 10.2.0) (205). **Supplementary tables 2 – 11** show the closest related strains for each isolate which were included in the phylogenetic tree.

## 2.4 Metabolite extraction and fractionation

Bacteria were inoculated from seven-day precultures and cultured (7 days, 160 rpm, 30 °C, Erlenmeyer flasks 250 mL) with HP20 resin (2.5 g) for metabolite extraction using ISP2 broth (50 mL), except extract LR16 which was cultured using ISP7 broth (50 mL). The cultures were then centrifuged (4000 rpm, 20 minutes), and the supernatants removed (leaving a cell pellet and resin). The cell-resin pellets were then frozen (-80 °C, overnight), lyophilised (12 hours, LABCONCO Freezone 2.5 drier) and extracted (250 mL Erlenmeyer flasks, 10 mL ethyl acetate (Fisher Scientific, HPLC-grade), 120 rpm, 2 hours, Start SSL1 orbital shaker). The extract was then filtered through chromatography paper (10 cm diameter) (Whatman brand 3 mm), dried under Nitrogen and the extract weight recorded (mg) (180).

Crude metabolite extracts were fractionated using solid phase extraction (SPE), with a C18 200 mg column (Thermo Scientific). The extract was first dissolved in methanol:water (MeOH:H<sub>2</sub>O) (Fisher Scientific, HPLC-grade) (80:20 v/v, 2 mL) and then eluted using 10 mL in sequence of the following solvent(s) (all Fisher Scientific, HPLC-grade): methanol: water (MeOH:H<sub>2</sub>O) (80:20 v/v); methanol (MeOH); acetonitrile (ACN); ethyl acetate (EtOAc). Each fraction was dried under Nitrogen and the weight recorded (mg). Antibiofilm testing used fractions dissolved in dimethyl sulfoxide (DMSO) (Fisher Scientific, HPLC-grade) (1% in dH<sub>2</sub>O) and bioactivity disk assays used fractions dissolved in EtOAc; both to a final concentration of 1 mg/mL.

## 2.5 Antibacterial bioactivity assays (plug and disk)

Overnight cultures (OD<sub>600</sub> calculated) of *P. aeruginosa* (PA14), *E. coli*, and *S. aureus* (5 mL), were used to inoculate molten soft nutrient agar (SNA) (< 50 °C) (15 mL) at an OD<sub>600</sub> of 0.01. This was then poured as a top layer onto nutrient agar (NA) plates (25 mL) in Petri dishes to

create a pathogen lawn. Once solidified, a plug was taken from a seven-day bacterial culture plates using the large end of 1 mL pipette tip. This was carefully placed on top of the pathogen lawn and the position noted. Alongside the isolated strains, positive antibiotic controls of chloramphenicol (20 µL, 2.5 µg/mL *E. coli* and *S. aureus*) or gentamicin (5 µL, 15 µg/mL, *P. aeruginosa*) were used and a sterile agar plug was used as a negative control. The Petri dishes were then incubated for 18 hours at 37 °C, and the radii measured. Each pathogen and plug combination were repeated in triplicate.

The disk assays were set as above, however instead of an agar bacterial culture plug, metabolite extracts were added to sterile filter disks (5 mm diameter, Whatman brand 3 mm chromatography paper) (20 µL) and dried before being transferred to the Petri dish with the SNA pathogen lawn.

## 2.6 Mass spectrometry of bacterial metabolite extracts

Crude metabolite extracts from liquid extraction and corresponding media controls were prepared at 1 mg/mL in acetonitrile and C18 untargeted metabolomics analysis was performed with the Exploris 240 instrument. Extracts were analysed by high-performance liquid chromatography-electrospray ionization quadrupole orbitrap mass spectrometry (HPLC-ESI-HRMS) using a Thermo Vanquish binary LC system coupled to a Thermo Exploris 240 orbitrap mass spectrometer. 5 µL of each extract was injected (15 µL) onto an Accucore C18 HPLC Column (2.6 µm, 100 mm × 2.1 mm I.D. (Thermo)). Mobile phase A consisted of 0.1% formic acid in water (v/v). Mobile phase B consisted of 0.1% formic acid in acetonitrile (v/v). Each sample was subsequently run on the following solvent gradient:

Retention (min)	Flow (mL/min)	%a	%b	Curve
0	0.3	99	1	5
0.5	0.3	99	1	5
2	0.3	50	50	5
10.5	0.3	1	99	8

11	0.3	1	99	5
11.5	0.3	99	1	7
14.9	0.3	99	1	5
15	0.3	99	1	5

Mass spectrometry analysis was performed under the following conditions: ESI source conditions were set as follows: ion spray voltage (pos 3700 V) sheath gas 40, aux gas 10, sweep gas 1, ion transfer tube temperature 300 °C, vaporizer temperature 280°C. The instrument was set to acquire over the  $m/z$  scan range of 70–1050, at 60k resolution and with and RF lens of 70%.

Other full scan filters included: exclusion override factor = 3, exclusion list peak window extension = 3, inclusion list peak fragmentation threshold = 80, preferred ions = [M+H]<sup>+</sup>+1; [M-H]<sup>-</sup>-1; [M+Na]<sup>+</sup>+1, exclusion duration = 10. MS/MS settings were as follows: resolution = 60k, FR Lens(%) = 65, EASY-IC = on, Intensity Filter = 5x10<sup>3</sup>, Precursor Fit Filter = Fit Threshold (%) 51 and Fit Window ( $m/z$ ) 0.7, Charge State = 1-2 (including undetermined charge states), Custom Dynamic Exclusion = exclude after n times = 1; exclusion duration = 3s; mass tolerance = ppm, low = 2; high = 2; exclude isotope = on, no target or exclusion masses used, desired apex window (%) = 50. ddMS2 was set at 5 scans, isolation window = 0.7, collision energy = normalized, resolution = 30k, scan range mode = auto.

## 2.7 Processing of mass spectrometry data

All mass spectrometry data was processed using the MZmine freeware (version 2.53) (<http://mzmine.sourceforge.net/> - accessed on February 24th 2023), which was employed for the data processing, peak detection, deconvolution, deisotoping, filtering, alignment and gap-filling to allow comparison of data files. Mass detection was undertaken via a centroid mass detector set at 1.00E3 for MS level 1 and 1.00E1 for MS level 2. Mass to charge ( $m/z$ ) tolerance was set at 0.01, with peaks detected above a threshold of 3.00E3. Minimum time span was set to 0.1. tR tolerance was set to 0.1. MS/MS data was converted from raw to

mzML format using FileZilla v3.52.2 (<https://filezillaproject.org/> - accessed on February 24<sup>th</sup> 2023) with the converted data uploaded to the GNPS server (193).

## 2.8 Molecular networking of mass spectrometry data

A classic molecular network was created using the online workflow (METABOLOMICS-SNETS-V2) on the GNPS website (<http://gnps.ucsd.edu> - accessed on February 24<sup>th</sup> 2023). The data was filtered by removing all MS/MS fragment ions within +/- 17 Da of the precursor  $m/z$ . MS/MS spectra were window filtered by choosing only the top 6 fragment ions in the +/- 50 Da window throughout the spectrum. The precursor ion mass tolerance was set to 2 Da and a MS/MS fragment ion tolerance of 0.5 Da. A network was then created where edges were filtered to have a cosine score above 0.7 and more than 3 matched peaks. Further, edges between two nodes were kept in the network only if each of the nodes appeared in each other's respective top 10 most similar nodes. Finally, the maximum size of a molecular family was set to 100, and the lowest scoring edges were removed from molecular families until the molecular family size was below this threshold. The spectra in the network were then searched against GNPS' spectral libraries. Cytoscape (version 3.9.1) (206) was used to visualise and annotate the molecular network, with each node corresponding to a consensus spectrum and each edge conforming to a modified cosine similarity score between pairs of nodes.

## 2.9 Initial biofilm formation and quantification (cuvettes)

For the initial biofilm quantification, overnight cultures of *P. aeruginosa* (PA14) were diluted to an OD<sub>600</sub> of 1 and seeded into a 6-well plate (1 mL, carried out in triplicate) (Corning™), and incubated (4 hours, 37 °C, static). Following this, the biofilm was dislodged by pipetting the media up and down, and transferred to a 1 mL cuvette. This was then read on a spectrophotometer at 600 nm. Following this, the protocol was carried out as before, however after the four-hour incubation, the wells were washed with phosphate-buffered saline (PBS) (Sigma). This was achieved by removing the media without dislodging the biofilm, adding 1 mL of PBS to the wells, and removed gently. A further 1 mL was added, and the biofilm was dislodged and read on the spectrophotometer as before.

## 2.10 Biofilm formation and quantification (96-well plates)

Both PA14 and LESB58 were diluted to an  $OD_{600}$  of 1 from overnight cultures, added (100  $\mu$ L) to a clear-walled, clear-bottomed 96-well plate (carried out in triplicate) (Thermo Scientific™) and incubated (37 °C, static) for 4 hours to allow for biofilm formation with minimal media evaporation. Post-incubation, absorbance was measured at 600 nm then the medium removed, and the wells washed with 100  $\mu$ L dH<sub>2</sub>O. After air-drying (15 minutes, room temperature (RT)), the wells were stained with 0.1% crystal violet (CV) in dH<sub>2</sub>O (w/v) for 15 minutes at RT, after which the CV was removed, and two further washes with PBS were carried out, and the plates air dried (15 minutes, RT). To quantify the CV-stained biofilms, 200  $\mu$ L ethanol (Fisher Scientific, HPLC-grade) (95%, in dH<sub>2</sub>O v/v) was added to each well to solubilise the CV and the absorbance read (570 nm). The biofilm formation was normalised against media only and *P. aeruginosa* only controls.

## 2.11 Electrochemical biofilm quantification methods

In order to carry out electrochemical measurements, 96-well plates with three-point carbon sensors in the base (PalmSens™) were used for all electrochemical measurements. These were fitted with a circuit board underneath and could be placed directly onto a specialised plate reader (DropSens Connector 96X) to input and measure electrical signals (**Figure 2.1**). To achieve this, desired measurements were set up as scripts on PStace software (version 5.9) run on a laptop (Lenovo IdeaPad 320S). A potentiostat (PalmSens4 version 1.7) and multiplexer (PalmSens MUX8-R2) were connected in sequence from the laptop to the plate reader, which enabled desired measurements to be carried out in specific wells (selected on the plate reader) in sequence, as each well forms its own circuit (**Figure 2.1B**). The plate reader was able to operate within the incubator (Panasonic MIR-154-PE) (**Figure 2.2**). As described previously, biofilms were formed in a 96-well plate at a seeding density of  $OD_{600}$  of 1. Measurements from each well were taken every 30 minutes for four hours.

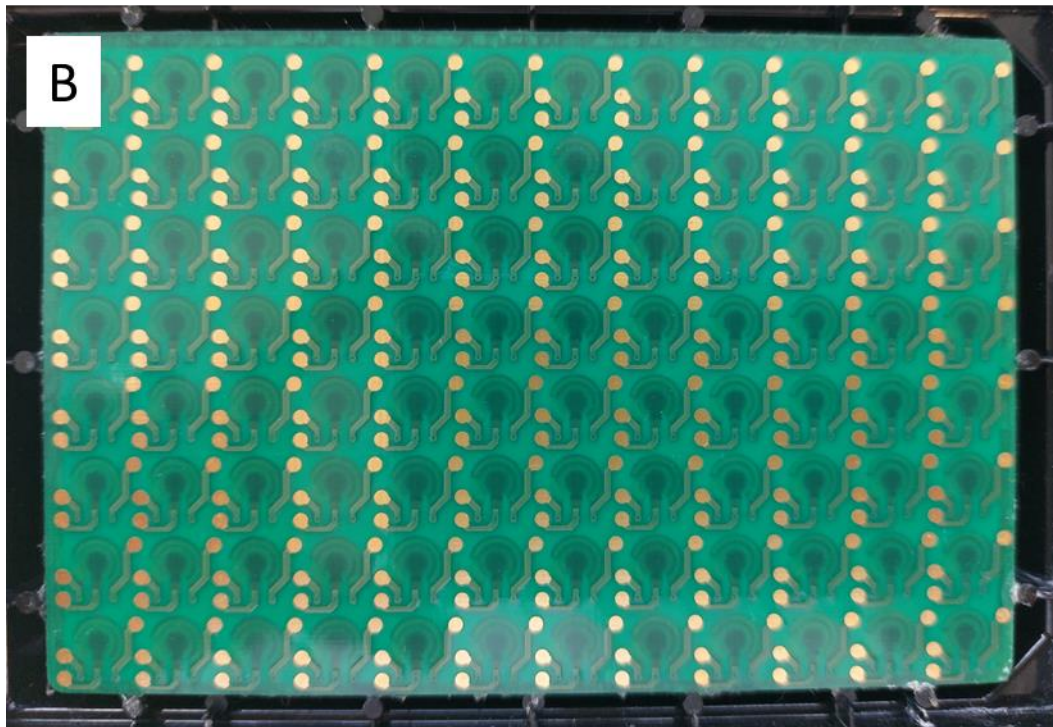
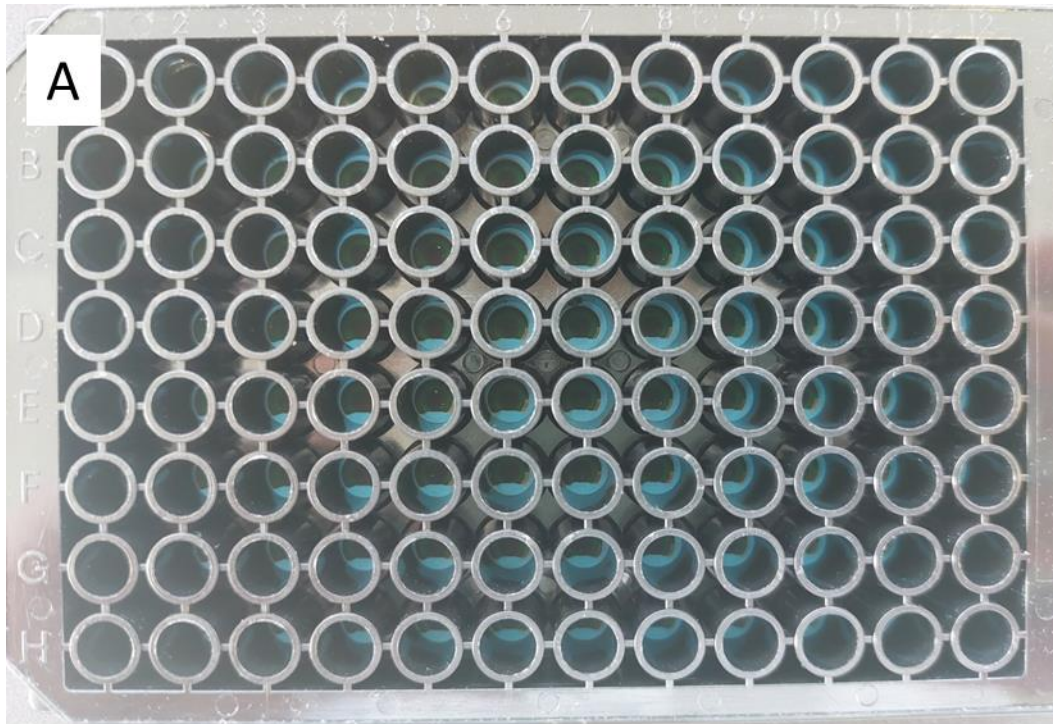


**Figure 2.1: Front and back of a PalmSens 96-well plate with sensors in the bottom. A) Top view: looking down into the wells, the three-point carbon sensors can be seen surrounded in blue. B) Bottom view: circuit board and gold contact points for each well.**

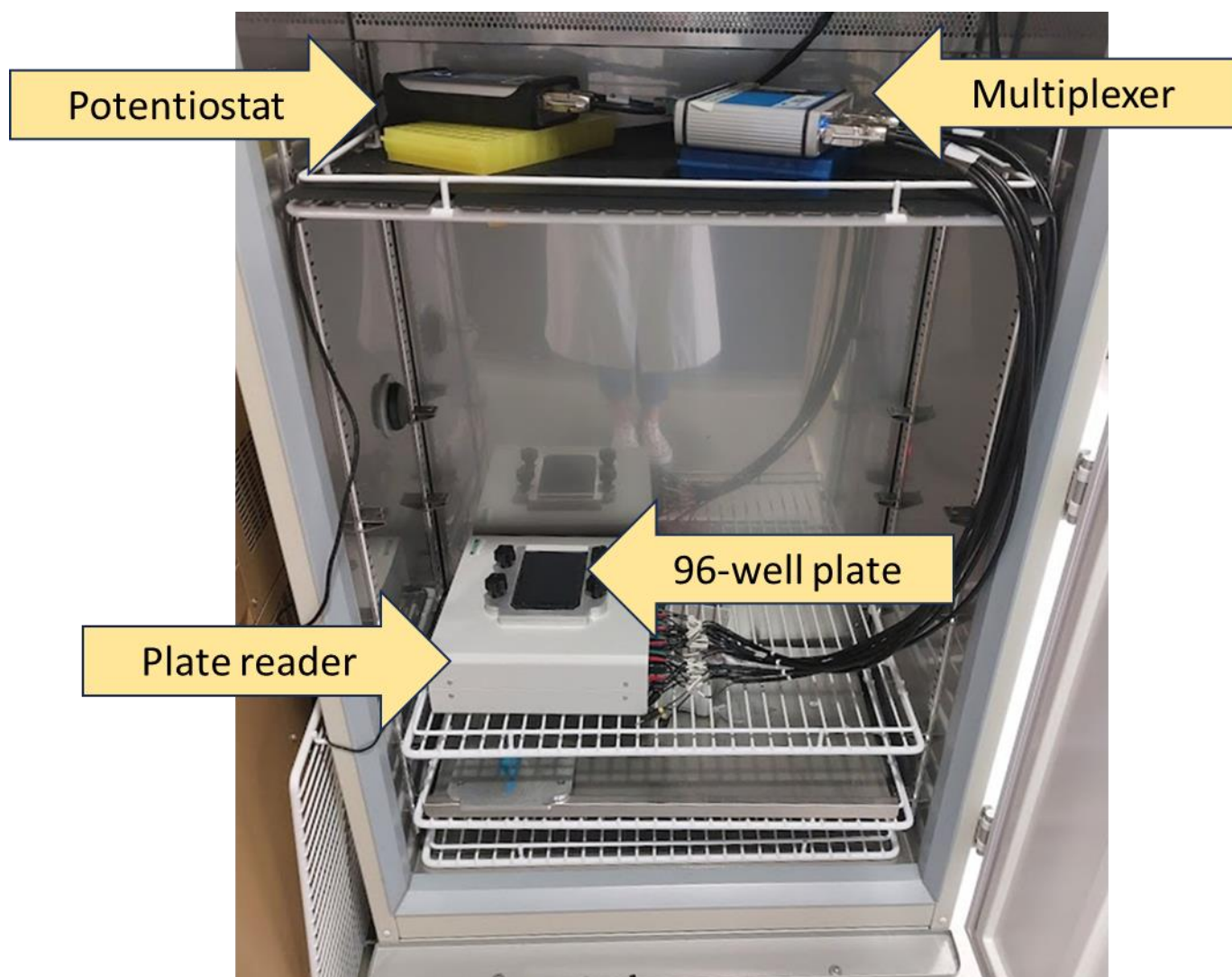


**Figure 2.2: Photograph of equipment set up for electrochemical measurements.** Photo taken inside the incubator with a laptop on bench behind the incubator (not seen). The laptop connects directly to the potentiostat, which is connected to the multiplexer on the top shelf. The multiplexer is then connected to the plate reader via 32 inputs. The multiwell plate sits on top of the plate reader; when in use, this is covered with a breathable membrane to maintain sterility. The multiplexer and potentiostat were on blocks to keep them at the same height to reduce strain on the wires.



Square wave voltammetry (SWV) measurements were carried out with a 5 A current, 3 mV step potential, and 15 Hz frequency. A range of potential differences (-0.5 – 0.5 V) was applied to the wells, and the current output ( $\mu\text{A}$ ) measured. This gave a peak intensity for metabolites within the media, if they are excited at a potential difference within the range. Peak height positively correlates to the quantity of the metabolite present in the media, thus allowing for quantification. The current at -0.35 V was recorded and used as the planktonic growth measurement. The data was normalised by dividing the respective well by the corresponding  $t=0$  value. In this way, the variations in background noise associated with each sensor were minimised (130).

For electrochemical impedance spectroscopy (EIS) measurements, 0.1 – 10,000 Hz frequencies were scanned at 0.01 V AC potential (11 frequencies per decades at 67 frequencies) and the EIS spectra measured against the open circuit potential. This output of raw impedance modulus ( $\Omega$ ) values was then analysed for trends; both over time at the same frequency, and at a range of frequencies at the same time point. An increase in biofilm formation on the sensor correlated with a decrease in the impedance modulus at a frequency of 10 Hz. Higher frequencies contained a large amount of noise. The data was again normalised by dividing the respective well by the corresponding  $t=0$  value to minimise the variations in background noise associated with each sensor (130).

## 2.12 Pyocyanin concentration curve

A standard curve was required to identify SWV peak(s) of interest for pyocyanin, therefore pyocyanin (Sigma Aldrich™) was dissolved in ethanol (100%) to a concentration of 1 mM. This stock was then diluted in  $\text{dH}_2\text{O}$  to 100  $\mu\text{M}$ , and then serially diluted seven-fold in  $\text{dH}_2\text{O}$  to 0.781  $\mu\text{M}$ . These dilutions were then measured using the same SWV protocol described above; with potential differences between -0.5 and 0.5 V applied to the wells.

## 2.13 Screening antibiofilm agents

Stock solutions of six *P. aeruginosa* antibiofilm agents were dissolved or diluted in  $\text{dH}_2\text{O}$  to the following stock concentrations; 4 mM  $\text{ZnCl}_2$ , 0.25  $\mu\text{g}/\text{mL}$  meropenem, 2% ethanol (v/v), 0.125  $\mu\text{g}/\text{mL}$  ciprofloxacin, 0.8% L-arginine (w/w), 3.125  $\mu\text{g}/\text{mL}$  gentamicin. These were then

serial diluted 1 in 2, seven-fold. Each agent was added to a 96-well plate (50  $\mu$ L) in triplicate, and 50  $\mu$ L PA14 or LESB58 added to each well. Control wells with antibiofilm + media, *P. aeruginosa* only, and LB media only were also set up in triplicate. As the agents were dissolved in dH<sub>2</sub>O, a solvent control was not used here. The biofilm formation was quantified with CV only and normalised against media only and *P. aeruginosa* only controls.

Bacterial metabolite extracts were assayed as above at a concentration of 1 mg/mL in DMSO, alongside a DMSO only control as well. These were assayed with SWV, and EIS measurements in addition to CV quantification.

## 2.14 Biofilm formation on Dacron graft material

Laser-cut Dacron graft disks (0.4 cm diameter) were gifted by Dr. McCormick in Biomedical Engineering at the University of Strathclyde, and disks were autoclaved prior to use.

Both PA14 and LESB58 biofilms were formed on Dacron graft disks, following the biofilm forming protocol established in 96-well plates. The disks were added to the media prior to the addition of pathogens, ensuring that they were at the bottom of the plate by submerging them with a pipette tip and incubated (4 hours). Due to the opacity of the Dacron graft, this was carried out without the absorbance read at 600 nm after four hours. The staining and de-staining was carried out as previously described, however following the CV-solubilisation in ethanol, the graft disks were removed, and the absorbance measured at 570 nm. The biofilm and control Dacron graft disks were kept photographed to visually observe the background stain.

The same biofilm formation protocol was carried out for the electrochemical quantification of both PA14 and LESB58 biofilms, with the Dacron graft on top of the sensor. Controls including with and without graft material were also carried out to ensure this did not interfere with the potential differences and frequencies across the sensor. The SWV and EIS measurements were carried out as before; SWV potential differences between -0.5 and 0.5 V, and EIS frequencies between 0.1 and 10,000 Hz. As previously, these measurements were taken every 30 minutes for four hours.

## 2.15 Statistical analysis

For all data sets subject to statistical analysis, a Shapiro-Wilk test was performed initially to confirm the dataset was normally distributed. Following the normality test, statistical differences between samples was carried out. For the comparison of two samples, an independent samples t-test was performed. Where there were more than two samples, a one-way ANOVA was carried out to determine if there was significant difference within the group. Following this confirmation, both Tukey's and Dunnet's posthoc tests were carried out, which compared all groups to each other and to the control, respectively. Significance from all tests was determined as  $\leq 0.05$ , with the exception of Shapiro-Wilk, in which  $\leq 0.05$  indicates that the samples are not normally distributed. All statistical analysis was carried out using SPSS (version 28.0.0.0 (190)).

## 2.16 Data storage and availability

All data which has formed part of this thesis is available on the University of Strathclyde PURE: <https://doi.org/10.15129/c4c133fe-7eae-4307-9b6a-d8b199d39c43>, and .mzML files are available on Global Natural Products Social Molecular Networking (GNPS) under user LRiordan.

## 3.0 The optimisation and use of both crystal violet and electrochemical measurements to quantify *Pseudomonas aeruginosa* biofilms

### 3.1 Introduction

Biofilms create an obstacle for basic quantification, due to some cells entering dormancy (32), as well as cell biomass and other debris (60). There can also be challenges with interpreting quantification results, due to the biofilm architecture and micro-colony structure (68,74). Due to this, there are no standardised methods for biofilm quantification (74). There are three categories for biofilm quantification; biomass assays, which quantify the extracellular matrix (ECM), along with both living and dead cells; viability assays, which quantify the living cells only; and matrix quantification, which quantifies the components of the ECM only (207). Assays which capture the activity of pre-formed biofilms are of clinical relevance, as these replicate the clinical context; as treatment occurs once a biofilm has become established (74).

Crystal violet (CV) staining was first used for the staining and quantification of biofilms by Fletcher in 1977 (208), and since then it has become the 'gold-standard' for biofilm quantification (62,74,83,87,176,207,209–215). CV staining is capable of capturing the activity of pre-formed biofilms, and is one of the most common published quantification methods (60,215). CV stains all negatively charged surface molecules and polysaccharides (207), including anionic proteins, nucleic acids and lipopolysaccharides (74), and has the advantage of giving data on the total biofilm biomass, but also does not discriminate between live and dead cells (74,207). It has been demonstrated to be repeatable both within and between species (207), and can be quantified using a spectrophotometer by dissolving the crystal violet in a solvent (207,216,217). Prior to this advance, quantification was achieved using laborious and inaccurate microscopy cell counts both with and without CV staining (208,218). Despite its popular use, CV can give considerable background stain (209), though this can be overcome with washing steps (74,218). Background staining is also less significant with greater biofilm biomass, as is often observed when quantifying *Pseudomonas aeruginosa* (74,209). However, published methods all show variations in washing and quantification techniques (56,60,72,74,119,207,216,218). These variations include using no

washing steps (218) or increased washing steps (176,209), as well as different solvents used to solubilise the CV, such as ethanol (83), glacial acetic acid (62), and isopropanol (176). In a study comparing both CV (quantifies biomass) and Congo Red (CR) (quantifies bacterial cell viability) as methods for biofilm quantification for isolates from urinary tract infections, CV was shown to have an accuracy of 89%, nearly 30% higher than CR (<60%). This was due to the limited sensitivity of CR (119). Unfortunately, the study did not differentiate between the nine bacterial species assessed. This is important, as other biofilm quantification assays comparing biofilm quantification techniques have found variation between and within bacterial and fungal species (207,219–221). In a large study comparing six biofilm quantification techniques, Peeters, *et al.*, tested fluorescein diacetate (FDA), dimethyl methylene blue (DMMB), 2,3-bis(2-methoxy-4-nitro-5-sulphophenyl)-5-[(phenylamino)carbonyl]-2H-tetrazolium hydroxide (XTT), Syto9, resazurin and CV for their ability to quantify the biofilms of *Burkholderia cenocepacia*, *Propionibacterium acnes*, *Candida albicans*, *Staphylococcus aureus* and *P. aeruginosa*, and found low standard deviations between replicates. This showed each method to be replicable and comparable between the different techniques. Both FDA and DMMB could not be used for *S. aureus* and *C. albicans* biofilm quantification, respectively. As well, XTT was unable to differentiate between the pathogens post-staining (207). Due to the inability of DMMB to quantify *C. albicans*, it may not be able to quantify the biofilms of other yeasts or fungi, such as *Candida auris* or *Aspergillus* spp.. These differences are potentially due to whether the pathogen is a fungus or bacterium, as well as the membrane composition of the bacteria (Gram-positive or Gram-negative). DMMB stains the ECM instead of the cells, and this positively correlates with biofilm quantity. However, this also means DMMB cannot be used in studies comparing planktonic to biofilm growth. Furthermore, both DMMB and CV require additional steps to give quantitative data. DMMB requires a decomplexation solution to remove the DMMB bound with the ECM, whereas CV requires solvent addition to solubilise the CV which has stained biofilm cells, which is then measured (207), as mentioned previously. Lastly, a recent review found that 75% of studies quantifying biofilms had used an endpoint, colourmetric assay, such as CV, and that 81% of these had used CV (215).

Further to the methods discussed above, laminar flow chambers (LFCs) (74), microscopy (74,222), and electrochemical impedance spectroscopy (EIS) have been used as biofilm quantification techniques (74). LFCs are used to grow biofilms under flow conditions, where

media flows over the top of the biofilm for set time periods, constantly replenishing the nutrients but adding shear stress to the biofilm (74). In 2018, a study coupled LFCs with microscopy, with the method validated by comparison with a CV biofilm staining assay (74). They found that combining these allowed biofilms to be grown under conditions closer to those found *in situ*, alongside enhanced biofilm visualisation (74). However, LFCs and microscopy both require trained personnel and specialised equipment, and as such, are not rapid or high-throughput methods (74). Furthermore, studying biofilms in LFCs does not correctly mimic all biofilms found in humans, such as cholesteatoma (87), which is not constantly under flow conditions. Another more complex method includes forming biofilms on 'pegs' within a 96-well plate, which can then be removed after biofilm formation, but before quantifying for increased measurement accuracy, thereby removing the background measurements. This is another costly method, and also requires specialised training and equipment (223). As this assay requires biofilms to be formed on these pegs in the plate, it does not alter the assay time or increase the throughput compared to CV quantification.

Studies have shown EIS to be a relatively rapid and inexpensive point-of-care diagnostic tool, using screen-printed electrodes for less than £2 per sensor (129), and it has even been found to outperform traditional microbiological techniques (129,130). For some bacterial strains, such as *Salmonella enterica* Typhis and *S. enterica* Typhimurium, EIS detection has been possible within as little as 60 minutes (127). However, *P. aeruginosa* has typically been measured over 24 – 69 hours (80,128,135). *Escherichia coli* also required longer measurement times (130). Another measurement, square wave voltammetry (SWV) involves the application of a range of potentials (V) to a liquid and the current output (A) is measured (130). Due to the potential being small, it has little to no effect on the bacteria (224). Using this, a user can gain information about the charged molecules in the media (128), and monitoring this allows changes to the media to be observed in real-time, *in situ*, and this can be applied to bacteria growing in liquid culture (130,224). In EIS, a range of frequencies are passed between two electrodes and the impedance modulus ( $\Omega$ ) between the electrodes is measured (225). Using a range of frequencies allows the user to gain information about the resistive and capacitive properties of the well, meaning that any build-up of cells or debris on the electrodes from a forming biofilm, is measured as a decrease in impedance modulus (130). Typically, impedance values are fit to a model, such as a Randle's

equivalence circuit (127,128,224), however changes in raw impedance values have also been employed previously to detect antibiotic resistance between two strains of *S. aureus* (129). Furthermore, these authors employed a normalisation technique for EIS which treats each well as a closed system as impedance is sensitive; by normalising each well against its  $t=0$ , any variations between sensors are taken into account. Both SWV and EIS allow for real-time monitoring of bacterial growth and biofilm formation, therefore EIS has been shown to be of greater benefit for biofilm detection than other methods (130). Previously, EIS has been used to detect pathogens, including *E. coli* O157:H7, on food products (226), and has also successfully distinguished between biofilm adhesion and maturation of *P. aeruginosa* (224). However, the authors did not investigate different biofilm concentrations or biofilm reduction measurements. Furthermore, EIS has also been applied to *S. aureus* growing alongside methicillin, determining that the system is sensitive enough to differentiate between methicillin-resistant or methicillin-sensitive *S. aureus* in under two hours; a promising tool for point-of-care diagnostics (130). A gel on top of an electrode can contain decreasing concentrations of antimicrobial, and this can be used as a rapid screening technique for antibiotic resistance (130). This offers a marked improvement on the 18–24-hour incubation for antibiotic susceptibility tests, and the 48-hour tests described earlier.

One of the main reasons *P. aeruginosa* was chosen for this study was due to its ability to produce electrochemically active metabolites, such as pyocyanin, which is produced by 90–95% of *P. aeruginosa* isolates (67). Pyocyanin production has been shown to increase with planktonic growth of *P. aeruginosa* within a closed system (128). Furthermore, pyocyanin is reduced at  $-0.35\text{ V}$  (227), and it is the chemical signal released during the reduction process which is measured (128). It was therefore hypothesized that measuring the bacterially produced pyocyanin could be an accurate method to quantify the planktonic growth of the *P. aeruginosa*. Furthermore, *P. aeruginosa* attachment has been seen within two hours, and plateaued at four hours (208). Therefore, it was hypothesized that biofilm formation of *P. aeruginosa* would be observable within four hours using EIS (**Figure 3.1**).

### 3.2 Aims and objectives:

The first aim of the work presented in this chapter was to design a model system for the monitoring of growth and inhibition of biofilm formation, using the clinically relevant pathogen, *P. aeruginosa*. Two strains were chosen due to their laboratory and clinical significance, PA14 and LESB58. The second aim was to develop electrochemical methods for biofilm quantification; specifically electrochemical impedance spectroscopy (EIS) and square wave voltammetry (SWV), and to compare these to the 'gold standard' crystal violet (CV) using PA14 and LESB58.

These aims were achieved through the following objectives:

1. To optimise *P. aeruginosa* biofilm growth in 96-well plates (required for downstream EIS measurements)
2. To quantify PA14 and LESB58 biofilms using CV
3. To quantify PA14 and LESB58 biofilms using SWV and EIS
4. To compare CV and electrochemical data for biofilm quantification

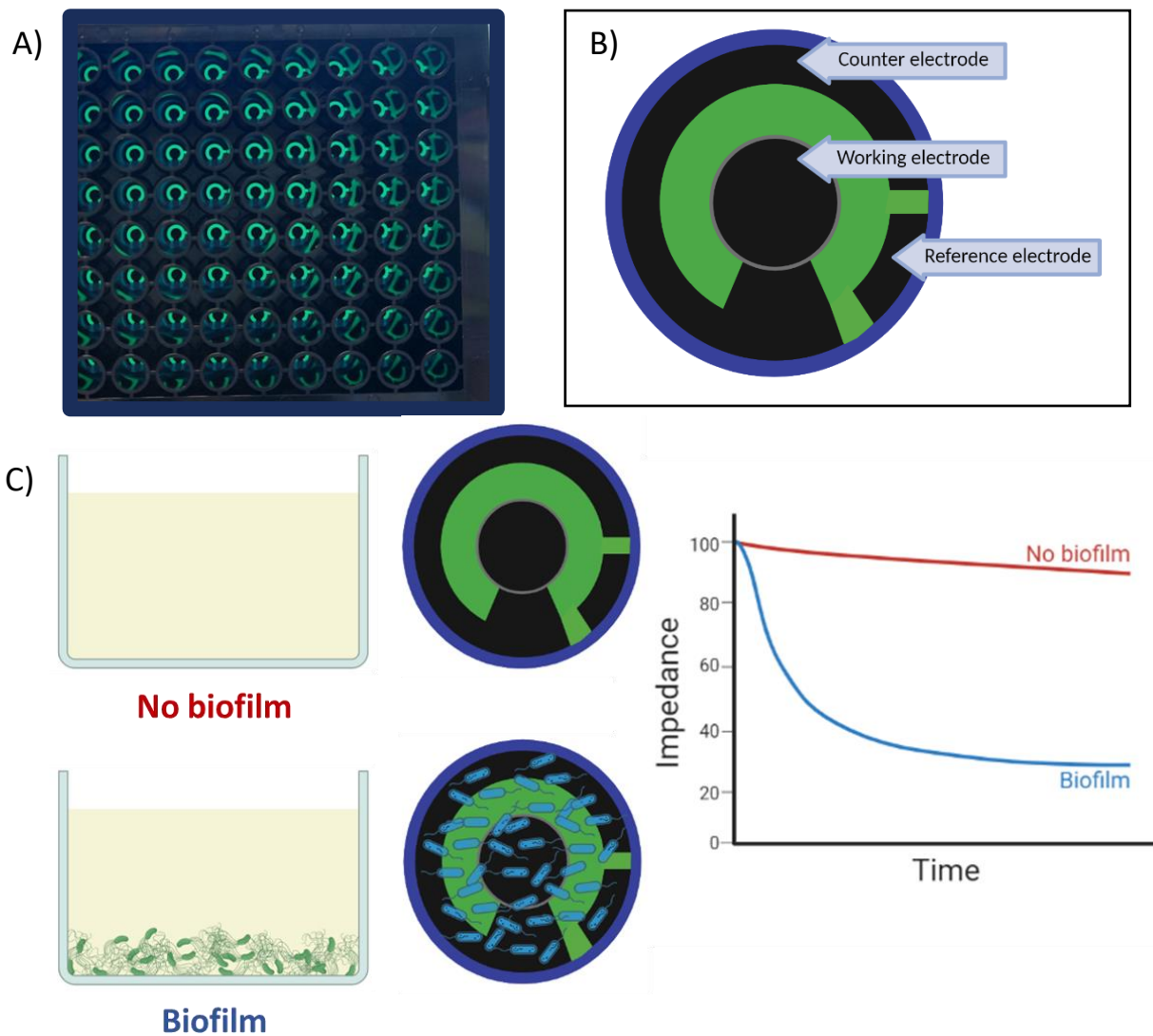


**Figure 3.1 DropSens™ plate layout and biofilm formation.** A) Close-up of DropSens™ 96-well plate with carbon sensors in the base of each well. B) Diagram showing the positioning of the counter, working and reference electrodes on the sensors present in the 96-well plate, C) Schematic of the difference observed when biofilm is present and not present on the sensor.

### 3.3 Results

First, it was important to assess the time frame of *P. aeruginosa* PA14 growth under the conditions by which biofilm growth would be evaluated (37 °C, static). This was done by dislodging the biofilm from the walls of the well (6-well plate), and then measuring the optical density at 600 nm (OD) as a proxy for biofilm growth, as is standard practice for non-filamentous, non-clumping bacteria. The results showed that OD<sub>600</sub> ranged from 0.060 - 0.084 with no statistical difference between replicates 1 – 3 ( $p \geq 0.05$ ,  $n=3$ ) suggesting uniform and consistent measurement (**Table 3.1**) across all replicates. The final ODs of the biofilm bacteria was unexpected, as the cells were seeded at 0.2 OD<sub>600</sub>, and therefore an abundance of adhered cells were anticipated. However, to more accurately use this method to quantify biofilm, it would be important to wash the planktonic cells, so that only biofilm cells adhered to the plate surface would be quantified. As such, three PBS washes were introduced and as expected, the cell density reduced by 10-fold (ranging from OD<sub>600</sub> 0.024-0.081) (**Table 3.1**), indicating that planktonic cells had been successfully removed. There was also more variation in measurements, with the results being statistically significant from one another ( $p \leq 0.05$ ), including more than a 3-fold difference between replicates 4 and 6. This suggests that this method is not accurate for biofilm quantification. The main disadvantage of this method, and one that could impact the success in ‘capturing’ biofilm cells in the measurement, is that pipetting is used to transfer the culture to the cuvette for measurements in the spectrophotometer. There was no method used to determine if all the biofilm cells had been removed from the wells for quantification, and this may account for the discrepancies between replicates. As such, the results were expected and next the ‘gold standard’ method of biofilm quantification, CV staining, was assessed. This allowed for biofilms to be quantified within a 96-well plate (necessarily for later electrochemical measurements) and therefore circumvented the cell-removal issues experienced during OD measurement.

**Table 3.1 Biofilm formation of *P. aeruginosa* quantified spectroscopically.** OD<sub>600</sub> of *P. aeruginosa* (PA14) biofilm after four hours incubation at 37 °C with ( $p \leq 0.05$ , n=3) and without a ( $p \geq 0.05$ , n=3) PBS wash.

Replicate	OD <sub>600</sub> (nm)	PBS wash
1	0.083	No
2	0.060	No
3	0.084	No
4	0.081	Yes
5	0.031	Yes
6	0.024	Yes

Following on from the initial biofilm formations in 6-well plates, decreasing seeding ODs of *P. aeruginosa* (PA14) were introduced to observe if decreasing quantities of biofilm could be detected. These were photographed after dH<sub>2</sub>O washing steps (**Supplementary Figure 3.1**). The lack of staining in the CV control after the biofilms were washed, confirmed that both the planktonic cells and the background stain were removed, as well, there was a visual decrease in the quantity of stain for decreasing OD<sub>600</sub> of *P. aeruginosa*.

From this, it was necessary to quantify the CV-stained biofilm, and therefore 95% ethanol (v/v) was used to solubilise the biofilm-bound CV. The biofilms were formed from seeding densities of 0.05 – 1 OD<sub>600</sub>. The addition of ethanol to the CV-stained wells solubilises the CV from the walls of the wells into the solvent, allowing for spectrophotometric quantification of the CV (**Figure 3.2**). The CV quantification of both PA14 and LESB58 at increased seeding densities (**Figures 3.2 and 3.3**) had clear linear trend lines. As the data was normalised, the end value was 100% biofilm formation, showing an 79.2% increase in biofilm formation between the lowest and highest seeding ODs for PA14. LESB58 showed a 109.7% increase. These both positively correlated to the initial OD that the *P. aeruginosa* were seeded at ( $r^2$  values of 94% and 92%, respectively; indicating the percentage of explained variation of the total variation). Furthermore, there was an overall increase in the standard deviation at the higher starting ODs, particularly compared with those at ODs 0.05 and 0.1 (**Figure 3.2**). The background staining which can be seen in the LB control (**Supplementary Figure 3.1**), may be a source of the large standard deviation of the replicates. Next, it was of interest to determine if *P. aeruginosa* biofilm formation could be viewed in real-time, rather than as an endpoint, as with CV quantification.

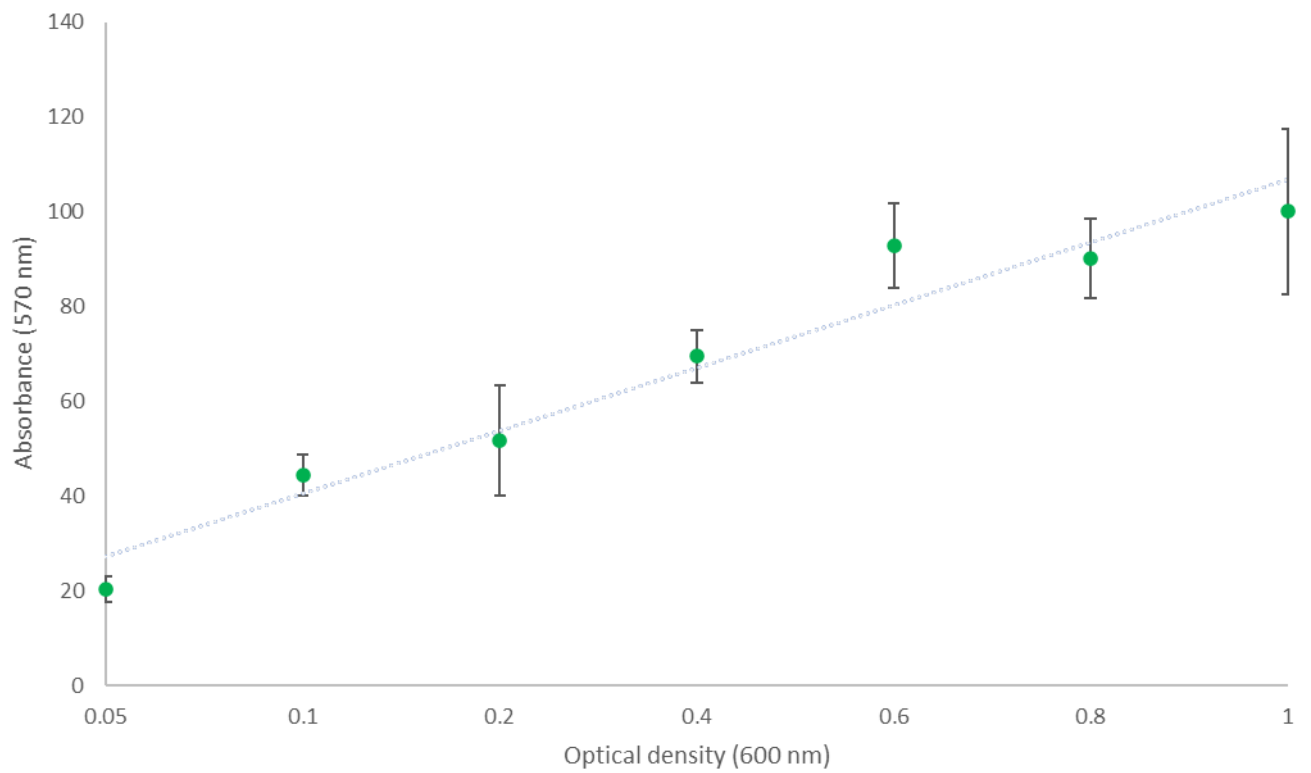


**Figure 3.2: Crystal violet quantification of *P. aeruginosa* (PA14) biofilms with increasing seeding densities ( $OD_{600}$  0.05 – 1).** Measured after four hours using spectroscopy readings at 570 nm of solubilised CV in ethanol (error bars show standard deviation,  $n=3$ ,  $r^2=94\%$ ).

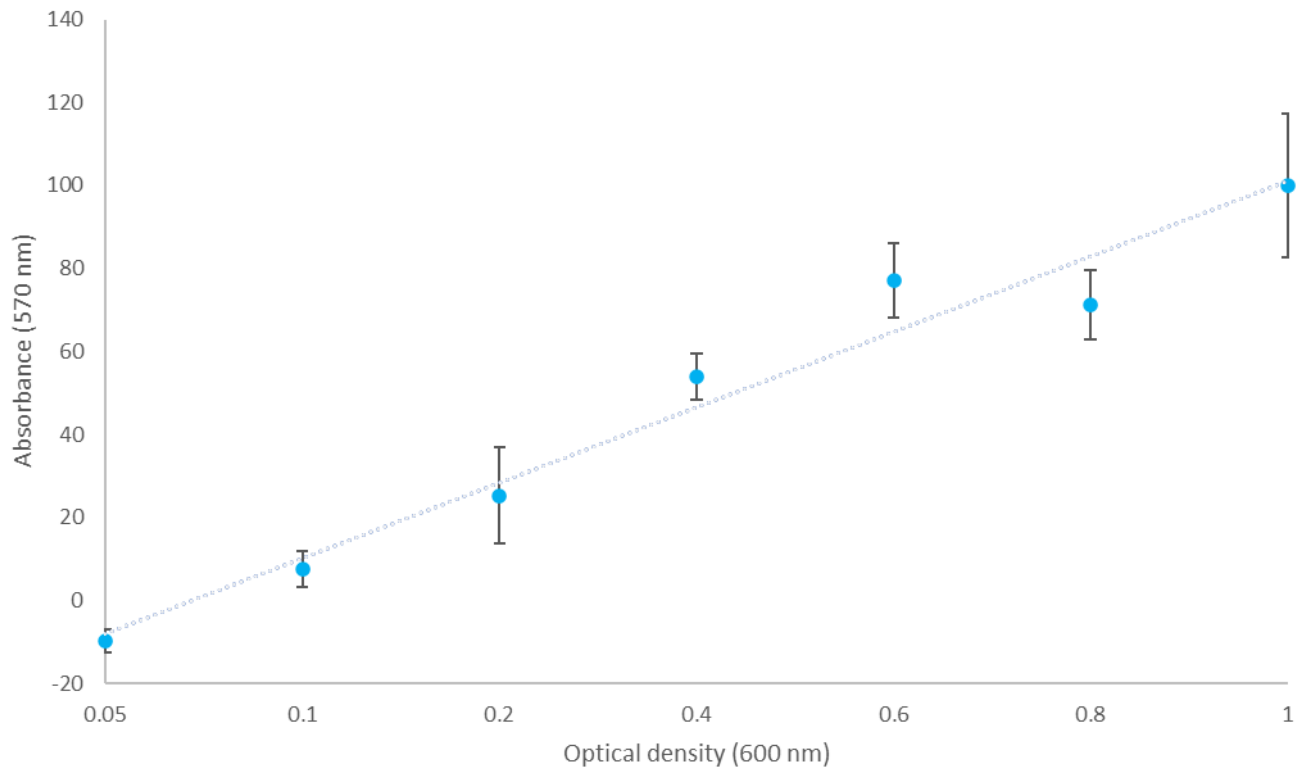


**Figure 3.3: Crystal violet quantification *P. aeruginosa* (LESB58) with increasing seeding densities ( $OD_{600}$  0.05 – 1).** Measured after four hours using spectroscopy readings (570 nm) of solubilised CV in ethanol (error bars show standard deviation,  $n=3$ ,  $r^2=92\%$ ).

As CV quantification provided challenges with accurate and repeatable measurements, as well as only allowing for endpoint reads, we chose to develop methods which enabled electrochemistry to be used to monitor biofilm formation in real-time and *in situ*. As mentioned previously, *P. aeruginosa* produces an electrochemically active secondary metabolite, pyocyanin, which can be measured using electrochemical techniques, used as a proxy for growth (128), as outlined in 2.11. Briefly, a range of potential differences (-0.5 – 0.5 V) was applied to the wells, and the current output ( $\mu\text{A}$ ) measured. Peak height positively correlates to the quantity of the metabolite present in the media, thus allowing for quantification. As proof of concept, increasing concentrations of a pyocyanin standard were quantified using SWV, with a potential difference at -0.35 V, as this is the potential at which pyocyanin is reduced (227), to create a pyocyanin concentration curve (**Figure 3.4**). This showed a strong positive correlation between the pyocyanin concentration of a solution and the resulting current ( $\mu\text{A}$ ) ( $r^2=99.9\%$ ). As pyocyanin production has been shown to increase with planktonic growth of *P. aeruginosa* in a closed system (128), it was therefore hypothesized that measuring the bacterially-produced pyocyanin could be an accurate method to quantify the planktonic growth of the *P. aeruginosa*.

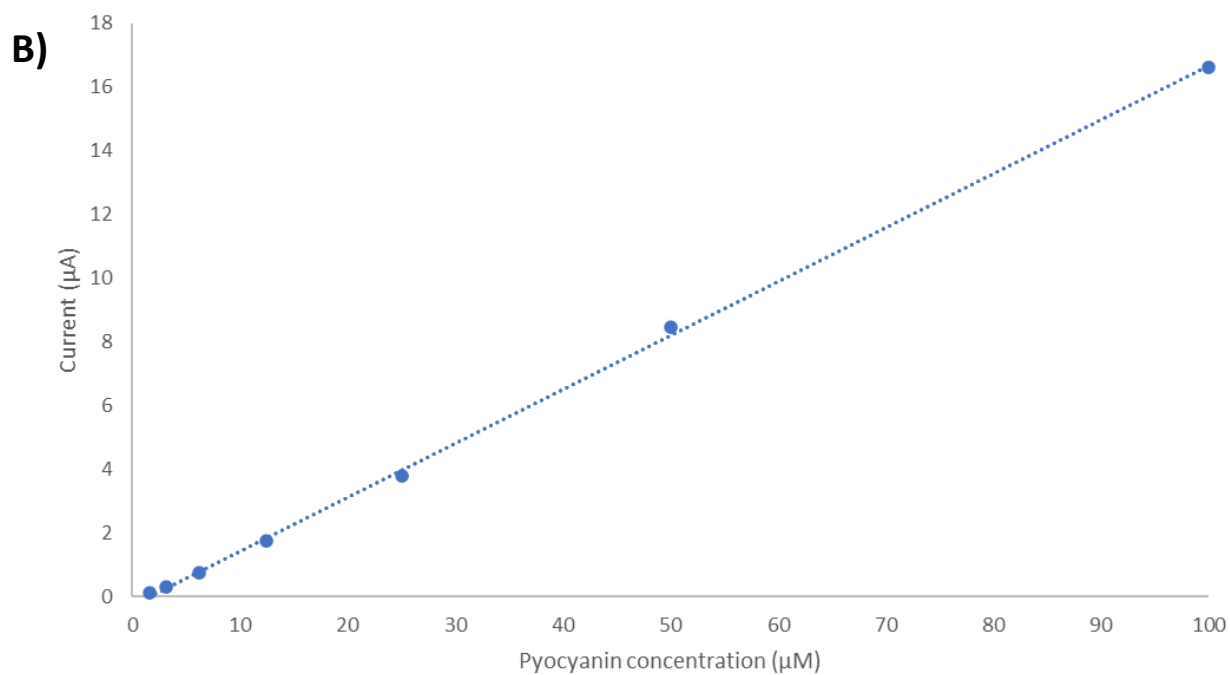
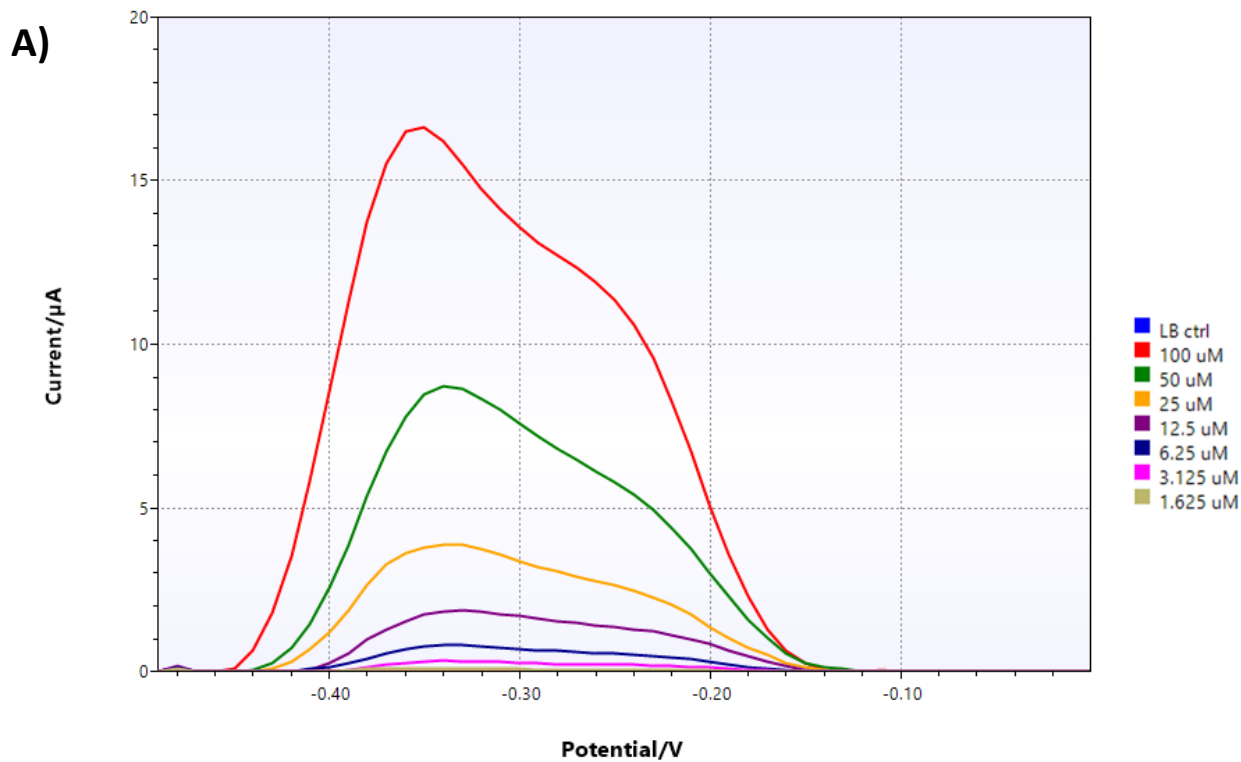


**Figure 3.4: SWV Pyocyanin concentration curve.** Pyocyanin serial diluted in LB (1.56 – 100  $\mu\text{M}$ ) and **A)** measured across a range of potential differences (V). **B)** Corresponding pyocyanin concentration curve showing increasing current output ( $\mu\text{A}$ ) with increasing pyocyanin concentrations at -0.35 V,  $r^2=99.9\%$ .

As such, the next experiment used the same set-up, but with both *P. aeruginosa* PA14 and LESB58 at increased seeding densities, as carried out earlier. The results showed a similar trend to the CV data (**Figures 3.5** and **3.6**, respectively). As hypothesized from the concentration curve, there was an increased current ( $\mu\text{A}$ ) output at increased seeding densities (shown as a percentage as the data has been normalised). For example, for PA14, OD 0.05 = 6.4% increase in current, compared to OD 0.8 = 70.6%. Similar trends were seen for LESB58, OD 0.05 = 1.2%, and OD 0.8 = 64.2%. This increased current output demonstrates increased pyocyanin production, and subsequently the density of *P. aeruginosa* cells. As both sets of data were normalised to the current at the highest concentration of pyocyanin ( $\text{OD}_{600} = 1$ ), **Figures 3.5** and **3.6** do not show the differences in pyocyanin production between PA14 and LESB58. Looking at the current output data prior to normalisation (**Supplementary Figure 3.2**), it can be observed that LESB58 produces more pyocyanin than PA14; LESB58 = 12.7  $\mu\text{A}$ , compared to 2.2  $\mu\text{A}$  for PA14, both at  $\text{OD}_{600} 1$ . This is likely because LESB58 has increased virulence compared to PA14, and pyocyanin is a virulence factor of *P. aeruginosa*. The pyocyanin concentration curve had an  $r^2$  value of 99.9%, compared to 91% for the SWV data (both PA14 and LESB58);  $r^2$  indicating the percentage of explained variation of the total variation. This is not unsurprising, as the concentration curve in **Figure 3.4** is pyocyanin and media only, whereas *P. aeruginosa* cultures produce other metabolites in addition to pyocyanin. These additional metabolites, such as pyoverdine, add additional variation to these wells, which is not measured by the concentration curve. Next, it was of interest to determine if biofilm formation could be observed over the four hours, rather than an endpoint read, as with CV.

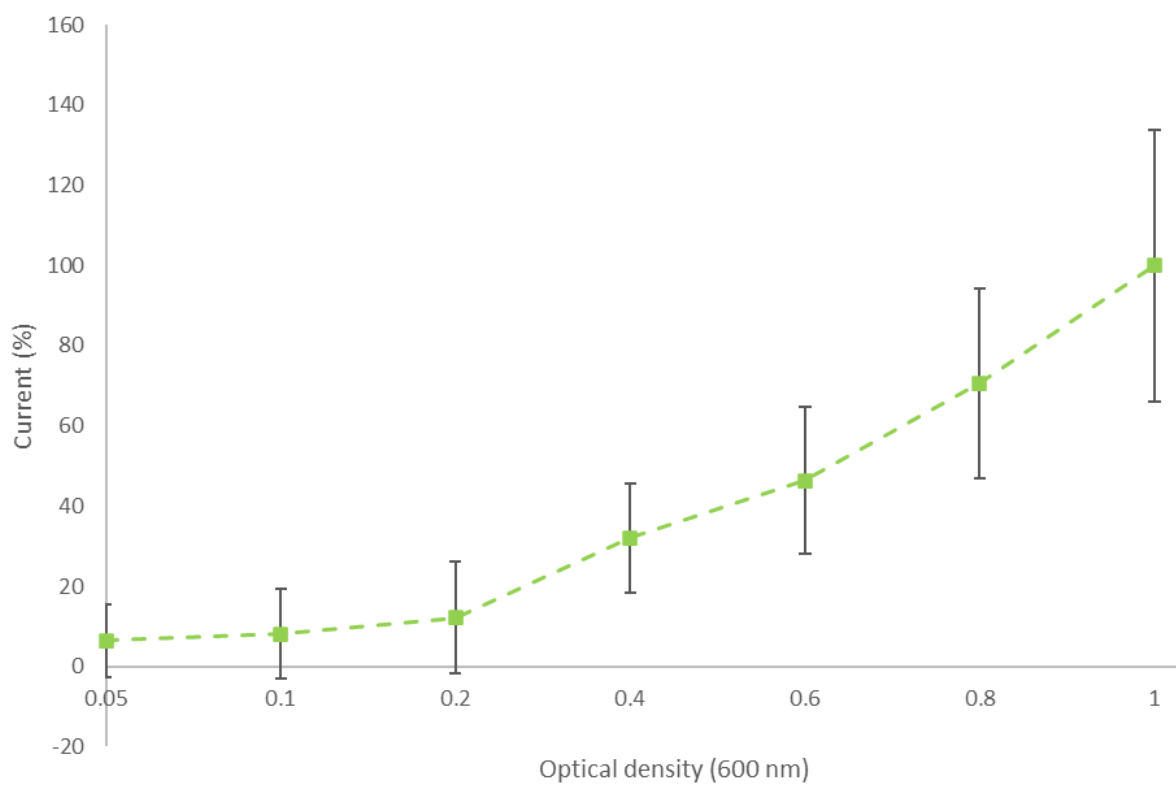


**Figure 3.5: SWV quantification of *P. aeruginosa* (PA14) with increasing seeding densities ( $OD_{600}$  0.05 – 1). Current ( $\mu A$ ) measured over four hours at -0.35 V, normalised four-hour time point shown (error bars show standard deviation,  $n=3$ ,  $r^2=91\%$ ).**

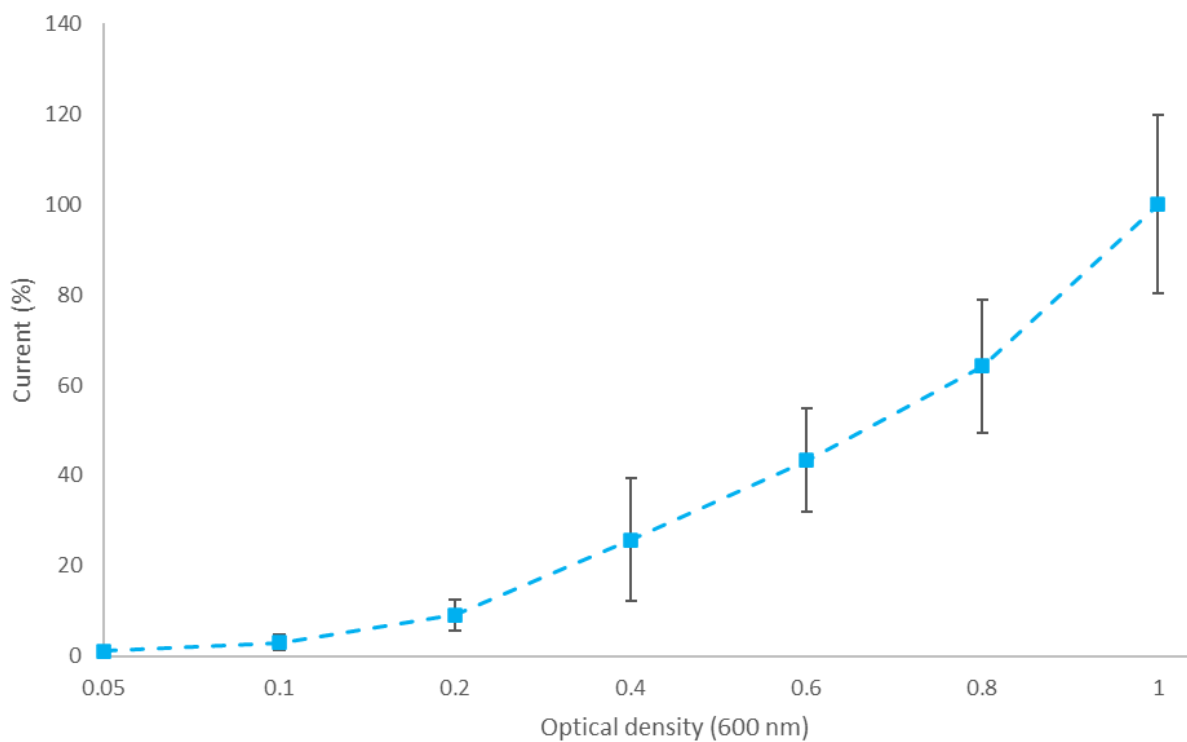


**Figure 3.6: SWV quantification of *P. aeruginosa* (LESB58) with increasing seeding densities (OD<sub>600</sub> 0.05 – 1).** Current ( $\mu\text{A}$ ) measured over four hours at  $-0.35\text{ V}$ , normalised four-hour time point shown (error bars show standard deviation,  $n=3$ ,  $r^2=91\%$ ).

As mentioned previously, SWV measurements at -0.35 V quantify the concentration of pyocyanin within the media (correlating to planktonic growth of *P. aeruginosa*). As such, it was hypothesized that EIS could be employed to quantify biofilm formation, as this instead measured the build-up of cells on the electrode, with a decrease in impedance modulus indicating biofilm formation. As expected, the EIS spectra of PA14 and LESB58 over four hours showed a decrease in normalised impedance modulus ( $\Omega$ ) from 1 to 0.54, and 1 to 0.43 for PA14 and LESB58, respectively (**Figure 3.7**), indicating that both strains had formed biofilms within the four hours. Furthermore, there was a significant difference observed in the quantity of biofilm formed by LESB58 after 1.5 hour ( $p = 0.046$ ,  $n=3$ ), when compared to 0 hours, and a significant difference in the quantity of biofilm formed by PA14 after just one hour ( $p = 0.00033$ ,  $n=3$ ) (**Figure 3.7**). Typically, impedance data is fit to a circuit model as a method of normalisation (128,129), however model-fitting was not carried out here, as significant differences between the LB control and both *P. aeruginosa* strains could be observed without this. Instead the data was normalised, as in a study by Hannah, *et al.* (130), by dividing by the corresponding  $t=0$  value for each condition. Lastly, there was no significant difference in biofilm between either strain of *P. aeruginosa* after 4 hours ( $p = 0.076$ ,  $n=3$ ), despite other studies indicating that LESB58 is a superior biofilm former, due to its lack of motility (52). The ability to detect biofilm formation in real-time, and within 90 minutes, for both strains has strong implications in the field of high throughput diagnostics, for example in real-time monitoring of medical implants. Therefore, it was lastly of interest to determine if an antibiofilm agent could be found to quantify biofilm reduction as well as growth.

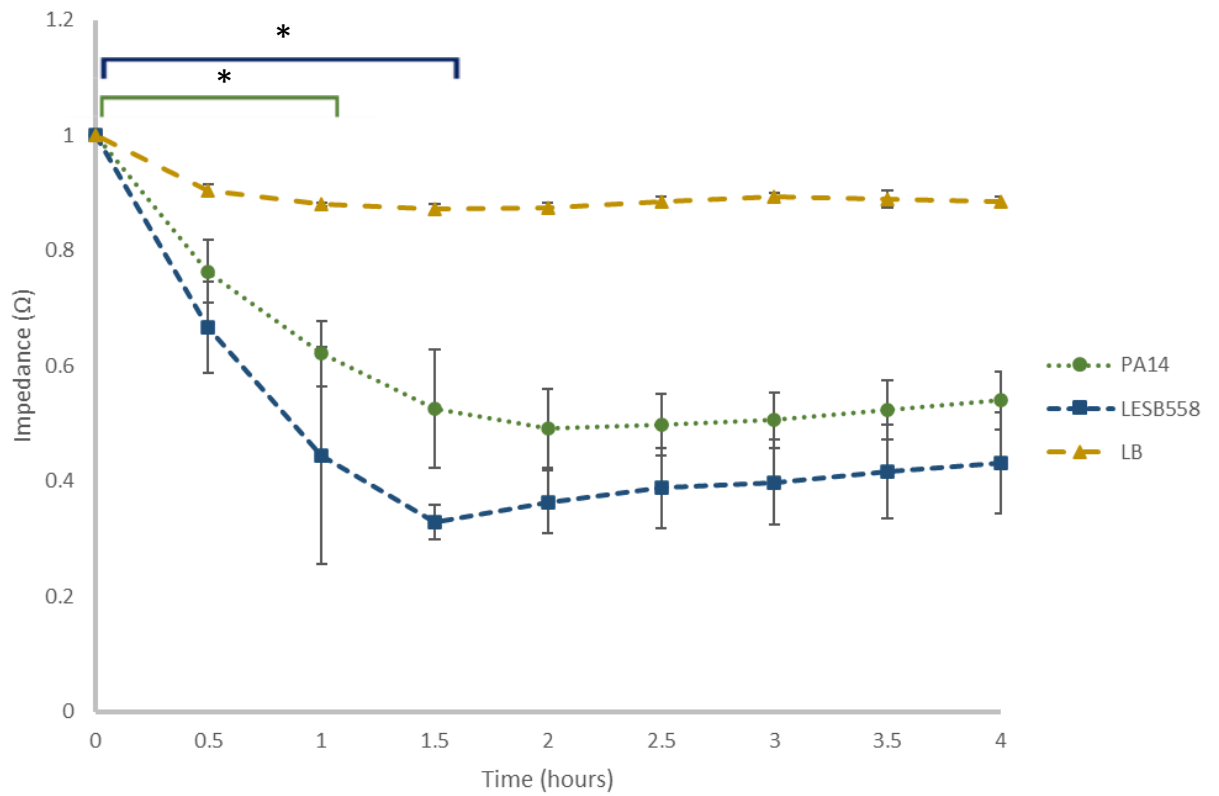


**Figure 3.7: EIS quantification of *P. aeruginosa* biofilms over four hours.** PA14 (dark green), LESB58 (dark blue) biofilms and LB media control (dark yellow) quantified using EIS (10 Hz) over four hours. Impedance normalised by dividing each data set by their t=0 value. Error bars show standard deviation, n=3, \* denotes significant difference ( $p < 0.05$ ).

As mentioned, a final challenge was to demonstrate that reduction in biofilm formation could also be quantified with CV initially and then EIS. Six antibiofilm agents were identified from literature and assayed using OD<sub>600</sub> measurements and CV (**Figure 3.8**), for their effect on both planktonic growth and biofilm growth, respectively, with a darker colour indication increased growth. These antibiofilm agents were measured against both PA14 (green) and LESB58 (blue); gentamicin (112), L-arginine (211), ciprofloxacin (74,83,211), ethanol (228), meropenem (211), and zinc chloride (229). The least successful antibiofilm agent tested was ciprofloxacin by both PA14 and LESB58; at all the concentrations, the biofilm formation is comparable to the no treatment control. At the highest concentration of ciprofloxacin, biofilm formation was 84.9% and 100% by PA14 and LESB58, respectively. A similar trend was seen with L-arginine, the lowest biofilm formation by PA14 at any concentration was 69.6% (0.4% L-arginine (w/w)), and 83.9% by LESB58 (0.1% L-arginine (w/w)). Both ethanol and meropenem had little to no effect on the planktonic and biofilm formation of PA14; ethanol inhibited 13% biofilm at the highest concentration (2% (v/v)), however this was accompanied by a 53% reduction in planktonic growth. The same trend was seen for ethanol with LESB58; there was no reduction in biofilm at the highest concentration, however planktonic growth was reduced by 58%. This reduction in planktonic growth but no reduction in biofilm formation is likely a stress response. This same response was seen at the higher gentamicin concentrations by LESB58 too. At the highest concentration (3.125 ug/mL), LESB58 had reduced planktonic growth (33.6%), but limited reduction in biofilm formation (73.2%). Interestingly, this was not observed by PA14 with gentamicin. Instead, the inverse was seen; the planktonic growth for PA14 has limited reduction (71.0%), compared just 14.5% biofilm formation at the highest gentamicin concentration. This indicates that the biofilm formation by PA14 is more readily disrupted than for LESB58. Whereas LESB58 increases biofilm formation in the presence of an environmental stress, PA14 appears to decrease biofilm formation. From these data, the most viable antibiofilm agent for both LESB58 and PA14 tested was zinc chloride. At 1 mM, the biofilm formation by PA14 and LESB58 was 64.0% and 0.0 %, respectively. This was accompanied by 100% and 98.0% planktonic growth. Further reduction in biofilm formation was observed by PA14 at higher zinc chloride concentrations; 25.2% at 2 mM, and -6.1% at 4 mM. However, at 4 mM, there was a reduction in planktonic growth of PA14 as well (65.3%).

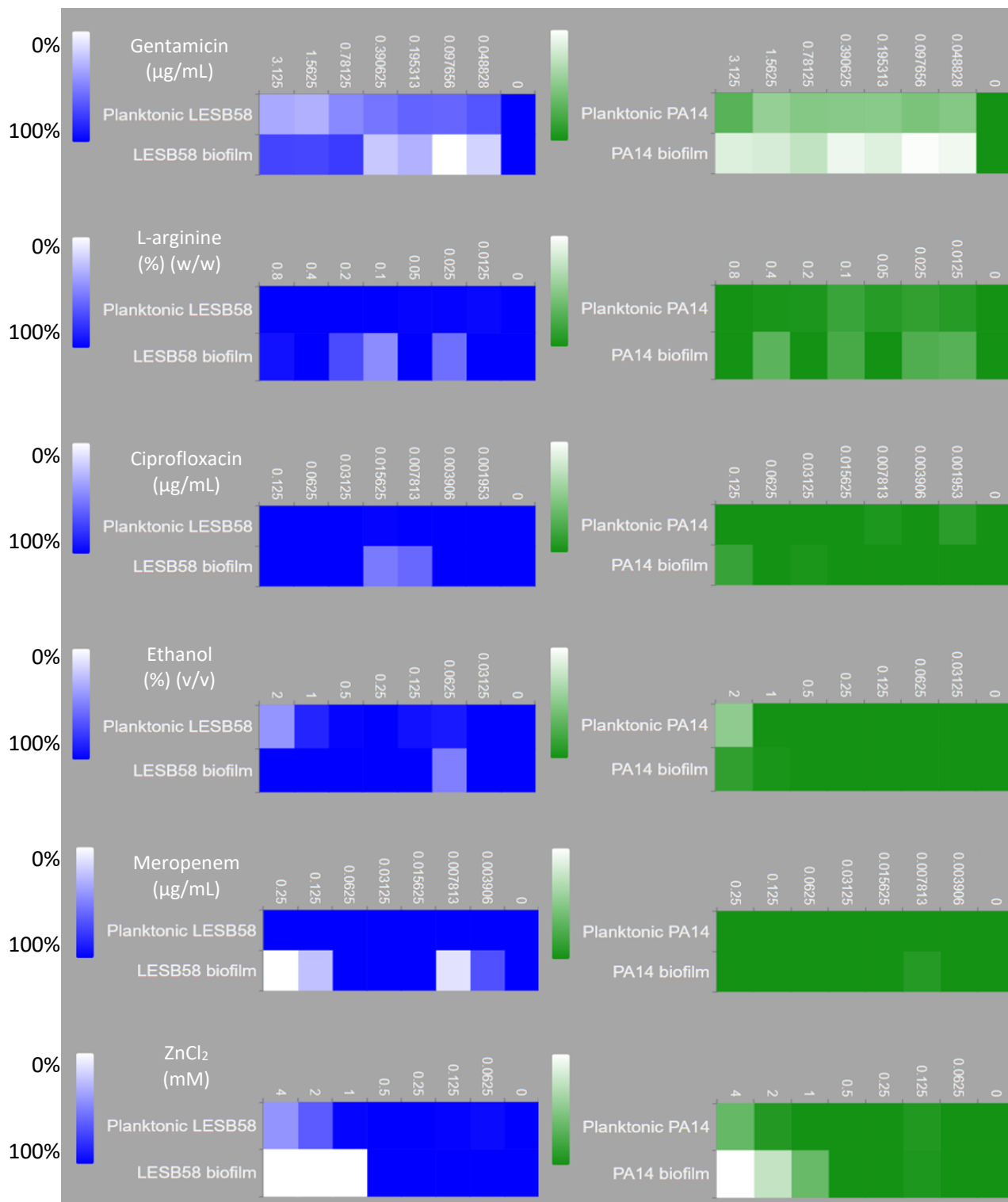


**Figure 3.8: Heatmap showing the efficacy of six antibiofilm agents recommended in the literature.** Antibiofilm agents assayed using OD<sub>600</sub> and CV measurements against both planktonic and biofilms of LESB58 (blue) and PA14 (green); (top to bottom) gentamicin, L-arginine, ciprofloxacin, ethanol, meropenem, zinc chloride (n=3 for each antibiofilm agent + *P. aeruginosa* strain). Growth is normalised against *P. aeruginosa* only and media only

controls and therefore given as a percentage; white indicating no growth (0%), and the darkening colours indicating increased growth.

### 3.4 Discussion

It has been previously shown that LESB58 forms more biofilm than PA14; a 2005 study compared the biofilm forming ability of environmental isolates to PAO1, another lab strain, and found that 83% of the isolates had up to 18-fold greater biofilm-forming ability than the laboratory strain, with the other 17% having the same biofilm forming ability (87). This aligns with the data here, as LESB58, a clinical isolate (51), formed more biofilm than PA14, although this was not statistically significant. However, the increase in biofilm formation from LESB58 compared to PA14 has been shown in the literature previously. In a 2022 study, there was a significant difference in the quantity of biofilm formed between PA14 and LESB58 (128). As well, another study found that LESB58 was able to form 43% more biofilm than both PA14 and PAO1 *in vivo*. Interesting, the site of LESB58 infection was in the bronchial lumen; where the infection was initiated (52). The reasoning behind this is potentially due to the reduced swimming and twitching motility exhibited by LESB58 when compared to both PA14 and PAO1 (52). The lack of motility could be attributed to the increased virulence of LESB58, increased virulence is metabolically expensive (76), as seen here with the increase in pyocyanin production, a virulence factor. In contrast to this, another large study compared to more than 200 *P. aeruginosa* isolates taken from humans, as well as animals which have had prolonged, close contact with humans, including dogs and snakes. These *P. aeruginosa* isolates were collected from various human and animal swabs (ear, eye, wound, vaginal, mouth, nasal, and skin) and body fluids (milk, urine, and sputum), and were compared with PAO1 for biofilm formation and human cell pathogenicity. Whereas the previous studies outlined, only 15% of the *P. aeruginosa* isolates could form biofilms stronger than PAO1, and 5% did not form any biofilm (62). However, the authors do not note where the isolate was taken from; an isolate from a urine sample would possibly be more likely to form biofilm than an isolate from an eye swab due to the environmental pressures the strain finds itself in. For example, LESB58 is an isolate from the cystic fibrosis (CF) human lung (51), and therefore has increased pressures to form biofilm. Furthermore, two of these studies focus on environmental isolates (62,87), rather than clinical isolates, and therefore the strains potentially have decreased virulence due to lesser environmental pressures (230). As well as this, because PA14 has increased pathogenicity in comparison to PAO1 (199), it therefore would have been interesting for both Milivojevic, *et al.*, and Wang, *et al.*, to assay against PA14 in addition to, or in replacement of, PAO1. Lastly, all these studies

comparing the pathogenicity of different strains, quantified biofilm formation using CV, an end-point methodology (52,62,87). Therefore, conclusions with regards to speed of biofilm formation cannot be obtained.

As discussed earlier, there is no standardised method in which biofilms are quantified in the literature, and there is no antibiofilm agent currently available on the US market (74,110). Previously, gentamicin has been seen to reduce the biofilm formation of PA14 and 52% of *P. aeruginosa* clinical isolates at sub-inhibitory concentrations (231). However, the results presented here showed that gentamicin increased the biofilm formation at similar concentrations. Similarly, Kao, *et al.*, looked at antimicrobial and host immune defence evasion by biofilms, and used D-amino acids to inhibit biofilm formation, finding that they only prevent biofilm formation for 72–168 hours. After this time the biofilms formed, and some D-amino acids even enhanced the formation of biofilms (72), as with gentamicin and LESB58 presented here. For this, the authors followed a similar protocol to the one carried out in this thesis for biofilm formation, and found that PAO1 forms biofilms quicker than PA14 (72). However, for both strains, the biofilms were grown at 30 °C instead of 37 °C, which would potentially hinder the biofilm formation of both strains, as both PAO1 and PA14 grow optimally at 37 °C.

Another inconsistency within the biofilm-quantification community is variations which occur within the CV-staining protocol. In the one of the earlier studies using CV, in 1998, CV was added directly to the media after the biofilms were grown, resulting in planktonic cells also being stained alongside the biofilm (218). Furthermore, the authors used 1% CV (218), a concentration used in several studies (210,217,218). This is in comparison to the 0.1% used in other studies (72,74,85,211), including this one. Two of the studies which used 0.1% CV, looked at reduction in biofilm formation using amino acids (72), and biofilm growth in different media (74), respectively. Both also included photographs alongside quantification of the biofilms with crystal violet, as with this study, to highlight the background staining. These studies also showed clear trends from the CV data, with similar margins of error as here; and larger error at higher absorbance (570 nm) values. This supports the data, and CV quantification protocol presented here, with a lower concentration of CV, as a useful method of biofilm quantification which can inform further assay development with EIS.

Electrochemical measurements, including EIS, have been used to quantify planktonic and biofilm cells previously. As mentioned above, electrochemical data and in particular impedance data, is fit to an equivalent circuit model, such as Randles (128,129,232). However, circuit fitting was not carried out here due to the trends in the data being apparent prior to model fitting. Hannah, *et al.*, found similarly, that when measuring the planktonic growth of *E. coli* on their gel-electrode system, there was no requirement for model fitting, and that changes in bacterial growth could be detected from raw impedance modulus values at 100 kHz (130). This is highly encouraging, as removal of part of the workflow allows electrochemical methods to be more accessible and therefore increase the likelihood of them being used in the clinical setting by non-specialists. However, the error associated with increased current values could pose issues of reliability in the clinical setting (233). Furthermore, increased variation between measurements and controls has previously been attributed to metabolites within the growth media which are not present in the standards, and increased concentrations of bacteria would hence lead to further variation compared to the standards (128). This study also aimed to quantify biofilms using hyperspectral imaging however were unable to quantify PA14 biofilms which were the same age as those measured in this thesis (128). This demonstrated the benefit of electrochemical methods over conventional methods, such as CV, but also lesser-used methods, such as hyperspectral imaging. A clear limitation of the study presented here, is the inability to directly measure planktonic growth, instead inferring from the pyocyanin concentration (128). However, previous studies have looked at planktonic only (130), or planktonic in one system and biofilm in another (128), rendering the results incomparable. Therefore, this middle-ground of using both SWV and EIS must be seen as a compromise that will be overcome outwith the scope of this project.

Using EIS to monitor *P. aeruginosa* biofilms has previously shown a decreasing impedance as well, with the authors also monitoring capacitance, which is inversely proportional to impedance (234). Furthermore, Kretzschmar, *et al.*, discussed the possibility that carbon electrodes limit the determination of some biofilm properties, due to the increased capacitance associated with the material, and subsequently automatically lowering the impedance measurements (234) when compared to other published data on different electrode materials, such as gold, where impedance data could be read at higher frequencies (211). Lastly, an increased electrical 'noise' has been associated with a multiplexer, which

also results in higher EIS frequencies being unusable (225), and therefore studies using single electrodes have been able to monitor higher frequencies (211). These factors may go some way to explaining why the trends in the EIS spectra here were only seen at lower frequencies (10 Hz).

### 3.5 Conclusions and future work

From this work, a standardised method for reliable biofilm quantification of two *P. aeruginosa* strains (PA14 and LESB58) has been achieved using CV, and translated into SWV and EIS measurements, using the CV measurements as a reliability indicator, to confirm these data. This work has also been carried out using *S. aureus*, *E. coli*, *Pseudomonas putida* (data not shown), however their biofilm formation was considerably lower, and therefore the assays were streamlined to include *P. aeruginosa* only. The use of two electrochemical techniques has enabled the real-time quantification, rather than endpoint measurements only of biofilm formation. In future work, it would be of interest to observe how *P. aeruginosa* responds to antibiotic or antibiofilm agents, and if this can be detected with the developed electrochemical system. Lastly, these electrochemical techniques have interesting patient-care applications, and it would be highly worthwhile to assay this with medically relevant materials, as a stepping-stone to point-of-care electrochemical sensing could be used to detect biofilms forming on implanted materials. These are the focuses of chapters four and five.

## 4.0 The antibiotic and antibiofilm potential of Actinomycetota isolated from marine sediment

### 4.1 Introduction

As mentioned previously, there is currently no antibiofilm agent which has been approved for use in humans to combat medical device or implant infections. This is despite the prevalence of topical wound cleaning agents, which reduce the formation of biofilms on the skin (235). These are unable to be used within patients due to their toxicity, for example primary active ingredients such as polyhexamethylene biguanide, is corrosive (236) and polyhexanide is a potential carcinogen (237). Biofilm eradication techniques are further complicated as, often in hospitals, the MIC of the planktonic cells (56) is used, rather than the MIC of the biofilm bacteria. As a result, the antibiotics used are often not sufficient; it has been shown that the concentration of antibiotic required to eradicate biofilms can be up to 1000-fold higher than the planktonic MIC (89,90). This may explain why the chemicals used in antibiofilm wound cleaners are so harsh, for example patients have lost their sight when these chemicals were applied to the eye (236). Furthermore, clinically used periacetic acid (56) and steam cleaning (due to the temperature) (238), have both been found to be toxic to mammalian cells and therefore not viable as antibiofilm agents *in vivo*.

As evidenced, the need for antibiofilm agents, particularly *in vivo*, is of great importance. As such, there has been significant interest in the isolation of both biofilm inhibitory and eradictory agents in recent years; those which prevent colonisation, and those which are active against a pre-formed biofilms, respectively (239). For example, metabolite extracts from algae have also been assayed for their antibiofilm activity whereby *Padina pavonica* demonstrated antibiotic efficacy against eight clinically relevant pathogens, including *Staphylococcus aureus*, *Escherichia coli*, and *Pseudomonas aeruginosa*. Despite the promising bioactivity against planktonic cells, the algal extract only had antibiofilm activity against *Enterococcus faecalis* and *Bacillus subtilis* (155). However, an antioxidant, glutathione, was found to disrupt *P. aeruginosa* biofilms in another study. This is due to the glutathione reacting with pyocyanin, which inhibits calcification in the cystic fibrosis (CF)

lung (240). These bacterial metabolites, such as pyocyanin (85), are of particular interest due to their ability to eradicate biofilms. In one study, pyocyanin was shown to eradicate 88% of *S. aureus* clinical isolate biofilms, and reduced the cell viability by 82% (85). Similarly, bacterial metabolite extracts from *Streptomyces* isolated from Central Java, were also found to inhibit and disrupt the biofilms of methicillin-resistant *S. aureus* (176). Lastly, antibiofilm agents which target animal pathogens are also of interest due to the economic burden associated with agricultural pathogens (151). Metabolite extracts from a *Streptomyces* sp., also isolated in Indonesia, were instead found to inhibit the biofilm formation of *Vibrio harveyi*, a fish pathogen (239).

The genus *Streptomyces* produces more than 50% of all clinically used antibiotics (141). Due to their ubiquitous nature (241,242), a wide variety of actinomycetes are present in marine sediments (243–245). Furthermore, as mentioned previously, Actinomycetota have been successfully isolated from a variety of ecosystems, including Arctic and Antarctic sediment cores (165,180,197), the rhizosphere of desert plants (242), medicinal plants (246), and the deep ocean (247). This location-diversity was shown previously; a study isolating Actinomycetota from Valparaiso Bay in Chile, isolated 68 different Actinomycetota strains across 17 genera (243). However, other studies have found there to be a predominance of *Streptomyces*, with 80% of strains isolated from a valley in Antarctica belonging to this genus, alongside *Nocardia* and *Pseudonocardia* (175), this is despite another more recent study finding no *Streptomyces* spp. in Antarctic sediment isolations (197). Furthermore, the Chilean study found that all of the isolated *Streptomyces* strains showed antibacterial bioactivity against at least one assayed pathogen, compared to just 57% of the non-*Streptomyces* isolates (243), with 83% of bioactive strains isolated from marine sediment from Diu Island belonging to the genus *Streptomyces* (245). Further, sediments isolated from different depths have shown changes in abundance of Actinomycetota species, with surface level sediments containing a higher frequency of *Streptomyces* spp. (165); a study collecting surface Antarctic sediments (0 – 2 cm depth) contained more than 80% *Streptomyces* (175). In contrast, studies isolating Antarctic strains from between 388 and 4730 m depth, isolated no *Streptomyces* spp. (180,197). Lastly, Jensen, *et al.*, isolated strains from the novel genera, *Salinospora*, and found that at 500 m depth, they made up the majority (58%) of isolated strains (200). In the majority of the studies outlined, these isolated strains have been taken

forward for metabolite extraction with the interest of extracting novel bioactive metabolites (155,248).

Here, antibiotic assays and liquid chromatography tandem mass spectrometry (MS/MS) were carried out with crude metabolite extracts. These were followed by molecular networking to visualise the relationship between the relative ion peaks in a single spectrum, as well as comparing them to other obtained spectra (197). Liquid chromatography mass spectrometry (LC-MS) is commonly used to separate biological molecules, such as metabolites from crude extracts. For natural product research, MS/MS is used to produce characteristic fragment ion patterns (180,183,244,249). In a 2021 study, LC-MS was used to analyse the crude extract from a sponge-associated *Streptomyces*. The authors identified this metabolite as 8-O-metyltetrangomycin and demonstrated its efficacy against *S. aureus* as a potential new antibiotic (143). A similar study in 2021 identified the presence and quantity of metabolites in the aerial and underground parts of five different herbs, and these were measured using LC-MS/MS instead. The authors then attempted to link the presence of isoquinoline alkaloids and polyphenolic compounds detected, as described above, to the antimicrobial activity against *P. aeruginosa*, *S. aureus*, and *Candida albicans* seen for each crude MeOH extract, however they found no correlation in the data sets (154). Similarly, however using electrospray ionisation mass spectrometry (ESI-MS), an antibiofilm agent with activity against *P. aeruginosa* was identified as taurocholic acid (186). ESI-MS has also been used to identify antibiotic tirandmycins from a novel *Streptomyces* strain isolated from a marine sponge from the coast of Wenchang, China (248). Lastly, by incorporating molecular networking into a workflow, matched and related ions can be identified (195,197). This allows for accelerated dereplication steps, as well as the detection of any unique compounds in the search for novel chemistry (250), and allow for prioritisation of any compounds of interest (195).

In this study, Actinomycetota were isolated from marine sediments collected from Scottish shores (**Figure 4.1**), and chosen for their actinomycete-like characteristics, including diffusion of metabolites into the surrounding agar, aerial and substrate mycelia. The bacteriostatic potential of the isolated strains was tested against three clinically relevant bacterial pathogens, *E. coli*, *S. aureus* and *P. aeruginosa*. Following this, specialised metabolites were extracted from these isolated strains. These metabolite extracts were

tested for both antibiotic activity against the same three pathogens, as well as their antibiofilm activity was tested against *P. aeruginosa* strain, PA14.

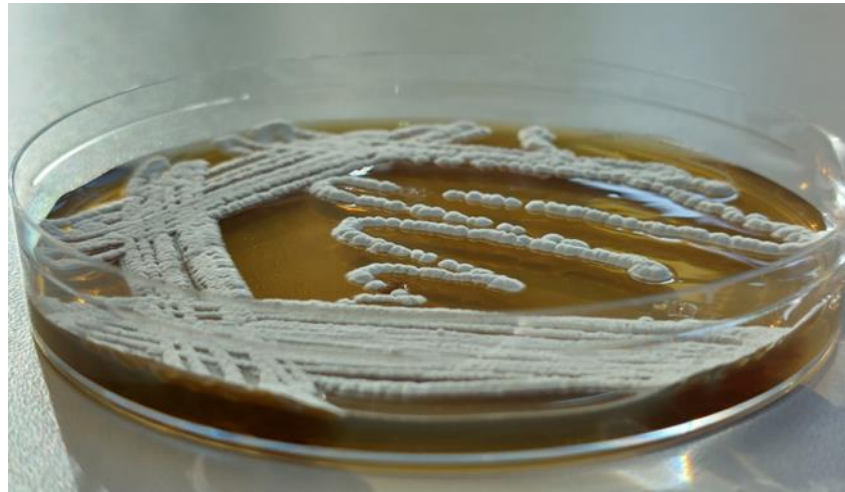


**Figure 4.1: Bacterial isolate LR16 on ISP7 agar.** Diffusion of metabolites into the agar can be seen from the colour change of the media, and the white aerial mycelia associated with *Streptomyces* can be seen on top of the colonies.

## 4.2 Aims and Objectives

The first aim of this chapter was to establish a marine Actinomycetota strain collection and prepare metabolite extracts from these strains. These extracts were then to be assayed for their antibacterial and antibiofilm efficacy against the clinically relevant pathogens *S. aureus*, *E. coli*, and *P. aeruginosa*, using the previously optimised electrochemical techniques, square wave voltammetry (SWV) and electrochemical impedance spectroscopy (EIS), as well as the literature gold-standard techniques, optical density (OD) and crystal violet (CV) measurements.

These aims were achieved through the following objectives:

1. To isolate marine actinomycetes, test their antibacterial activity, and taxonomically and phylogenetically identify them using 16S rRNA gene sequencing
2. To culture these strains and extract their bacterial metabolites, and assess the antibiofilm activity using CV and EIS methodologies
3. To fractionate these bacterial crude extracts and assess their antibiofilm activity using CV and EIS methodologies

## 4.3 Results

Initially, 20 environmental strains (LR1 – LR20) were isolated from Scottish marine sediments and chosen due to their actinomycete-like morphology. As such, all strains isolated had a dry, rough, matte appearance, with a non-spreading morphology (LR16 shown in **Figure 4.1**). In addition, 16 of the 20 strains isolated could be seen to be producing pigmented metabolites which were secreted into the surrounding media. Due to the success of antimicrobial compound production by Actinomycetota, all 20 strains were tested for their antibacterial activity against three clinically relevant pathogens: *S. aureus*, *E. coli*, and *P. aeruginosa*, as a Gram-positive, Gram-negative, and model biofilm former, respectively (**Figure 4.2**). As anticipated, there was no zone of inhibition (ZOI) around any of the negative controls (agar-only plug), showing that the agar had no antibacterial activity. However, none of the strains isolated showed antibacterial activity against *P. aeruginosa*, potentially as *P. aeruginosa* is a Gram-negative pathogen; the outer membrane makes Gram-negative

bacteria harder to kill than Gram-positive pathogens. However, as there was observed antibacterial activity against *E. coli*, it is possible that the efflux pumps are targeted; due to *P. aeruginosa* having twice as many efflux pumps than *E. coli* (1.9% of *P. aeruginosa* genome, compared to 1% of *E. coli*) (251,252). Furthermore, 55% of the environmental strains isolated showed no bioactivity against any of the three pathogens tested (*S. aureus*, *E. coli*, or *P. aeruginosa*) (**Figure 4.2**). This was surprising due to the success of actinomycetes, mainly *Streptomyces*, to produce antimicrobial metabolites. However, the reported success of actinomycetes may be overestimated due to the lack of negative data published. Many factors could have an impact here, for example, the strains were only grown on a single medium (ISP2 or ISP7), as well, the plugs were taken after seven days of growth; a longer time may allow for the diffusion of a greater number of metabolites into the agar. In these plug assays, LR9 showed the largest ZOI against *S. aureus* and *E. coli*, at 8 mm and 8.7 mm (radii), respectively. Due to lack of antibacterial activity against *P. aeruginosa*, all nine isolated strains with bioactivity against *S. aureus* or *E. coli* were taken forward for metabolite extraction.

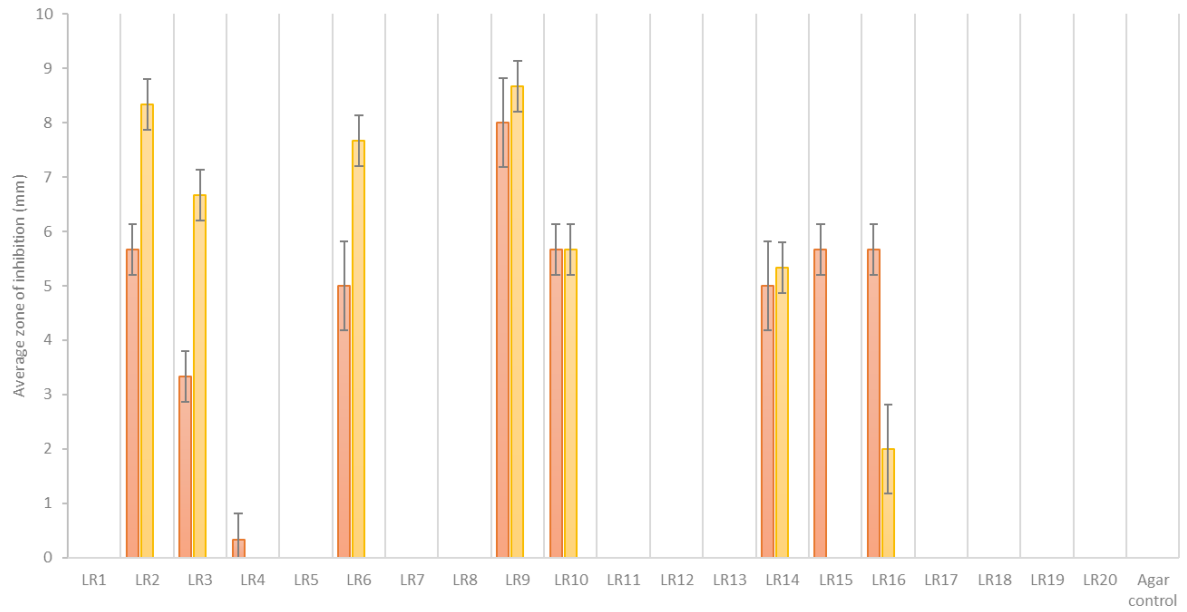


**Figure 4.2: Antibacterial activity of isolated strains.** Average zones of inhibition (radius, mm) of 20 environmental bacteria (LR1 – LR20 strains) against three pathogens (*S. aureus*; red, *E. coli*; yellow, *P. aeruginosa*; green), error bars represent standard deviation (n=3).

Given the scope of the work in **Chapter 3** on biofilm formation and quantification, one of the key objectives of this study was to discover antibiofilm activity from metabolites produced by environmental bacterial strains. As none of the LR strains showed antibacterial activity against *P. aeruginosa*, strains from the wider KRD culture collection were assessed against the same three clinically relevant pathogens (**Figure 4.3**). A further 11 KRD strains were selected based on a previous study from the group which found all 11 strains to have antibacterial bioactivity against at least one of the ESKAPE pathogens (180). It is important to note that of the ESKAPE pathogens, only *E. coli*, *S. aureus* and *P. aeruginosa* were tested here, so it was anticipated that not all strains would exhibit antibacterial activity due to the reduced panel of pathogens. Of the 11 KRD strains tested, three showed anti-*P. aeruginosa* bioactivity (KRD175, KRD153, KRD182), and therefore were also taken forward for metabolite extractions. Two of these three strains were previously identified based on 16S rRNA gene sequencing; KRD175 and KRD182 were found to belong to the genera *Rhodococcus* and *Pseudonocardia*, respectively (180). Interestingly, the antibacterial bioactivity observed from testing the KRD strains compared to the LR strains was less potent (smaller ZOI). For example, the KRD strains had a maximum ZOI of 3.2 mm (KRD182), compared to 8.7 mm (LR9). LR and KRD strains were all isolated from marine sediment, and all (apart from KRD182 and LR16) were grown on ISP2 agar (consistent carbon, nitrogen, and nutrients). As such, the taxonomy of the bioactive LR strains was determined to identify if they belonged to the genus *Streptomyces*. To confirm this, gene amplification of the 16S rRNA gene of the LR strains was carried out.

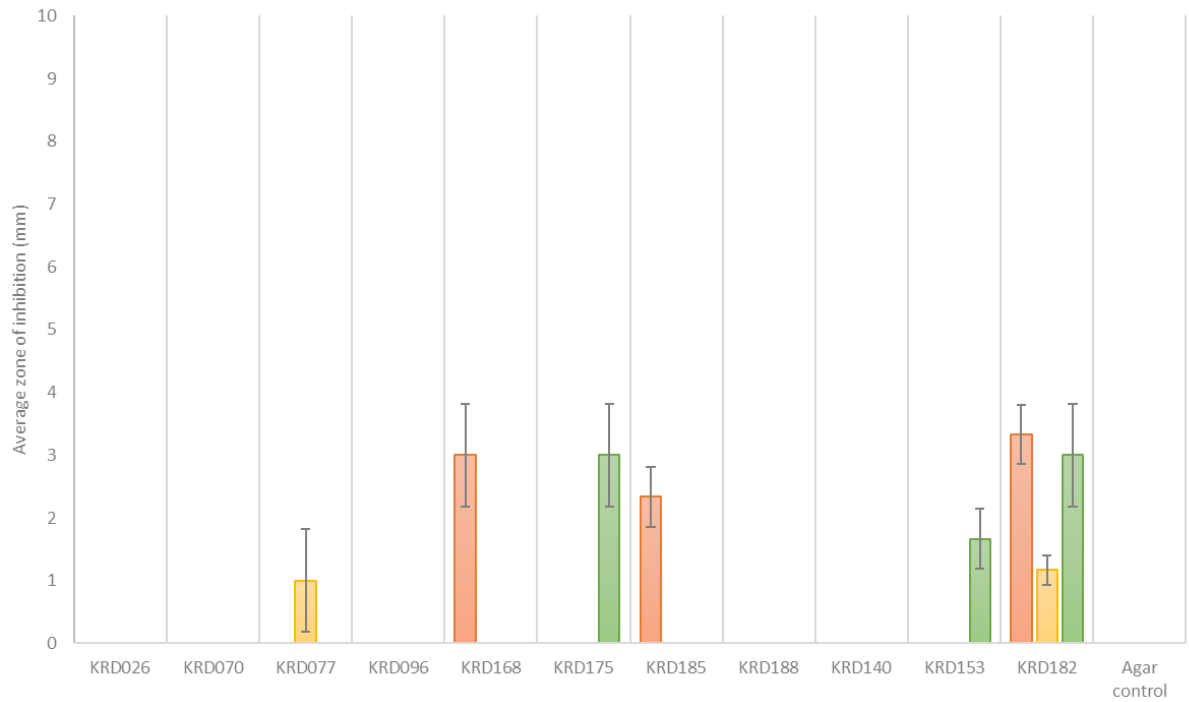


**Figure 4.3: Antibacterial activity of environmental isolates.** Average zones of inhibition (radius, mm) of 11 environmental bacteria (KRD strains) against three pathogens (*S. aureus*; red, *E. coli*; yellow, *P. aeruginosa*; green), error bars represent standard deviation (n=3).

The strains which showed antibacterial activity were nine LR isolates (LR2, LR3, LR4, LR6, LR9, LR10, LR14, LR15, LR16) and three KRD isolates with bioactivity against *P. aeruginosa* (KRD153, KRD175, KRD182). As such, prior to metabolite extraction work, their phylogenetic relationships were investigated by constructing a maximum likelihood phylogenetic tree. 16S rRNA gene sequences already existed for KRD175 and KRD182, and therefore these two were not included. Based on the BLAST analysis of 16S rRNA gene sequences to the NCBI database, strains LR2, LR3, LR4, LR6, LR9, LR10, LR14, LR15, and LR16 belong to the genus *Streptomyces*, as was previously hypothesised, and KRD153 belonged to the genus *Micrococcus*.

Phylogenetic analysis of these sequences revealed five major clades (A-E, **Figure 4.4**), which all belong to the genus *Streptomyces*, except clade E which contained *Micrococcus* spp.. However, the branches for LR4, LR15, and LR16 are supported by low bootstrap values (9%, 9%, 2%, respectively), indicating that these isolates cannot be phylogenetically delineated. Further, there are several branches with low bootstrap values; this is likely due to the highly conserved nature of the 16S rRNA gene, a known issue surrounding its use for phylogenetic analysis, particularly within the *Streptomyces* genus (253). Interestingly, when the phylogeny data is compared to the bioactivity data, KRD153 is the only strain which showed bioactivity against *P. aeruginosa* and is also the only strain which does not belong to the genus *Streptomyces*. However, *Streptomyces* spp. are infamous for their ability to produce a wide range of natural products, many with antimicrobial activity (145,254). Therefore, looking at the isolated LR strains belonging to the genus *Streptomyces*, all LR strains in clade A (LR10, LR9, LR6, LR3, LR2) show a high level of bioactivity against both *S. aureus* and *E. coli*, with all strains showing greater bioactivity against *E. coli* than *S. aureus*, with the exception of LR10. Additionally, two of the three strains in clade B (LR15 and LR4) showed no bioactivity against *E. coli*, and the third strain, LR16, showed around 66% less bioactivity against *E. coli* than *S. aureus*. In the future, it would be of interest to assay the bioactivity of the reference strains in all clades against the same three pathogens (*E. coli*, *S. aureus*, *P. aeruginosa*) to determine if this trend between clades holds up. This bioactivity data could be used to further highlight any relationships between strain phylogeny and antibacterial bioactivity.

Lastly, the media which were used to isolate these environmental actinomycetes were ISP2 and ISP7. These were chosen to capture taxonomic diversity within the order Actinomycetales, however these media only yielded strains belonging to the genus

*Streptomyces*. For example, all LR strains in clade A (LR10, LR9, LR6, LR3, and LR2) were isolated on ISP2 media. Therefore, it would be valuable to attempt further bacterial isolation work using a broader variety of media, as well as culture the isolated strains onto a range of media, using the one strain many compounds (OSMAC) approach (180), to elicit further antimicrobial activity from the strains. Following on from the phylogenetic analysis, the isolated strains which showed antibacterial activity were cultured to assess their produced metabolites for antibacterial activity.

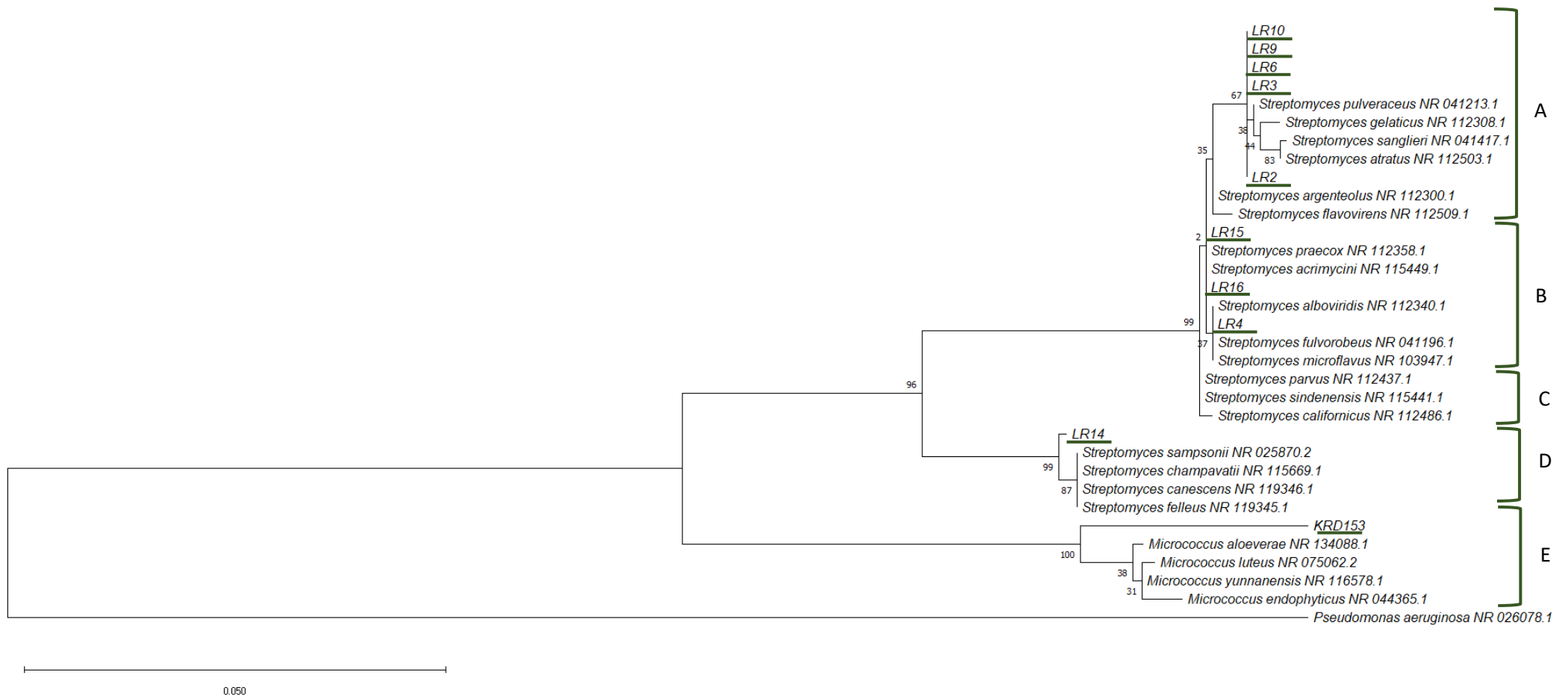


**Figure 4.4: Phylogenetic relationships of environmental isolates and closely related sequences.** Both partial and complete 16S rRNA gene sequences of 10 environmental isolates (underlined in dark green) and closely related sequences obtained from an NCBI BLAST (BLASTN) search. The tree was constructed using the maximum likelihood method and Tamura-Nei model, with the percentage of bootstrap replicates (1000 re-samplings) supporting the proposed branching order shown at the relevant nodes. *P. aeruginosa* was used as an outgroup. Scale bar shows 0.050 nucleotide substitutions per site.

The 12 bioactive actinomycetes (of the 31 total; 20 LR, 11 KRD strains) were all cultured and their metabolites were extracted from liquid media, with the strains grown in ISP2 or ISP7 broth for seven days prior to extraction. The resulting crude extracts were tested for antibacterial activity against the same three pathogens, to assess whether the produced bioactive metabolites were extracted from bacterial culture. Results showed that there was no bioactivity against *P. aeruginosa* from any of the crude extracts, this was expected from the nine LR strains which were not bioactive previously using the plug assay. However, surprisingly the three KRD strains also showed no bioactivity against *P. aeruginosa*, despite showing bioactivity in the plug assay. Furthermore, there was also no antibacterial activity observed against *E. coli* or *S. aureus* either (data not shown), despite earlier bioactivity in plug assays. This could be due to the active metabolite not being extracted by the EtOAc due to the polarity of the solvent (249), although this would seem unlikely for all the extracts. Furthermore, the earlier bioactivity was assayed using plugs from agar plates (also a seven-day incubation). Therefore, it would be of interest to carry out the solvent metabolite extractions from agar plates and compare the bioactivity of the crude extract with those from the liquid extraction as carried out here. Lastly, it would also be interesting to carry out solvent extractions of metabolites using a wider range of solvent polarity, such as more polar MeOH and less polar dichloromethane, to see if additional bioactive metabolites could be extracted.

As there was no antibacterial activity from any of the crude metabolite extracts, they were instead tested for their ability to inhibit *P. aeruginosa* biofilm formation. This was carried out using a CV assay, as antibiotic and antibiofilm agents target different cellular pathways and inhibition mechanisms. All 12 crude solvent extracts, those from strains which had previously shown antibacterial activity using the plug assays, were tested (LR2, LR3, LR4, LR6, LR9, LR10, LR14, LR15, LR16, KRD153, KRD175, KRD182). Of these 12 extracts, all except LR9 showed biofilm-inhibitory activity against *P. aeruginosa* (**Figure 4.5**). This was interesting as nine of the 12 extracts did not show antibacterial activity against *P. aeruginosa* using the plug assay, and none showed bioactivity when metabolite extracts were tested. As mentioned previously, antibiotics often target different pathways to antibiofilm agents, and it is therefore likely that these extracts are targeting biofilm-related pathways which are not bacteriostatic or bactericidal. As the extract is added before the biofilm forms, the pathways targeted are possibly involved in biofilm formation, such as the production of EPS or

sequestering host molecules, rather than biofilm maintenance or dispersal. LR16 crude extract had the highest *P. aeruginosa* biofilm inhibition (73.2%) after four hours compared to controls. Interestingly, LR16 was the only isolated strain which was cultured, and the metabolites extracted, on ISP7. As the other strains were grown on ISP2, they may be undergoing carbon catabolite repression due to the three carbon sources in ISP2 media. This may result in reduced specialised metabolite production. Further, LR9 was grown on ISP2, and had the greatest antibacterial activity against *S. aureus* and *E. coli* (**Figure 4.2**). Here, LR9 increased the formation of biofilm, rather than inhibiting it; 107.1% biofilm growth (-7.1% biofilm inhibition) compared to the *P. aeruginosa* and DMSO control. LR9 had the most potent antibacterial bioactivity in the plug assay, despite the fact that there was no observed bioactivity when metabolite extracts of the culture were tested. Therefore, the antibacterial activity of the extract may be eliciting a stronger biofilm response due to stress; an increase in biofilm formation as a method to protect cells and raise the minimum inhibitory concentration (MIC) required to kill them. This has been demonstrated previously; subinhibitory concentrations of gentamicin (1 µg/mL) increase the quantity of LESB58 biofilm formed when compared to the MIC (10 µg/mL) (**Supplementary Figure 4.1**). With the exception of LR9, all of the strains in clade A show similar biofilm inhibition abilities (range: 35.6 – 46.2%). There is no discernible difference between the antibiofilm activity of *Streptomyces* spp. and KRD153 (*Micrococcus* sp.), as KRD153 showed 48.9% inhibition, whereas the *Streptomyces* spp. inhibited between -7.1% and 73.2% biofilm formation. As all the crude metabolite extracts were normalised against *P. aeruginosa* and solvent, and LB and solvent controls, the antibiofilm activity can be attributed to the crude metabolite extracts, rather than the DMSO they are dissolved in. Furthermore, ISP2 and ISP7 media were solvent extracted, and showed no antibiotic or antibiofilm activity against PA14 or LESB58 demonstrating that the antibiofilm activity observed was a result of the bacterially produced metabolites (**Supplementary Figure 4.2**).

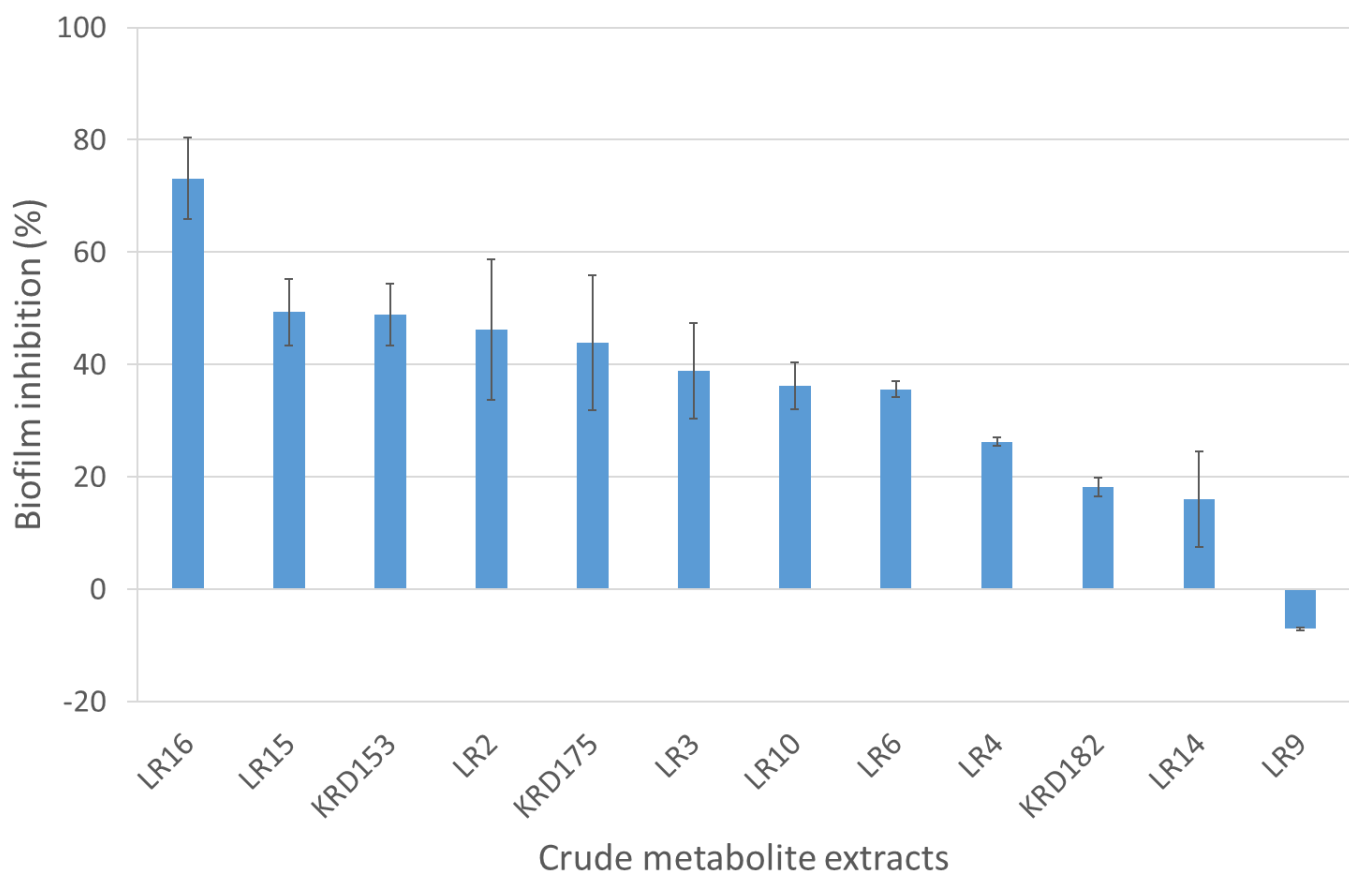


**Figure 4.5: Biofilm inhibition of *P. aeruginosa* by environmental bacterial metabolite crude extracts (in DMSO).** Antibiofilm activity measured after four hours using CV, normalised against *P. aeruginosa*+DMSO and the corresponding media only control (IPS2 or ISP7) to give a percentage of biofilm inhibition. Error bars represent standard deviation (n=3).

The most potent antibiofilm extracts (extracts LR15, LR16, and KRD153) were taken forward for fractionation using four organic solvents (MeOHdH<sub>2</sub>O, MeOH, ACN, EtOAc, in decreasing polarity), to separate the potential antibiofilm metabolites into fractions by polarity. This also enabled fractionated and non-fractionated metabolite extracts to be compared alongside antibiofilm bioactivity data to further dereplicate the potential antibiofilm metabolites responsible for the observed bioactivity. Although it was expected that the fractions would not exhibit antibacterial activity (against *S. aureus*, *E. coli* and *P. aeruginosa*), ahead of antibiofilm testing, they were assessed for antibacterial activity in case the deconvolution of metabolites in each extract tested enabled unmasking of bioactive constituents. Unfortunately, this was not the case, and no bioactivity was observed (data not shown). As the extracts previously showed antibiofilm activity against *P. aeruginosa*, it was of greater interest to assay if any of the 12 fractions showed antibiofilm activity. As the crude metabolite extracts showed strong antibiofilm activity, it was reassuring to see the fractionated extracts retained this bioactivity (**Figure 4.6**). The MeOHdH<sub>2</sub>O fraction of LR16 showed 71% biofilm inhibition. As the fractions were normalised against the corresponding fractionated media control, therefore biofilm inhibition can be attributed to the metabolites present in the fraction. Lastly, the MeOHdH<sub>2</sub>O fractions for extract LR15 and KRD153 show more than 100% biofilm growth (negative biofilm inhibition); likely a stress response resulting in an increase in biofilm formation, as seen with extract LR9 previously (**Figure 4.5**). When testing LR15 fractions, the less polar MeOH and ACN fractions showed 35% and 19% biofilm inhibition respectively. KRD153 had three fractions that showed biofilm inhibition, MeOH (5%), ACN (29%) and EtOAc (17%). Similarly, LR16 has two further antibiofilm fractions; MeOH (7%) and EtOAc (39% biofilm inhibition). Alongside the bacterial metabolite extraction and subsequent fractionation, corresponding media blanks were also extracted and fractionated. As these had no antibacterial or antibiofilm activity when assayed against either *P. aeruginosa*, it can be concluded that the results observed from testing the extracts and fractions correspond to the bacterial metabolites produced, and not the media (**Supplementary Figures 4.3 and 4.4**).

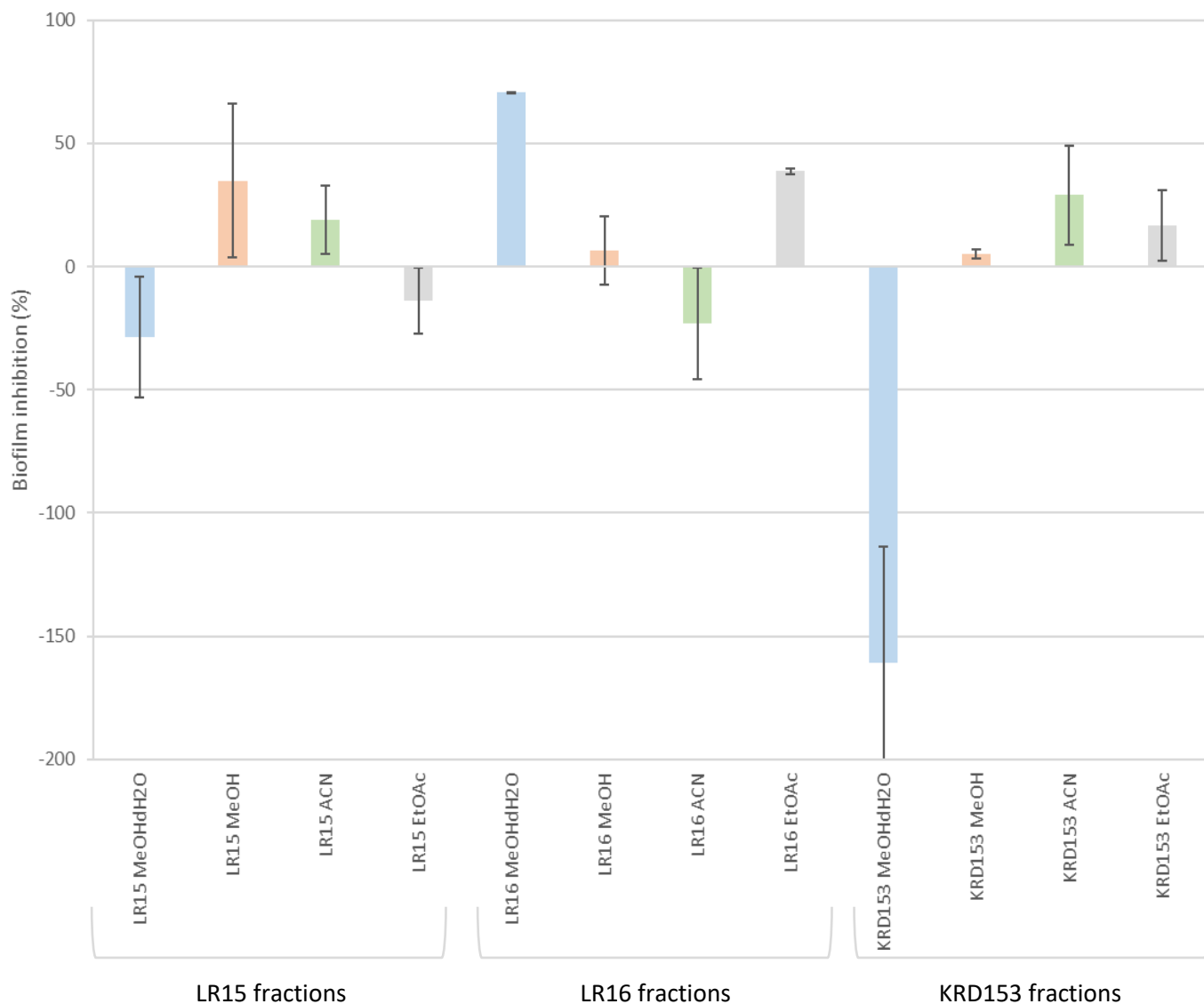


**Figure 4.6: *P. aeruginosa* biofilm inhibition of fractions of crude extracts from three strains (four fractions per extract) which showed most antibiofilm activity previously.** Antibiofilm activity of fractions (MeOHdH<sub>2</sub>O; blue, MeOH; orange, ACN; green, EtOAc; grey) measured after four hours using CV and normalised against *P. aeruginosa* + corresponding media fraction to give percentage biofilm inhibition. Error bars show standard deviation (n=3).

The three crude metabolite extracts with antibiofilm activity (KRD153, LR15 and LR16) and their four solvent metabolite fractions (12 total, various antibiofilm activities), underwent untargeted metabolomics analysis by LC-MS/MS. Using this data, comparative metabolomics was conducted using molecular networking. These networks are comprised of nodes, each representing a molecular ion connected by edges based on the structural similarity of the metabolites. As such, structurally related analogues of metabolites cluster together into molecular families and some unique metabolites, unrelated to anything in the network can be seen as singletons. Each node colour corresponds to a fraction or extract, with the media and solvent controls greyed out, as such all coloured nodes are bacterially produced metabolites.

In the molecular network of KRD153 crude extract and fractions (**Figure 4.7**), there are 653 nodes, with 539 nodes belonging to media and solvent controls (83%), which is an unexpectedly large proportion. However, it is well known that *Micrococcus* is slow growing, and as such, it might be at a disadvantage with a seven-day extraction. It would be interesting to normalise this to growth stage in the future, or to optimize the extraction media for strains to maximise produced metabolites. There was also very little overlap between crude extract and fractions, with only 23 nodes (3.5% of total nodes, 20% of non-control nodes) shared between the crude extract and any fractions shared suggesting that perhaps metabolites got retained on the column during fractionation or that the quantities of metabolites compared are so low it is not an accurate comparison. The crude extract (red) shared no produced metabolites (nodes) with the MeOH:H<sub>2</sub>O or MeOH fractions (dark and pale oranges), indicating that there are less metabolites present in these fractions. Although the numbers and percentage of the overall network are low, these conclusions should be treated with caution. This is in-line with the biofilm inhibition data in **Figure 4.6**, as the fractions from extract KRD153 with antibiofilm activity were the ACN (yellow) and EtOAc (blue) fractions. These two fractions shared 12 produced metabolites with the crude extract (red). Further, there is a node ( $m/z$  284.961), which is only shared between the crude extract and the ACN and EtOAc fractions. This node has a match to a GNPS spectrum library; tris(2-chloroethyl) phosphate (TCEP), which is a plastic, and likely a contamination from laboratory consumables (185). There are 11 further molecular ions which were found in all three extracts, however none of these 11 had matches to the GNPS spectrum metabolite libraries. This is somewhat expected, as two of these nodes are singletons at the bottom of the

molecular network (highlighted in blue), with singletons suggesting chemical novelty, and therefore may not exist within the GNPS library (255). These singletons would be interesting to pursue further in the future, however it may be first necessary to repeat the extraction and analysis due to the TCEP node present.

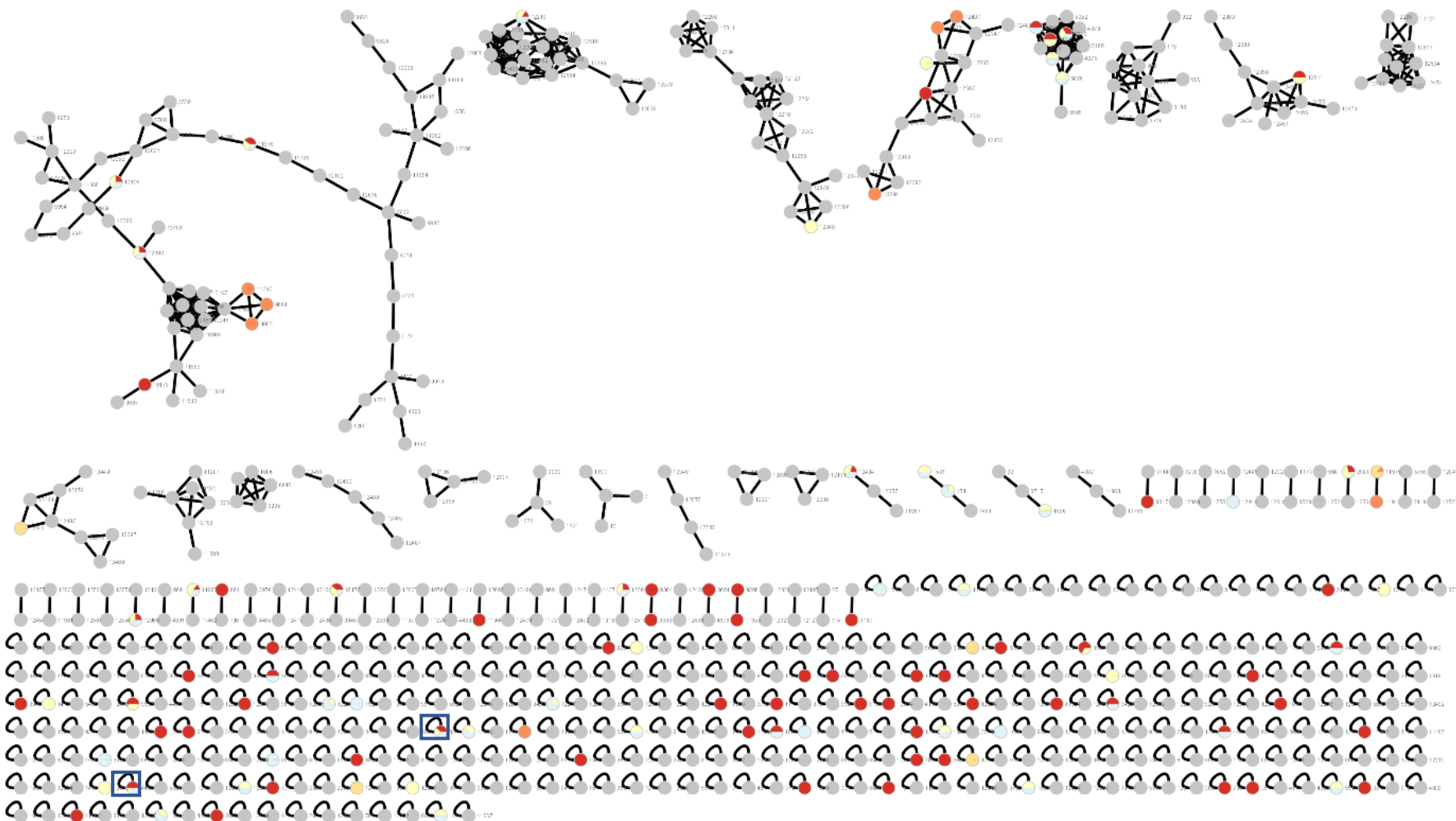


**Figure 4.7: Classical molecular network of KRD153 crude extract and its four fractions.** Extract KRD153 (red) and the 4 fractions; MeOH/H<sub>2</sub>O (dark orange), MeOH (pale orange ACN (yellow), EtOAc (light blue), features from ISP2 medium and solvent blanks are depicted in grey. Where a metabolite is present in more than one fraction, this is shown as a pie chart within the node with the colours of the shared features. Number of nodes = 653, number of edges = 827.

The molecular network for extract LR15 (**Figure 4.8**) is slightly larger than for KRD153, with 722 nodes, 535 of which belonging to the media and solvent controls; the number of nodes representing controls is comparable to the molecular network for KRD153 and is therefore reaffirming that there are nearly 200 nodes of interest from the LR15 extract and fractions. Interestingly, there are 45 nodes belonging to metabolite fractions which are not shared with LR15 crude extract (24%), which is unexpected, as the fractions contain metabolites which are also present in the crude extract. Furthermore, there are 123 nodes belonging to the crude extract that are not shared with any of the fractions (66%). Lastly, the antibiofilm fractions identified in **Figure 4.6** were MeOHdH<sub>2</sub>O and EtOAc fractions. There are only three molecular ions ( $m/z$  245.174, 421.148, and 515.245) (highlighted in blue) which are shared between the crude extract (red) and the MeOHdH<sub>2</sub>O fraction (dark orange), however only one of these produced metabolites ( $m/z$  421.148) has a spectral match in the GNPS library; methyl 2-[[4-hydroxy-3-(3-methylbut-2-enyl)phenyl]methyl]-3-(4-hydroxyphenyl)-4-methoxy-5-oxofuran-2-carboxylate. Interestingly, this metabolite is a singleton on the molecular network, which indicates chemical novelty. However, looking at the chemical formula, this is an analogue of olomoucine (256); olomoucine has a methyl group which has been replaced by a hydroxy group. Olomoucine is a cyclin-dependent kinase (CDK) inhibitor, and as CDKs are a target of many cancers, olomoucine has been investigated as a potential anticancer agent (256). Lastly, there are no nodes which are shared between the crude extract and EtOAc fraction (blue). These data align with the antibiofilm data clearly, as there were potential antibiofilm metabolites seen in the crude extract, and antibiofilm activity in the MeOHdH<sub>2</sub>O fraction. Furthermore, there were no potential ions in the EtOAc fraction, and limited antibiofilm activity from the EtOAc fraction. Finally, looking at the nodes which are shared with the standards, there is an ion peak ( $m/z$  261.159) shared between the media blank and the crude extract (highlighted in green) which has a spectral match in the GNPS library to cyclo(L-Phe-D-Pro). This peptide is a stereoisomer of the antifungal natural product, cyclo(L-Phe-L-Pro) (257). Further, cyclo(L-Phe-D-Pro) has been extracted from marine bacteria previously (258). Therefore, this is potentially one of the antibiofilm metabolites present in the crude extract.

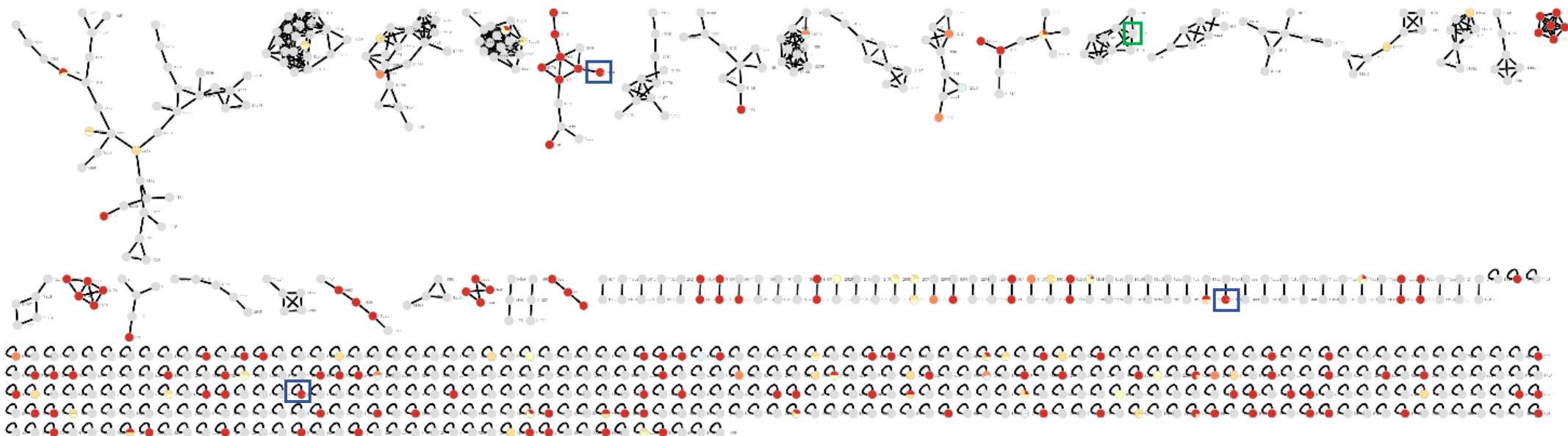


**Figure 4.8: Classical molecular network of LR15 crude extract and its four fractions.** Extract LR15 (red) and the 4 fractions; MeOHdH<sub>2</sub>O (dark orange), MeOH (pale orange), ACN (yellow), EtOAc (light blue), features from ISP2 medium and solvent blanks are depicted in grey. Where a metabolite is present in more than one fraction, this is shown as a pie chart within the node with the colours of the shared features. Number of nodes = 722, number of edges = 865.

Lastly, there are fewer shared nodes between the crude extract and any of the solvent fractions for extract LR16 (**Figure 4.9**), compared to both extract KRD153 and extract LR15. Despite this, there are a similar number of nodes for extract LR16 (723), as there were for extract LR15 (722), however there are 434 nodes pertaining to the media and solvent controls; nearly 100 fewer than both previous molecular networks. As mentioned previously, LR16 was grown in a minimal media (one carbon source), compared to isolates LR15 and KRD153 which were grown on ISP2 (three carbon sources). This potentially explains the difference in the media blanks; there may be less media ion peaks for extract LR16. There are 119 nodes that correspond to the crude extract only (red), and a further 73 which correspond to the crude extract and MeOHdH<sub>2</sub>O fraction (dark orange); which corresponds to the antibiofilm activity of the MeOHdH<sub>2</sub>O fraction seen in **Figure 4.6**. There is a large molecular family containing 10 produced metabolites belonging to the crude extract and MeOHdH<sub>2</sub>O fraction only (*m/z*; 273.206, 245.174, 285.242, 217.143, 239.161, 195.162, 259.190, 227.164, 255.195, 199.133) (**Figure 4.9, insert**). However, there were no spectral matches in the GNPS library with previously identified metabolites for any of these nodes. The shared ions between the crude extract and the antibiofilm efficacy of the MeOHdH<sub>2</sub>O fraction further supports the hypothesis that the MeOHdH<sub>2</sub>O fraction has antibiofilm properties. Further, there are 45 nodes pertaining to the EtOAc fraction (blue), not including media and solvent controls, which is expected as the EtOAc fraction also showed antibiofilm activity. Therefore, as expected, the MeOH and ACN fractions showed only 12 and 14 produced metabolites each, respectively.

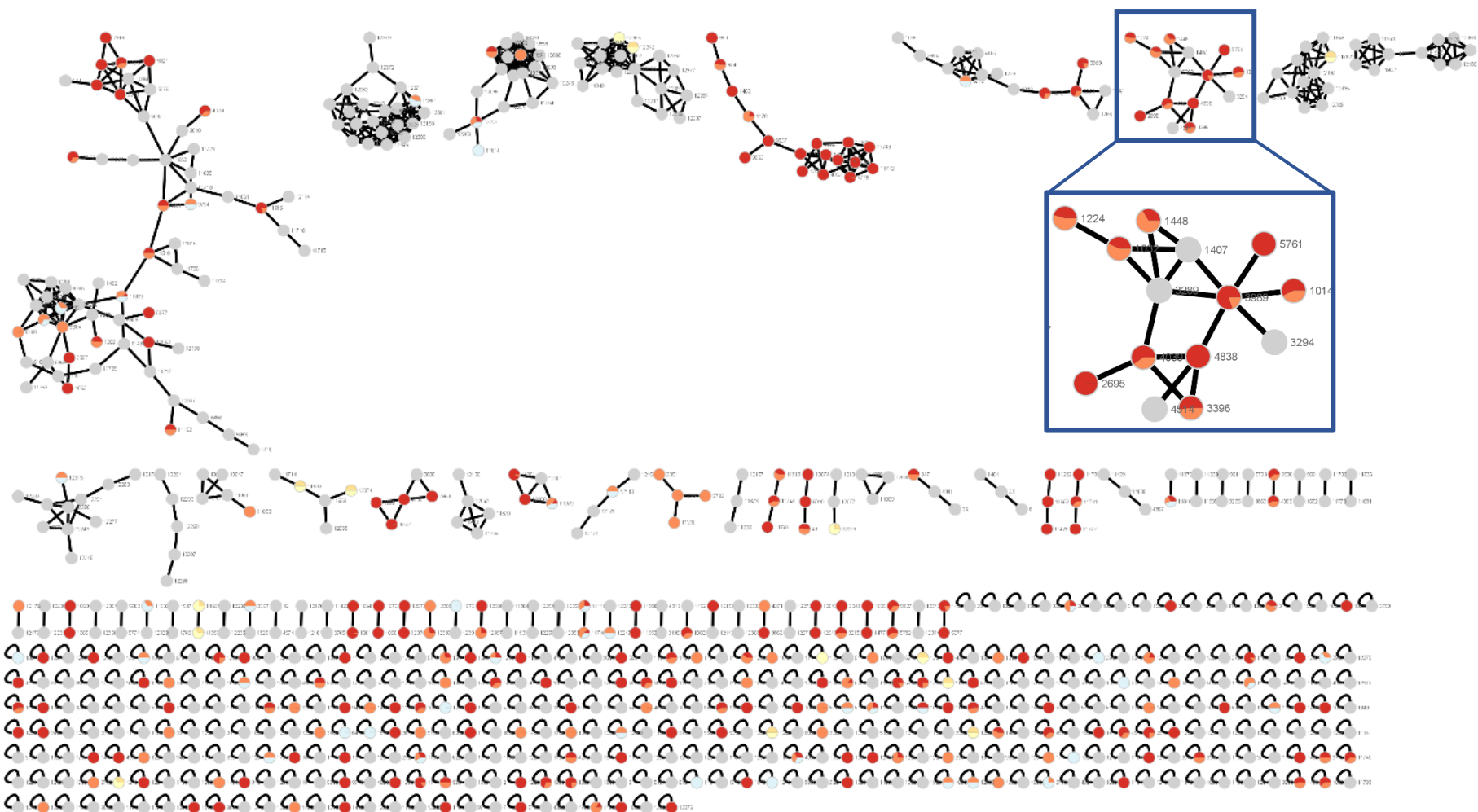


**Figure 4.9: Classical molecular network of LR16 crude extract and its four fractions.** Extract LR16 (red) and the 4 fractions; MeOHdH<sub>2</sub>O (dark orange), MeOH (pale orange), ACN (yellow), EtOAc (light blue), features from ISP7 medium and solvent blanks are depicted in grey. Where a metabolite is present in more than one fraction, this is shown as a pie chart within the node with the colours of the shared features. Number of nodes = 723, number of edges = 906. Insert – close-up of molecular family shared between the crude extract and MeOHdH<sub>2</sub>O fraction.

Finally, as the crude metabolite extract LR16 had the most potent antibiofilm activity compared to the other crude extracts (73% biofilm inhibition), the biofilm inhibition of LR16 extract were assayed using EIS (**Figure 4.10**). From the CV data, extract LR16 inhibited biofilm formation, it was therefore anticipated that there would be little to no decrease in impedance modulus; a decrease in impedance modulus indicates biofilm formation, as demonstrated in **Chapter 3**. PA14+extract (LR16) was measured by EIS alongside a PA14+DMSO control, as the extract was dissolved in DMSO. This showed DMSO had no biofilm-inhibitory effects, as after four hours, the impedance modulus values of PA14 and PA14+DMSO were 0.62136  $\Omega$  and 0.68556  $\Omega$ , respectively (no significant difference,  $p = 0.273$ ,  $n=3$ ). As expected from the LR16 extract CV data, after four hours, there was a significant difference between PA14+extract and LB+extract ( $p = 0.044$ ,  $n=3$ ), as well as the PA14+extract and PA14 control ( $p = 0.039$ ,  $n=3$ ). Demonstrating that the extract is inhibiting biofilm formation, and that this was being measured by EIS. Further, in the presence of the extract, there is a reduction in biofilm formation within 90 minutes, although this was not significant until four hours ( $p = 0.022$ ,  $n=3$ ). It may be that if the concentration of extract was greater than 1 mg/mL, it may reduce the biofilm formation further (resulting in an overall increase in impedance modulus). Lastly, the LB and the LB+extract controls show no significant difference between each other over the four hours ( $p = 0.803$ ,  $n=3$ ). As the desirable outcome for this experiment was to align with the LB controls, it was next necessary to assay further concentrations of extract LR16; to determine if the extract was influencing the LB or *P. aeruginosa*.

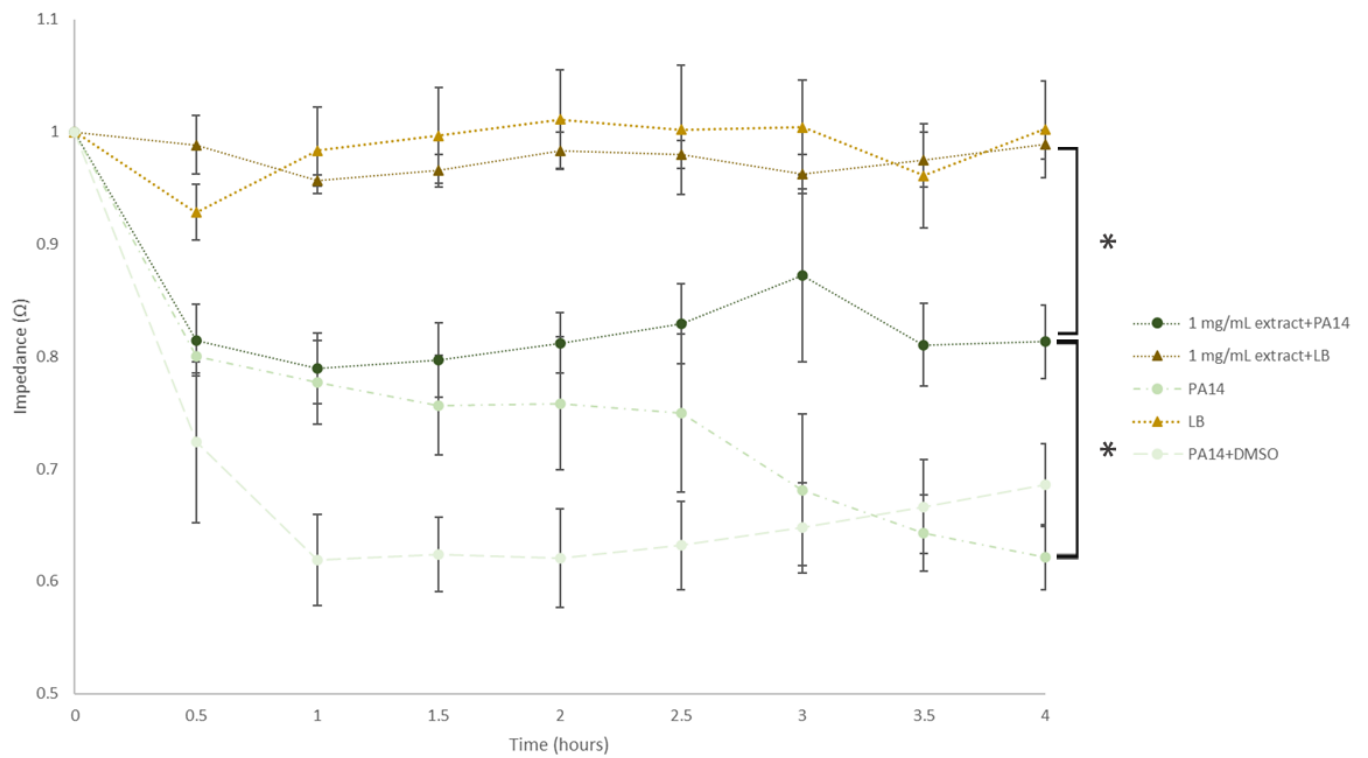


**Figure 4.10: EIS quantification of *P. aeruginosa* (PA14) biofilm inhibition by LR16 (1 mg/mL).** Impedance modulus quantified at 10 Hz over four hours with PA14 starting at  $OD_{600}=1$ . Data normalised by dividing each data set by their  $t=0$  value. Error bars show standard deviation,  $n=3$ , \* denotes significant difference ( $p < 0.05$ ).

Lastly, it was necessary to determine if higher impedance modulus values observed in **Figure 4.10** were caused by extract LR16 either inhibiting *P. aeruginosa* biofilm (and therefore a dose-dependent response would be observed) or impacting the LB media. A higher impedance modulus values indicates a lack of biofilm formation, as discussed previously. Therefore, two further concentrations of extract LR16 were assayed against *P. aeruginosa* (0.5 mg/mL and 0.25 mg/mL) (**Figure 4.11**). As hypothesized, the decreasing concentrations of extract LR16 against PA14 showed a dose dependent response, with a decrease in impedance modulus for the lower concentrations of extract, indicating biofilm formation. At 4 hours, the impedance modulus for 1 mg/mL, 0.5 mg/mL, 0.25 mg/mL, and 0 mg/mL were 0.81305  $\Omega$ , 0.75622  $\Omega$ , 0.67400  $\Omega$ , and 0.62136  $\Omega$ , respectively. Despite the large error, there was a significant difference between the lowest and highest concentrations of extract LR16 (1 and 0.25 mg/mL) after four hours ( $p = 0.044$ ,  $n=3$ ). Further, the lower concentrations of LR16 + LB controls showed no significant difference between any of the concentrations ( $p > 0.05$ ,  $n=3$ ) (**Supplementary Figure 4.5**). It can therefore be concluded that extract LR16 was inhibiting *P. aeruginosa* biofilm forming ability, rather than interfering with the LB control. As the lowest concentration of extract LR16 + PA14 followed the same trend as the PA14 only control, and shows no significant difference ( $p = 0.997$ ,  $n=3$ ), it appears that this concentration is not having any inhibitory effect on the biofilm. In the future, it would be insightful to assay higher concentrations of the LR16 extract to see if the biofilm response continued beyond 1 mg/mL.

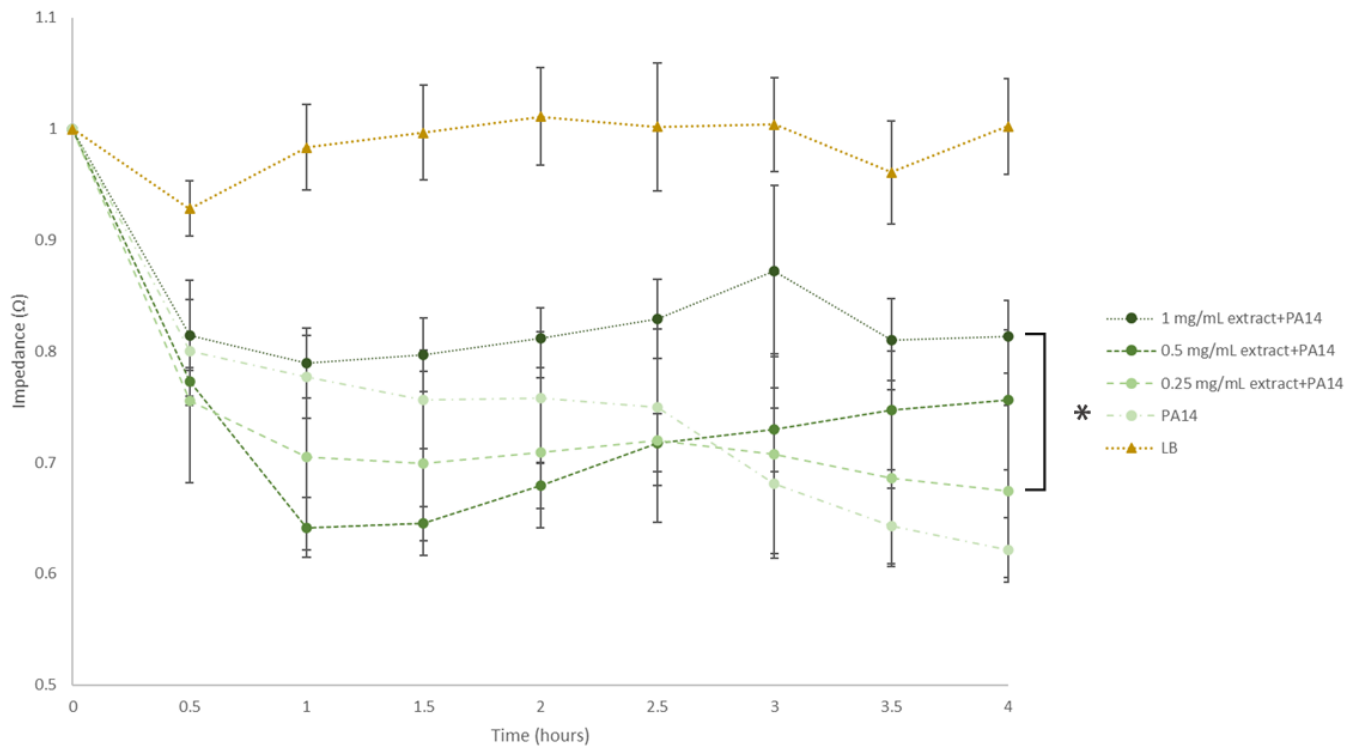


**Figure 4.11: EIS quantification of *P. aeruginosa* (PA14) biofilm inhibition by extract LR16 at decreasing concentrations.** Impedance modulus quantified at 10 Hz over four hours, with LR16 at 1, 0.5, 0.25, 0 mg/mL and LB media control (dark yellow), PA14 starting at  $OD_{600}=1$ . Data normalised by dividing each data set by their  $t=0$  value. Error bars show standard deviation,  $n=3$ , \* denotes significant difference ( $p < 0.05$ ).

#### 4.4 Discussion

The ISP media were originally designated for the identification of *Streptomyces* spp., with ISP2 belonging to the core four which are used in *Streptomyces* identification (ISPs 2, 3, 4, and 5) (202). However, other environmental bacterial genera have been isolated using ISP media, not just *Streptomyces*. Within the last 24 months, two novel species of *Pseudonocardia* have been isolated on ISP2 agar, *Pseudonocardia oceani* and *Pseudonocardia abyssalis* (247). Although, the authors incubated the isolation plates for four times the incubation period carried out here. Other similar studies have also carried out four-week incubations of ISP2 isolation plates in the hope of rarer actinomycete discovery (197). Despite these slow to culture strains, metabolite extraction and or bioactivity were sometimes carried out in relatively short time periods, such as seven to 14 days (33,10). It is therefore possible that slower growing Actinomycetota genera (not *Streptomyces*) were not isolated due to the seven-day standard incubation time of this study. However, within the Actinomycetales order, the genus *Streptomyces* produces 68% of all Actinomycetota-produced natural products (137), which accounts for up to 80% of all bioactive natural products (140).

All the environmental strains isolated as part of this thesis (LR strains) belong to the genus *Streptomyces*. In the phylogenetic analysis, clade A contains five of the environmental isolates, and the type strains also in this clade show some interesting bioactivity. *Streptomyces pulveraceus* was isolated more than 60 years ago, and previously shown to have antibiotic properties against both Gram-positive and Gram-negative bacteria (259). Interestingly, when *S. pulveraceus* was characterised, the authors found that it had stronger bioactivity against *E. coli* than *S. aureus*, as seen with four of the five strains in clade A (not LR10). Furthermore, the authors also found that there was no antibacterial bioactivity against *P. aeruginosa* using a plug assay (259), which again was seen here for all strains within clade A. It is therefore likely that one of the strains present in this clade is *S. pulveraceus*, although due to the low bootstrap values, these conclusions should be made with caution. As well, due to the low bootstrap values, it is possible that the LR strains in clade A are the same strain; however they exhibited differing morphologies and bioactivity profiles. Furthermore, the isolation of fostriecin, a type-1 polyketide synthase antibiotic isolated from *S. pulveraceus* in 1961 (260), supports the possibility that one of the strains in Clade A is *S. pulveraceus*, due to the observed antibacterial activity from those strains.

Fostriecin has also been shown to exhibit antitumour properties (260), no studies could be found looking into the antibiofilm activity of fostriecin, however none of the strains within clade A exhibited more than 50% biofilm inhibition, with LR9 encouraging the formation of biofilm when compared to the PA14 only control. Another type strain in clade A is *Streptomyces sanglieri*, which was described in 2002 (261). *S. sanglieri* is another soil isolate, and a known antibiotic producer; producing lactonamycin Z, which has been shown to have antibacterial activity against *S. aureus* (262). Furthermore, lactonamycin Z is another known antitumour compound (262). It is not unexpected that *S. sanglieri* produces an antitumour compound as well as an antibiotic, given the genetic similarities between *S. sanglieri* and *S. pulveraceus*. Lastly, *Streptomyces gelaticus* is another antibiotic producing *Streptomyces* sp.. *S. gelaticus* produces elaiomycin, which has been shown to have antibiotic activity against *E. coli* and *S. aureus*, as well as *P. aeruginosa*, despite the other strains within this clade showing no anti-*P. aeruginosa* bioactivity (263).

Fostriecin and lactonamycin Z are only a few of the antibiotics which have been found to have other biomedical properties (260,262). There has been a recent resurgence in drug repurposing; the re-screening of compounds approved for human use for potential antimicrobial activity, given the antimicrobial resistance crisis. For example, antiviral properties of a fish poison were found by Buranda, *et al.*, in 2018 (147). As well, antidepressants and antipsychotic medications were found to 'reverse' the antimicrobial phenotype of the screened pathogens; both Gram-positive and Gram-negative (264). Although not a novel treatment, it allows for the use of pre-approved antibiotics to be repurposed. Therefore drug development time is shortened, as the drug's safety profile is already known and preclinical tests have already been carried out; saving both time and money (265).

This is not the first description of the extraction of an antibiofilm agent from *Streptomyces*. In 2021, an antibiofilm agent active against *S. aureus* was described, with antibiofilm activity against antibiotic resistant strains too (176). The described experiments did not test against any other pathogens, so it is not clear if the isolated strain and extract would have antibiofilm activity against any other pathogens, including Gram-negative strains. Further, only strains which showed bioactivity against *S. aureus* in a disk diffusion were tested for their antibiofilm activity against *S. aureus*. By this selection criteria, bacterial isolates LR15 and LR16 would not have undergone extractions, and the subsequent antibiofilm activity would

not have been observed. Similarly, a *Streptomyces* strain (MUSC 125) isolated in Malaysia was found to have both antibiotic and antibiofilm activity against *S. aureus* (216). As in the 2021 study, the authors did not assay any other pathogens, and therefore it is not known if the extract, MUSC 125, has any bioactivity against Gram-negative pathogens. Finally, another 2021 study extracted angucycline from marine *Streptomyces* and found it to be a viable antibiofilm agent with low toxicity to zebrafish (143). Once again, this was only tested against *S. aureus*, and therefore any ability to inhibit Gram-negative biofilms is unknown. This tendency to test solely against Gram-positive pathogens is of concern, as Gram-negative bacteria are typically harder to treat than Gram-positive bacteria, and when comparing biofilms, *P. aeruginosa* was found to form stronger biofilms than *S. aureus* (74). Finally, all antibiofilm assays described above, and 80% of antibiofilm testing described a recent mini-review (60), use end-point assays, such as CV and other staining techniques, to determine whether the antibiofilm agent is successful (60,74,143,155,176,216). The use of EIS to monitor biofilm response to antibiofilm agents could revolutionise biofilm drug discovery; to allow researchers to identify the time to kill (TTK) and MIC in real-time.

Lastly, although there were no spectral matches for the metabolites extracted from LR16, which showed the strongest antibiofilm activity, one of the metabolites extracted from LR15 was cyclo(D-Pro-L-Phe) (referred to as DL). This metabolite has been synthesized previously, and shown to exhibit strong antibiotic activity (MIC = 0.10 µg/mL) against the fish pathogen, *Vibrio anguillarum* (258). Furthermore, due to the two chiral carbons present, there are three other stereoisomers this metabolite can form; cyclo(D-Pro-D-Phe), cyclo(L-Pro-D-Phe), cyclo(L-Pro-L-Phe), referred to as DD, LD, and LL, respectively. Three of the four isomers were isolated from bacteria derived from marine organism, *Pecten maximus* (258). These three isomers, not LL, have been shown to have the antibiotic activity against *V. anguillarum*, with DD exhibiting the lowest MIC at 0.03 µg/mL (258). Despite not showing antibacterial activity, in another study LL, isolated from a jellyfish-derived marine fungus, was shown to be neuroprotective against oxidative stress-induced neurodegeneration (257). Although the LR15 crude extract, and MeOHdH<sub>2</sub>O and EtOAc fractions demonstrated antibiofilm activity against *P. aeruginosa*, one of the stereoisomers, LD, has previously showed strong growth promoting activity towards *E. coli*, both planktonically and in biofilm (266). This is despite the fact that there was no activity against the other two pathogens tested here (*E. coli* and *S. aureus*). Furthermore, LD is the stereoisomer least similar to DL, due to both chiral carbons

being in the opposite position to DL (the isolated metabolite), and therefore this may be why the published activity is in such contrast to that of extract LR15.

#### 4.5 Conclusions and future work

From this work, an antibiofilm agent produced by a marine bacterial isolate (extract LR16) was found to be bioactive against *P. aeruginosa* biofilms. Extract LR16 showed no biostatic or biocidal activity when assayed by disk diffusion, however prevented the formation of *P. aeruginosa* (PA14) biofilms when assayed with CV. This activity solely against *P. aeruginosa* biofilms has strong implications in the treatment of CF and burns patients, which are prone to *P. aeruginosa* colonisation. The antibiofilm extracts were successfully assayed with EIS measurements which showed real-time biofilm quantification and subsequent reduction of biofilms when exposed to marine extracts. Most of the assays in this chapter have been carried out solely in *P. aeruginosa*, as the electrochemical assays were developed and optimised for *P. aeruginosa* only. In the future, as the bacterial isolates at the beginning of this chapter were assayed against *S. aureus*, *E. coli*, and *P. aeruginosa*, it would be of interest to determine if any of the crude extracts showed antibiofilm activity against the other pathogens. Although the biofilm quantification would likely be able to be carried out with EIS, as this quantifies the build-up on the sensor, SWV measurements were optimised for the detection of pyocyanin, a *P. aeruginosa* metabolite. It would also be of interest to whole genome sequence strain LR16. This *Streptomyces* sp. appears to produce a metabolite not currently produced by close relatives, and therefore a whole genome sequence would identify the producing strain and give some indication as to whether the metabolite is known or not. Lastly, high pressure liquid chromatography could be employed to separate the antibiofilm metabolite from the LR16 MeOH:H<sub>2</sub>O fraction in the first step towards identification of the antibiofilm agent. This would then enable further assays using the pure antibiofilm metabolite in determining a potential mechanism of action against *P. aeruginosa*.

## 5.0 Real world applications of electrochemical sensing

### 5.1 Introduction

The colonisation of medical implants by pathogens, and the subsequent biofilm formation is a significant health threat and considerable complication of some common medical procedures (56). For infections associated with vascular grafts, mortality occurs in 33% of patients, and of the surviving 67% of patients, 75% require at least one limb amputation (106). These medical implant infections touch all areas of medicine, including coma (96) and cancer patients (267). For example, one study found 18.8% of patients undergoing post-mastectomy breast reconstruction surgery following a mastectomy developed an infection, of these 73% had positive wound cultures. These salvaged cultures showed the most common infective species was *Staphylococcus aureus* (37.5% of all cultures), and the most common Gram-negative pathogen was *Pseudomonas aeruginosa*, with Gram-negative bacteria responsible for more than 30% of all implant infections (267,268). As well as initial biofilm formation, implant infections have also been shown to reoccur. One study demonstrated that *P. aeruginosa* infections recur more frequently than any other pathogen studied, required more surgical interventions and had poorer patient outcomes (98). This is potentially due to *P. aeruginosa* colonisation hindering wound healing through the secretion of pseudolysin and protease IV (269). Another study also found that the most common infective species was *S. aureus*, likely due to its commensal colonisation of the skin, and found that implant infection rates vary wildly in India (between 1.6% and 38%) (46). This is possibly in part due to discrepancies in the classification of a surgical site infection, with some studies including all infections within a year of surgery that require antibiotics (267), in contrast to only infections requiring hospitalisation (46), and only including infections for a few months post-surgery instead (268).

The material associated with an implant infection may play a role in infection frequency, however one study looking at two different types of graft material; polytetrafluoroethylene (PTFE) and Dacron graft, showed only a 1.7% difference in infection incidence between the two materials (97). Dacron graft is a woven, polyester material commonly used for aortic grafts (97,270). One retrospective study looked at a cohort of patients receiving a synthetic graft bypass for the femoral artery, and showed that 5% of patients developed an implant infection (97). Similarly, another study found graft-related infections affected 6% of patients

(270). However, it has also been noted that the infection rate of aortic grafts can be as high as 58% of patients in a higher risk category, such as patients with complications from smoking, diabetes, or obesity (97). Despite how commonly Dacron graft is used, it has been shown to have high levels of bacterial adhesion both *in vitro* (108) and *in vivo* (271) compared to other commercially available options. These include silver-infused graft materials, which attempt to use silver as biofilm-preventative (108), and iodine-infused wound dressings (272). This was demonstrated nearly 50 years ago *in vivo*, with signs of infection found in 33% of Dacron graft-recipient animals, compared to 0% of those treated with comparison graft material (271). Furthermore, a common pathogen associated with Dacron graft implant infections, *P. aeruginosa*, has been found in more than 10% of all implant infections (270), and *P. aeruginosa* infection on grafts were more likely to recur and require further surgeries (98). Lastly, implanted materials are often not discovered to have biofilms present until the implant is removed (57), or the patient develops sepsis and has become critically ill (57,96,273). Therefore, the ability to detect biofilms in real-time would have a significant impact in reducing the number of patients developing sepsis and other biofilm-associated infections (274). As mentioned previously, *P. aeruginosa* is a key pathogen in cystic fibrosis (CF) lung biofilms (112), and as such, much work has been undertaken to understand strains of this species further.

In 2006, Liberati, *et al.*, made a complete, nonredundant library of *P. aeruginosa* (PA14) transposon insertion mutants (PA14NR) to aid in genome-level studies of *P. aeruginosa*, and more specifically, the strain PA14. The authors colony purified the mutants, and therefore they were able to be used in genome-scale screens (199). These knockouts have allowed researchers to identify pathways which are inhibited by the redundancy of a gene. For example, studies of *Isp1A*, from the mutant library, was used for the screening of *P. aeruginosa* phage, and subsequently observe phage evolution. The authors showed which phage targeted the type IV pilus in *P. aeruginosa*, and which prophages prevent this targeted attack (275). Other work focused on mutations giving rise to antibiotic resistance and susceptible *P. aeruginosa* strains, and therefore which genes are ideal targets for antimicrobial therapy. For example, the gene *oprD* was shown to increase resistance to carbapenem antibiotics and dissemination *in vivo*, therefore inhibition of the *oprD* gene could lead to carbapenem-susceptible *P. aeruginosa* strains (276). The insertion mutant library has also been used to screen the effect of drugs on proteins or genes, including meta-

bromo-thiolactone, which inactivated two genes associated with quorum sensing, virulence, and biofilm formation (114). Finally, two drugs were screened against insertion mutants affecting biofilm formation, showing that *IsamiC* and *IsamiR* were involved in binding the antibiofilm agents to the protein AmiC (277).

There are many mechanisms and genes involved in biofilm formation, such as quorum sensing (*las* and *rhl* genes) (64) and pyocyanin production (*phzM*) (278). Therefore these pathways and redundancy library are pivotal to *P. aeruginosa* biofilm research (199,277). Many of these mutants reduce the quorum-sensing ability of *P. aeruginosa* (279), and this may therefore inhibit planktonic growth. It is therefore crucial to measure both planktonic and biofilm growth. Phenazine biosynthesis and the genes involved in this pathway are all implicated in pyocyanin production and biofilm formation (114). *lasR* and *rhlR* encode for quorum sensing receptor proteins; the inactivation of the associated genes reduces the virulence of PA14, including biofilm formation, and prevents quorum-sensing mediated killing (114,280). Alongside regulators *lasR* and *rhlR*, are the inducer enzymes, *lasI* and *rhlI*, which are located next to their respective regulator (further from the origin of replication) on the PA14 genome (**Figure 5.1**) (64). These pairs of regulators and inducers are the two main quorum sensing component systems in *P. aeruginosa*; clinical studies have found *las* enzymes in 94% of clinical isolates. The *las*-negative isolates were also found to be weaker biofilm formers (64). Interestingly, the elastase activity of *P. aeruginosa* is inactivated when *lasR* is inhibited, but not when *lasI* is inhibited; despite *lasI* inducing *lasR* (67). Another gene for targeting of biofilm formation is *phzM*. *phzM* is implicated in the pyocyanin biosynthesis pathway (**Figure 5.2**), which mediates the production *P. aeruginosa* virulence factors. These factors aid in biofilm formation and include pyocyanin. As demonstrated in this biosynthesis pathway, the *phzM* insertion mutant (*IsphzM*) prevents the conversion of phenazine-1-carboxylic acid to 5-methylpyrazine-1-carboxylic acid. 5-methylpyrazine-1-carboxylic acid is then converted via a different enzyme, *phzS* (278), however without the presence of *phzM*, *phzS* converts it to 1-hydroxyphenazine (**Figure 5.2**). The final insertion mutant used in this study was *IspqSA*. The disruption of the *pqsA* gene affects *P. aeruginosa* virulence by limiting the ability to form biofilms (281,282), disrupting quorum sensing ability (114,280–282), and reducing pyoverdine (281) and eDNA production (280). However, the reduction in pyoverdine production is biofilm dependent; and therefore this is not always observed by this mutant (281). Lastly, it is of interest to note that bacterially-produced metabolites, such

as actinorhodin, albaflavenone, pyocyanin, and pyoverdine, are often linked to lifecycle stage of the bacterium; with some metabolites, such as albaflavenone, produced once *Streptomyces coelicolor* germinates (189).

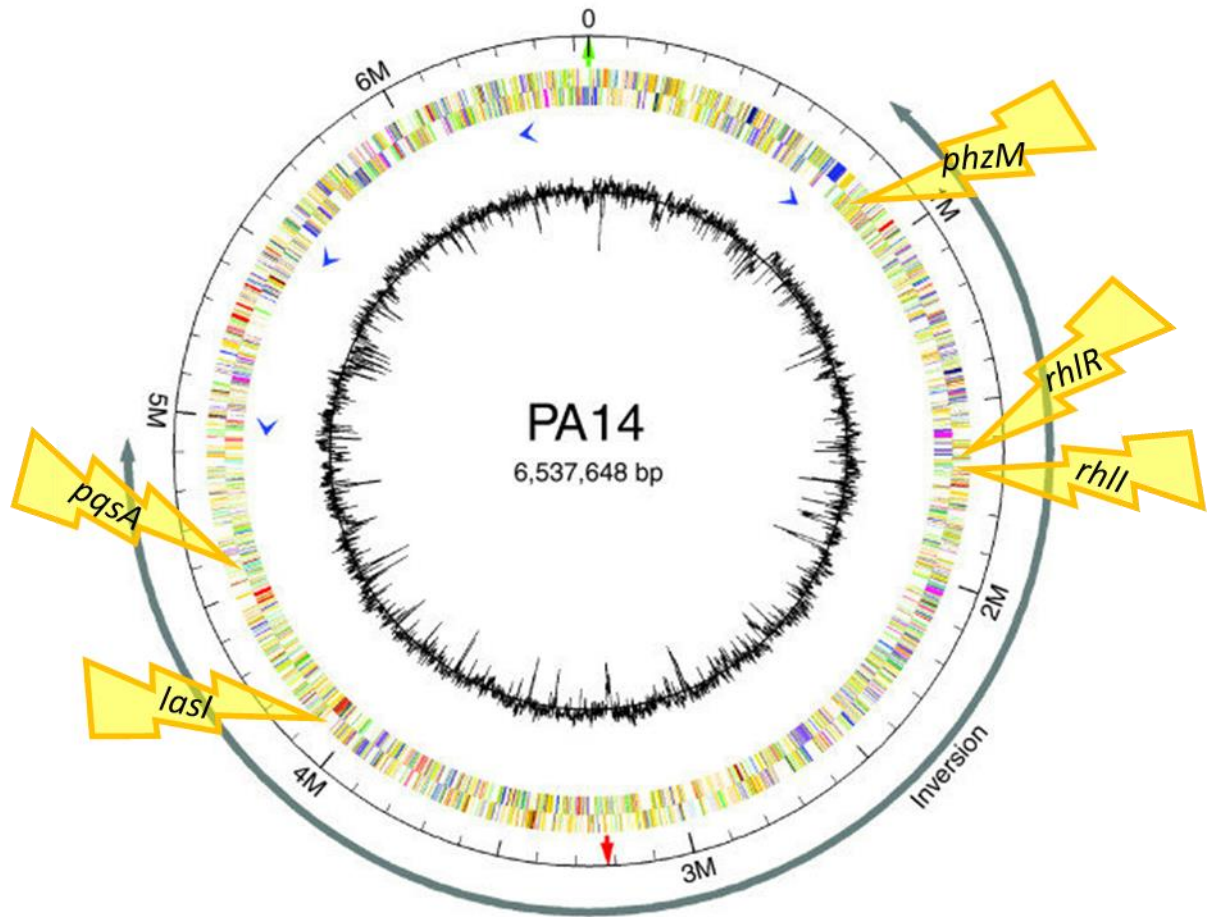


**Figure 5.1: Genome map of PA14.** Sites of insertion mutants used in this study, *phzM*, *rhIR*, *rhII*, *lasI*, and *pqsA*, marked around the edge. Circular map from Lee, *et al.* (54). The origin and terminus of replication indicated by the green and red arrows, respectively.

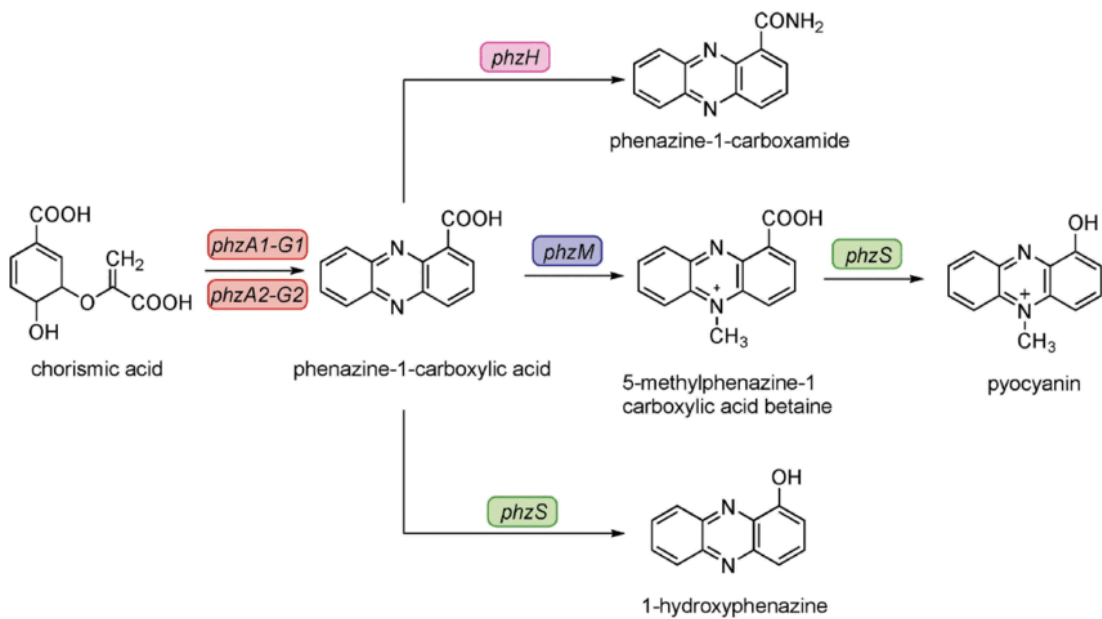


**Figure 5.2: Pyocyanin biosynthesis pathway.** Biosynthesis of pyocyanin and phenazines from chorismic acid and the *phz* genes associated with each step within the pathway. *phzM* is highlighted in purple in the centre. Pathway from Dong, *et al*, 2020 (283).

## 5.2 Aims and objectives:

The first aim of the work presented in this chapter was to design and establish a method for real-time biofilm growth and inhibition on medically relevant materials, assayed with *P. aeruginosa*, of which, PA14 and LESB58 were used, and Dacron graft was chosen as the medically relevant material of choice. The second aim was to assay the previously fractionated metabolite extracts against the biofilms of the two *P. aeruginosa* strains (PA14 and LESB58) using the previously established electrochemical techniques, square wave voltammetry (SWV) and electrochemical impedance spectroscopy (EIS), and to compare these to the literature 'gold standard' biofilm quantification technique, crystal violet (CV).

These aims were achieved through the following objectives:

1. To establish a method for biofilm formation on medically relevant materials
2. To quantify biofilms in real-time on medically relevant materials using both CV and EIS

To assay with EIS the fractionated metabolite extracts against these clinically relevant biofilms, formed using the established method for biofilm formation

### 5.3 Results

Initially, five insertion mutants of PA14, *Islasl*, *IsphzM*, *IspqsA*, *IsrhII*, and *IsrhIR*, were chosen for their ability to disrupt biofilm formation through reduced quorum sensing (281,282), or reduced eDNA (280) or virulence factor production (281). These mutants of PA14 were assayed for their ability to form biofilm and grow planktonically. Due to the pathways these mutants disrupt, it was hypothesised that at least one of the five insertion mutants would demonstrate a limited ability to form biofilm, but none of the insertion mutants would impact planktonic growth. As such, it would demonstrate their ability to be used in antibiofilm drug screening assays. This assessment was carried out using optical density (OD) and crystal violet (CV) measurements to quantify both planktonic and biofilm growth, respectively, in addition to the previously optimised electrochemical methods, SWV and EIS. Of the five insertion mutants assayed, three showed significantly less biofilm formation than the PA14 wild-type (WT) control ( $p < 0.001$  for all three mutants) (**Figure 5.3**); insertion mutants *Islasl*, *IsphzM*, and *IspqsA* had CV absorbance reads of 0.12, 0.15, and 0.14, respectively, each less than 50% of WT control (0.30 at 570 nm). These three insertion mutants were also not statistically significant from the LB media only control. As these PA14 mutants formed less than 50% biofilm compared to the WT PA14 strain, it suggested that the genes disrupted are involved biofilm formation. Furthermore, for the three insertion mutants which did not form biofilm, *lasI*, *phzM*, and *pqsA*, there was no statistically significant difference between the planktonic growth when compared to the PA14 control, as measured with absorbance reads at 600 nm prior to CV staining ( $p = 1.000$ ,  $p = 0.744$ ,  $p = 1.000$ , respectively, all  $n=3$ ). This further suggests that the mutants disrupt biofilm formation but not planktonic growth. The insertion mutants inactivating the *rhl* gene (*IsrhII* and *IsrhIR*) did not impact the formation of biofilm, and therefore it is likely that this gene is not essential for the formation of biofilm in PA14. The three mutants which impacted biofilm formation (*Islasl*, *IsphzM*, and *IspqsA*) were therefore taken forward to assay with the electrochemical techniques developed previously, to determine if these techniques could differentiate between WT PA14 and the mutants for both planktonic and biofilm growth. The biofilm growth could be quantified with EIS and the planktonic growth with SWV. It was therefore hypothesized that there would be an increase in current with SWV, indicative of planktonic growth. It was further hypothesized, there would be a limited decrease in impedance modulus indicating biofilm formation.

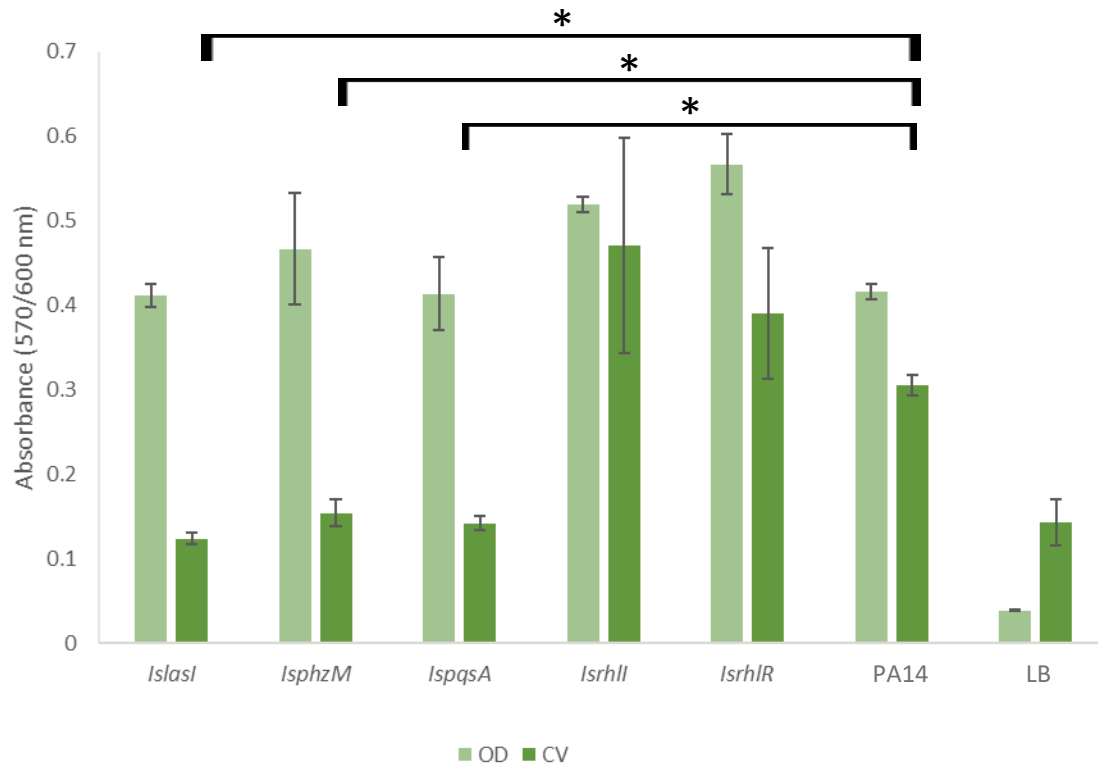


**Figure 5.3: Planktonic and biofilm growth of five PA14 insertion mutants.** Optical density (measured at 600 nm) (light green) and crystal violet (measured at 570 nm) (dark green) measurements of PA14 insertion mutants; *lasI*, *phzM*, *pqsA*, *rhlI*, *rhlR*, and PA14 WT and LB (media only) controls after four hours incubation. Error bars represent standard deviation, \* denotes statistical significance ( $p < 0.05$ ),  $n=3$ .

The three PA14 insertion mutants which inhibited biofilm formation when measured with CV (*IslasI*, *IsphzM*, and *IspqSA*) were assayed with both EIS (**Figure 5.4**) and SWV (**Figure 5.5**), to determine if the planktonic growth (SWV) and lack of biofilm formation (EIS) could be seen in real time using electrochemical techniques. An increase in pyocyanin production results in an increase in current in SWV, which positively correlates to planktonic growth of *P. aeruginosa* in a closed system (128), and in EIS, a lower impedance modulus value indicates biofilm formation on the sensor. As anticipated, the impedance modulus measurements (normalised against their corresponding  $t = 0$  value) after 4 hours for the three mutants and two controls were 0.92  $\Omega$  (*IspqSA*), 0.91  $\Omega$  (*IsphzM*), 0.88  $\Omega$  (*IslasI*), 0.60  $\Omega$  (PA14 WT strain control), 0.98  $\Omega$  (LB media control). As seen with the CV data previously (**Figure 5.3**), this confirmed that none of the three insertion mutant strains assayed formed biofilm within the four hours ( $p > 0.05$  for all three mutants compared to the LB media control). Furthermore, these three mutants were also assayed with SWV to look at quantification of the planktonic growth. This was important as all three were able to be quantified planktonically with OD<sub>600</sub> measurements previously, and this ability to be quantified in real-time allows for antibiofilm agent screening. However, only one insertion mutant, *IsphzM*, was able to be quantified with SWV (13.4  $\mu\text{A}$ ) at -0.35 V, the potential difference at which pyocyanin is detectable (128). This is used here as a proxy for planktonic growth, as shown in **Chapter 3**, and therefore *IsphzM* was the only mutant able to be quantified planktonically using electrochemical techniques. *IspqSA* and *IslasI* had current outputs of 0.07  $\mu\text{A}$  and 0.03  $\mu\text{A}$ , respectively, with no significant difference from the LB media control (0  $\mu\text{A}$ ;  $p = 0.536$  and  $p = 0.878$ , both  $n=3$ ). As SWV measurements have been optimised in **Chapter 3** using pyocyanin production as a proxy for planktonic growth, it is therefore likely that these two mutants are not producing pyocyanin, suggesting the insertion mutants have an inactivated phenazine biosynthesis pathway, reducing or eliminating pyocyanin production (135), and hence their planktonic growth cannot be quantified with SWV at -0.35 V. This was unfortunate as the phenazine biosynthetic pathway is only one gene cluster in the genome. Sequencing would be needed to confirm this hypothesis, and in future additional pigmented metabolites could be used to quantify *P. aeruginosa* planktonic growth, such as pyoverdine (281). These data show that biofilm reduction can be quantified using *P. aeruginosa* mutants without the addition of an antibiofilm agent. As mentioned, this has implications in the discovery and screening of

potential antibiofilm agents, as well as determination of which genes or biosynthetic pathway is affected by as a result of a drug or change in genotype, as has been previously shown (114,276,277).

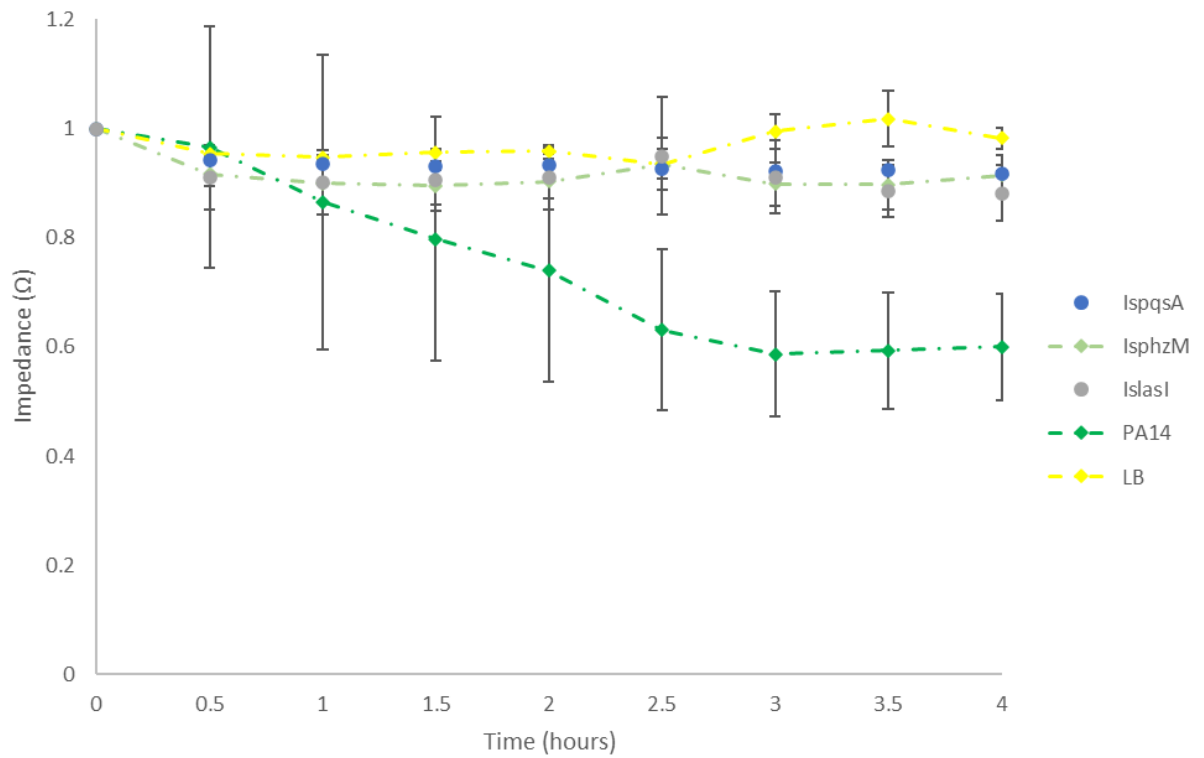


**Figure 5.4: Biofilm growth of three PA14 insertion mutants measured with EIS.** Impedance modulus measurements ( $\Omega$ ) over four hours of three PA14 insertion mutants; *lasI*, *phzM*, *pqsA*, PA14 WT and LB (media only) controls. Error bars represent standard deviation, n=3.

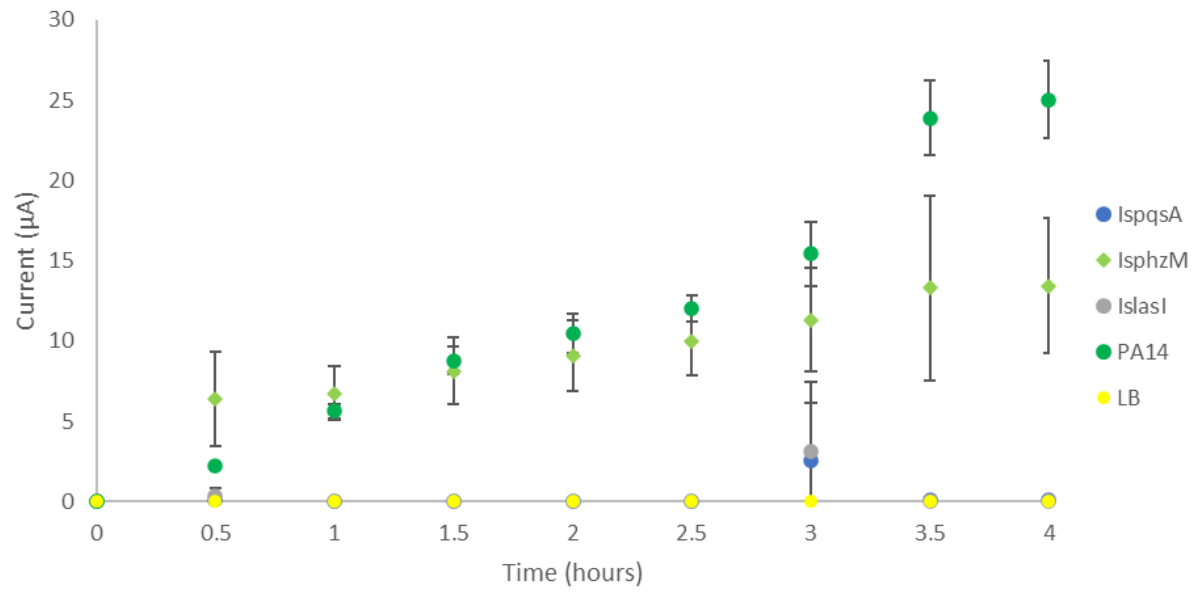


**Figure 5.5: Planktonic growth of three PA14 insertion mutants measured with SWV.** Current output ( $\mu\text{A}$ ) of PA14 insertion mutants; *lasI*, *phzM*, *pqsA*, PA14 WT and LB (media only) controls over four hours incubation. Error bars represent standard deviation,  $n=3$ .

In **Chapter 4**, an antibiofilm metabolite extract, LR16, was identified and assayed using SWV and EIS to assess planktonic growth (not impacted) and biofilm formation (reduced), respectively. Following on from this, extract LR16 was fractionated using four organic solvents (MeOHdH<sub>2</sub>O, MeOH, ACN, and EtOAc). Here, these solvent fractions were assayed with the previously developed electrochemical techniques, SWV and EIS. The goal of this work was to identify which fraction(s) contained the bioactive metabolite(s), and therefore make a step towards dereplicating the chemistry responsible for the phenotype. These assays were conducted using two strains of *P. aeruginosa*, PA14 and LESB58, as used previously. It was hypothesized that none of the fractions would inhibit planktonic growth of either PA14 or LESB58, as PA14 planktonic growth was not impacted previously. Furthermore, it was also hypothesized that at least one fraction would demonstrate antibiofilm activity against PA14 as the crude extract reduced PA14 biofilm formation by 75%. It would therefore seem likely that the biofilm formation of LESB58 would also be reduced, however as LESB58 is the stronger biofilm former (51), this was suggested tentatively.

Firstly, planktonic growth was measured using SWV to assess whether the metabolite fractions affected bacterial growth. Ideally, this would not vary and then biofilm formation would be able to be studied using EIS. As mentioned previously, here SWV measures the pyocyanin concentration within the media; this correlates to the planktonic growth of *P. aeruginosa* and has been used as a proxy here. The SWV results over four hours show that both strains of *P. aeruginosa*, PA14 (**Figure 5.6**) and LESB58 (**Figure 5.7**), grew planktonically in the presence of all four metabolite solvent fractions; an increase in current ( $\mu\text{A}$ ) indicates an increase in bacterial cell count.

After 4 hours, PA14 had a current of 1.46  $\mu\text{A}$ , lower than PA14 in the presence of all four metabolite fractions: 1.90, 4.16, 4.57, and 4.80  $\mu\text{A}$  for MeOHdH<sub>2</sub>O, MeOH, ACN, and EtOAc, respectively (**Figure 5.6**). However, none of these are statistically significant from the PA14 control (MeOHdH<sub>2</sub>O  $p = 0.878$ , MeOH  $p = 0.716$ , ACN  $p = 0.571$ , EtOAc  $p = 0.075$ ,  $n=3$  for all). Further, none of the fractions are statistically significant from one another ( $p > 0.05$  for all combinations). It can therefore be concluded the fractions are not inhibiting the planktonic growth of PA14; there is an increase in growth alongside the EtOAc fraction (light grey), but this is not significant ( $p = 0.075$ ,  $n=3$ ), likely due to the large amounts of error associated with SWV at higher current measurements (233). However, after four hours,

there is statistical significance between the LB control and the EtOAc fraction ( $p = 0.011$ ,  $n=3$ ), showing that this fraction does not inhibit planktonic growth. This supports some of the conclusions presented in **Chapter 4**, which saw no antibacterial activity from the metabolite extract fractions when assayed by zone of inhibition measurements against *P. aeruginosa* (PA14), as well as *S. aureus* and *Escherichia coli*. These data further support the use of SWV at  $-0.35$  V as a measurement of planktonic growth.

The bioactivity of the metabolite fractions against LESB58 were not assayed in **Chapter 4**, and therefore it was of interest to assay the effect of the fractions against this *P. aeruginosa* strain. This was because, as demonstrated previously, LESB58 forms an increased quantity of biofilm compared to PA14. After four hours, the current measurements ( $\mu\text{A}$ ) for LESB58 with the four fractions were 1.70, 2.53, 1.93, and 3.19  $\mu\text{A}$ , for MeOHdH<sub>2</sub>O, MeOH, ACN, and EtOAc, respectively (**Figure 5.7**). As seen with the PA14 only control, the LESB58 only control also had a lower current output than the fractions (1.65  $\mu\text{A}$  after four hours), and therefore less planktonic growth. As observed with PA14, there is no significant difference between the LESB58 only control and any of the four fractions ( $p > 0.997$  for all four fractions). This is to be expected, as there was no significance between PA14 only and any of the fractions (**Figure 5.6**), as well, there was no bioactivity seen against PA14 from any of the fractions in **Chapter 4**. As mentioned previously, the initial fraction is typically bactericidal, due to containing concentrated salts (165,284), however these data shows that both strains of *P. aeruginosa* are growing planktonically in the presence and absence of fractions, possibly indicating that there are limited salts within the MeOHdH<sub>2</sub>O fraction. These data were reassuring; the bacterial growth of both PA14 and LESB58 was not affected by the presence of any of the metabolite fractions or media fractions (demonstrated as they were used in normalisation of the data). As a result of the SWV data showing planktonic growth in the presence of all fractions, next, the ability of the fractions to impact biofilm formation for both *P. aeruginosa* strains were studied using EIS.

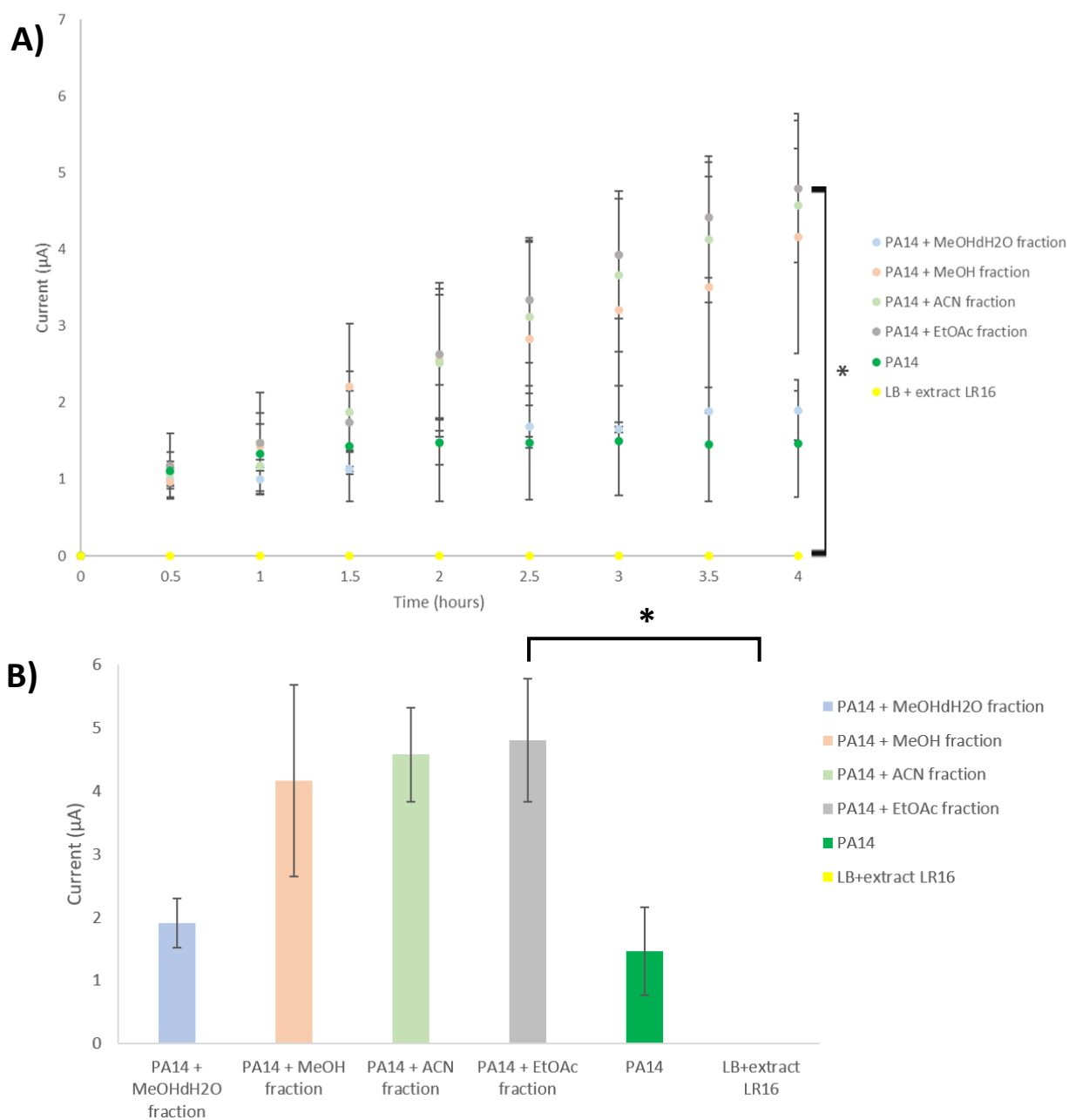


**Figure 5.6: Planktonic growth of PA14 grown alongside of four extract fractions measured with SWV. A)** Current output (µA) at -0.35 V of fractions (MeOHdH2O, MeOH, ACN, EtOAc) of extract LR16 against PA14 over four hours, normalised against their corresponding PA14 only and media only fractions. **B)** Four-hour timepoint represented as a bar graph. Error bars represent standard deviation, \* denotes statistical significance ( $p < 0.05$ ),  $n=3$ .

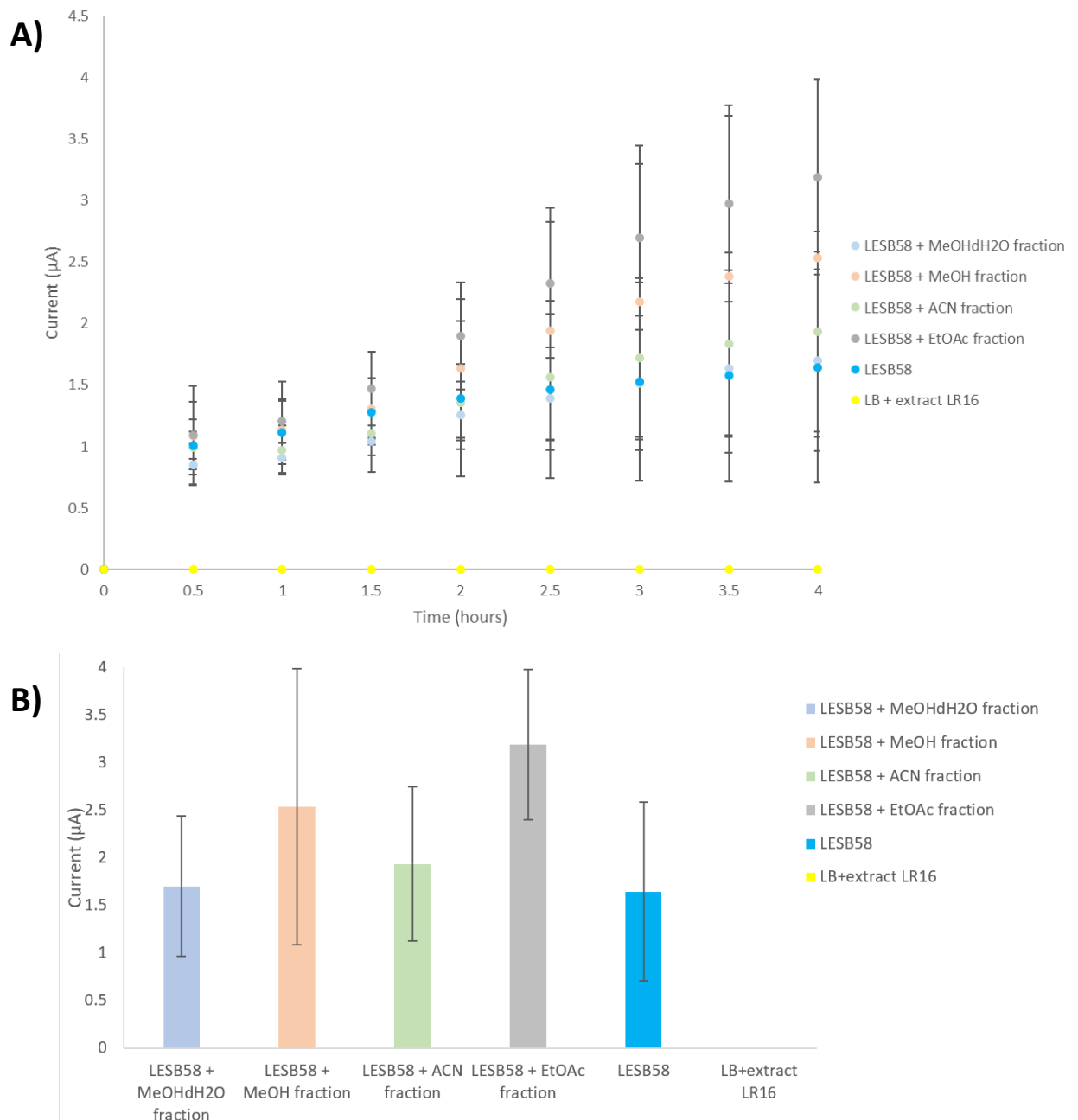


**Figure 5.7: Planktonic growth LESB58 grown alongside of four extract fractions measured with SWV. A)** Current output (µA) at -0.35 V of fractions of extract LR16 (MeOHdH2O, MeOH, ACN, EtOAc) against LESB58 over four hours, normalised against their corresponding PA14 only and media only fractions. **B)** Four-hour timepoint represented as a bar graph. Error bars represent standard deviation, n=3.

After demonstrating that all four fractions from both the extract LR16 and the media blank extract (**Supplementary Figures 4.2 and 4.3**) had no negative impact on the planktonic growth of either *P. aeruginosa* strain, the fractions were assayed using EIS for their ability to inhibit biofilm formation. As was shown in **Chapter 3**, a decrease in impedance modulus ( $\Omega$ ) over time, correlates to biofilm formation. Here, the results of each of the four fractions to inhibit biofilm formation of both strains are presented by fraction. To start, the MeOHdH<sub>2</sub>O fraction was tested. This is the most polar fraction and typically contains salts which can be inhibitory. Within an hour, the impedance modulus for both PA14 and LESB58 controls decreases, demonstrating that both strains are forming biofilm as expected and shown in **Chapter 3**. In the presence of the MeOHdH<sub>2</sub>O fraction (**Figure 5.8**), both strains have a limited decrease in impedance modulus over the four hours (LESB58+fraction = 0.851  $\Omega$ , PA14+fraction = 0.835  $\Omega$ ) which is not statistically significant from the LB only control (0.983  $\Omega$ ,  $p > 0.05$  for both strains). This shows that the MeOHdH<sub>2</sub>O fraction is inhibiting the biofilm formation for both PA14 and LESB58. After four hours, the quantity of biofilm formed without the presence of the fraction is statistically significant for both PA14 ( $p = 0.050$ ,  $n=3$ ) and LESB58 ( $p = 0.011$ ,  $n=3$ ) only controls. As demonstrated in both **Chapter 4** and **Figures 5.6 and 5.7**, the bacterial cells are not dying in the presence of salts in this fraction, as may be expected (165,284), so they are able to grow planktonically in the presence of both the extract and fractions. This demonstrates that the MeOHdH<sub>2</sub>O fraction is inhibiting the biofilm formation of *P. aeruginosa*. Next, it was of interest to assay the remaining fractions for their ability to also inhibit biofilm formation.

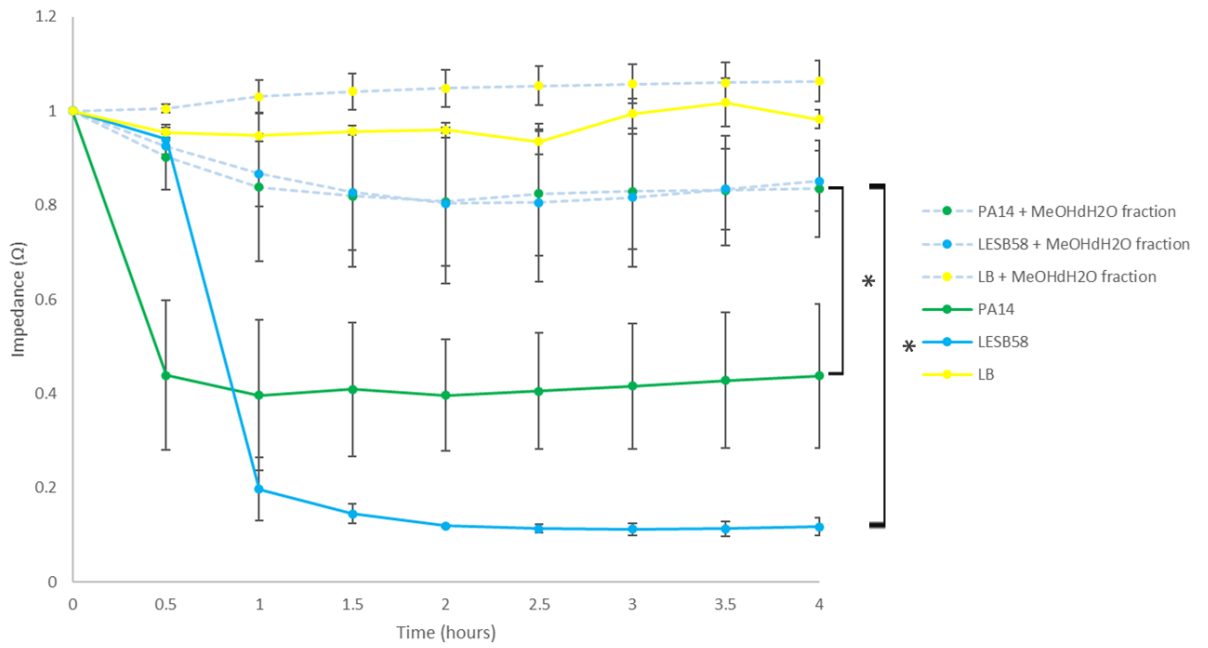


**Figure 5.8: Biofilm growth of PA14 and LESB58 grown alongside MeOHdH<sub>2</sub>O extract fraction.** EIS measurements at 10 Hz of fractionated extract LR16 (MeOHdH<sub>2</sub>O fraction) against both PA14 and LESB58. Error bars represent standard deviation, \* denotes statistical significance ( $p < 0.05$ ),  $n=3$ .

Going in decreasing polarity, the biofilm formation of LESB58 is significantly reduced after four hours in the presence of the MeOH fraction, shown as a higher impedance modulus (0.866  $\Omega$ ) than the LESB58 only control (0.118  $\Omega$ ) (**Figure 5.8**), and this reduction in biofilm formation is significant ( $p = 0.049$ ,  $n=3$ ). However, there is limited reduction in PA14 biofilm formation in the presence of the MeOH fraction (0.630  $\Omega$ ), and this is not significant ( $p = 1.000$ ,  $n=3$ ). This is likely due to the large standard deviations for both PA14 + MeOH fraction and the PA14 only control. However, this difference in the inhibition of biofilm between the two *P. aeruginosa* strains could also be due to the strains. Looking at the PA14 and LESB58 controls, LESB58 forms more biofilm than PA14 (shown as a lower impedance modulus value); 0.118  $\Omega$  compared to 0.438  $\Omega$  for LESB58 and PA14, respectively. This was also demonstrated in **Chapter 3**. As mentioned previously, LESB58 is more pathogenic than PA14, containing a higher number of virulence factors (285), however this is offset by LESB58 by having little to no motility compared to PA14 (52). Due to the difference in biofilm inhibition between the two strains of *P. aeruginosa* (by the MeOH fraction), it was hypothesized that the remaining two metabolite fractions may not show the same inhibition against one strain as the other strain.

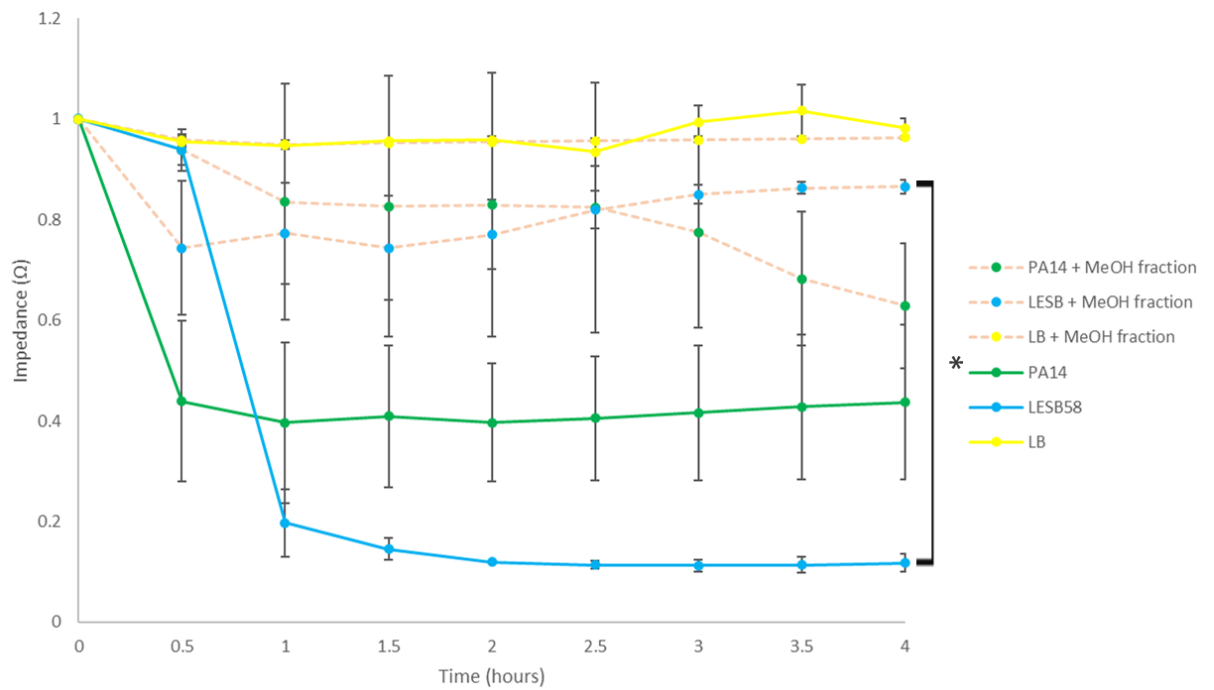


**Figure 5.9: Biofilm growth of PA14 and LESB58 grown alongside MeOH extract fraction.** EIS measurements at 10 Hz of fractionated extract LR16 (MeOH fraction) against both PA14 and LESB58. Error bars represent standard deviation, \* denotes statistical significance ( $p < 0.05$ ),  $n=3$ .

As suggested previously, there was a difference in biofilm formation between PA14 and LESB58 in the presence of the ACN fraction (**Figure 5.10**), as seen with the MeOH fraction. In the presence of the ACN fraction, the impedance modulus for LESB58 is 0.716  $\Omega$ , which is significant ( $p = 0.042$ ,  $n=3$ ) when compared to the LESB58 only control. This is in comparison to 0.594  $\Omega$  and 0.438  $\Omega$  ( $p = 0.995$ ,  $n=3$ ) for the PA14 + ACN fraction and PA14 only control. The PA14 biofilm formation in the presence of both the MeOH and ACN fractions is expected, as there was no antibiofilm activity observed from these two fractions against PA14 in the initial CV assay in **Chapter 4**. Therefore, there was antibiofilm activity expected from the EtOAc fraction, as this reduced the PA14 biofilm formation previously (**Chapter 4**).

Unexpectedly, however, there was no biofilm inhibition seen from the EtOAc against PA14 (**Figure 5.11**). This was demonstrated as there is no significant difference between the PA14 + EtOAc fraction (0.590  $\Omega$ ) and PA14 only (0.438  $\Omega$ ) ( $p = 1.000$ ,  $n=3$ ). Furthermore, the EtOAc fraction is the only metabolite extract fraction which did not inhibit the biofilm formation of LESB58; 0.492  $\Omega$  after four hours, compared to 0.118  $\Omega$  for the LESB58 control ( $p = 0.273$ ,  $n=3$ ). Typically, the bioactive metabolites would be expected to be present in only one fraction, and therefore the antibiofilm bioactivity from three fractions (MeOHdH<sub>2</sub>O, MeOH, and ACN) against LESB58 is unexpected; the bioactivity of only one fraction (MeOHdH<sub>2</sub>O) against PA14 is more expected. Furthermore, the antibiofilm activity of the MeOHdH<sub>2</sub>O fraction aligns with the molecular network of LR16 extract and fractions in **Chapter 4**, which showed that there are singletons and molecular ions not present in the GNPS library which are found in only the MeOHdH<sub>2</sub>O fraction, and are therefore likely candidates for the antibiofilm metabolite. For all fractions (**Figures 5.8 – 5.11**), there was no significant difference between the LB only and the LB + solvent fraction controls. Therefore, the observed antibiofilm activity, increased impedance modulus, seen from the fractions can be attributed to produced bacterial metabolites interacting with *P. aeruginosa*, rather than the LB media. This was confirmed by control assays with DMSO, which the fractions were dissolved in, against both PA14 and LESB58, which also showed no inhibitory effect. Lastly, it was of interest to determine if the biofilm forming ability of both strains is impacted by the presence of medically relevant materials, if these biofilms can be quantified with EIS, and if the presence of metabolite extract fraction impacts these biofilms. Due to the presence of an additional surface, it was anticipated that the quantity of biofilm would

increase, and this would potentially decrease the efficacy of the metabolite extract fractions against both PA14 and LESB58.

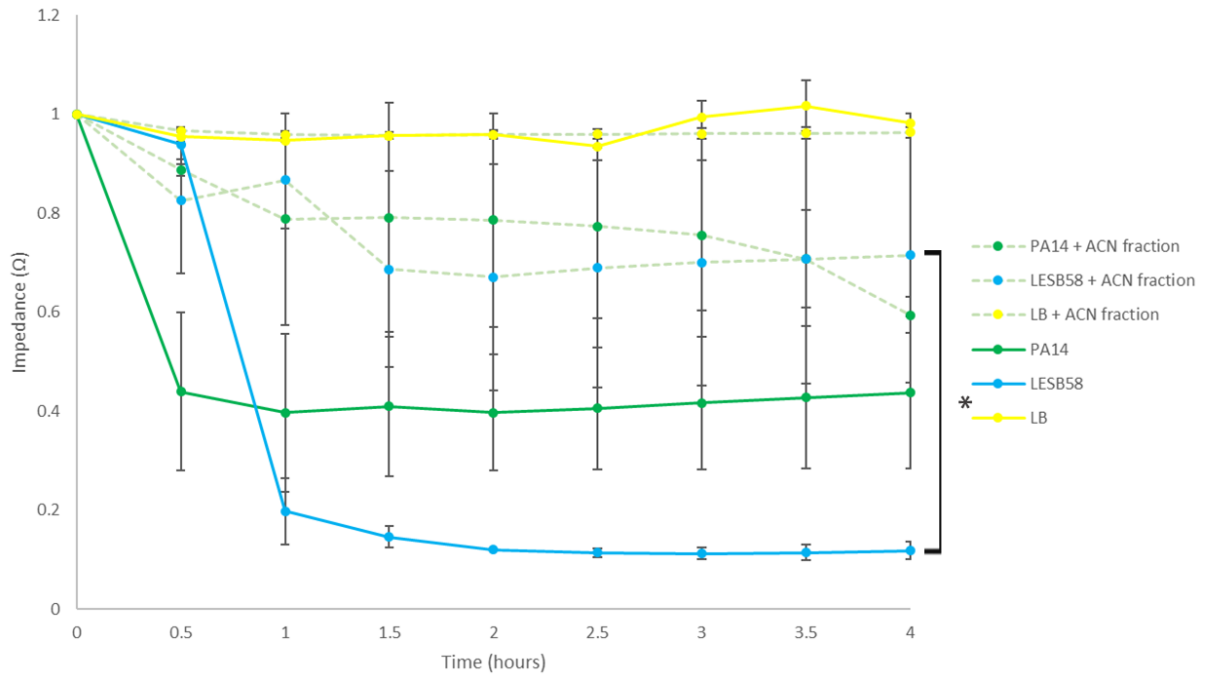


**Figure 5.10: Biofilm growth of PA14 and LESB58 grown alongside ACN extract fraction.** EIS measurements at 10 Hz of fractionated extract LR16 (ACN fraction) against both PA14 and LESB58. Error bars represent standard deviation, \* denotes statistical significance ( $p < 0.05$ ),  $n=3$ .

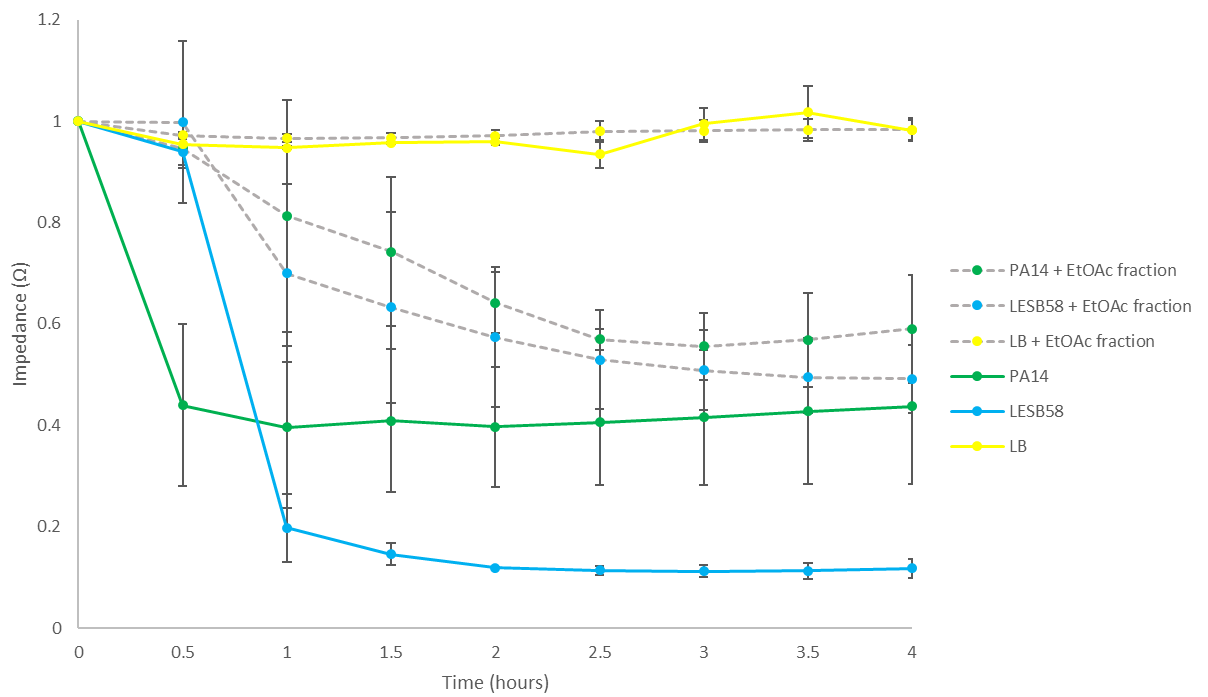


**Figure 5.11: Biofilm growth of PA14 and LESB58 grown alongside EtOAc extract fraction.**

EIS measurements at 10 Hz of fractionated extract LR16 (EtOAc fraction) against both PA14 and LESB58. Error bars represent standard deviation, n=3.

Due to the prevalence of biofilms forming on medical devices and implants, it was of interest to assay if the quantity of biofilm formed by both PA14 and LESB58 was affected by the presence of Dacron graft; a common material used in reconstructive vascular graft surgeries (97). Further, these biofilms were also grown in the presence of the fractions of extract LR16 to observe if the addition of a surface affected the antibiofilm ability of the extract. These assays were carried out using EIS only, as graft material with CV carried too much background stain to distinguish between *P. aeruginosa* and media only controls (**Supplementary Figure 5.1**). As all fractions were dissolved in DMSO, *P. aeruginosa* + DMSO was assayed alongside the fractions and the percentage of biofilm was calculated to a no DMSO control, as DMSO is a known antibiofilm agent.

As expected, the biofilm formation of PA14 increased in the presence of Dacron graft; shown as the inhibition of PA14 biofilm formation decreased. This was measured as a higher normalised impedance modulus, compared to a lower impedance modulus which indicates biofilm formation. However unexpectedly, this was not significant between any of the fractions with and without the graft ( $p > 0.05$  for all four combinations) (**Table 5.1**). This is potentially due to the large error observed from EIS measurements, as impedance is highly sensitive (286). Furthermore, there was no significant difference between the biofilm formation between the graft and no graft controls in the presence of DMSO only ( $p = 0.407$ ,  $n=3$ ), demonstrating that the DMSO is not affecting the Dacron graft. However, it can be seen that the DMSO without the addition of the solvent fractions had an antibiofilm effect, 45.1% inhibition of PA14 when compared to PA14 only control (0% inhibition), there was significantly greater biofilm inhibition from the MeOHdH<sub>2</sub>O fraction; 80.3% inhibition ( $p = 0.048$ ,  $n=3$ ). This aligns with the MeOHdH<sub>2</sub>O EIS data above (**Figure 5.8**), as this fraction previously showed the highest antibiofilm activity. Furthermore, the addition of the Dacron graft allowed PA14 to overcome the biofilm inhibitory effects of the MeOHdH<sub>2</sub>O fraction of extract LR16. The MeOHdH<sub>2</sub>O fraction inhibited PA14 biofilm formation by 80.3%, however in the presence of Dacron graft, the biofilm formation is restored to that of the no fraction control, 41.8% biofilm inhibition, which is not significant from the DMSO only control (45.1%,  $p = 0.444$ ,  $n=3$ ). This is potentially due to the increased surface area the Dacron graft has afforded PA14; as the graft is ridged, *P. aeruginosa* has a greater surface area with which to adhere to. Lastly, the limited bioactivity of the remaining three fractions to inhibit PA14 biofilm was expected, all three showed no significant difference when compared to the no

fraction controls earlier (**Figures 5.9 – 5.11**). Here, the remaining three fractions (MeOH, ACN, EtOAc) also showed limited biofilm inhibition both with and without the presence of the Dacron graft (30.8 – 55.4% inhibition), with no significant difference between the fractions and DMSO control in the presence of graft material ( $p = 0.156, 0.676, 0.342, n=3$  for all), as well as the fractions and DMSO without the Dacron graft ( $p > 0.994, n=3$ ). Due to the ability of PA14 to overcome the antibiofilm effects of the MeOH:H<sub>2</sub>O fraction in the presence of Dacron graft, it was exciting to assay the antibiofilm activity of the fractions against LESB58.

**Table 5.1: PA14 biofilm inhibition in the presence and absence of Dacron graft.** Percentage of PA14 biofilm inhibition compared to PA14 only control after four hours when incubated alongside four solvent fractions of extract LR16 and Dacron graft, impedance modulus measured over four hours and normalised. \* Denotes statistical significance, n=3.

PRESENCE OF GRAFT	SOLVENT FRACTION	BIOFILM INHIBITION (%)
Y	DMSO control	45.1 *
N		49.5
Y	MeOHdH2O	41.8
N		80.3 *
Y	MeOH	39.3
N		38.8
Y	ACN	37.1
N		31.7
Y	EtOAc	55.4
N		30.8

The LESB58 data (**Table 5.2**) showed that the biofilm formation in the presence of the DMSO control is not affected by the presence or absence of graft material, as in the control wells, there was 35.7% and 34.7% biofilm inhibition with and without the graft material, respectively ( $p = 1.000$ ,  $n=3$ ). When exposed to the antibiofilm fractions which previously showed a significant decrease in biofilm formation (MeOHdH<sub>2</sub>O, MeOH, ACN; **Figures 5.8 – 5.10**), there was a similar significant increase in biofilm inhibition; 90.0%, 91.8% and 73.4% inhibition for the same three fractions. However, in the presence of Dacron graft, the biofilm inhibition is returned to that of the control for both the MeOH and ACN fractions, 29.4% and 44.5% respectively, and this difference between the graft and no graft for the MeOH fraction is statistically significant ( $p = 0.016$ ,  $n=3$ ). This is potentially due to the increased virulence of LESB58 (285), allowing the strain to produce more biofilm overall, as seen previously. Interestingly though, the MeOHdH<sub>2</sub>O fraction is still able to inhibit LESB58 biofilm formation in the presence of the graft (86.7% inhibition). This is potentially due to the limited motility of LESB58 compared to PA14, and this may be a potential mechanism which the metabolite fraction is targeting. As there was no significant difference between the DMSO control with and without Dacron graft for both PA14 and LESB58 ( $p = 0.407$ ,  $p = 1.000$ , both  $n=3$ ), it can be concluded that the graft material is not impacting the impedance modulus or the physical sensor. Therefore, the change in impedance modulus observed in the presence of the Dacron graft is due to *P. aeruginosa* biofilm formation.

**Table 5.2: LESB58 biofilm inhibition growth in the presence and absence of Dacron graft**

Percentage of LESB58 biofilm inhibition after four hours when incubated alongside four solvent fractions of extract LR16 and Dacron graft. Normalised against PA14 +/- Dacron graft and LB +/- Dacron graft controls. \* Denotes statistical significance, n=3.

PRESENCE OF GRAFT	SOLVENT FRACTION	BIOFILM INHIBITION (%)
Y	DMSO control	35.7
N		34.7
Y	MeOHdH2O	86.7
N		90.0
Y	MeOH	29.4 *
N		91.8 *
Y	ACN	44.5
N		73.4
Y	EtOAc	31.5
N		45.9

## 5.4 Discussion

The data shown here offer an insight into the way in which biofilms and antibiofilm agents may be used with real-world, bench-to-bedside applications. As demonstrated here, biofilms forming on surfaces are more resistant to antibiotics and antibiofilm agents than both planktonic cells and biofilms formed without a surface present. It was shown previously that biofilms forming on surfaces require more than 100-fold stronger antibiotic concentration, compared to the removal of planktonic cells (56). This has also been dramatically demonstrated with *Legionella pneumophila*, which showed that planktonic cells were 210,000-fold more susceptible to iodination than biofilm cells attached to stainless steel. Furthermore, biofilm cells which had been removed during washing steps (named unattached by the authors) were only 135-fold less resistant than the biofilm-bound cells – still nearly 200,000 times the resistance of planktonic *L. pneumophila* (287), demonstrating the clear need for agents which specifically target biofilm formation.

Despite this evidence, there are currently no commercially available, licensed antibiofilm agents on the market (74,110,111). However a known antibiofilm agent used throughout this study is DMSO (215,288). In a study similar to this one, the authors dissolved their metabolites of interest in DMSO, yet found that the solvent was killing the planktonic bacteria (288). This DMSO-killing of planktonic cells was not seen here, however this may be because the authors used 32% DMSO (288); nearly 100-fold higher than the concentration used in this study (0.5%). Further adding to this, another report found that DMSO is bactericidal at ~30% (215), although, Yahya, *et al.*, found DMSO to have no bioactivity against *P. aeruginosa* at 0.5%, the concentration used here (288). The results here showed some biofilm inhibition at 0.5% DMSO when compared to the no-DMSO control, however no bactericidal effects were seen when considering the SWV data. Despite the EIS data demonstrating that DMSO had a slight inhibitory effect on the biofilm of both PA14 and LESB58, the antibiofilm efficacy of the LR16 extract and fractions was still visible as additional activity when compared to the DMSO and *P. aeruginosa* controls. This impact on biofilm forming ability is further supported by a study which showed that DMSO may affect the *las* and *rhl* systems. As mentioned previously, these are the main genes responsible for quorum sensing in *P. aeruginosa* (273). The loss of function of these would therefore decrease the ability of *P. aeruginosa* to form biofilms (215,273); supporting the data here.

As the *las* and *rhl* systems regulate quorum sensing (273), is it unsurprising that *IsrhlR*, *IsrhlI*, and *IslasI* were not suitable for SWV measurements here. These genes have previously been the target of the natural product, cinnamaldehyde (150), and are reportedly associated with a reduction in pyocyanin production (114,280). Therefore, as pyocyanin is used as the proxy measurement for planktonic growth in this study, these insertion mutants could not be quantified using SWV at -0.35 V, which was optimised for the detection of pyocyanin in **Chapter 3**. Furthermore, the reduced biofilm forming ability of *IsphzM* is unsurprising, as the *phzM* gene encodes a pyocyanin precursor, with pyocyanin required for biofilm formation, through the promotion of extracellular DNA (eDNA) release (289). However, as *IsphzM* has disrupted pyocyanin production, it would therefore be expected that the insertion mutant would not be able to be quantified with SWV, as seen with the other insertion mutants which disrupted the production of pyocyanin. The reduced pyocyanin production by a *phzM* mutant has been previously shown using high performance liquid chromatography (HPLC); PAO1  $\Delta phzM$  when compared to the PAO1 WT did not produce pyocyanin. Furthermore, the mutant strain was plated out onto PIA agar, and the characteristic-blue pigment did not diffuse out (290). Lastly, another *P. aeruginosa* mutant,  $\Delta pmtA$ , showed decreased expression of *phzM* which was accompanied by corresponding decreases in pyocyanin production and biofilm formation, mirroring the decrease in *phzM* expression (81). It would be highly interesting to assay extract LR16 with several of the antibiofilm insertion mutants mentioned here, to determine which pathways extract LR16 is interacting with, and which genes are being up or down regulated; as approximately 95% of *P. aeruginosa* isolates produce pyocyanin (81). Furthermore, as there is a high concentration of pyocyanin in the lungs of CF patients, the pathways involved in pyocyanin production are attractive drug targets (67). That being said, as both PA14 and LESB58 planktonic growth were both still quantifiable with SWV in the presence of the crude extract and metabolite fractions, the metabolite is unlikely to inhibit pyocyanin production. Due to the fact that the SWV measurements have used pyocyanin as a proxy for planktonic growth throughout this thesis; as pyocyanin is measured at -0.35 V, a decrease in current would have been observed for the *P. aeruginosa* strains if pyocyanin production was inhibited.

Finally, the future of monitoring and eradication of biofilms requires multiple different approaches, including the use of sensors and introduction of antibiofilm agents. One of the main advantages of anti-virulence, antibiofilm, and bacteriostatic drugs, is these provide less

evolutionary pressure of pathogens to evolve, as the pathogens are not being killed (291,292). There has been a large number of antibiofilm drug investigations, with many showing promise, such as extract LR16 here, cinnamaldehyde (150), curcumin (280), and 6-gingerol (280). Both curcumin and 6-gingerol have been shown to inhibit *P. aeruginosa* biofilm formation by interacting with a few of the genes considered and assayed here; the *las* and *rhl* genes (280).

## 5.5 Conclusions and future work

To conclude, the antibiofilm extract LR16, has been shown to inhibit *P. aeruginosa* biofilms of two strains, PA14 and LESB58, and this bioactivity has been further investigated through the fractionation of extract LR16. The MeOHdH<sub>2</sub>O fraction showed the highest levels of antibiofilm activity against both *P. aeruginosa* strains, comparable to that of the crude extract, indicating that the antibiofilm metabolite is present in this fraction. However, LESB58 biofilm formation was also inhibited by two further fractions (MeOH and ACN fractions). Furthermore, both strains were able to overcome the biofilm inhibitory effects of the MeOHdH<sub>2</sub>O LR16 fraction in the presence of implant material (Dacron graft). This was not seen for LESB58 in the presence of other fractions. In the future it would be of interest to assay if this effect is seen with other medically relevant materials, such as medical-grade stainless steel (316L). The use of stainless steel would pose a hurdle with regards to electrochemical methods, however it would allow for easier functionalisation. A further direction would be to determine if Dacron graft could be functionalised with the MeOHdH<sub>2</sub>O fraction of LR16, as a potential antibiofilm implant material. One of the key limitations of this study is the sole assaying of *P. aeruginosa* strains. It would be key to determine if other clinically relevant biofilm forming strains could be quantified with EIS. However, the quantification of planktonic cells would not be possible, as this was optimised *P. aeruginosa*, as it produces pyocyanin. As this may be an implant technology, it would be necessary to assay mammalian cells with the electrochemical techniques to determine if the cells interfere with the EIS frequencies or SWV potential differences, as well, if the mammalian cells are killed, or otherwise impacted, by the quantification techniques. Lastly, systematically assaying the LR16 extract and four fractions against a series of PA14 biofilm insertion mutants, could allow the determination of the mode of action of the active

metabolite, although further work on identifying the bioactive metabolite(s) should be carried out first.

## 6.0 General discussion, future work, and conclusions

### 6.1 Discussion

Biofilms were first recorded by the inventor of the microscope, Anton Von Leeuwenhoek, as 'microbial aggregates' (293). However the term 'biofilm' was not coined until more than 300 years later, by Prof. Bill Costerton, in an article modestly named "How Bacteria Stick" (294). This acknowledgement of biofilm-forming bacteria comes more than 70 years after the synthesis of the very first antibacterial agent, Salvarsan, used to treat syphilis (174). Furthermore, antimicrobial resistant *Treponema pallidum* was seen in 1931 (295), 14 years before Fleming received the Nobel Prize in Medicine for his discovery of penicillin (296,297). In this, Fleming warned against potential antimicrobial resistant strains arising in his acceptance speech (298), despite not knowing how the bacteria may become resistant. As seen here, one of the main mechanisms bacteria use to afford themselves resistance is through the formation of biofilms (299). Further, the issues associated with the inhibition and eradication of biofilms have been known for as long as biofilms have been recorded (294). These include decreased diffusion of antibiotics across the biofilm (57) and increased antibiotic concentrations required to inhibit them (56), often attributed to the chemical and physical properties of the biofilm, such as increased efflux pumps (39) and dormant cells (57). Furthermore, biofilms were first quantified in 1977 using crystal violet (CV) (208). Despite the technological advancements over the last 46 years, this is still the gold standard which is used today.

The work described in **Chapter 3** demonstrated how variable the quantification of biofilms is. In particular, there is considerable variation using CV, despite being the most commonly used biofilm quantification method (215). For example, additional PBS washes of the biofilm pre-staining (150), post-staining (73), solvent variation (56), and increased concentrations of CV (207,288). Important for the work carried out here, was that the quantification of biofilm-bound CV is an indirect measurement; the biofilm-bound CV is resolubilised into a solvent and then this is measured (85,288). Here, the aim was to develop a method which could be used to quantify the biofilm as it was forming, rather than an endpoint method, such as CV. This chapter successfully concluded that biofilms could be quantified using electrochemical impedance spectroscopy (EIS) and its output of raw impedance modulus reads could give quantifiable measurements during formation. This is the first time this has been shown for

*Pseudomonas aeruginosa* biofilms without the need for post-measurement model fitting. This advancement makes *P. aeruginosa* biofilm detection more readily accessible and is a huge step towards *in vivo* quantification. *P. aeruginosa* biofilms have been quantified previously using EIS, however as mentioned, importantly the data required circuit fitting (128,135,300,301). This increases processing time and makes the technology less accessible for non-specialists (128), thereby limiting its use, something the work in this thesis circumvents. In fact, to our knowledge, the only other instance of biofilm quantification using the raw impedance values was focussed on *Escherichia coli* biofilms (130). The 2020 study demonstrated the use of impedance measurements for phenotypic antibiotic (streptomycin) susceptibility testing (130), and as such, demonstrates another exciting potential for real-world applications. For example, real-time antibiotic susceptibility measurements for isolated strains in clinical settings.

As the work in **Chapter 3** successfully quantified biofilms using optimised CV and EIS biofilm techniques, **Chapter 5** took this further, and used these electrochemical techniques and applied them to quantify biofilm on real-world implant material; something which is not possible with CV or other staining techniques. To our knowledge, this real-time quantification of biofilms forming on materials has not been carried out previously. Previously published methods involve the removal of biofilm from surfaces (58,83,86,302,303), and therefore there is no way to determine the speed of biofilm formation or how effective antibiofilm treatments are in real-time. Furthermore, as the biofilm is removed from the surface prior to quantification, these assays are always endpoint, and there is no standardised method to ensure all of the bacterial cells are removed (86,302). This objective and the use of EIS here was successful for the quantification of *P. aeruginosa* biofilms on Dacron grafts; ubiquitously used in medical procedures, such as aortobifemoral bypass and revascularisation procedures (57,107). However, there are several areas for improvement, for example, the variability of EIS should be decreased. This is symptomatic of the high sensitivity of impedance measurements (226). Additionally, increased error has previously been associated with the use of a multiplexer (used to gather the data from multiple wells) (129,225), which are also each on their own circuit (129); creating variability between them. In a real-world application, such as a medical implant, there would only be a single sensor; the multiplexer and use of the multi-well plate are symptomatic of the optimisation and laboratory-based process. Despite these conditions

increasing error, the possibilities that the ability to quantify biofilm on medically relevant materials in real-time opens up, such as integration into point of care devices, outweighs these issues arising, particularly as significant difference was still seen for the measurements.

It is clear from the work on Dacron grafts that new antibiofilm agents are greatly needed, often the mechanism of action of an antibiofilm agent differs from than of an antibiotic (299). As such, **Chapter 4** added a biodiscovery component to this thesis, and we hypothesized that we could quantify how effective antibiofilm agents may be by utilising our developed electrochemical methods. Furthermore, the isolation of marine organisms and antibiofilm bioactivity screening has been carried out previously with similar results. Such that, from the screening of isolated strains, only a low percentage are found to have antibiofilm activity (143); 3% to 12.5% (216,304). Also shown here was the isolation of strains which promoted the formation of biofilms, which has also been reported in the literature (110,154). The use of electrochemical measurements to evaluate antibiotics has been carried out previously; the efficacy of gentamicin, fosfomycin, and amoxicillin against both *E. coli* and *P. aeruginosa* showed clear antibiotics susceptibility profiles (127). However, to our knowledge, this is the first-time electrochemical measurements have been used to evaluate novel antibiofilm agents, and as such, provides an exciting advance to evaluate how effective these agents are over time, as well as a potential novel screening technique for antibiotic and antibiofilm compounds.

## 6.2 Future work

The work in this thesis opens the door for biofilm quantification *in vivo*. We demonstrated the possibility to quantify *P. aeruginosa* biofilms in real-time within 60 minutes. One of the most exciting applications for this technology is the possibility of use in implantable medical devices. As such, the next logical step would be to determine if other pathogens can be quantified; especially mixed-species biofilms, as these are of greater clinical significance than single-species biofilms (282). Following this, integration of sensors onto graft material would be necessary, with attention to obstacles, such as the creation of additional spaces for biofilm to form (under the sensor, for example). An endpoint of this work would be a sensor on a medical implant to detect a biofilm forming within a patient, without surgical

intervention and before the patient develops sepsis. To make this application widespread, further medically relevant materials would also need to be assayed, such as latex or silicone. However, medical grade, 316L, stainless steel could create an issue with quantification, as the metal would interfere with the measurements.

In terms of progressing the antibiofilm agent discovery work, it would be insightful to identify the producing strain via whole genome sequencing. This could be compared to genomes of phylogenetically related species, potentially giving insight into the biosynthetic gene cluster encoding the enzymes responsible for metabolite biosynthesis. Having this further information could aid additional dereplication of the mass spectrometry data, as although fractionation afforded some narrowing down of the metabolites responsible for the bioactivity, more work would be needed, including separation by high-performance liquid chromatography (HPLC) followed by structure elicitation using nuclear magnetic resonance (NMR). The identity and structure of the antibiofilm metabolites could then be used in conjunction with the Liberati, *et al.*, PA14 insertion mutant library (199) to systematically assay which insertion mutants were affected by the antibiofilm metabolite. This would potentially allow a mechanism of action of the antibiofilm metabolites to be elucidated. Lastly, once the mode of action of the antibiofilm metabolite is known, this will be able to give insights as to the pathogens it will likely be active against (for example, Gram-negative only), as well as if it will have changes in activity against antimicrobial resistant strains.

Bringing these aspects together, the functionalising of Dacron graft or other material using the antimicrobial metabolites would allow the creation of antibiofilm surfaces for use in medical implants, as well as the functionalising of surfaces for the slow release of drugs. Furthermore, the EIS sensors could be integrated with the functionalised surfaces; EIS would potentially provide a mechanism to detect when a released drug had run out, for example, in a contraceptive implant. This functionalising of surfaces could first be carried out with medical devices and equipment (non-implantable surfaces); this would provide a useful stepping-stone in acquiring proof of principle data. This is particularly pertinent, as although this thesis focussed on implantable medical devices, the real-time biofilm quantification methods developed here have strong applications in water treatment, food manufacturing (286), and in point of care diagnostics (305), such as antibiotic susceptibility profiling (127,130), where the currently employed methods are slow and, at times, ineffective (207).

### 6.3 Conclusions

To conclude, *P. aeruginosa* biofilms were detected and quantified in real-time using electrochemical measurements, including impedance modulus, and these biofilms have been inhibited by a potentially novel antibiofilm agent isolated from marine bacteria. The development of this methodology for quantifying biofilms by EIS without the need for circuit fitting offers exciting opportunities for future work into assaying biofilm formation on medically relevant materials in real-time, as well as the screening of antibiofilm compounds. Further, the identification of an antibiofilm agent, LR16, which did not show planktonic inhibition opens up the possibility for changing the way environmental strains are screened for bioactivity, and an exciting advancement in the field of antibiotic discovery. These findings offer avenues for future exploration and provide a solid foundation for revolutionising the field of implantable medical devices.

## 7.0 References

1. Murray CJ, Ikuta KS, Sharara F, Swetschinski L, Robles Aguilar G, Gray A, et al. Global burden of bacterial antimicrobial resistance in 2019: a systematic analysis. *The Lancet*. 2022;6736(21).
2. O’neill J. Tackling drug-resistant infections globally. *Review on Antimicrobial Resistance*. 2016;1–84.
3. Rice LB. Federal Funding for the Study of Antimicrobial Resistance in Nosocomial Pathogens: No ESKAPE. *J Infect Dis*. 2008;197(8):1079–81.
4. Public Health England. English surveillance programme for antimicrobial utilisation and resistance (ESPAUR) 2021-2022. 2022;1–143.
5. CDC. U.S. Department of Health & Human Services. 2020 [cited 2020 Apr 27]. Antibiotic/Antimicrobial Resistance | CDC. Available from: <https://www.cdc.gov/drugresistance/about.html>
6. Balasubramanian R, Van Boeckel TP, Carmeli Y, Cosgrove S, Laxminarayan R. Global incidence in hospital-associated infections resistant to antibiotics: An analysis of point prevalence surveys from 99 countries. *PLoS Med*. 2023 Jun 1;20(6).
7. WHO. 2020. [cited 2020 Apr 15]. Tuberculosis. Available from: <https://www.who.int/news-room/fact-sheets/detail/tuberculosis>
8. Migliori GB, De Iaco G, Besozzi G, Centis R, Cirillo DM. First tuberculosis cases in Italy resistant to all tested drugs. *Weekly releases (1997–2007)*. 2007;12(20):3194.
9. Velayati AA, Masjedi MR, Farnia P, Tabarsi P, Ghanavi J, ZiaZarifi AH, et al. Emergence of new forms of totally drug-resistant tuberculosis bacilli: Super extensively drug-resistant tuberculosis or totally drug-resistant strains in Iran. *Chest*. 2009;136(2):420–5.
10. Rodrigues C, Ajbani KK, Amale RA, Udwadia ZF. Totally Drug-Resistant Tuberculosis in India. 2012;54:579–81.
11. Kumarasamy KK, Toleman MA, Walsh TR, Bagaria J, Butt F, Balakrishnan R, et al. Emergence of a new antibiotic resistance mechanism in India, Pakistan, and the UK: a molecular, biological, and epidemiological study. *Lancet Infect Dis*. 2010;10:597–602.
12. Sengupta S, Chattopadhyay MK, Grossart HP. The multifaceted roles of antibiotics and antibiotic resistance in nature. *Front Microbiol*. 2013;4(47).
13. Jevons MP. “Celbenin” - resistant Staphylococci. *Br Med J*. 1961;1(124).
14. Hutchings M, Truman A, Wilkinson B. Antibiotics: past, present and future. *Curr Opin Microbiol*. 2019 Oct 1;51:72–80.
15. Butler MS, Paterson DL. Antibiotics in the clinical pipeline in October 2019. *Journal of Antibiotics*. 2020;73(6):329–64.

16. Gove M, Hancock M. Tackling antimicrobial resistance 2019–2024 – The UK’s five-year national action plan. HM Government. 2019.
17. Chan M. Global action plan on antimicrobial resistance. World Health Organization. 2017;1–28.
18. Denham J. UK Antimicrobial Resistance Strategy and Action Plan. 2000.
19. CDC. Antibiotic resistance threats in the United States. 2019.
20. Xiao Y, Zhang J, Zheng B, Zhao L, Li S, Li L. Changes in Chinese Policies to Promote the Rational Use of Antibiotics. *PLoS Med.* 2013;10(11):1–4.
21. Moore CE. Changes in antibiotic resistance in animals. *Science* (1979). 2019;365(6459):1251–2.
22. Aslam B, Wang W, Arshad MI, Khurshid M, Muzammil S, Rasool MH, et al. Infection and Drug Resistance Dovepress Antibiotic resistance: a rundown of a global crisis. 2018;
23. Van Boeckel TP, Brower C, Gilbert M, Grenfell BT, Levin SA, Robinson TP, et al. Global trends in antimicrobial use in food animals. *Proc Natl Acad Sci U S A.* 2015 May 5;112(18):5649–54.
24. Moser KA, Zhang L, Spicknall I, Braykov NP, Levy K, Marrs CF, et al. The Role of Mobile Genetic Elements in the Spread of Antimicrobial-Resistant *Escherichia coli* from Chickens to Humans in Small-Scale Production Poultry Operations in Rural Ecuador. *Am J Epidemiol.* 2018;187(3):558–67.
25. Zhou F, Yu T, Du R, Fan G, Liu Y, Liu Z, et al. Clinical course and risk factors for mortality of adult inpatients with COVID-19 in Wuhan, China: a retrospective cohort study. *The Lancet.* 2020;395:1054–62.
26. Auta A, Hadi MA, Oga E, Adewuyi EO, Abdu-Aguye SN, Adeloye D, et al. Global access to antibiotics without prescription in community pharmacies: A systematic review and meta-analysis. *Journal of Infection.* 2019;78(1):8–18.
27. Aminov RI. A brief history of the antibiotic era: Lessons learned and challenges for the future. *Front Microbiol.* 2010;1(DEC):1–7.
28. Ahmed MN, Porse A, Sommer MOA, Høiby N, Ciofu O. Evolution of antibiotic resistance in biofilm and planktonic *Pseudomonas aeruginosa* populations exposed to subinhibitory levels of ciprofloxacin. *Antimicrob Agents Chemother.* 2018;62(8).
29. WHO. 2021 AWaRe classification [Internet]. [cited 2024 Feb 29]. Available from: <https://www.who.int/publications/i/item/2021-aware-classification>
30. Iskandar K, Murugaiyan J, Halat DH, Hage S El, Chibabhai V, Adukkadukkam S, et al. Antibiotic Discovery and Resistance: The Chase and the Race. *Antibiotics.* 2022;11(2):1–38.
31. Fisher RA, Gollan B, Helaine S. Persistent bacterial infections and persister cells. *Nature Publishing Group.* 2017;15:453–64.

32. Cabral DJ, Wurster JI, Belenky P. Antibiotic persistence as a metabolic adaptation: Stress, metabolism, the host, and new directions. *Pharmaceuticals*. 2018;11(1).
33. Reygaert WC. An overview of the antimicrobial resistance mechanisms of bacteria. *AIMS Microbiol*. 2018;4(3):482–501.
34. Kankwatira AM, Okoro CK, Dougan G, Parkhill J, Gordon MA, Quail MA, et al. High-Resolution Single Nucleotide Polymorphism Analysis Distinguishes Recrudescence and Reinfection in Recurrent Invasive Nontyphoidal Salmonella Typhimurium Disease. *Clinical Infectious Diseases*. 2012;54(7):955–63.
35. Russo TA, Stapleton A, Wenderoth S, Hooton TM, Stamm WE. Chromosomal restriction fragment length polymorphism analysis of escherichia coli strains causing recurrent urinary tract infections in young women. *Journal of Infectious Diseases*. 1995;172(2):440–5.
36. Blair JMA, Richmond GE, Piddock LJV. Multidrug efflux pumps in Gram-negative bacteria and their role in antibiotic resistance. *Future Microbiol*. 2014;9(10):1165–77.
37. Du D, Wang-Kan X, Neuberger A, van Veen HW, Pos KM, Piddock LJV, et al. Multidrug efflux pumps: structure, function and regulation. *Nat Rev Microbiol*. 2018;16(9):523–39.
38. Coyne S, Courvalin P, Périchon B. Efflux-mediated antibiotic resistance in *Acinetobacter* spp. *Antimicrob Agents Chemother*. 2011;55(3):947–53.
39. Gillis RJ, White KG, Choi KH, Wagner VE, Schweizer HP, Iglewski BH. Molecular basis of azithromycin-resistant *Pseudomonas aeruginosa* biofilms. *Antimicrob Agents Chemother*. 2005;49(9):3858–67.
40. Bordi C, de Bentzmann S. Hacking into bacterial biofilms: a new therapeutic challenge. *Ann Intensive Care*. 2011;1(1):19.
41. Blair JMA, Smith HE, Ricci V, Lawler AJ, Thompson LJ, Piddock LJ V. Expression of homologous RND efflux pump genes is dependent upon AcrB expression: implications for efflux and virulence inhibitor design. *Journal of Antimicrobial Chemotherapy*. 2015;70:424–31.
42. McMillan EA, Gupta SK, Williams LE, Jové T, Hiott LM, Woodley TA, et al. Antimicrobial resistance genes, cassettes, and plasmids present in salmonella enterica associated with United States food animals. *Front Microbiol*. 2019;10(APR):1–18.
43. Peterson LR. Bad Bugs, No Drugs: No ESKAPE Revisited. *Clinical Infectious Diseases*. 2009;49(6):992–3.
44. Tacconelli E, Magrini N. World health organization releases global priority list of antibiotic-resistant bacteria to guide research, discovery, and development of new antibiotics. WHO. Geneva; 2017.
45. Mulani MS, Kamble EE, Kumkar SN, Tawre MS, Pardesi KR. Emerging strategies to combat ESKAPE pathogens in the era of antimicrobial resistance: A review. *Front Microbiol*. 2019;10(APR).

46. Skender K, Machowska A, Singh V, Goel V, Marothi Y, Lundborg CS, et al. Antibiotic Use, Incidence and Risk Factors for Orthopedic Surgical Site Infections in a Teaching Hospital in Madhya Pradesh, India. *Antibiotics*. 2022;11(748):1–16.
47. Marturano JE, Lowery TJ. ESKAPE pathogens in bloodstream infections are associated with higher cost and mortality but can be predicted using diagnoses upon admission. *Open Forum Infect Dis*. 2019;6(12):1–8.
48. Ochoa SA, López-Montiel F, Escalona G, Cruz-Córdova A, Dávila LB, López-Martínez B, et al. Características patogénicas de cepas de *Pseudomonas aeruginosa* resistentes a carbapenémicos, asociadas con la formación de biopelículas. *Bol Med Hosp Infant Mex*. 2013;70(2):138–50.
49. Cai J, Deng T, Shi J, Chen C, Wang Z, Liu Y. Daunorubicin resensitizes Gram-negative superbugs to the last-line antibiotics and prevents the transmission of antibiotic resistance. *iScience*. 2023;26(6):106809.
50. Oren A, Garrity GM. Valid publication of the names of forty-two phyla of prokaryotes. *Int J Syst Evol Microbiol*. 2021;71(10).
51. Moore MP, Lamont IL, Williams D, Paterson S, Kukavica-Ibrulj I, Tucker NP, et al. Transmission, adaptation and geographical spread of the *Pseudomonas aeruginosa* Liverpool epidemic strain. *Microb Genom*. 2021;7(3).
52. Kukavica-Ibrulj I, Bragonzi A, Paroni M, Winstanley C, Sanschagrin F, O'Toole GA, et al. In vivo growth of *Pseudomonas aeruginosa* strains PAO1 and PA14 and the hypervirulent strain LESB58 in a rat model of chronic lung infection. *J Bacteriol*. 2008;190(8):2804–13.
53. Ude S, Arnold DL, Moon CD, Timms-Wilson T, Spiers AJ. Biofilm formation and cellulose expression among diverse environmental *Pseudomonas* isolates. *Environ Microbiol*. 2006;8(11):1997–2011.
54. Lee DG, Urbach JM, Wu G, Liberati NT, Feinbaum RL, Miyata S, et al. Genomic analysis reveals that *Pseudomonas aeruginosa* virulence is combinatorial. *Genome Biol*. 2006;7(10).
55. Cheng K, Smyth RL, Govan JRW, Doherty C, Winstanley C, Denning N, et al. Spread of  $\beta$ -lactam-resistant *Pseudomonas aeruginosa* in a cystic fibrosis clinic. *Lancet*. 1996;348:639–42.
56. Akinbobola AB, Sherry L, McKay WG, Ramage G, Williams C. Tolerance of *Pseudomonas aeruginosa* in in-vitro biofilms to high-level peracetic acid disinfection. *Journal of Hospital Infection*. 2017;97(2):162–8.
57. Høiby N, Bjarnsholt T, Givskov M, Molin S, Ciofu O. Antibiotic resistance of bacterial biofilms. *Int J Antimicrob Agents*. 2010;35(4):322–32.
58. Riordan L, Smith EF, Mills S, Hudson J, Stapley S, Nikoi N dei, et al. Directly bonding antimicrobial peptide mimics to steel and the real world applications of these materials. *Materials Science and Engineering C*. 2019;102(December 2018):299–304.

59. McCallum SJ, Gallagher MJ, Corkill JE, Hart CA, Ledson MJ, Walshaw MJ. Spread of an epidemic *Pseudomonas aeruginosa* strain from a patient with cystic fibrosis (CF) to non-CF relatives. *Thorax*. 2002;57(February 2000):559–61.
60. Wilson C, Lukowicz R, Merchant S, Valquier-Flynn H, Caballero J, Sandoval J, et al. Quantitative and Qualitative Assessment Methods for Biofilm Growth: A Mini-review. *Nature Rev Drug Discovery*. 2016;5(6):1–8.
61. Dawadi P, Khadka C, Shyaula M, Syangtan G, Joshi TP, Pepper SH, et al. Prevalence of metallo- $\beta$ -lactamases as a correlate of multidrug resistance among clinical *Pseudomonas aeruginosa* isolates in Nepal. *Science of the Total Environment*. 2022;850(August):157975.
62. Milivojevic D, Šumonja N, Medić S, Pavic A, Moric I, Vasiljevic B, et al. Biofilm-forming ability and infection potential of *Pseudomonas aeruginosa* strains isolated from animals and humans. *Pathog Dis*. 2018;76(4):1–14.
63. Stover CK, Pham XQ, Erwin AL, Mizoguchi SD, Warrenner P, Hickey MJ, et al. Complete genome sequence of *Pseudomonas aeruginosa* PAO1, an opportunistic pathogen. *Nature*. 2000;406(6799):959–64.
64. Elnegery AA, Mowafy WK, Zahra TA, Abou El-Khier NT. Study of quorum-sensing LasR and RhlR genes and their dependent virulence factors in *Pseudomonas aeruginosa* isolates from infected burn wounds. *Access Microbiol*. 2021;3(3):1–11.
65. Davey ME, Caiazza NC, O'Toole GA. Rhamnolipid Surfactant Production Affects Biofilm Architecture in. *Microbiology (N Y)*. 2003;185(3):1027–36.
66. Kamath S, Kapatral V, Chakrabarty AM. Cellular function of elastase in *Pseudomonas aeruginosa*: Role in the cleavage of nucleoside diphosphate kinase and in alginate synthesis. *Mol Microbiol*. 1998;30(5):933–41.
67. Passador L, Cook JM, Gambello MJ, Rust L, Iglewski BH. Expression of *Pseudomonas aeruginosa* virulence genes requires cell-to-cell communication. *Science (1979)*. 1993;260(5111):1127–30.
68. Conibear TCR, Collins SL, Webb JS. Role of mutation in *Pseudomonas aeruginosa* biofilm development. *PLoS One*. 2009;4(7):e6289.
69. De Bentzmann S, Plésiat P. The *Pseudomonas aeruginosa* opportunistic pathogen and human infections. *Environ Microbiol*. 2011;13(7):1655–65.
70. Keogh RH, Szczesniak R, Taylor-Robinson D, Bilton D. Up-to-date and projected estimates of survival for people with cystic fibrosis using baseline characteristics: A longitudinal study using UK patient registry data. *Journal of Cystic Fibrosis*. 2018;17(2):218–27.
71. Emerson J, Rosenfeld M, McNamara S, Ramsey B, Gibson RL. *Pseudomonas aeruginosa* and other predictors of mortality and morbidity in young children with cystic fibrosis. *Pediatr Pulmonol*. 2002;34(2):91–100.

72. Kao WTK, Frye M, Gagnon P, Vogel JP, Chole R. D-amino acids do not inhibit *Pseudomonas aeruginosa* biofilm formation. *Laryngoscope Investig Otolaryngol*. 2017;2(1):4–9.
73. Mikkelsen H, McMullan R, Filloux A. The *Pseudomonas aeruginosa* reference strain PA14 displays increased virulence due to a mutation in *ladS*. *PLoS One*. 2011;6(12).
74. Haney EF, Trimble MJ, Cheng JT, Vallé Q, Hancock REW. Critical assessment of methods to quantify biofilm growth and evaluate antibiofilm activity of host defence peptides. *Biomolecules*. 2018;8(2):1–22.
75. Martin K, Baddal B, Mustafa N, Perry C, Underwood A, Constantidou C, et al. Clusters of genetically similar isolates of *Pseudomonas aeruginosa* from multiple hospitals in the UK. *J Med Microbiol*. 2013;62(PART7):988–1000.
76. Winstanley C, Langille MGI, Fothergill JL, Kukavica-Ibrulj I, Paradis-Bleau C, Sanschagrin F, et al. Newly introduced genomic prophage islands are critical determinants of in vivo competitiveness in the liverpool epidemic strain of *pseudomonas aeruginosa*. *Genome Res*. 2009;19(1):12–23.
77. Anwar H, Costerton JW. Enhanced activity of combination of tobramycin and piperacillin for eradication of sessile biofilm cells of *Pseudomonas aeruginosa*. *Antimicrob Agents Chemother*. 1990;34(9):1666–71.
78. Friedheim E, Michaelis L. Potentiometric Study of Pyocyanine. *Journal of Biological Chemistry*. 1931;91(1):355–68.
79. Abdelaziz AA, Kamer AMA, Al-Monofy KB, Al-Madboly LA. *Pseudomonas aeruginosa*'s greenish-blue pigment pyocyanin: its production and biological activities. *Microb Cell Fact*. 2023;22(1):1–14.
80. Webster TA, Sismaet HJ, Chan IPJ, Goluch ED. Electrochemically monitoring the antibiotic susceptibility of *Pseudomonas aeruginosa* biofilms. *Analyst*. 2015;140(21):7195–201.
81. Thees A V., Pietrosimone KM, Melchiorre CK, Marden JN, Graf J, Lynes MA, et al. *PmtA* Regulates Pyocyanin Expression and Biofilm Formation in *Pseudomonas aeruginosa*. *Front Microbiol*. 2021;12(November):1–16.
82. Liao C, Huang X, Wang Q, Yao D, Lu W. Virulence Factors of *Pseudomonas Aeruginosa* and Antivirulence Strategies to Combat Its Drug Resistance. Vol. 12, *Frontiers in Cellular and Infection Microbiology*. Frontiers Media S.A.; 2022.
83. Moskowitz SM, Foster JM, Emerson J, Burns JL. Clinically Feasible Biofilm Susceptibility Assay for Isolates of *Pseudomonas aeruginosa* from Patients with Cystic Fibrosis. *J Clin Microbiol*. 2004;42(5):1915–22.
84. Podos SD, Thanassi JA, Leggio M, Pucci MJ. Bactericidal activity of ACH-702 against nondividing and biofilm staphylococci. *Antimicrob Agents Chemother*. 2012;56(7):3812–8.

85. Kamer AMA, Abdelaziz AA, Al-Monofy KB, Al-Madboly LA. Antibacterial, antibiofilm, and anti-quorum sensing activities of pyocyanin against methicillin-resistant *Staphylococcus aureus*: in vitro and in vivo study. *BMC Microbiol.* 2023;23(1):1–19.
86. Donlan RM. Biofilm Formation: A Clinically Relevant Microbiological Process. *Clinical Infectious Diseases.* 2001;33(8):1387–92.
87. Wang EW, Jung JY, Pashia ME, Nason R, Scholnick S, Chole RA. Otopathogenic *Pseudomonas aeruginosa* strain as competent biofilm formers. *Archives of otolaryngology - head and neck surgery.* 2005;131(11):983–9.
88. Ryder C, Byrd M, Wozniak DJ. Role of polysaccharides in *Pseudomonas aeruginosa* biofilm development. *Curr Opin Microbiol.* 2007;10(6):644–8.
89. Xu Y, Dhaouadi Y, Stoodley P, Ren D. Sensing the unreachable: challenges and opportunities in biofilm detection. *Curr Opin Biotechnol.* 2020;64:79–84.
90. Kalia VC, Prakash J, Koul S, Ray S. Simple and Rapid Method for Detecting Biofilm Forming Bacteria. *Indian J Microbiol.* 2017;57(1):109–11.
91. Cochran WL, McFeters GA, Stewart PS. Reduced susceptibility of thin *Pseudomonas aeruginosa* biofilms to hydrogen peroxide and monochloramine. *J Appl Microbiol.* 2000;88(1):22–30.
92. Werner E, Roe F, Bugnicourt A, Franklin MJ, Heydorn A, Molin S, et al. Stratified growth in *Pseudomonas aeruginosa* biofilms. *Appl Environ Microbiol.* 2004;70(10):6188–96.
93. Rukavina Z, Vanić Ž. Current trends in development of liposomes for targeting bacterial biofilms. Vol. 8, *Pharmaceutics.* MDPI AG; 2016.
94. Bisht K, Ann Wakeman C. Discovery and therapeutic targeting of differentiated biofilm subpopulations. Vol. 10, *Frontiers in Microbiology.* Frontiers Media S.A.; 2019.
95. Gilbert-Girard S, Reigada I, Savijoki K, Yli-Kauhaluoma J, Fallarero A. Screening of natural compounds identifies ferutinin as an antibacterial and anti-biofilm compound. Vol. 37, *Biofouling.* 2021. p. 791–807.
96. Marrie TJ, Costerton JW. Scanning and transmission electron microscopy of in situ bacterial colonization of intravenous and intraarterial catheters. *J Clin Microbiol.* 1984;19(5):687–93.
97. Siracuse JJ, Nandivada P, Giles KA, Hamdan AD, Wyers MC, Chaikof EL, et al. Prosthetic graft infections involving the femoral artery. *J Vasc Surg.* 2013;57(3):700–5.
98. Tseng YH, Lin CC, Wong MY, Kao CC, Lu MS, Lu CH, et al. *Pseudomonas aeruginosa* Infections Are Associated with Infection Recurrence in Arteriovenous Grafts Treated with Revision. *Medicina (B Aires).* 2023;59(1294).
99. NBIC. National Biofilms Innovation Centre Annual Report 2021. 2021;

100. Lee J, Kang CI, Lee JH, Joung M, Moon S, Wi YM, et al. Risk factors for treatment failure in patients with prosthetic joint infections. *J Hosp Infect.* 2010;75(4):273–6.
101. Seebach E, Kubatzky KF. Chronic Implant-Related Bone Infections-Can Immune Modulation be a Therapeutic Strategy? *Front Immunol.* 2019;10(July):1724.
102. Wildemann B, Jandt KD. Infections @ Trauma / Orthopedic Implants: Recent Advances on Materials, Methods, and Microbes - A Mini-Review. *Materials.* 2021;14(19):1–11.
103. Tapscott DC, Wottowa C. *Orthopedic Implant Materials.* Treasure Island, Florida: StatPearls Publishing; 2023. 7 p.
104. Ratner B. Vascular Grafts: Technology Success/Technology Failure. *BME Front.* 2023;4(Cdi):1–11.
105. Nazer RI, Alhothali A, Albarrati A. In vitro modeling of crimped Dacron vascular grafts for aortic root replacement. *Am J Cardiovasc Dis.* 2023;13(2):59–67.
106. Fitridge R, Thompson M. *Mechanisms of Vascular Disease: A reference book for vascular specialists.* 2011th ed. Barr Smith Press. Adelaide, Australia: Barr Smith Press; 2011. 553 p.
107. Ugurlucan M, Oztas DM, Onal Y, Canbay C, Sayin OA, Barbuoglu M, et al. Treatment of Dacron Grafting Dilatation with Endovascular Stent Grafting. *Aorta.* 2016;4(5):162–6.
108. Tello-Díaz C, Palau M, Muñoz E, Gomis X, Gavaldà J, Fernández-Hidalgo N, et al. Methicillin-Susceptible *Staphylococcus aureus* Biofilm Formation on Vascular Grafts: an In Vitro Study . *Microbiol Spectr.* 2023;11(2).
109. Walker JN, Horswill AR. A coverslip-based technique for evaluating *Staphylococcus aureus* biofilm formation on human plasma. *Front Cell Infect Microbiol.* 2012;2(March):39.
110. Condren AR, Kahl LJ, Boelter G, Kritikos G, Banzhaf M, Dietrich LEP, et al. Biofilm Inhibitor Taurolithocholic Acid Alters Colony Morphology, Specialized Metabolism, and Virulence of *Pseudomonas aeruginosa*. *ACS Infect Dis.* 2020;6(4):603–12.
111. Stewart PS. Prospects for anti-biofilm pharmaceuticals. *Pharmaceuticals.* 2015;8(3):504–11.
112. Döring G, Hoiby N, Assael B, Ballmann M, Bush A, Button B, et al. Early intervention and prevention of lung disease in cystic fibrosis: A European consensus. *Journal of Cystic Fibrosis.* 2004;3(2):67–91.
113. De Kievit TR, Kakai Y, Register JK, Pesci EC, Iglewski BH. Role of the *Pseudomonas aeruginosa* las and rhl quorum-sensing systems in rhlI regulation. *FEMS Microbiol Lett.* 2002;212(1):101–6.
114. O’Loughlin CT, Miller LC, Siryaporn A, Drescher K, Semmelhack MF, Bassler BL. A quorum-sensing inhibitor blocks *Pseudomonas aeruginosa* virulence and biofilm formation. *PNAS.* 2013;110(44):17981–6.

115. Bodelón G, Montes-García V, López-Puente V, Hill EH, Hamon C, Sanz-Ortiz MN, et al. Detection and imaging of quorum sensing in *Pseudomonas aeruginosa* biofilm communities by surface-enhanced resonance Raman scattering Europe PMC Funders Group. *Nat Mater*. 2016;15(11):1203–11.
116. Amabili M, Balasubramanian P, Ferrari G, Franchini G, Giovanniello F, Tubaldi E. Identification of viscoelastic properties of Dacron aortic grafts subjected to physiological pulsatile flow. *Journal of Mechanical Behaviour of Biomedical Materials*. 2020;110.
117. Herten M, Bisdas T, Knaack D, Becker K, Osada N, Torsello GB, et al. Rapid in vitro quantification of *S. aureus* biofilms on vascular graft surfaces. *Front Microbiol*. 2017 Dec 5;8(DEC).
118. Donlan RM, William Costerton J. Biofilms: Survival Mechanisms of Clinically Relevant Microorganisms. *Clin Microbiol Rev*. 2002;15(2):167–93.
119. Panda P, Chaudhary U, Dube S. Comparison of four different methods for detection of biofilm formation by uropathogens. *Indian J Pathol Microbiol*. 2016;59(2):177–9.
120. Tsalik EL, Bonomo RA, Fowler VG. New Molecular Diagnostic Approaches to Bacterial Infections and Antibacterial Resistance. *Annu Rev Med*. 2018;379–94.
121. Singh PK, Schaefer AL, Parsek MR, Moninger TO, Welsh MJ, Greenberg EP. Quorum-sensing signals indicate that cystic fibrosis lungs are infected with bacterial biofilms. *Nature*. 2000;407(October):762–4.
122. Rasmussen BB, Nielsen KF, MacHado H, Melchiorson J, Gram L, Sonnenschein EC. Global and phylogenetic distribution of quorum sensing signals, acyl homoserine lactones, in the family of vibrionaceae. *Mar Drugs*. 2014;12(11):5527–46.
123. Lasa I, Penadés JR. Bap: A family of surface proteins involved in biofilm formation. *Res Microbiol*. 2006;157(2):99–107.
124. Antypas H, Choong FX, Libberton B, Brauner A, Richter-Dahlfors A. Rapid diagnostic assay for detection of cellulose in urine as biomarker for biofilm-related urinary tract infections. *NPJ Biofilms Microbiomes*. 2018;26.
125. Tietze S, Singer F, Lasota S, Ebert S, Landskron J, Drese KS, et al. Monitoring of Soft Deposition Layers in Liquid-Filled Tubes with Guided Acoustic Waves Excited by Clamp-on Transducers. *Sensors*. 2018;18(526).
126. Sellmyer MA, Lee I, Hou C, Weng CC, Li S, Lieberman BP, et al. Bacterial infection imaging with [<sup>18</sup>F]fluoropropyl-trimethoprim. *PNAS*. 2017;114(31):8372–7.
127. Domingo-Roca R, Lasserre P, Riordan L, Macdonald AR, Dobrea A, Duncan KR, et al. Rapid assessment of antibiotic susceptibility using a fully 3D-printed impedance-based biosensor. *Biosens Bioelectron X*. 2023;13:100308.
128. Dunphy RD, Lasserre P, Riordan L, Duncan KR, McCormick C, Murray P, et al. Combining hyperspectral imaging and electrochemical sensing for detection of *Pseudomonas aeruginosa* through pyocyanin production. *Sensors & Diagnostics*. 2022;1(4):841–50.

129. Hannah S, Addington E, Alcorn D, Shu W, Hoskisson PA, Corrigan DK. Rapid antibiotic susceptibility testing using low-cost, commercially available screen-printed electrodes. *Biosens Bioelectron.* 2019;145(July).
130. Hannah S, Dobrea A, Lasserre P, Blair EO, Alcorn D, Hoskisson PA, et al. Development of a Rapid, Antimicrobial Susceptibility Test for *E. coli* Based on Low-Cost, Screen-Printed Electrodes. *Biosensors (Basel).* 2020;10(11).
131. Macdonald JR. Impedance spectroscopy. *Ann Biomed Eng.* 1992;20:289–305.
132. Ramírez N, Regueiro A, Arias O, Contreras R. Electrochemical impedance spectroscopy: An effective tool for a fast microbiological diagnosis. *Biotechnología Aplicada.* 2009;26(2):72–8.
133. Alatraktchi FA, Andersen SB, Johansen HK, Molin S, Svendsen WE. Fast selective detection of pyocyanin using cyclic voltammetry. *Sensors (Switzerland).* 2016;16(3).
134. Bellin DL, Sakhtah H, Zhang Y, Price-Whelan A, Dietrich LEP, Shepard KL. Electrochemical camera chip for simultaneous imaging of multiple metabolites in biofilms. *Nat Commun.* 2016 Jan 27;7.
135. Ward AC, Connolly P, Tucker NP. *Pseudomonas aeruginosa* can be detected in a polymicrobial competition model using impedance spectroscopy with a novel biosensor. *PLoS One.* 2014;9(3).
136. Ait Barka E, Vatsa P, Sanchez L, Gaveau-Vaillant N, Jacquard C, Klenk HP, et al. Taxonomy, Physiology, and Natural Products of Actinobacteria. *Microbiology and Molecular Biology Reviews.* 2015;80:1–43.
137. Chen J, Xu L, Zhou Y, Han B. Natural products from actinomycetes associated with marine organisms. *Mar Drugs.* 2021;19(11).
138. Katz L, Baltz RH. Natural product discovery: past, present, and future. *J Ind Microbiol Biotechnol.* 2016;43(2–3):155–76.
139. Gavriilidou A, Kautsar SA, Zaburannyi N, Krug D, Müller R, Medema MH, et al. Compendium of specialized metabolite biosynthetic diversity encoded in bacterial genomes. *Nat Microbiol.* 2022;7(5):726–35.
140. Alam K, Mazumder A, Sikdar S, Zhao YM, Hao J, Song C, et al. Streptomyces: The biofactory of secondary metabolites. *Front Microbiol.* 2022;13(September):1–21.
141. Hoskisson PA, van Wezel GP. *Streptomyces coelicolor*. *Trends Microbiol.* 2019;27(5):468–9.
142. Kronheim S, Daniel-Ivad M, Duan Z, Hwang S, Wong AI, Mantel I, et al. A chemical defence against phage infection. *Nature.* 2018;564(7735):283–6.
143. Jabila Mary TR, Kannan RR, Iniyan AM, Ramachandran D, Prakash Vincent SG. Cell wall distraction and biofilm inhibition of marine *Streptomyces* derived angucycline in methicillin resistant *Staphylococcus aureus*. *Microb Pathog.* 2021;150(September 2020).

144. Manderscheid N, Helaly SE, Kulik A, Wiese J, Imhoff JF, Fiedler H peter, et al. Elaiomycins K and L , new azoxy antibiotics from *Streptomyces* Sp. Tu 6399\*. *J Antibiot (Tokyo)*. 2013;66(64):85–8.
145. Li X, Li B, Cai S, Zhang Y, Xu M, Zhang C, et al. Identification of rhizospheric actinomycete *streptomyces lavendulae* sps-33 and the inhibitory effect of its volatile organic compounds against *ceratocystis fimbriata* in postharvest sweet potato (*Ipomoea batatas* (L.) Lam.). *Microorganisms*. 2020;8(3).
146. Rashad FM, Fathy HM, El-Zayat S, Elghonaimy AM. Isolation and characterization of multifunctional *Streptomyces* species with antimicrobial, nematocidal and phytohormone activities from marine environments in Egypt. *Microbiol Res*. 2015;175:34–47.
147. Buranda T, Gineste C, Wu Y, Bondu V, Perez D, Lake KR, et al. A high-throughput flow cytometry screen identifies molecules that inhibit hantavirus cell entry. *SLAS Discovery*. 2018;23(7):634–45.
148. Cohen A, Harley EH, Rees KR. Antiviral Effect of Daunomycin. *Nature*. 1969;222:36–8.
149. Dias DA, Urban S, Roessner U. A Historical overview of natural products in drug discovery. *Metabolites*. 2012;2(2):303–36.
150. Topa SH, Palombo EA, Kingshott P, Blackall LL. Activity of cinnamaldehyde on quorum sensing and biofilm susceptibility to antibiotics in *Pseudomonas aeruginosa*. *Microorganisms*. 2020;8(3).
151. Intra B, Mungsuntisuk I, Nihira T, Igarashi Y, Panbangred W. Identification of actinomycetes from plant rhizospheric soils with inhibitory activity against *Colletotrichum* spp., the causative agent of anthracnose disease. *BMC Res Notes*. 2011;4(98):1–9.
152. Zucker L. Chapter 6 - Arnica. *Complementary Therapies for Physical Therapy*. 2008;75–83.
153. Merfort I. Caffeoylquinic acids from flowers of *Arnica Montana* and *Arnica chamissonis*. *Phytochemistry*. 1992;31(6):2111–3.
154. Zielińska S, Dziągwa-becker M, Junka A, Piątczak E, Jezierska-domaradzka A, Brożyna M, et al. Screening papaveraceae as novel antibiofilm natural-based agents. *Molecules*. 2021;26(16):1–20.
155. Makhlof MEM, El-sheekh MM, El-sayed AIM. In vitro antibiofilm, antibacterial, antioxidant and antitumor activities of the brown alga *Padina pavonica* biomass extract. *Int J Environ Health Res*. 2023;1–18.
156. Buijs Y, Bech PK, Vazquez-Albacete D, Bentzon-Tilia M, Sonnenschein EC, Gram L, et al. Marine Proteobacteria as a source of natural products: Advances in molecular tools and strategies. Vol. 36, *Natural Product Reports*. 2019. p. 1333–50.
157. Baltz RH. Gifted microbes for genome mining and natural product discovery. *J Ind Microbiol Biotechnol*. 2017;44(4–5):573–88.

158. Sowani H, Kulkarni M, Zinjarde S, Javdekar V. *Gordonia* and Related Genera as Opportunistic Human Pathogens Causing Infections of Skin, Soft Tissues, and Bones. In: *The Microbiology of Skin, Soft Tissue, Bone and Joint Infections*. 1st ed. Elsevier Inc.; 2017. p. 105–21.
159. Feeney MA, Newitt JT, Addington E, Gallardo LA, Allan C, Balis L, et al. ActinoBase : tools and protocols for researchers working on *Streptomyces* and other filamentous actinobacteria. *Microb Genom*. 2022;1–11.
160. Lucas X, Senger C, Erxleben A, Grüning BA, Döring K, Mosch J, et al. StreptomeDB: a resource for natural compounds isolated from *Streptomyces* species. *Nucleic Acids Res*. 2013;41:D1130–6.
161. Fenical W, Jensen PR. Developing a new resource for drug discovery: Marine actinomycete bacteria. *Nat Chem Biol*. 2006;2(12):666–73.
162. Kuroda H, Hosokawa N. Gram-ghost bacilli. *J Gen Fam Med*. 2019;20(1):31–2.
163. Silva G da C, Kitano IT, Ribeiro IA de F, Lacava PT. The Potential Use of Actinomycetes as Microbial Inoculants and Biopesticides in Agriculture. *Frontiers in Soil Science*. 2022;2(February):1–20.
164. Mast Y, Stegmann E, Lu Y. Editorial: Regulation of Antibiotic Production in Actinomycetes. *Front Microbiol*. 2020;11(July):10–2.
165. Schneider YK, Hagestad OC, Li C, Hansen EH, Andersen JH. Selective isolation of Arctic marine actinobacteria and a down-scaled fermentation and extraction strategy for identifying bioactive compounds. *Front Microbiol*. 2022;13(November):1–16.
166. Waksman SA, Woodruff HB. Bacteriostatic and Bactericidal Substances Produced by a Soil Actinomycetes. *Proceedings of the Society for Experimental Biology and Medicine*. 1940;45(2):609–14.
167. Waksman SA, Woodruff HB. Streptothricin, a New Selective Bacteriostatic and Bactericidal Agent, Particularly Active Against Gram-Negative Bacteria. *Proceedings of the Society for Experimental Biology and Medicine*. 1942;49(2):207–10.
168. Schatz A, Bugle E, Waksman SA. Streptomycin, a Substance Exhibiting Antibiotic Activity Against Gram-Positive and Gram-Negative Bacteria. *Proceedings of the Society for Experimental Biology and Medicine*. 1944;55(1):66–9.
169. Schniete JK, Cruz-Morales P, Selem-Mojica N, Fernández-Martínez LT, Hunter IS, Barona-Gómez F, et al. Expanding primary metabolism helps generate the metabolic robustness to facilitate antibiotic biosynthesis in *Streptomyces*. *mBio*. 2018;9(1).
170. Harir M, Bendif H, Bellhcene M, Fortas Z, Pogni R. *Streptomyces* Secondary Metabolites. In: *Basic Biology and Applications of Actinobacteria*. 2018. p. 44.
171. Bruner-Montero G, Wood M, Horn HA, Gemperline E, Li L, Currie CR. Symbiont-Mediated Protection of *Acromyrmex* Leaf-Cutter Ants from the Entomopathogenic Fungus *Metarhizium anisopliae*. *mBio*. 2021;12(6).

172. de Lima Procópio RE, da Silva IR, Martins MK, de Azevedo JL, de Araújo JM. Antibiotics produced by *Streptomyces*. *Brazilian Journal of Infectious Diseases*. 2012 Sep;16(5):466–71.
173. Emery E. The preparation “606.” *The Lancet*. 1910;1543–8.
174. Nichols HJ. Further observations on certain features of experimental syphilis and yaws in the rabbit. *Journal of Experimental Medicine*. 1911;14(2):196–216.
175. Babalola OO, Kirby BM, Le Roes-Hill M, Cook AE, Cary SC, Burton SG, et al. Phylogenetic analysis of actinobacterial populations associated with Antarctic Dry Valley mineral soils. *Environ Microbiol*. 2009;11(3):566–76.
176. Dinda AP, Asnani A, Anjarwati DU. The Activities of *Streptomyces* W-5A as Antibacterial and Antibiofilm towards Methicillin-resistant *Staphylococcus aureus* 2983. *Proceedings of the 1st Jenderal Soedirman International Medical Conference in conjunction with the 5th Annual Scientific Meeting (Temilnas) Consortium of Biomedical Science Indonesia*. 2021;(JIMC 2020):109–15.
177. Jiang H, Dong H, Zhang G, Yu B, Chapman LR, Fields MW. Microbial diversity in water and sediment of Lake Chaka, an athalassohaline lake in northwestern China. *Appl Environ Microbiol*. 2006;72(6):3832–45.
178. Pérez-Corral DA, de Jesús Ornelas-Paz J, Olivas-Orozco GI, Acosta-Muñiz CH, Salas-Marina MÁ, Berlanga-Reyes DI, et al. Molecular, Morphological and Biochemical Characterization of Actinomycetes and Their Antagonistic Activity Against Phytopathogenic Fungi. *Revista Fitotecnia Mexicana*. 2022;45(1):103–15.
179. Romano S, Jackson SA, Patry S, Dobson ADW. Extending the “one strain many compounds” (OSMAC) principle to marine microorganisms. *Mar Drugs*. 2018;16(7):1–29.
180. Soldatou S, Eldjárn GH, Ramsay A, van der Hoof JJJ, Hughes AH, Rogers S, et al. Comparative Metabologenomics Analysis of Polar Actinomycetes. *Mar Drugs*. 2021;19(2):1–23.
181. McLafferty FW. A century of progress in molecular mass spectrometry. *Annual Review of Analytical Chemistry*. 2011;4:1–22.
182. Gohlke RS, McLafferty FW. *Early Gas Chromatography / Mass*. American Society for Mass Spectrometry. 1993;4:367–71.
183. El-Aneed A, Cohen A, Banoub J. Mass spectrometry, review of the basics: Electrospray, MALDI, and commonly used mass analyzers. *Appl Spectrosc Rev*. 2009;44(3):210–30.
184. Pitt JJ. Principles and Applications of Liquid Chromatography-Mass Spectrometry in Clinical Biochemistry. 2009;30(February):19–34.
185. Schauer KL, Broccardo CJ, Webb KM, Covey PA, Prenni JE. Mass spectrometry contamination from tinuvin 770, a common additive in laboratory plastics. *Journal of Biomolecular Techniques*. 2013;24(2):57–61.

186. Sanchez LM, Cheng AT, Warner CJA, Townsley L, Peach KC, Navarro G, et al. Biofilm formation and detachment in gram-negative pathogens is modulated by select bile acids. *PLoS One*. 2016;11(3):1–16.
187. Kim MC, Winter JM, Asolkar RN, Boonlarpradab C, Cullum R, Fenical W. Marinoterpins A-C: Rare Linear Merosesterterpenoids from Marine-Derived Actinomycete Bacteria of the Family Streptomycetaceae. *Journal of Organic Chemistry*. 2021;
188. Lee C, Ni CK. Soft Matrix-Assisted Laser Desorption/Ionization for Labile Glycoconjugates. *J Am Soc Mass Spectrom*. 2019;30(8):1455–63.
189. Čihák M, Kameník Z, Šmídová K, Bergman N, Benada O, Kofronová O, et al. Secondary metabolites produced during the germination of *Streptomyces coelicolor*. *Front Microbiol*. 2017;8(DEC):1–13.
190. Elshafie HS, De Martino L, Formisano C, Caputo L, De Feo V, Camele I. Chemical Identification of Secondary Metabolites from Rhizospheric Actinomycetes Using LC-MS Analysis: In Silico Antifungal Evaluation and Growth-Promoting Effects. *Plants*. 2023;12(9).
191. Arango C, Acosta-Gonzalez A, Parra-Giraldo CM, Sánchez-Quitian ZA, Kerr R, Díaz LE. Characterization of Actinobacterial Communities from Arauca River Sediments (Colombia) Reveals Antimicrobial Potential Presented in Low Abundant Isolates. *Open Microbiol J*. 2018;12(1):181–94.
192. McCann A, Kune C, La Rocca R, Oetjen J, Arias AA, Ongena M, et al. Rapid visualization of lipopeptides and potential bioactive groups of compounds by combining ion mobility and MALDI imaging mass spectrometry. *Drug Discov Today Technol*. 2021;39:81–8.
193. Wang M, Carver JJ, Phelan V V., Sanchez LM, Garg N, Peng Y, et al. Sharing and community curation of mass spectrometry data with Global Natural Products Social Molecular Networking. *Nat Biotechnol*. 2016;34(8):828–37.
194. de Jonge NF, Louwen JJR, Chekmeneva E, Camuzeaux S, Vermeir FJ, Jansen RS, et al. MS2Query: reliable and scalable MS2 mass spectra-based analogue search. *Nat Commun*. 2023;14(1):1–18.
195. Purves K, Macintyre L, Brennan D, Hreggviðsson G, Kuttner E, Ásgeirsdóttir ME, et al. Using molecular networking for microbial secondary metabolite bioprospecting. *Metabolites*. 2016;6(1).
196. Yu J, Hermann M, Smith R, Tomm H, Metwally H, Kolwich J, et al. Hyperspectral Visualization-Based Mass Spectrometry Imaging by LMJ-SSP: A Novel Strategy for Rapid Natural Product Profiling in Bacteria. *Anal Chem*. 2022;
197. Millán-Aguiñaga N, Soldatou S, Brozio S, Munnoch JT, Howe J, Hoskisson PA, et al. Awakening ancient polar actinobacteria: Diversity, evolution and specialized metabolite potential. *Microbiology (United Kingdom)*. 2019;165(11):1169–80.

198. Lee DG, Urbach JM, Wu G, Liberati NT, Feinbaum RL, Miyata S, et al. Genomic analysis reveals that *Pseudomonas aeruginosa* virulence is combinatorial. *Genome Biol.* 2006;7(10).
199. Liberati NT, Urbach JM, Miyata S, Lee DG, Drenkard E, Wu G, et al. An ordered, nonredundant library of *Pseudomonas aeruginosa* strain PA14 transposon insertion mutants. *Proc Natl Acad Sci U S A.* 2006;103(8):2833–8.
200. Jensen PR, Gontang E, Mafnas C, Mincer TJ, Fenical W. Culturable marine actinomycete diversity from tropical Pacific Ocean sediments. *Environ Microbiol.* 2005;7(7):1039–48.
201. Bertani G. Studies on lysogenesis. I. The mode of phage liberation by lysogenic *Escherichia coli*. *J Bacteriol.* 1951;62(3):293–300.
202. Shirling EB, Gottlieb D. Methods for characterization of *Streptomyces* species. *Int J Syst Bacteriol.* 1966;16(3):313–40.
203. Bergkessel M, Guthrie C. Colony PCR. In: *Methods in Enzymology.* 2013. p. 299–309.
204. Tamura K, Nei M. Estimation of the number of nucleotide substitutions in the control region of mitochondrial DNA in humans and chimpanzees. *Mol Biol Evol.* 1993;10(3):512–26.
205. Kumar S, Stecher G, Li M, Knyaz C, Tamura K. MEGA X: Molecular evolutionary genetics analysis across computing platforms. *Mol Biol Evol.* 2018;35(6):1547–9.
206. Shannon P, Markiel A, Ozier O, Baliga NS, Wang JT, Ramage D, et al. Cytoscape: A Software Environment for Integrated Models of Biomolecular Interaction Networks. *Genome Res.* 2003;13(22):2498–508.
207. Peeters E, Nelis HJ, Coenye T. Comparison of multiple methods for quantification of microbial biofilms grown in microtiter plates. *J Microbiol Methods.* 2008 Feb 1;72(2):157–65.
208. Fletcher M. The effects of culture concentration and age, time, and temperature on bacterial attachment to polystyrene. *Can J Microbiol.* 1977;23(1):1–6.
209. Stiefel P, Rosenberg U, Schneider J, Mauerhofer S, Maniura-Weber K, Ren Q. Is biofilm removal properly assessed? Comparison of different quantification methods in a 96-well plate system. *Appl Microbiol Biotechnol.* 2016;100:4135–45.
210. Djordjevic D, Wiedmann M, Mclandsborough LA. Microtiter Plate Assay for Assessment of *Listeria monocytogenes* Biofilm Formation. *Appl Environ Microbiol.* 2002;68(6):2950–8.
211. Van Duuren JBJH, Müsken M, Karge B, Tomasch J, Wittmann C, Häussler S, et al. Use of Single-Frequency Impedance Spectroscopy to Characterize the Growth Dynamics of Biofilm Formation in *Pseudomonas aeruginosa*. *Sci Rep.* 2017;7(1):1–11.
212. Hancock V, Klemm P. Global gene expression profiling of asymptomatic bacteriuria *Escherichia coli* during biofilm growth in human urine. *Infect Immun.* 2007;75(2):966–76.

213. Nilsson M, Chiang WC, Fazli M, Gjermansen M, Givskov M, Tolker-Nielsen T. Influence of putative exopolysaccharide genes on *Pseudomonas putida* KT2440 biofilm stability. *Environ Microbiol.* 2011;13(5):1357–69.
214. Guiton PS, Hung CS, Kline KA, Roth R, Kau AL, Hayes E, et al. Contribution of autolysin and sortase A during *Enterococcus faecalis* DNA-dependent biofilm development. *Infect Immun.* 2009;77(9):3626–38.
215. Summer K, Browne J, Hollanders M, Benkendorff K. Out of control: The need for standardised solvent approaches and data reporting in antibiofilm assays incorporating dimethyl-sulfoxide (DMSO). *Biofilm.* 2022;4(August).
216. Kemung HM, Tan LT hern, Chan K gan, Ser H leng, Law JW fei, Lee L han, et al. *Streptomyces* sp. Strain MUSC 125 from Mangrove Soil in Malaysia with Anti-MRSA, Anti-Biofilm and Antioxidant Activities. *Molecules.* 2020;25(3545):1–20.
217. Woodward MJ, Sojka M, Sprigings KA, Humphrey TJ. The role of SEF14 and SEF17 fimbriae in the adherence of *Salmonella enterica* serotype Enteritidis to inanimate surfaces. *J Med Microbiol.* 2000;49(5):481–7.
218. O'Toole GA, Kolter R. Initiation of biofilm formation in *Pseudomonas fluorescens* WCS365 proceeds via multiple, convergent signalling pathways: A genetic analysis. Vol. 28, *Molecular Microbiology.* 1998. p. 449–61.
219. Kuhn DM, Chandra J, Mukherjee PK, Ghannoum M a. Comparison of Bio lms Formed by. *Society.* 2002;70(2):878–88.
220. Shailaja A, Bruce TF, Gerard P, Powell RR, Pettigrew CA, Kerrigan JL. Comparison of cell viability assessment and visualization of *Aspergillus niger* biofilm with two fluorescent probe staining methods. *Biofilm.* 2022;4(June):100090.
221. Culotti A, Packman AI. *Pseudomonas aeruginosa* Promotes *Escherichia coli* Biofilm Formation in Nutrient-Limited Medium. *PLoS One.* 2014;9(9):1–9.
222. Mountcastle SE, Vyas N, Villapun VM, Cox SC, Jabbari S, Shelton RM, et al. Biofilm viability checker: An open-source tool for automated biofilm viability analysis from confocal microscopy images. *NPJ Biofilms Microbiomes.* 2021;44:1–12.
223. Ceri H, Olson ME, Stremick C, Read RR, Morck D. The Calgary Biofilm Device. *J Clin Microbiol.* 1999;37(6):1771–6.
224. Kim T, Kang J, Lee JH, Yoon J. Influence of attached bacteria and biofilm on double-layer capacitance during biofilm monitoring by electrochemical impedance spectroscopy | Enhanced Reader. *Water Res.* 2011;45:4615–22.
225. Barreiro M, Sánchez P, Vera J, Viera M, Morales I, Dell'Osa AH, et al. Multiplexing Error and Noise Reduction in Electrical Impedance Tomography Imaging. *Frontiers in Electronics.* 2022;3(March):1–11.
226. Barreiros dos Santos M, Aguil JP, Prieto-Simón B, Sporer C, Teixeira V, Samitier J. Highly sensitive detection of pathogen *Escherichia coli* O157: H7 by electrochemical impedance spectroscopy. *Biosens Bioelectron.* 2013;45(1):174–80.

227. Webster TA, Sismaet HJ, Conte JL, Chan I ping J, Goluch ED. Electrochemical detection of *Pseudomonas aeruginosa* in human fluid samples via pyocyanin. *Biosens Bioelectron.* 2014;60:265–70.
228. Natan M, Jacobi G, Banin E, Ashkenazi S. Prevention and treatment of *Pseudomonas aeruginosa*-based biofilm with ethanol. *Israel Medical Association Journal.* 2020;22(5):299–302.
229. Lee JH, Kim YG, Cho MH, Lee J. ZnO nanoparticles inhibit *Pseudomonas aeruginosa* biofilm formation and virulence factor production. *Microbiol Res.* 2014;169(12):888–96.
230. Faruque SM, Kamruzzaman M, Meraj IM, Chowdhury N, Nair GB, Sack RB, et al. Pathogenic potential of environmental *Vibrio cholerae* strains carrying genetic variants of the toxin-coregulated pilus pathogenicity island. *Infect Immun.* 2003;71(2):1020–5.
231. Yousefpour Z, Davarzani F, Owlia P. Evaluating of the effects of sub-MIC concentrations of gentamicin on biofilm formation in clinical isolates of *pseudomonas aeruginosa*. *Iran J Pathol.* 2021;16(4):403–10.
232. Russell C, Ward AC, Vezza V, Hoskisson P, Alcorn D, Steenson DP, et al. Development of a needle shaped microelectrode for electrochemical detection of the sepsis biomarker interleukin-6 (IL-6) in real time. *Biosens Bioelectron.* 2019;126(September 2018):806–14.
233. Cornish-Bowden A. *Fundamentals of Enzyme Kinetics.* 4th ed. *Fundamentals of enzyme kinetics.* Weinheim: Wiley-Blackwell; 1982.
234. Kretzschmar J, Harnisch F. Electrochemical impedance spectroscopy on biofilm electrodes – conclusive or euphonious? *Curr Opin Electrochem.* 2021;29(April):100757.
235. Paleczny J, Junka AF, Krzyz P. Comparison of antibio fi lm activity of low-concentrated hypochlorites vs polyhexanide- containing antiseptic. 2023;(March):1–14.
236. Patel N V, Mathur U, Sawant S, Acharya M, Gandhi A. Three Consecutive Cases of Ocular Polyhexamethylene Biguanide ( PHMB ) Toxicity Due to Compounding Error. *Cureus.* 2023;15(5):1–6.
237. Fjeld H, Lingaas E. Polyhexanide – safety and efficacy as an antiseptic. *Tidsskr Nor Legeforen.* 2016;136(8):707–11.
238. NHS. *The Revised Healthcare Cleaning Manual.* UK; 2009.
239. Miller T, Waturangi DE. Antibiofilm properties of bioactive compounds from Actinomycetes against foodborne and fish pathogens. *Sci Rep.* 2022;12(18614):1–14.
240. Klare W, Das T, Ibugo A, Buckle E, Manefield M, Manos J. Glutathione-disrupted biofilms of clinical *Pseudomonas aeruginosa* strains exhibit an enhanced antibiotic effect and a novel biofilm transcriptome. *Antimicrob Agents Chemother.* 2016;60(8):4539–51.

241. Ward AC, Bora N. Diversity and biogeography of marine actinobacteria. *Curr Opin Microbiol.* 2006;9(3):279–86.
242. Alswat AM, Jalal RS, Shami AY, Mazen A, Alsaedi ZS, Baz L, et al. Investigating the metagenomics of the bacterial communities in the rhizosphere of the desert plant *Senna italica* and their role as plant growth promoting factors. *Notulae Botanicae Horti Agrobotanici Cluj-Napoca.* 2023;51(1):1–18.
243. Claverías FP, Undabarrena A, González M, Seeger M, Cámara B. Culturable diversity and antimicrobial activity of Actinobacteria from marine sediments in Valparaíso bay, Chile. *Front Microbiol.* 2015;6(JUL):1–11.
244. Duncan K, Haltli B, Gill KA, Kerr RG. Bioprospecting from Marine Sediments of New Brunswick, Canada: Exploring the Relationship between Total Bacterial Diversity and Actinobacteria Diversity. *Mar Drugs.* 2014;12:899–925.
245. Jose PA, Jha B. Intertidal marine sediment harbours Actinobacteria with promising bioactive and biosynthetic potential. *Sci Rep.* 2017;7(1):1–15.
246. Nakaew N, Lumyong S, Sloan WT, Sungthong R. Bioactivities and genome insights of a thermotolerant antibiotics-producing *Streptomyces* sp. TM32 reveal its potentials for novel drug discovery. *Microbiologyopen.* 2019;8(11):1–7.
247. Parra J, Soldatou S, Rooney LM, Duncan KR. *Pseudonocardia abyssalis* sp. nov. and *pseudonocardia oceani* sp. nov., two novel actinomycetes isolated from the deep southern ocean. *Int J Syst Evol Microbiol.* 2021;71(9):1–8.
248. Huang X, Kong F, Zhou S, Huang D, Zheng J, Zhu W. *Streptomyces tirandamycinicus* sp. nov., a novel marine sponge-derived actinobacterium with antibacterial potential against streptococcus agalactiae. *Front Microbiol.* 2019;10(MAR):1–11.
249. Kirkwood JS, Maier C, Stevens JF. Simultaneous, untargeted metabolic profiling of polar and nonpolar metabolites by LC-Q-TOF mass spectrometry. *Curr Protoc Toxicol.* 2013;1(SUPPL.56):1–17.
250. Quinn RA, Nothias LF, Vining O, Meehan M, Esquenazi E, Dorrestein PC. Molecular Networking As a Drug Discovery, Drug Metabolism, and Precision Medicine Strategy. *Trends Pharmacol Sci.* 2017;38(2):143–54.
251. Rampioni G, Pillai CR, Longo F, Bondì R, Baldelli V, Messina M, et al. Effect of efflux pump inhibition on *Pseudomonas aeruginosa* transcriptome and virulence. *Sci Rep.* 2017;7(1):1–14.
252. Teelucksingh T, Thompson LK, Cox G. The Evolutionary Conservation of *Escherichia coli* Drug Efflux Pumps Supports Physiological Functions. *J Bacteriol.* 2020;202(22):1–17.
253. Komaki H. Recent Progress of Reclassification of the Genus *Streptomyces*. *Microorganisms.* 2023;11(4).
254. Quinn GA, Abdelhameed AM, Alharbi NK, Cobice D, Adu SA, Swain MT, et al. The isolation of a novel streptomyces sp. CJ13 from a traditional irish folk medicine

- alkaline grassland soil that inhibits multiresistant pathogens and yeasts. Vol. 11, Applied Sciences (Switzerland). 2021. p. 1–13.
255. Schmid R, Petras D, Nothias LF, Wang M, Aron AT, Jagels A, et al. Ion identity molecular networking for mass spectrometry-based metabolomics in the GNPS environment. *Nat Commun.* 2021;12(3832).
  256. Garrett MD, Fattaey A. CDK inhibition and cancer therapy. *Curr Opin Genet Dev.* 1999;9(1):104–11.
  257. Li D dan, Wang Y, Kim E La, Hong J, Jung JH. Neuroprotective Effect of Cyclo-(L-Pro-L-Phe) Isolated from the Jellyfish-Derived Fungus *Aspergillus flavus*. *Mar Drugs.* 2021;19(417):1–18.
  258. Fdhila F, Vazquez V, Sanchez JL, Riguera R. DD-Diketopiperazines: Antibiotics Active against *Vibrio anguillarum* Isolated from Marine Bacteria Associated with Cultures of *Pecten maximus*. *J Nat Prod.* 2003;66(10):17–9.
  259. Shibata M, Higashide E, Kanzaki T, Yamamoto H, Nakazawa K. Studies on Streptomycetes. *Agr Biol Chem.* 1960;25(3):171–5.
  260. Walsh AH, Cheng A, Honkanen RE. Fostriecin, an antitumor antibiotic with inhibitory activity against serine/threonine protein phosphatases types 1 (PPI) and 2A (PP2A), is highly selective for PP2A. *FEBS Lett.* 1997;416(3):230–4.
  261. Manfio GP, Atalan E, Czerwinska JZ, Rodriguez C, Collins MD, Goodfellow M. Classification of novel soil streptomycetes as *Streptomyces aureus* sp. nov., *Streptomyces laceyi* sp. nov. and *Streptomyces sanglieri* sp. nov. *Antonie Van Leeuwenhoek.* 2003;83:245–55.
  262. Holtzel A, Dieter A, Schmid DG, Brown R, Goodfellow M, Beil W, et al. Lactonamycin Z, an Antibiotic and Antitumor Compound Produced by *Streptomyces sanglieri* Strain AK 623. *J Antibiot (Tokyo).* 2003;56(12):1058–61.
  263. Mueller JV. Investigations of the biosynthesis of elaiomycin. Rice University; 1984.
  264. Ayaz M, Subhan F, Ahmed J, Khan AU, Ullah F, Sadiq A, et al. Citalopram and venlafaxine differentially augments antimicrobial properties of antibiotics. *Acta Poloniae Pharmaceutica - Drug Research.* 2015;72(6):1269–78.
  265. Rác B, Spengler G. Repurposing Antidepressants and Phenothiazine Antipsychotics as Efflux Pump Inhibitors in Cancer and Infectious Diseases. *Antibiotics.* 2023;12(1).
  266. Domzalski A, Margent L, Vigo V, Dewan F, Vara N, Pilarsetty K, et al. Unambiguous Stereochemical Assignment of Cyclo(Phe-Pro), Cyclo(Leu-Pro), and Cyclo(Val-Pro) by Electronic Circular Dichroic Spectroscopy. *Molecules.* 2021;26(5981).
  267. Boustany AN, Elmaraghi S, Agochukwu N, Cloyd B, Dugan AJ, Rinker B. A breast prosthesis infection update: Two-year incidence, risk factors and management at single institution. *Indian Journal of Plastic Surgery.* 2018;51:7–14.
  268. Löwik CAM, Zijlstra WP, Knobben BAS, Ploegmakers JJW, Dijkstra B, De Vries AJ, et al. Obese patients have higher rates of polymicrobial and Gram-negative early

- periprosthetic joint infections of the hip than non-obese patients. *PLoS One*. 2019;14(4):1–11.
269. Prasad ASB, Shruptha P, Prabhu V, Srujan C, Nayak UY, Anuradha CKR, et al. *Pseudomonas aeruginosa* virulence proteins pseudolysin and protease IV impede cutaneous wound healing. *Laboratory Investigation*. 2020;100(12):1532–50.
  270. Wilson WR, Bower TC, Creager MA, Amin-Hanjani S, O’Gara PT, Lockhart PB, et al. Vascular Graft Infections, Mycotic Aneurysms, and Endovascular Infections: A Scientific Statement from the American Heart Association. Vol. 134, *Circulation*. 2016. 412–460 p.
  271. Bergamini TM, Bandyk DF, Govostis D, Kaebnick HW, Towne JB. Infection of vascular prostheses caused by bacterial biofilms. *J Vasc Surg*. 1988;7(1):21–30.
  272. Stuermer EK, Plattfaut I, Dietrich M, Brill F, Kampe A, Wiencke V, et al. In vitro Activity of Antimicrobial Wound Dressings on *P. aeruginosa* Wound Biofilm. *Front Microbiol*. 2021;12(May):1–10.
  273. Guo Q, Wu Q, Bai D, Liu Y, Chen L, Jin S, et al. Potential use of dimethyl sulfoxide in treatment of infections caused by *Pseudomonas aeruginosa*. *Antimicrob Agents Chemother*. 2016;60(12):7159–69.
  274. Vyas HKN, Xia B, Mai-Prochnow A. Clinically relevant in vitro biofilm models: A need to mimic and recapitulate the host environment. *Biofilm*. 2022;4:100069.
  275. Bondy-denomy J, Qian J, Westra ER, Buckling A, Guttman DS, Davidson AR, et al. Prophages mediate defense against phage infection through diverse mechanisms. *ISME J*. 2016;22:2854–66.
  276. Skurnik D, Roux D, Cattoir V, Danilchanka O, Lu X, Yoder-Himes DR, et al. Enhanced in vivo fitness of carbapenem-resistant *oprD* mutants of *Pseudomonas aeruginosa* revealed through high-throughput sequencing. *PNAS*. 2013;110(51):20747–52.
  277. Louis M, Tahrioui A, Lendon CJ, Clamens T, Lefranc B, Kipnis E, et al. The natriuretic peptide receptor agonist osteocrin disperses *Pseudomonas aeruginosa* biofilm. *Biofilm*. 2023;5(December 2022).
  278. Serafim B, Bernardino AR, Freitas F. and Applications of *Pseudomonas* spp . Phenazines. 2023;
  279. Preda VG, Săndulescu O. Communication is the key: biofilms, quorum sensing, formation and prevention. *Discoveries*. 2019;7(3):e10.
  280. Gonçalves ASC, Leitão MM, Simões M, Borges A. The action of phytochemicals in biofilm control. Vol. 40, *Natural Product Reports*. 2022. 595–627 p.
  281. Kang D, Turner KE, Kirienco N V. PqsA promotes pyoverdine production via biofilm formation. *Pathogens*. 2018;7(1).
  282. Murray EJ, Dubern JF, Chan WC, Chhabra SR, Williams P. A *Pseudomonas aeruginosa* PQS quorum-sensing system inhibitor with anti-staphylococcal activity sensitizes polymicrobial biofilms to tobramycin. *Cell Chem Biol*. 2022;29(7):1187-1199.e6.

283. Dong L, Pang J, Wang X, Zhang Y, Li G, Hu X, et al. Mechanism of pyocyanin abolishment caused by *mvaT mvaU* double knockout in *Pseudomonas aeruginosa* PAO1. *Virulence*. 2020 Jan 1;11(1):57–67.
284. Seng LY, Al-Shaikh M, Hascakir B. Intermolecular interaction between heavy crude oils and surfactants during surfactant-steam flooding process. *ACS Omega*. 2020;5(42):27383–92.
285. Jani M, Mathee K, Azad RK. Identification of novel genomic islands in liverpool epidemic strain of *Pseudomonas aeruginosa* using segmentation and clustering. Vol. 7, *Frontiers in Microbiology*. 2016.
286. Chiriaco MS, Parlange I, Sirsi F, Poltronieri P, Primiceri E. Impedance sensing platform for detection of the food pathogen *listeria monocytogenes*. Vol. 7, *Electronics (Switzerland)*. 2018.
287. Cargill KL, Pyle BH, Sauer RL, McFeters GA. Effects of culture conditions and biofilm formation on the iodine susceptibility of *Legionella pneumophila*. *Can J Microbiol*. 1992;38(5):423–9.
288. Yahya MFZR, Alias Z, Karsani SA. Antibiofilm activity and mode of action of DMSO alone and its combination with afatinib against Gram-negative pathogens. *Folia Microbiol (Praha)*. 2018;63(1):23–30.
289. Das T, Manefield M. Pyocyanin Promotes Extracellular DNA Release in *Pseudomonas aeruginosa*. *PLoS One*. 2012;7(10).
290. Mavrodi D V., Bonsall RF, Delaney SM, Soule MJ, Phillips G, Thomashow LS. Functional analysis of genes for biosynthesis of pyocyanin and phenazine-1-carboxamide from *Pseudomonas aeruginosa* PAO1. *J Bacteriol*. 2001;183(21):6454–65.
291. Baquero F, Levin BR. Proximate and ultimate causes of the bactericidal action of antibiotics. *Nat Rev Microbiol*. 2021;19(2):123–32.
292. Baym M, Stone LK, Kishony R. Multidrug evolutionary strategies to reverse antibiotic resistance. *Science (1979)*. 2016;351.
293. Chandki R, Banthia P, Banthia R. Biofilms: A microbial home. *J Indian Soc Periodontol*. 2011;15(2):111–4.
294. Costerton JW, Geesey GG, Cheng KJ. How Bacteria Stick. *Sci Am*. 1978;238(1):86–95.
295. Miller TH. The problem of arsphenamine-resistant syphilis. *JAMA*. 1931;97(1):11–4.
296. Fleming A. ON THE ANTIBACTERIAL ACTION OF CULTURES OF A PENICILLIUM , WITH SPECIAL REFERENCE TO THEIR USE IN THE ISOLATION OF B . INFLUENZAE. *The British Journal of Experimental Pathology*. 1929;10(3):226–36.
297. Fleming A. The Discovery of Penicillin. *Br Med Bull*. 1944;2(1):4–5.
298. Lilistrand G. The Nobel Prize in Physiology or Medicine Award Ceremony Speech. In: *The Nobel Prize*. 1945. p. 1–8.

299. Pamp SJ, Gjermansen M, Johansen HK, Tolker-Nielsen T. Tolerance to the antimicrobial peptide colistin in *Pseudomonas aeruginosa* biofilms is linked to metabolically active cells, and depends on the *pmr* and *mexAB-oprM* genes. *Mol Microbiol.* 2008;68(1):223–40.
300. Chabowski K, Junka AF, Szymczyk P, Piasecki T, Sierakowski A, Mączyńska B, et al. The Application of Impedance Microsensors for Real-Time Analysis of *Pseudomonas aeruginosa* Biofilm Formation. *Pol J Microbiol.* 2015;64(2):115–20.
301. Hannah AJ, Ward AC, Connolly P. Rapidly Detected Common Wound Pathogens via Easy-to-Use Electrochemical Sensors. *Journal of Biomedical Engineering and Biosciences.* 2021;8.
302. Estivill D, Arias A, Torres-Lana A, Carrillo-Munoz AJ, Arevalo MP. Biofilm formation by five species of *Candida* on three clinical materials. *J Microbiol Methods.* 2011;86(2):238–42.
303. Mandakhalikar KD, Rahmat JN, Chiong E, Neoh KG, Shen L, Tambyah PA. Extraction and quantification of biofilm bacteria: Method optimized for urinary catheters. *Sci Rep.* 2018;8(8069):1–9.
304. Dhandapani R, Thangavelu S, Ragunathan L, Paramasivam R, Velmurugan P, Muthupandian S. Potential Bioactive Compounds from Marine *Streptomyces* sp. and Their In Vitro Antibiofilm and Antibacterial Activities Against Antimicrobial-Resistant Clinical Pathogens. *Appl Biochem Biotechnol.* 2022;194(10):4702–23.
305. Donnelly S, Ward AC, MacGregor G, Connolly P. Cystic Fibrosis Patient Monitor. *BioMedEng*19. 2019;78.

## 8.0 Supplementary information

### 8.1 Supplemental tables

**Supplementary table 2.1: FASTA sequences of 16s rRNA genes of isolated environmental strains**

Strain ID	FASTA sequence
LR2	>LR2  NNNNNTGCAAGTCGAACGATGAAGCCCTTCGGGGTGGATTAGTGGCGAACGG GTGAGTAACACGTGNNCNNTCTGCCCTTCACTCTGGGACAAGCCCTGGAAACG GGGTCTAATACCGGATAAACTCTGTCCCGCATGGGACGGGGTTGAAAGCTCC GGCGGTGAAGGATGAGCCCGCGCCTATCAGCTTGTGGTGGGGTATGGCCT ACCAAGGCGACGACGGGTAGCCGGCCTGAGAGGGCGACCGGCCAACTGGGA CTGAGACACGGCCAGACTCCTACGGGAGGCAGCAGTGGGGAATATTGCACAA TGGGCGAAAGCCTGATGCAGCGACGCCGCGTGAGGGATGACGGCCTTCGGGT GTAAACCTCTTTCAGCAGGGAAGAAGCGAAAGTGACGGTACCTGCAGAAGAAG CGCCGGCTAACTACGTGCCAGCAGCCGCGTAATACGTAGGGCGCAAGCGTTG TCCGGAATTATTGGGCGTAAAGAGCTCGTAGGCGCCTGTACGTCGGATGTG AAAGCCCGGGGCTTAACCCGGGTCTGCATTGATACGGGCGAGCTAGAGTGT GGTAGGGGAGATCGGAATCCTGGTGTAGCGGTGAAATGCGCAGATATCAGGA GGAACACCGGTGGCGAAGGCGGATCTCTGGGCCATTACTGACGCTGAGGAGCG AAAGCGTGGGAGCGAACAGGATTAGATACCCTGGTAGTCCACGCCGTAAACG TTGGGAACTAGGTGTTGGCGACATTCCACGTCGTCGGTGCCGACGTAACGCAT TAAGTCCCCGCCTGGGGAGTACGGCCGCAAGGCTAAAACCTCAAAGGAATTGA CGGGGGCCCGCACAAGCAGCGGAGCATGTGGCTTAATTGACGCAACGCGAAG AACCTTACCAAGGCTTGACATACCCGAAAGCATCAGAGATGGTGCCCCCTT GTGGTCGGTGTACAGGTGGTGCATGGCTGTCTGTCAGCTCGTGTCTGAGATGTT GGGTAAAGTCCCGCAACGAGCGCAACCCTTGTCTGTGTTGCCAGCATGCCCTT CGGGGTGATGGGACTCACAGGAGACTGCCGGGGTCAACTCGGAGGAAGGTG GGGACGACGTCAAGTCATCATGCCCTTATGTCTTGGGCTGCACACGTGCTACA ATGGCCGGTACAATGAGCTGCGATGCCGCGAGGCGGAGCGAATCTCAAAAAGC CGGTCTCAGTTCGGATTGGGTCTGCAACTCGACCCCATGAAGTCGGAGTTGCT AGTAATCGCAGATCAGCATTGCTGCGGTGAATACGTTCCCGGGCCTTGACACA CCGCCCGTCACGTCACGAAAGTCGTAACACCCGAAGCCGGTGGCCCAACCCCT TGTGGGAGGGAGNNNNNC
LR3	>LR3  NNNNNTGCANGTCGAACGATGAAGCCCTTCGGGGTGGATTAGTGGCGAACGG GTGAGTAACACGTGGGCAATCTGCCCTTCACTCTGGGACAAGCCCTGGAAACG GGGTCTAATACCGGATAAACTCTGTCCCGCATGGGACGGGGTTGAAAGCTCC GGCGGTGAAGGATGAGCCCGCGCCTATCAGCTTGTGGTGGGGTATGGCCT ACCAAGGCGACGACGGGTAGCCGGCCTGAGAGGGCGACCGGCCAACTGGGA CTGAGACACGGCCAGACTCCTACGGGAGGCAGCAGTGGGGAATATTGCACAA

---

TGGGCGAAAGCCTGATGCAGCGACGCCGCGTGAGGGATGACGGCCTTCGGGTT  
GTAACCTCTTTCAGCAGGGAAGAAGCGAAAGTGACGGTACCTGCAGAAGAAG  
CGCCGGCTAACTACGTGCCAGCAGCCGCGTAATACGTAGGGCGCAAGCGTTG  
TCCGGAATTATTGGGCGTAAAGAGCTCGTAGGCGGCTTGTCACGTCGGATGTG  
AAAGCCCAGGGCTTAACCCCGGGTCTGCATTGCATACGGGCAGGCTAGAGTGT  
GGTAGGGGAGATCGGAATTCCTGGTGTAGCGGTGAAATGCGCAGATATCAGGA  
GGAACACCGGTGGCGAAGGCGGATCTCTGGGCCATTACTGACGCTGAGGAGCG  
AAAGCGTGGGAGCGAACAGGATTAGATACCCTGGTAGTCCACGCCGTAAACG  
TTGGGAACTAGGTGTTGGCGACATTCCACGTCGTCGGTGCCGCAGCTAACGCAT  
TAAGTTCCCCGCCTGGGGAGTACGGCCGCAAGGCTAAAACCTCAAAGGAATTGA  
CGGGGGCCCCGCACAAGCAGCGGAGCATGTGGCTTAATTGCAGCAACGCGAAG  
AACCTTACCAAGGCTTGACATACACCGGAAAGCATCAGAGATGGTGCCCCCTT  
GTGGTCGGTGTACAGGTGGTGCATGGCTGTCGTCAGCTCGTGTCTGAGATGTT  
GGGTTAAGTCCCGCAACGAGCGCAACCCTTGTCTGTGTTGCCAGCATGCCCTT  
CGGGGTGATGGGGACTCACAGGAGACTGCCGGGGTCAACTCGGAGGAAGGTG  
GGGACGACGTCAAGTCATCATGCCCTTATGTCTTGGGCTGCACACGTGCTACA  
ATGGCCGGTACAATGAGCTGCGATGCCGCGAGGCGGAGCGAATCTCAAAAAGC  
CGGTCTCAGTTCGGATTGGGTCTGCAACTCGACCCCATGAAGTCGGAGTTGCT  
AGTAATCGCAGATCAGCATTGCTGCGGTGAATACGTTCCCGGGCCTTGACACA  
CCGCCCGTCACGTACGAAAGTCGTAACACCCGAAGCCGGTGGCCCAACCCCT  
TGTTGGAGGGAGNNNNNCGAA

LR4

>LR4

NNNNNTCTGCCCTTCACTCTGGGACAAGCCCTGGAAACGGNGTCTAATACCGG  
ATAAACTCTGTCCTGCATGGGACGGGGTAAAAGCTCCGGCGGTGAAGGATG  
AGCCCGCGCCTATCAGCTTGTGGTGGGGTAATGGCTACCAAGGCGACGAC  
GGGTAGCCGGCCTGAGAGGGCGACCGGCCACACTGGGACTGAGACACGGCCC  
AGACTCCTACGGGAGGCAGCAGTGGGGAATATTGCACAATGGGCGAAAGCCTG  
ATGCAGCGACGCCGCGTGAGGGATGACGGCCTTCGGGTTGTAAACCTCTTTCAG  
CAGGGAAGAAGCGAAAGTGACGGTACCTGCAGAAGAAGCGCCGGCTAACTAC  
GTGCCAGCAGCCGCGTAATACGTAGGGCGCAAGCGTTGTCCGGAATTATTGG  
GCGTAAAGAGCTCGTAGGCGGCTTGTCACGTCGGATGTGAAAGCCCGGGGCTT  
AACCCCGGTCTGCATTCGATACGGGCTAGCTAGAGTGTGGTAGGGGAGATCG  
GAATTCCTGGTGTAGCGGTGAAATGCGCAGATATCAGGAGGAACACCGGTGGC  
GAAGGGCGGATCTCTGGGCCATTACTGACGCTGAGGAGCGAAAGCGTGGGGA  
GCGAACAGGATTAGATACCCTGGTAGTCCACGCCGTAAACGTTGGGAACTAGG  
TGTTGGCGACATTCCACGTCGTCGGTGCCGCAGCTAACGCATTAAGTTCCCCGC  
CTGGGGAGTACGGCCGCAAGGCTAAAACCTCAAAGGAATTGACGGGGGCCCCGC  
ACAAGCAGCGGAGCATGTGGCTTAATTGCAGCAACGCGAAGAACCTTACCAA  
GGCTTGACATATAACCGAAAGCATCAGAGATGGTGCCCCCTTGTGGTTCGGTAT  
ACAGGTGGTGCATGGCTGTCGTCAGCTCGTGTCTGAGATGTTGGGTTAAGTCC  
CGCAACGAGCGCAACCCTTGTCTGTGTTGCCAGCATGCCCTTCGGGGTATGG  
GGACTCACAGGAGACTGCCGGGGTCAACTNGGAGGAAGGTGGGGACGACGTC  
AAGTCATCANGCNCCNNATGTNTTGGGCTGCACNNGTNTACAATGGCCGTA  
CAATGAGCTGCGATGCCGCGAGGCGGAGCGAATCTCAAAAAGCCGGTCTCAGT

---

---

TCGGANTGGGGTNNNGCAACTNGACCNCNTGAAGTCGGAGTTGNTAGTAATCG  
CAGANNNNNN

LR6

>LR6

NNNNNGCAAGTCGAACGATGAAGCCCTTCGGGGTGGATTAGTGGCGAACGGG  
TGAGTAACACGTNNGNAATCTGCCCTTCACTCTGGGACAAGCCCTGGAAACGG  
GGTCTAATACCGGATAAACTCTGTCCCGCATGGGACGGGGTTGAAAGCTCCG  
GCGGTGAAGGATGAGCCCGCGCCTATCAGCTTGTGGTGGGGTGGATGGCCTA  
CCAAGGCGACGACGGGTAGCCGGCCTGAGGGGCGACCGGCCAACTGGGACT  
GAGACACGGCCCAGACTCTACGGGAGGCAGCAGTGGGGAATATTGCACAATG  
GGCGAAAGCCTGATGCAGCGACGCCGCTGAGGGATGACGGCCTCGGGTTGT  
AAACCTCTTTCAGCAGGGAAGAAGCGAAAGTGACGGTACCTGCAGAAGAAGCG  
CCGGCTAACTACGTGCCAGCAGCCGCGTAATACGTAGGGCGCAAGCGTTGTC  
CGGAATTATTGGGCGTAAAGAGCTCGTAGGCGGCTGTACGTCGGATGTGAA  
AGCCCGGGGCTTAACCCGGGTCTGCATTGATACGGGCAGGCTAGAGTGTGG  
TAGGGGAGATCGGAATTCCTGGTGTAGCGGTGAAATGCGCAGATATCAGGAGG  
AACACCGGTGGCGAAGGCGGATCTCTGGGCCATTACTGACGCTGAGGAGCGAA  
AGCGTGGGGAGCGAACAGGATTAGATACCCTGGTAGTCCACGCCGTAAACGTT  
GGGAACTAGGTGTTGGCGACATTCCACGTGTCGGTGCCGCAGCTAACGCATTA  
AGTTCCCCGCCTGGGGAGTACGGCCGCAAGGCTAAAACCTCAAAGGAATTGACG  
GGGGCCCGCACAAGCAGCGGAGCATGTGGCTTAATTGACGCAACCGGAAGAA  
CCTTACCAAGGCTTGACATACCCGGAAAGCATCAGAGATGGTGCCCCCTTGT  
GGTCGGTGTACAGGTGGTGCATGGCTGTCGTCAGCTCGTGTGTCGTGAGATGTTG  
GGTTAAGTCCCACAACGAGCGCAACCCTTGTCTGTGTTGCCAGCATGCCCTTC  
GGGGTGTGGGGACTCACAGGAGACTGCCGGGTCAACTCGGAGGAAGGTGG  
GGACGACGTCAAGTCATCATGCCCTTATGTCTTGGGCTGCACACGTGCTACAA  
TGGCCGGTACAATGAGCTGCGATGCCGCGAGGCGGAGCGAATCTCAAAAAGCC  
GGTCTCAGTTCGGATTGGGGTCTGCAACTCGACCCCATGAAGTCGGAGTTGCTA  
GTAATCGCAGATCAGCATTGCTGCGGTGAATACGTTCCCGGGCCTTGTACACAC  
CGCNGTCAAGTACGAAAGTTCGGTAACACCCGAAGCCGGTGGCCCAACCCCT  
TGNGGGAGGGAGNNNNNCGA

LR9

>LR9

NNNNTGCANGTCGAACGATGAAGCCCTTCGGGGTGGATTAGTGGCGAACGGG  
TGAGTAACACGTGGGCAATCTGCCCTTCACTCTGGGACAAGCCCTGGAAACGG  
GGTCTAATACCGGATAAACTCTGTCCCGCATGGGACGGGGTTGAAAGCTCCG  
GCGGTGAAGGATGAGCCCGCGCCTATCAGCTTGTGGTGGGGTGGATGGCCTA  
CCAAGGCGACGACGGGTAGCCGGCCTGAGAGGGGCGACCGGCCAACTGGGAC  
TGAGACACGGCCCAGACTCTACGGGAGGCAGCAGTGGGGAATATTGCACAAT  
GGGCGAAAGCCTGATGCAGCGACGCCGCTGAGGGATGACGGCCTTCGGGTT  
GTAAACCTCTTTCAGCAGGGAAGAAGCGAAAGTGACGGTACCTGCAGAAGAAG  
CGCCGGCTAACTACGTGCCAGCAGCCGCGTAATACGTAGGGCGCAAGCGTTG  
TCCGGAATTATTGGGCGTAAAGAGCTCGTAGGCGGCTGTACGTCGGATGTG  
AAAGCCCGGGGCTTAACCCGGGTCTGCATTGATACGGGCAGGCTAGAGTGT  
GGTAGGGGAGATCGGAATTCCTGGTGTAGCGGTGAAATGCGCAGATATCAGGA  
GGAACACCGGTGGCGAAGGCGGATCTCTGGGCCATTACTGACGCTGAGGAGCG  
AAAGCGTGGGGAGCGAACAGGATTAGATACCCTGGTAGTCCACGCCGTAAACG

---

---

TTGGGAACTAGGTGTTGGCGACATTCCACGTCGTCGGTGCCGCAGCTAACGCAT  
TAAGTTCCCCGCCTGGGGAGTACGGCCGCAAGGCTAAAACCTCAAAGGAATTGA  
CGGGGGCCCGCACAAGCAGCGGAGCATGTGGCTTAATTCGACGCAACGCGAAG  
AACCTTACCAAGGCTTGACATACACCGGAAAGCATCAGAGATGGTGCCCCCTT  
GTGGTCGGTGTACAGGTGGTGCATGGCTGTCGTCAGCTCGTGTCTGTGAGATGTT  
GGGTTAAGTCCCGCAACGAGCGCAACCCTTGTCTGTGTTGCCAGCATGCCCTT  
CGGGGTGATGGGGACTCACAGGAGACTGCCGGGGTCAACTCGGAGGAAGGTG  
GGGACGACGTCAAGTCATCATGCCCTTATGTCTTGGGCTGCACACGTGCTACA  
ATGGCCGGTACAATGAGCTGCGATGCCGCGAGGCGGAGCGAATCTCAAAAAGC  
CGGTCTCAGTTCGGATTGGGGTCTGCAACTCGACCCCATGAAGTCGGAGTTGCT  
AGTAATCGCAGATCAGCATTGCTGCGGTGAATACGTTCCCGGGCCTTGACACA  
CCGCCGTCACGTACGAAAGTCGTAACACCCGAAGCCGGTGGCCCAACCCCT  
TGNNGAGGANNNNCG

LR10 >LR10

NNNNNTGCAAGTCGAACGATGAAGCCCTTCGGGGTGGATTAGTGCGAACGG  
GTGAGTAACACGTGGGCAATCTGCCCTTCACTCTGGGACAAGCCCTGGAAACG  
GGGTCTAATACCGGATAAACTCTGTCCCGCATGGGACGGGGTTGAAAGCTCC  
GGCGGTGAAGGATGAGCCCGCGCCTATCAGCTTGTGGTGGGGTGTGGCCT  
ACCAAGGCGACGACGGGTAGCCGGCCTGAGAGGGCGACCGGCCACTGGGA  
CTGAGACACGGCCAGACTCCTACGGGAGGCAGCAGTGGGGAATATTGCACAA  
TGGGCGAAAGCCTGATGCAGCGACCCGCGTGAGGGATGACGGCCTTCGGGT  
GTAAACCTCTTTCAGCAGGGAAGAAGCGAAAGTGACGGTACCTGCAGAAGAAG  
CGCCGGCTAACTACGTGCCAGCAGCCGCGTAATACGTAGGGCGCAAGCGTTG  
TCCGGAATTATTGGGCGTAAAGAGCTCGTAGGCGCTTGTACGTCGGATGTG  
AAAGCCCGGGGCTTAACCCCGGGTCTGCATTGATACGGGCAGGCTAGAGTGT  
GGTAGGGGAGATCGGAATCCTGGTGTAGCGGTGAAATGCGCAGATATCAGGA  
GGAACACCGGTGGCGAAGGCGGATCTCTGGGCCATTACTGACGCTGAGGAGCG  
AAAGCGTGGGGAGCGAACAGGATTAGATACCCTGGTAGTCCACGCCGTAAACG  
TTGGGAACTAGGTGTTGGCGACATTCCACGTCGTCGGTGCCGCAGCTAACGCAT  
TAAGTTCCCCGCCTGGGGAGTACGGCCGCAAGGCTAAAACCTCAAAGGAATTGA  
CGGGGGCCCGCACAAGCAGCGGAGCATGTGGCTTAATTCGACGCAACGCGAAG  
AACCTTACCAAGGCTTGACATACACCGGAAAGCATCAGAGATGGTGCCCCCTT  
GTGGTCGGTGTACAGGTGGTGCATGGCTGTCGTCAGCTCGTGTCTGTGAGATGTT  
GGGTTAAGTCCCGCAACGAGCGCAACCCTTGTCTGTGTTGCCAGCATGCCCTT  
CGGGGTGATGGGGACTCACAGGAGACTGCCGGGGTCAACTCGGAGGAAGGTG  
GGGACGACGTCAAGTCATCATGCCCTTATGTCTTGGGCTGCACACGTGCTACA  
ATGGCCGGTACAATGAGCTGCGATGCCGCGAGGCGGAGCGAATCTCAAAAAGC  
CGGTCTCAGTTCGGATTGGGGTCTGCAACTCGACCCCATGAAGTCGGAGTTGCT  
AGTAATCGCAGATCAGCATTGCTGCGGTGAATACGTTCCCGGGCCTTGACACA  
CCGCCGTCACGTACGAAAGTCGTAACACCCGAAGCCGGTGGCCCAACCCCT  
TGNNNGAGGGNNNNNN

LR14 >LR14

NNNNNTCTGCCCTGCACTCTGGGACAAGCCCTGGNNACGGGGTCTAATACCG  
GATATGACCGTCTGCCGCATGGTGGATGGTGTAAAGCTCCGGCGGTGCAGGAT  
GAGCCCGGNNCTATCANNTTGTGGTGAGGTAGTGGCTCACCNAGGCGACGA

---

---

CGGGTANCCGGCCTGAGAGGGCGACCGGCCACACTGGGACTGAGNCACGNNC  
CAGACTNNNNCGGGAGGCAGCAGTGGGGAATATTGCACAATGGGCGAAAGCC  
TGATGCAGCGACGCCGCTGAGGGATGACGGCCTTCGGGTTGTAAACCTCTTTC  
AGCAGGGAAGAAGCGAAAGTGACGGTACCTGCAGAAGAAGCGCCGGCTAACT  
ACGTGCCAGCAGCCGCGGTAATACGTAGGGCGCAAGCGTTGTCCGGAATTATT  
GGGCGTAAAGAGCTCGTAGGCGGCTTGTACGTCGTTGTGAAAGCCCGGGGC  
TTAACCCCGGTCTGCAGTCGATACGGGCAGGCTAGAGTTCGGTAGGGGAGAT  
CGGAATTCCTGGTGTAGCGGTGAAATGCGCAGATATCAGGAGGAACACCGGTG  
GCGAAGGCGGATCTCTGGGCCGATACTGACGCTGAGGAGCGAAAGCGTGGGG  
AGCGAACAGGATTAGATACCCTGGTAGTCCACGCCGTAAACGGTGGGCACTAG  
GTGTGGGCAACATTCCACGTTGTCCGTGCCGCAGCTAACGCATTAAGTGCCCCG  
CCTGGGGAGTACGGCCGAAGGCTAAAACCTCAAAGGAATTGACGGGGGCCCG  
CACAAGCGGCGGAGCATGTGGCTTAATTCGACGCAACGCGAAGAACCTTACCA  
AGGCTTGACATACCCGAAACGTCTGGAGACAGGCGCCCCCTGTGGTCTGGT  
GTACAGGTGGTGCATGGCTGTCTGTCAGCTCGTGTCTGAGATGTTGGGTTAAGT  
CCCGCAACGAGCGCAACCCTGTCCCGTGTGCCAGCAGGCCCTTGTGGTGTG  
GGGACTCACGGGAGACCGCCGGGTCAACTCGGAGGAAGGTGGGGACGACGT  
CAAGTCATCATGCCCTTATGTCTTGGGCTGCACACGTGCTACAATGGCCGGTAC  
AATGAGCTGCGATACCGTGAGGTGGAGCGAATCTCAAAAAGCCGGTCTCAGTT  
CGGATTGGGGTCTGCAACTCGACCCCATGAAGTCGGAGTCGCTAGTAATCGCA  
GATCAGCATTGCTGCGGTGAATACGTTCCCGGGCCTGTACACNNNNNN

LR15

>LR15

NNNNNNNGNATNACACTCTGTCCCGCATGGGACGGGGTTAANAGCTCCGGCG  
GNGAAGGATGAGCCCGGCCTATCAGCTTGTGGTGGGGNAATGGCCTACCA  
AGGCGACGACGGGTAGCCGGCCTGAGAGGGCGACCGGCCACACTGGGACTGA  
GACACGGCCAGACTCCTACGGGAGGCAGCAGTGGGGAATATTGCACAATGGG  
CGAAAGCCTGATGCAGCGACGCCGCTGAGGGATGACGGCCTTCGGGTTGTAA  
ACCTCTTTCAGCAGGGAAGAAGCGAAAGTGACGGTACCTGCAGAAGAAGCGCC  
GGCTAACTACGTGCCAGCAGCCGCGGTAATACGTAGGGCGCAAGCGTTGTCCG  
GAATTATTGGGCGTAAAGAGCTCGTAGGCGGCTTGTACGTCGGATGTGAAAG  
CCCGGGGCTTAACCCCGGTCTGCATTGATACGGGCTAGCTAGAGTGTGGTA  
GGGGAGATCGGAATTCCTGGTGTAGCGGTGAAATGCGCAGATATCAGGAGGA  
ACACCGGTGGCGAAGGCGGATCTCTGGGCCATTACTGACGCTGAGGAGCGAAA  
GCGTGGGGAGCGAACAGGATTAGATACCCTGGTAGTCCACGCCGTAAACGTTG  
GGAAGTAGGTGTTGGCGACATCCACGTCGTCGGTGCCGCAGCTAACGCATTAA  
GTTCCCGCCTGGGGAGTACGGCCGAAGGCTAAAACCTCAAAGGAATTGACGG  
GGGCCCGACAAGCAGCGGAGCATGTGGCTTAATTCGACGCAACGCGAAGAAC  
CTTACCAAGGCTTGACATATACCGGAAAGCATCAGAGATGGTGCCCCCTTGTG  
GTCGGTATACAGGTGGTGCATGGCTGTCTGTCAGCTCGTGTCTGAGATGTTGG  
GTTAAGTCCCGCAACGAGCGCAACCCTTGTCTGTGTTGCCAGCATGNCCTTCG  
GGGTGATGGGGANTCACAGGAGACTGCCGGGGTCAACTCGGAGGAAGGTGGG  
GACGACGTCAAGTCATCANGCCCNATGTCTTGGGCTGCACNCGTNNNTACAAT  
GGCCGGTACAATGAGCTGCGATGCCGCGAGNCGGAGCGAATCTCAAAAANCC  
GGTCTCAGTTCGGANNGGGTCTGCAACTNNNCNCCATGAAGTCGGAGTTNNT  
AGTAATCGCAGATNNNCNTN

---

---

LR16

>LR16

NCNNNCTCCTACGGGAGGCANNAGNGNGGAANATTGCACNNTGNNCGAAAN  
CCTGATGCNNGACGNCGCGTGAGGNANGACGGCCTTCGGGTTGTAAACCTCT  
TTCAGCAGGGAAGAAGCGAAAGTGACGGTACCTGCAGAAGAAGCGCCGGCTA  
ACTACGTGCCAGCAGCCGCGTAATACGTAGGGCGCAAGCGTTGTCCGGAATT  
ATTGGGCGTAAAGAGCTCGTAGGCGGCTTGTACGTGCGATGTGAAAGCCCGG  
GGCTTAACCCCGGGTCTGCATTTCGATACGGGCTAGCTAGAGTGTGGTAGGGGA  
GATCGGAATTCCTGGTGTAGCGGTGAAATGCGCAGATATCAGGAGGAACACCG  
GTGGCGAAGGCGGATCTCTGGGCCATTACTGACGCTGAGGAGCGAAAGCGTG  
GGGAGCGAACAGGATTAGATACCCTGGTAGTCCACGCCGTAAACGTTGGGAAC  
TAGGTGTTGGCGACATTCCACGTCGTCGGTGCCGCAGCTAACGCATTAAGTTCC  
CCGCCTGGGGAGTACGGCCGCAAGGCTAAAACCAAAGGAATTGACGGNNGG  
CCCGCACAAGCAGCGGAGCATGTGGCTTAATTCGACGCAACGCGAAGAAACCT  
TACCAAGGCTTGACATATACCGGAAAGCATCAGAGATGGTGCSCCCTTGTGGT  
CGGTATACAGGTGGTGCATGGCTGTCGTCAGCTCGTGTGTCGTGAGATGTTGGGT  
AAGTCCCGCAACGAGCGCAACCCTTGTCTGTGTTGCCAGCATGCCCTTCGGGG  
TGATGGGGACTCACAGGAGACTGCCGGGTCAACTCGGAGGAAGGTGGGGAC  
GACGTCAAGTCATCATGCCCTTATGTCTTGGGCTGCACACGTGCTACAATGGCC  
GGTACAATGAGCTGCGATGCCGCGAGGCGGAGCGAATCTCAAAAAGCCGGTCT  
CAGTTCGGATTGGGGTCTGCAACTCGACCCCATGAAGTCGGAGTTGCTAGTAAT  
CGCAGATCAGCATTGNNNNGGTGAATACGTTCCCGGGCNTNGTACACACCGCC  
CGTCACGTCACGAAAGTCGGTAACACCCGANGCCGGNGGCCCAACCCCTTNG  
GGAGGGNNGNNNN

KRD153

>KRD153

ATTCNNTGCAACGCGAAGAACCTGACCAAGNCTTGACATGTTCTAGATCCCCGT  
AGAGAAAAGGTTTCCCTTTGGGGTGGGATTATGAAATGGGGGTTGGTGCATG  
GTTGTCGTCAGCTCGTGTGTCGTGAGATGTTGGGTTAAGTCNCGCAACGAGCGCA  
ACCCTCGTCCATGTTGCCAGCACGTCGTGGTGGGGACTCATGGGAGACTCCG  
GGGTCAACATACTCGGAGGAAGGTGAGGACGCCAAAAACGTCAAATCATCATG  
CCCCTTATGTCTTGGTGGGGGCTTACGCATNNTNNAATGGCCGGTACAATGG  
GTTGCGATACTGTGAGGTGGAGCTAATCCCAAAAAGCCGGAGCTCTCAATTCGG  
ATTGGGGGCCGCTCGATCTGCAACTCGACCCCGAANATGAAGTCGGAGTCGCT  
NGTAATCGCAGATCAGCAACGCTGACGGTGAATACGTNNNNCGGN

---

**Supplementary table 2.2: Closest related strains, and percentage similarity, to LR2 according to NCBI BLAST search**

Strain	Percentage similarity
<i>Streptomyces pulveraceus</i>	99%
<i>Streptomyces sanglieri</i>	99%
<i>Streptomyces globisporus</i>	99%
<i>Streptomyces albovinaceus</i>	99%
<i>Streptomyces rubiginosohelvolus</i>	99%
<i>Streptomyces atratus</i>	99%
<i>Streptomyces mediolani</i>	99%
<i>Streptomyces griseinus</i>	99%
<i>Streptomyces gelaticus</i>	99%
<i>Streptomyces plurocolorescens</i>	99%

**Supplementary table 2.3: Closest related strains, and percentage similarity, to LR3 according to NCBI BLAST search**

Strain	Percentage similarity
<i>S. pulveraceus</i>	99%
<i>S. sanglieri</i>	99%
<i>S. globisporus</i>	99%
<i>S. albovinaceus</i>	99%
<i>S. rubiginosohelvolus</i>	99%
<i>S. atratus</i>	99%
<i>S. mediolani</i>	99%
<i>S. griseinus</i>	99%
<i>S. gelaticus</i>	99%
<i>S. plurocolorescens</i>	99%

**Supplementary table 2.4: Closest related strains, and percentage similarity, to LR4 according to NCBI BLAST search**

Strain	Percentage similarity
<i>Streptomyces microflavus</i>	99%
<i>Streptomyces alboviridis</i>	99%
<i>Streptomyces fulvorobeus</i>	99%
<i>Streptomyces pratensis</i>	99%
<i>Streptomyces caviscabies</i>	99%
<i>Streptomyces luridiscabiei</i>	99%
<i>Streptomyces acrimycini</i>	99%
<i>Streptomyces praecox</i>	99%
<i>Streptomyces cyaneofuscatus</i>	99%
<i>Streptomyces fimicarius</i>	99%

**Supplementary table 2.5: Closest related strains, and percentage similarity, to LR6 according to NCBI BLAST search**

Strain	Percentage similarity
<i>S. pulveraceus</i>	99%
<i>S. sanglieri</i>	99%
<i>S. globisporus</i>	99%
<i>S. albovinaceus</i>	99%
<i>S. rubiginosohelvolus</i>	99%
<i>S. atratus</i>	99%
<i>S. mediolani</i>	99%
<i>S. griseinus</i>	99%
<i>S. gelaticus</i>	99%
<i>S. plurocolorescens</i>	99%

**Supplementary table 2.6: Closest related strains, and percentage similarity, to LR9 according to NCBI BLAST search**

Strain	Percentage similarity
<i>S. pulveraceus</i>	99%
<i>S. sanglieri</i>	99%
<i>S. globisporus</i>	99%
<i>S. albovinaceus</i>	99%
<i>S. rubiginosohelvolus</i>	99%
<i>S. atratus</i>	99%
<i>S. mediolani</i>	99%
<i>S. griseinus</i>	99%
<i>S. gelaticus</i>	99%
<i>S. plurocolorescens</i>	99%

**Supplementary table 2.7: Closest related strains, and percentage similarity, to LR10 according to NCBI BLAST search**

Strain	Percentage similarity
<i>S. pulveraceus</i>	98%
<i>S. sanglieri</i>	98%
<i>S. globisporus</i>	98%
<i>S. albovinaceus</i>	98%
<i>S. rubiginosohelvolus</i>	98%
<i>S. atratus</i>	98%
<i>S. mediolani</i>	98%
<i>S. griseinus</i>	98%
<i>S. gelaticus</i>	98%
<i>S. plurocolorescens</i>	98%

**Supplementary table 2.8: Closest related strains, and percentage similarity, to LR14 according to NCBI BLAST search**

Strain	Percentage similarity
<i>Streptomyces sampsonii</i>	99%
<i>Streptomyces champavatii</i>	99%
<i>Streptomyces albidoflavus</i>	99%
<i>Streptomyces odorifer</i>	99%
<i>Streptomyces canescens</i>	99%
<i>Streptomyces felleus</i>	99%
<i>Streptomyces limosus</i>	99%
<i>Streptomyces coelicolor</i>	99%
<i>Streptomyces griseochromogenes</i>	99%
<i>Streptomyces resistomycificus</i>	99%

**Supplementary table 2.9: Closest related strains, and percentage similarity, to LR15 according to NCBI BLAST search**

Strain	Percentage similarity
<i>S. pratensis</i>	98%
<i>S. caviscabies</i>	98%
<i>S. acrimycini</i>	98%
<i>S. praecox</i>	98%
<i>S. cyaneofuscatus</i>	98%
<i>S. fimicarius</i>	98%
<i>S. flavofuscus</i>	98%
<i>Streptomyces anulatus</i>	98%
<i>Streptomyces baarnensis</i>	98%
<i>S. microflavus</i>	98%

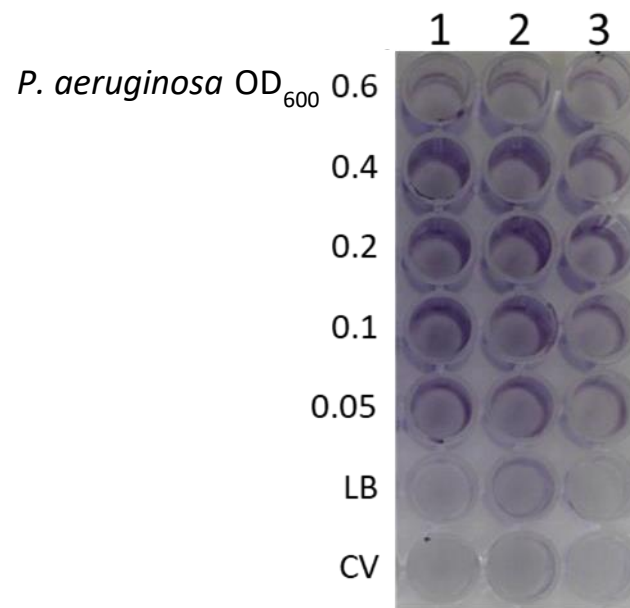
**Supplementary table 2.10: Closest related strains, and percentage similarity, to LR16 according to NCBI BLAST search**

Strain	Percentage similarity
<i>S. microflavus</i>	98%
<i>S. globisporus</i>	98%
<i>S. pratensis</i>	98%
<i>S. caviscabies</i>	98%
<i>S. acrimycini</i>	98%
<i>Streptomyces sindenensis</i>	98%
<i>S. praecox</i>	98%
<i>S. cyaneofuscatus</i>	98%
<i>S. alboviridis</i>	98%
<i>S. albovinaceus</i>	98%

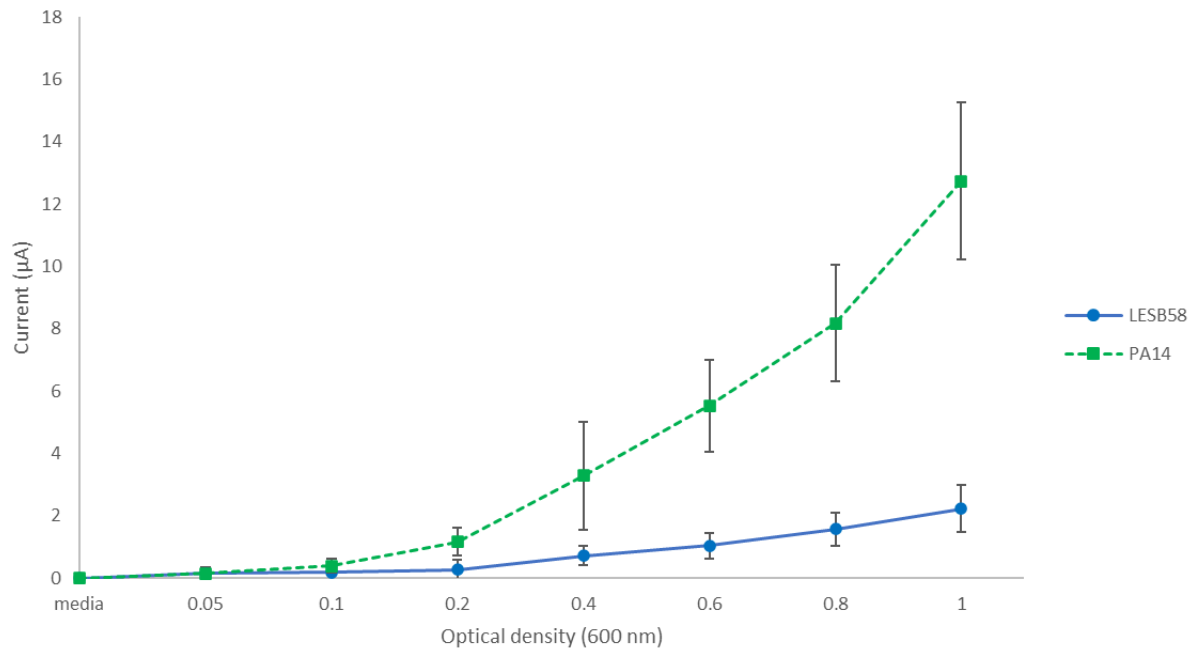
**Supplementary table 2.11: Closest related strains, and percentage similarity, to KRD153 according to NCBI BLAST search**

Strain	Percentage similarity
<i>Micrococcus aloeverae</i>	98%
<i>Micrococcus yunnanensis</i>	98%
<i>Micrococcus endophyticus</i>	98%
<i>Micrococcus luteus</i>	98%
<i>Micrococcus flavus</i>	98%
<i>Micrococcus antarcticus</i>	98%
<i>Paeniglutamicibacter gangotriensis</i>	98%
<i>Micrococcus cohnii</i>	98%
<i>Arthrobacter rhombi</i>	98%
<i>Micrococcus lylae</i>	98%

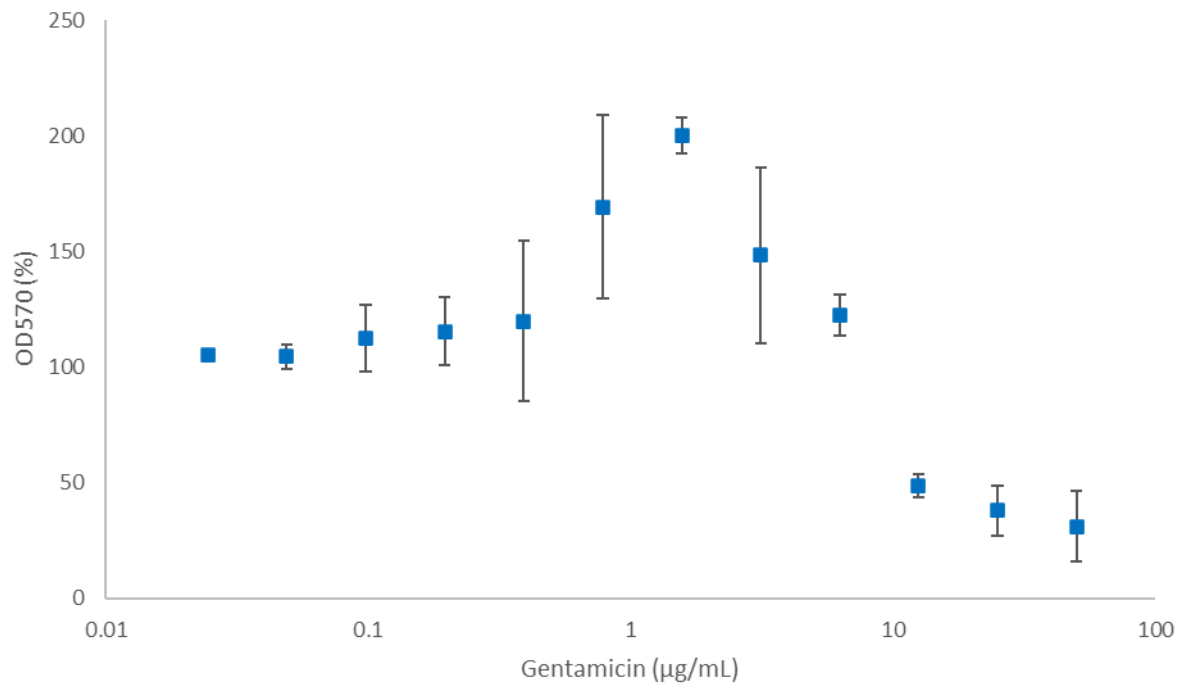
## 8.2 Supplemental figures



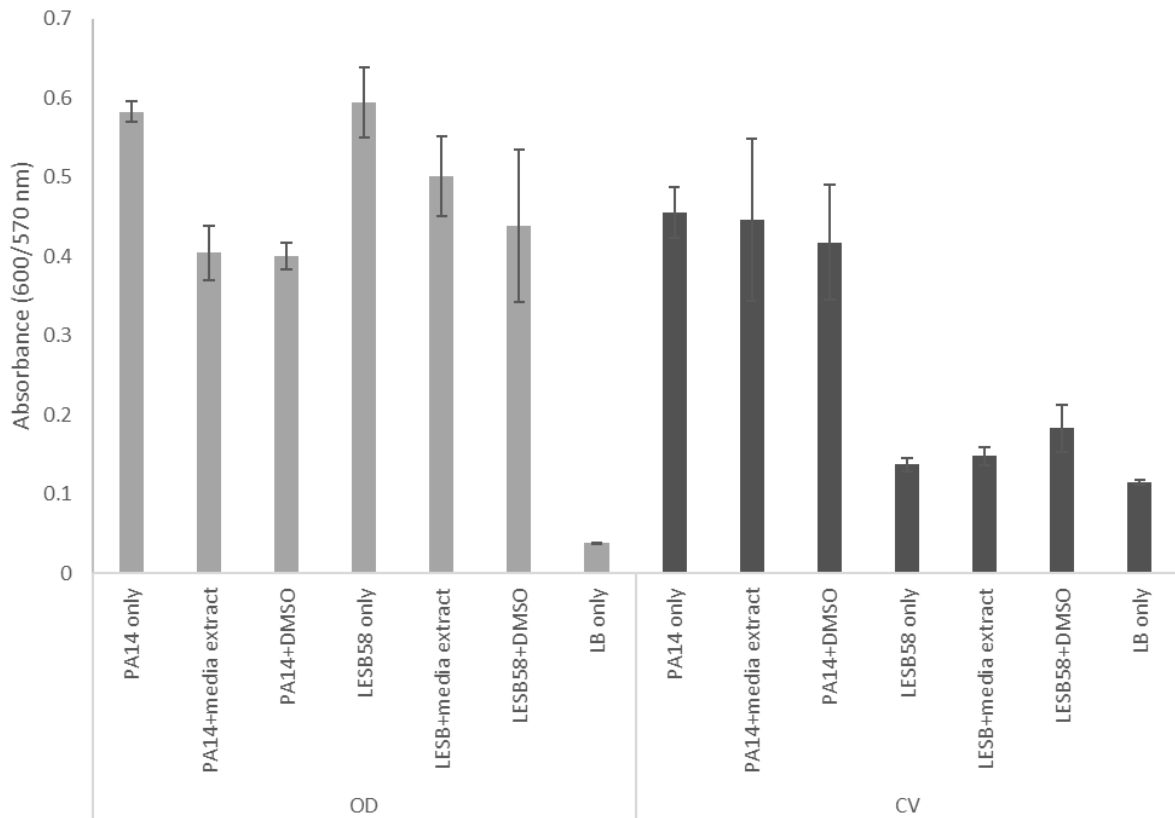
**Supplementary Figure 3.1: CV-stained *P. aeruginosa* (PA14) biofilms at decreasing seeding densities (OD<sub>600</sub> 0.05 – 0.6).** Biofilms, LB only control, and CV only control stained after four-hour incubation (n = 3).



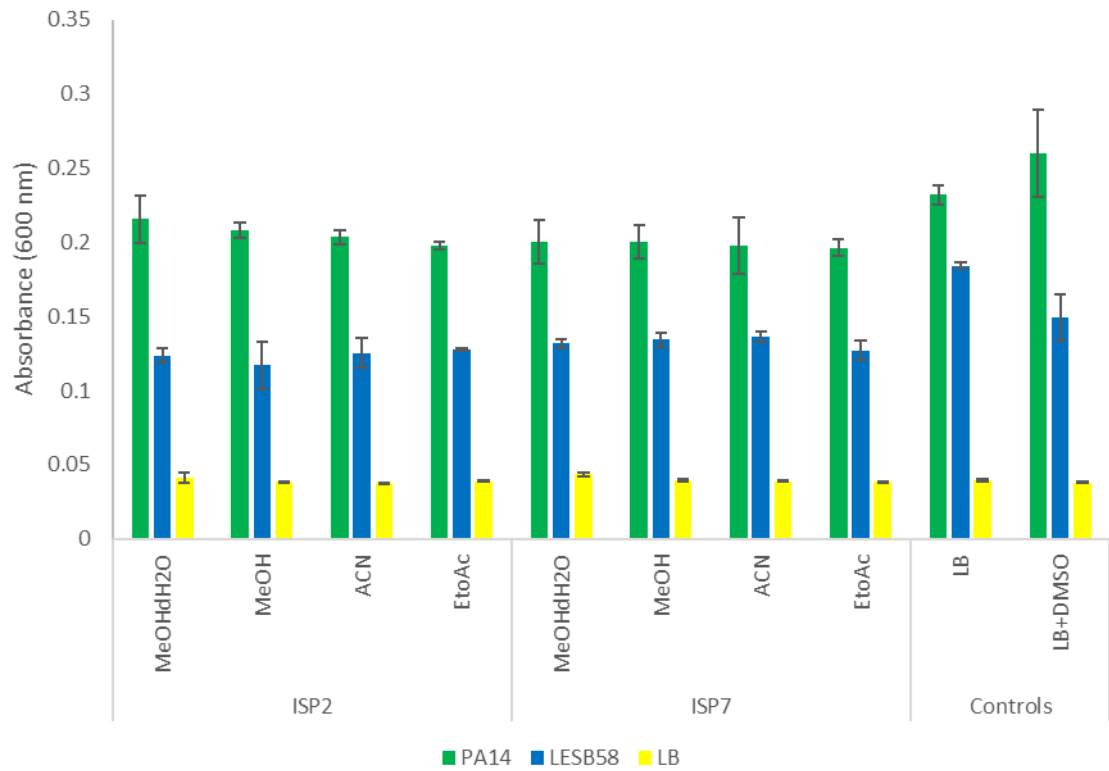
**Supplementary Figure 3.2: SWV quantification of *P. aeruginosa* (PA14 and LESB58) with increasing seeding densities (OD600 0.05 – 1).** Current (µA) measured at -0.35 V over a four-hour incubation, pre-normalised four-hour time points shown (error bars show standard deviation, n=3,  $r^2=91\%$ ).



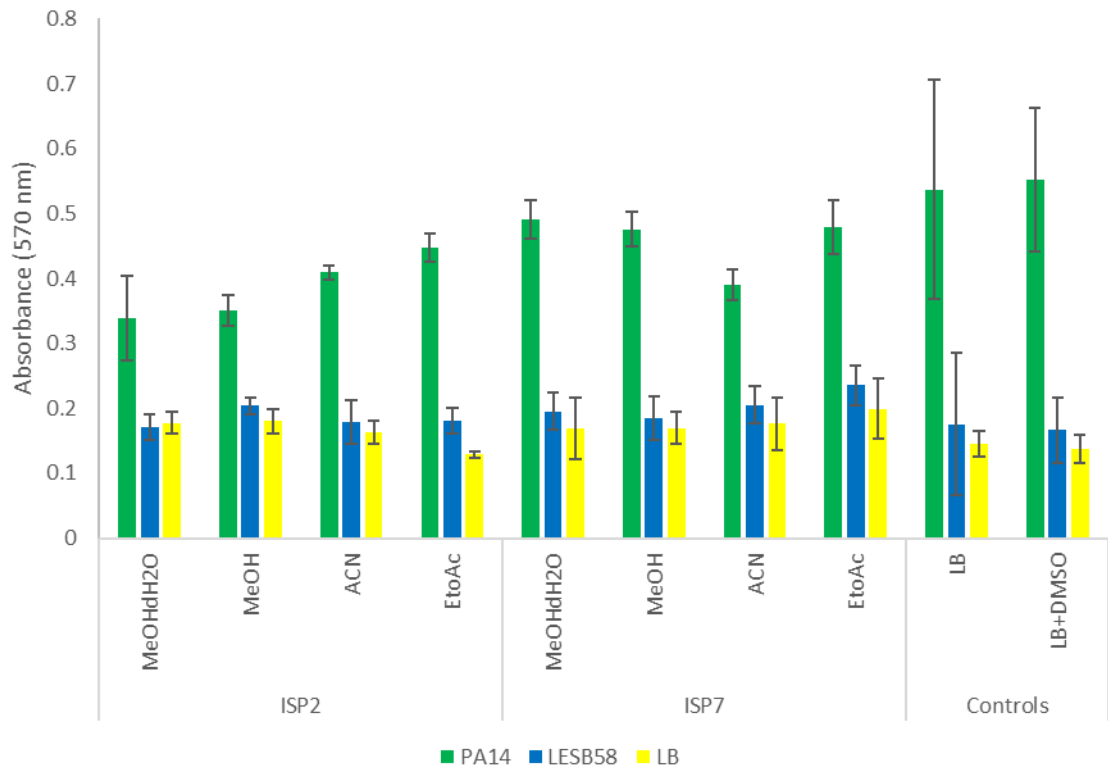
**Supplementary Figure 4.1: Biofilm formation of LESB58 in the presence of increasing concentrations gentamicin (µg/mL).** Biofilm formation measured with absorbance (570 nm) absorbed CV solubilised in ethanol, error bars show standard deviation, n=3. Gentamicin bactericidal at 10 µg/mL.



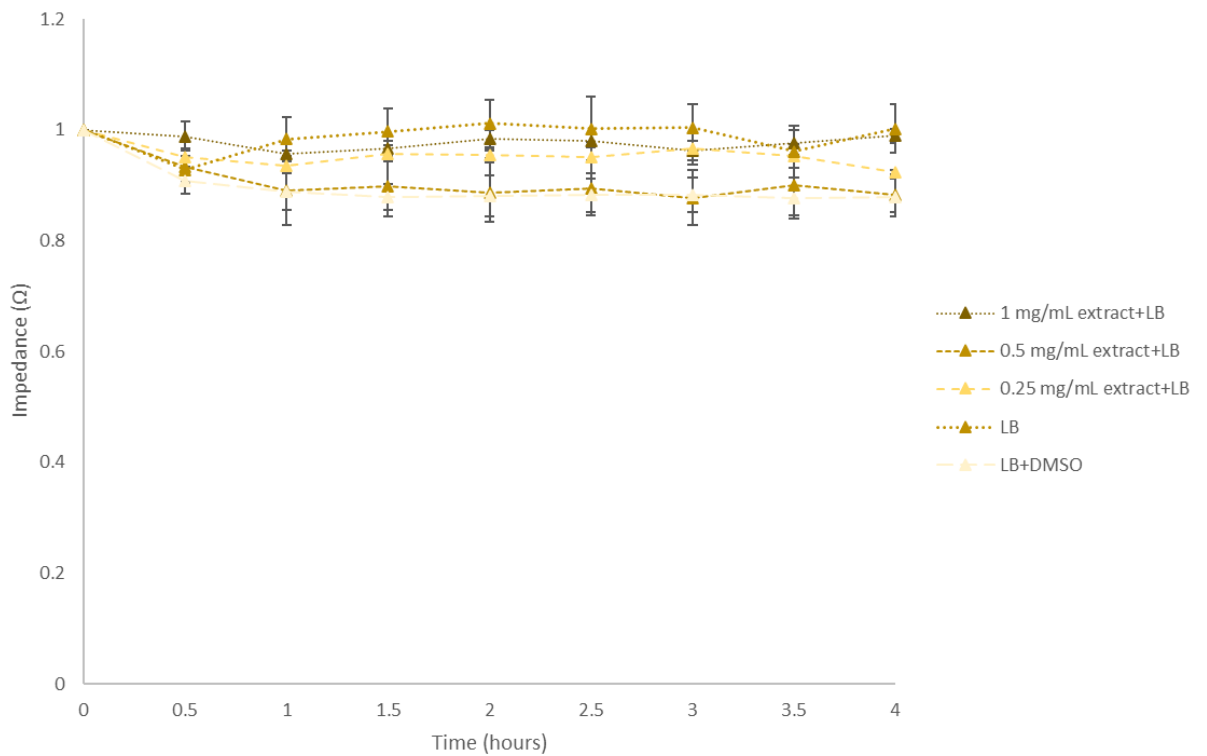
**Supplementary Figure 4.2: OD and CV measurements of controls against both PA14 and LESB58.** Controls include bacteria only, bacteria+extracted media blank, bacteria+DMSO, and LB media only, for both PA14 and LESB58. OD measurements (600 nm) are shown in pale grey, CV measurements (570 nm) are shown in dark grey. Biofilms measured after four hours incubation, error bars show standard deviation, n=3.



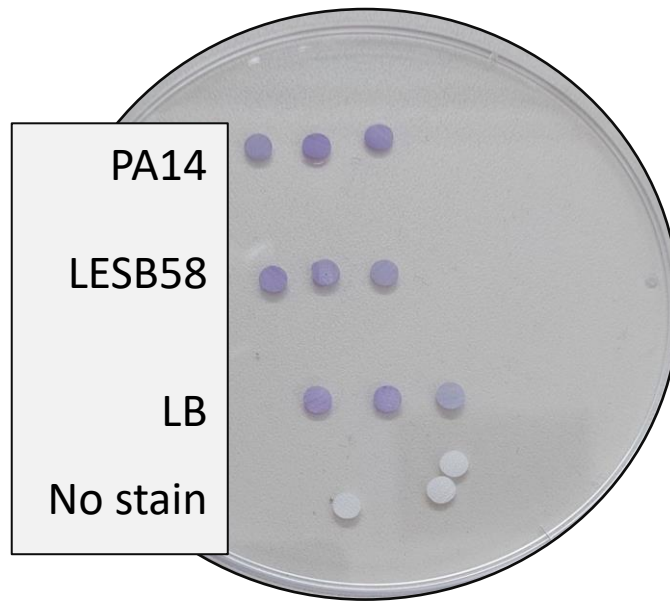
**Supplementary Figure 4.3: OD measurements of media solvent fractions against *P. aeruginosa* (PA14 and LESB58).** Solvent fractions of MeOHdH2O, MeOH, ACN, EtOAc for both ISP2 and ISP7, and LB, and LB+DMSO controls for PA14 (green), LESB58 (blue), LB (yellow). All fractions dissolved in DMSO. OD measured (600 nm) after four hours incubation, error bars show standard deviation, n=3.



**Supplementary Figure 4.4: CV measurements of media solvent extractions against *P. aeruginosa* (PA14 and LESB58).** Solvent fractions of MeOHdH2O, MeOH, ACN, EtOAc for both ISP2 and ISP7, and LB, and LB+DMSO controls for PA14 (green), LESB58 (blue), LB (yellow). All fractions dissolved in DMSO. Biofilms measured at 570 nm after four hours incubation, error bars show standard deviation, n=3.



**Supplementary Figure 4.5: EIS measurements of decreasing concentrations of extract LR16 (1 – 0.25 mg/mL) over four hours.** Extract LR16 in the presence of LB, with LB only and LB + DMSO controls. Impedance measured at 10 Hz over four hours, normalised by dividing each data set by their t=0 value, error bars show standard deviation, n=3, no statistical significance at any time points.



**Supplementary Figure 5.1: Photograph of Dacron graft post-CV staining.** *P. aeruginosa* (PA14 and LESB58) biofilms formed on Dacron graft and then stained with CV, along with an LB media control. Images show the retention of CV stain by the Dacron graft, including in the LB media only control, and subsequent inability for CV to be used to quantify biofilms on graft.